

LOUGHBOROUGH
UNIVERSITY OF TECHNOLOGY
LIBRARY

AUTHOR/FILING TITLE

LI, W

ACCESSION/COPY NO.

040129505

VOL. NO.

CLASS MARK

27 JUN 1997

Loan copy

28 OCT 1997

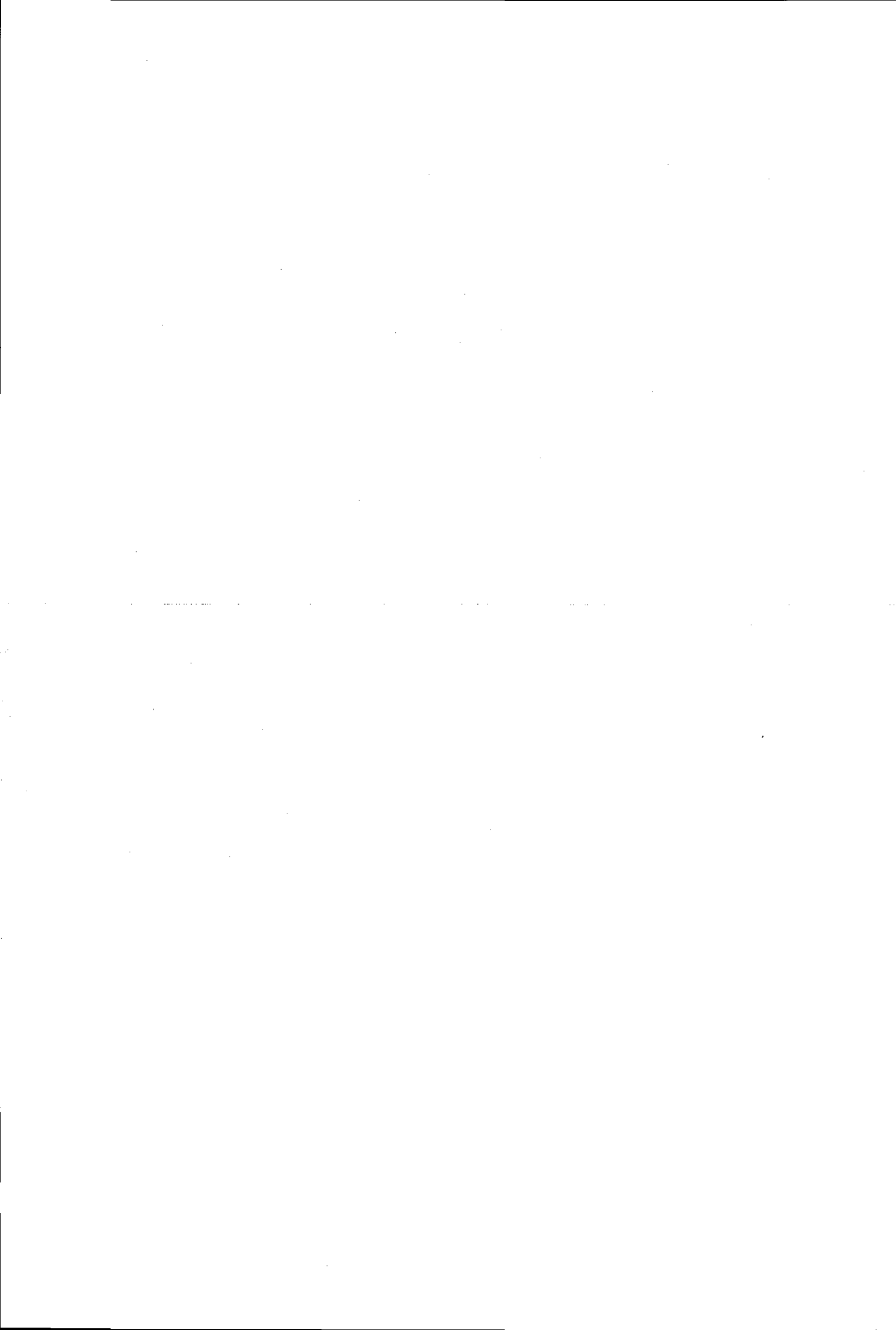
26 JUN 1998

25 JUN 1999

0401295052



BADMINTON PRESS
18 THE HALFCROFT
SYSTON
LEICESTER, LE7 1LD
ENGLAND



THE DYNAMICS OF PERFECT STEERING
BOGIE VEHICLES AND ITS IMPROVEMENT
WITH A RECONFIGURABLE MECHANISM

by

WEI LI


A Doctoral Dissertation

Submitted in partial fulfilment of the requirements for the award of
doctor of philosophy of the Loughborough University of Technology

October 1995

Supervised by: Professor A. H. Wickens

© by WEI LI, 1995

 Loughborough University
Date <i>Sept 96</i>
Class
Acc No. <i>040129505</i>

9648138

*To my daughter, my wife and my mother
for their support, encouragement and suffering
with all my love forever*

ABSTRACT

Even since railway vehicles were invented, railway scientists and engineers have been putting a lot of effort in finding the solution to the fundamental conflict between vehicle stability in the lateral plane and vehicle's capability of negotiating curves. Many configurations of railway bogie vehicles have been proposed and applied to minimise the conflict. The purpose of the research project is i) to create new configurations that can decouple the basic conflict, ii) to investigate dynamic behaviour of the new configurations and iii) to conceive a new mechanism that can improve the dynamics of the new configurations.

Three configurations of body-steered bogie vehicles have been set up in the research. The sufficient conditions for them to be capable of perfect steering have been derived. They are called perfect steering vehicles when they satisfy these sufficient conditions. Their curving ability, stability and ride performance have been investigated. To overcome the disadvantages of the perfect steering vehicles, the reconfigurable mechanism has been conceived. The improvement in the dynamic behaviour of the perfect steering vehicles with the reconfigurable mechanism has been demonstrated. A computer program has been developed to undertake the simulation.

The steering capability of the perfect steering vehicles is much better than that of conventional bogie vehicles. There are two modes of instability in the perfect steering vehicles: low conicity instability and conventional instability in the perfect steering vehicle. The perfect steering vehicles can decouple the conflict between their conventional stability and curving. The improvement of stability and ride performance of the perfect steering vehicles is, however, limited by the low conicity instability.

When the reconfigurable mechanism is applied, a body-steered bogie vehicle can become a perfect steering vehicle when on curves and can become a conventional bogie vehicle when in other circumstances. Low conicity instability can be eliminated when the reconfigurable mechanism is used. This class of vehicles possess the advantages of both conventional bogie vehicles and perfect steering vehicles, and thus, provide a very valuable solution for the fundamental conflicts between the stability and steering ability and between ride performance and stability of railway vehicles. The findings in this thesis have great significance in developing perfect steering vehicles.

ACKNOWLEDGEMENT

I would like to express my heartfelt gratitude to Professor A. H. Wickens for his guidance, supervising, his continuous encouragement and financial support through my study.

CONTENTS

	ABSTRACT	
	AKNOWLEDGEMENTS	
	CONTENTS	i
	NOTATION	v
Chapter 1	INTRODUCTION	1
1.1,	General Definitions -----	1
1.2,	The Fundamental Conflicts in Railway Vehicles -----	5
1.3,	A Review of Bogie Configuration -----	7
1.4,	Controlled Suspensions Systems in Railway Vehicles -----	14
1.5,	Research into Railway Vehicle Dynamics -----	19
1.6,	The Objectives of This Research -----	21
Chapter 2	DYNAMIC EQUATIONS	23
2.1,	Coordinate System and Accelerations -----	23
2.2,	Track Definitions -----	26
2.3,	Dynamic Equation of Unconstrained Wheelset -----	27
2.4,	Dynamic Equations of a Railway Bogie Vehicle -----	30
2.5,	Perfect Steering Conditions -----	32
2.6,	Displacement Vector -----	33
2.7,	Ride Performance -----	35
2.7.1,	Power Spectral Density (PSD) and Root Mean Square (rms) -	35
2.7.2,	PSD of Track Irregularities -----	36

2.7.3,	The Transfer Function of a Railway Bogie Vehicle -----	38
2.8,	Computer Programming -----	40
Chapter 3	PERFECT STEERING BOGIE VEHICLE MODELS AND THEIR CAPABILITY IN NEGOTIATING CURVES	42
3.1,	Perfect Steering Bogie Vehicles -----	42
3.1.1,	Configurations -----	43
3.1.2,	Perfect Steering Linkages -----	49
3.2,	Perfect Steering and Flange Clearance -----	51
3.3,	Geometric Errors in the Steering Linkage -----	53
3.4,	Effects of Cant Deficiency -----	59
3.5,	Kinematic State of Perfect Steering Vehicles on a Cubic Parabola Transition -----	62
3.6,	Summary -----	65
Chapter 4	STABILITY OF THE PERFECT STEERING BOGIE VEHICLES	72
4.1,	Stability Criteria -----	72
4.2,	Eigenvalues of Bogie Vehicles -----	75
4.3,	Instability Modes of the Perfect Steering Vehicles -----	78
4.3.1,	Low Speed Instability in Low Conicity -----	79
4.3.2,	Dynamic Instability in Low Conicity -----	79
4.3.3,	Conventional Instability -----	80
4.4,	Theoretical Analysis of Low Conicity Instability -----	81
4.4.1,	Bogie Sub-system -----	81

4.4.2,	Instability at Low Speed -----	83
4.4.3,	Dynamic Instability in Low Conicity -----	94
4.5,	Influences of the Parameters in the Steering Linkages and Suspensions -----	96
4.5.1,	Conicity -----	96
4.5.2,	Effective Stiffnesses -----	98
4.5.3,	Primary Lateral Stiffness -----	100
4.5.4,	Some Considerations -----	101
4.5.5,	Influences of the Secondary Suspension Parameters -----	103
4.5.6,	Influences of the Geometric Errors in Steering Linkages -----	104
4.6,	Summary -----	105
Chapter 5	RIDE PERFORMANCE OF THE PERFECT STEERING BOGIE VEHICLES	108
5.1,	Indices of Ride Performance -----	109
5.2,	Coupling between Steering Linkages and Suspensions ---	112
5.2.1,	An Example -----	112
5.2.2,	Complication Associated with Perfect Steering Vehicles -----	117
5.3,	Simulation Results -----	118
5.3.1,	Ride Quality -----	118
5.3.2,	Strokes -----	122
5.3.3,	Influences of the Parameters in the Suspensions and Steering Linkages -----	124
5.3.4,	Geometric Errors -----	135
5.4,	Summary -----	135
Chapter 6	SUMMARY OF THE DYNAMIC BEHAVIOUR OF THE PERFECT STEERING VEHICLES	138

Chapter 7 THE IMPROVEMENT OF PERFECT STEERING BOGIE VEHICLE DYNAMICS BY A RECONFIGURABLE MECHANISM 145

7.1, Reconfigurable Mechanism ----- 145

7.1.1, Concept of the Reconfigurable Mechanism ----- 145

7.1.2, Reconfigurable Mechanism in Perfect Steering Vehicles ----- 146

7.1.3, Two Devices ----- 150

7.2, The Relationship between Effective Stiffnesses and Yaw Stiffnesses ----- 155

7.3, Optimisation of Stiffnesses when the Reconfigurable Mechanism is Applied ----- 157

7.4, Improvement in Dynamic Behaviour ----- 161

7.5, Summary ----- 169

Chapter 8 CONCLUSIONS AND FUTURE DEVELOPMENTS 172

8.1, Contributions and Findings ----- 172

8.2, Commercial Application Remarks ----- 177

8.3, Future Development Remarks ----- 178

References

Appendix A

Appendix B

Appendix C

Appendix D

Notation

a_0	half gauge (m)
a	half wheelset base (m) or acceleration (m/s^2)
a_γ	longitudinal geometric parameter of vehicle (m)
a_w	weighted acceleration (m/s^2)
$a_{A,B,C,D,E}$	acceleration at point A, B, C, D, or E in Fig.5.1 (m/s^2)
\mathbf{a}	compatibility matrix
\mathbf{a}_{LL}	sub-compatibility matrix of leading bogie
A_a	roughness parameter of alignment irregularity (in^2/cpf)
A_c	roughness parameter of cross level irregularity (in^2/cpf)
\mathbf{A}	coefficient matrix of vehicle disturbances
b_γ	lateral geometric parameters of vehicle (m)
c_γ	viscous damping or geometric parameter (N-s or N-s/m)
\mathbf{C}	viscous damping matrix
d	distance between joint A and joint B in Fig.7.1 (m)
\mathbf{D}	system damping matrix
\mathbf{E}	system elastic matrix
\mathbf{E}_L	elastic sub-matrix of leading bogie
f	frequency (Hz)
f_{11}	longitudinal creepage coefficient (N)
f_{22}	lateral creepage coefficient (N)
f_{33}	creepage coefficient
f_{23}	creepage coefficient
F	force (N)
\mathbf{F}	force matrix
\mathbf{F}_{cant}	force vector caused by cant deficiency
\mathbf{F}_{creep}	creep force vector caused by curvature
\mathbf{F}_E	elastic force vector caused by curvature
g_γ	geometric parameters defined by Eq.(3-2) or Eq.(3-5) (m^2)
g	gravity acceleration (m/s^2)
\mathbf{G}	creepage damping matrix
h_γ	vertical geometric parameters of vehicle (m)
h_0	height from the floor level to the carbody weight centre (m)
$H(\omega)$	transfer function
$H^*(\omega)$	conjugate of transfer function $H(\omega)$

I	inertia of a mass (kg-m ²)
j	wheelset number of vehicle
k_γ	stiffness (N/m or N-m)
$k_{e\gamma}$	effective stiffness in steering linkages (N/m ³)
k_b	bending stiffness (N-m)
k_s	shear stiffness (N/m)
k_{py}	primary lateral stiffness (N/m)
$k_{p\psi}$	primary yaw stiffness (N-m)
$k_{p\phi}$	primary roll stiffness (N-m)
k_{sy}	secondary lateral stiffness (N/m)
$k_{s\psi}$	secondary yaw stiffness (N-m)
$k_{s\phi}$	secondary roll stiffness (N-m)
k_{bs}	stiffness between steering linkage lever and carbody (N/m)
k_{wo}	stiffness between steering linkage lever and outboard wheelset (N/m)
k_{wi}	stiffness between steering linkage lever and inboard wheelset (N/m)
k_{bwo}	stiffness between carbody and outboard wheelset (N/m)
k_{bwi}	stiffness between carbody and inboard wheelset (N/m)
k_{pwo}	primary bending stiffness of outboard wheelset (N/m)
k_{pwi}	primary bending stiffness of inboard wheelset (N/m)
k_{wwb}	inter wheelset bending stiffness (N/m)
k_{wws}	inter wheelset bending stiffness (N/m)
K	system stiffness matrix
l	half full length of vehicle (m)
l_0	half distance between two pivots (m)
l_i	geometric parameters of steering linkage levels (m)
L	length of transition curve (m)
m	mass (kg) or number of springs
M_γ	moment (N-m)
M	system inertia matrix
n	number of degrees of freedom or order of Eigen-Equation
N	normal force (N)
N	creepage stiffness matrix
p_i	coefficients of Eigen-Equation
P	degeneracy of elastic matrix E
q	general displacement
\bar{q}	relative displacement between reference and local coordinates
\hat{q}	relative displacement between the inertia axes of a mass and its local coordinates

\dot{q}	dq/dt
q'	dq/dx
δq	relative displacement between two \hat{q}
Δq	relative displacement between two \bar{q}
Q	force vector
r_0	nominal rolling radius of a wheelset (m)
r_L	rolling radius of the left wheel on a wheelset (m)
r_R	rolling radius of the right wheel on a wheelset (m)
R	radius of a curve (m)
$R(\tau)$	correlation function
$S(\omega)$	power spectrum density
t_i	time lag between wheelsets (s)
T	force acted on joint B in Fig.7.1 (N)
W	gravity of a mass (N)
W_i	weighted factors of acceleration rms
$W(f)$	single side power spectrum density
v_0	vehicle forward speed (m/s or km/h)
v_c	critical speed (m/s or km/h)
V_{\max}	vehicle maximum speed on curve (km/h)
x	longitudinal coordinate or displacement (m)
X	disturbance matrix
y	lateral coordinate or displacement (m)
y_L	end of transition curve (m)
y_a	track alignment irregularity (m)
y_{rR}	lateral displacement of right side rail (m)
y_{rL}	lateral displacement of left side rail (m)
z	vertical coordinate or displacement (m)
z_c	track cross-level irregularity (m)
z_{rR}	vertical displacement of right side rail (m)
z_{rL}	vertical displacement of left side rail (m)
α	yaw stiffness ratio ($k_{p\psi}/k_{s\psi}$) or angle of corned pin in Fig.7.8
β	stiffness ratio ($k_e/k_{p\psi}$)
δ	contact angle between rail and wheel
Δ_γ	Routh's array
$\Delta_\gamma(\omega)$	terms in transfer function $H(\omega)$
ϕ	roll direction, roll angle (rad) or spatial frequency (cpf)
ϕ_{1a}	low spatial break frequency (cpf) of alignment irregularity

ϕ_{2a}	high spatial break frequency (cpf) of alignment irregularity
ϕ_{1c}	low spatial break frequency (cpf) of cross level irregularity
ϕ_{2c}	high spatial break frequency (cpf) of cross level irregularity
ϕ_d	cant deficiency (rad)
λ	conicity or eigenvalue
λ_e	equivalent conicity
$\phi_?$	mean ratio of rms
μ	friction coefficient
$\vartheta_?$	proportion of rms
θ	pitch direction or pitch angle (rad)
Θ	angular velocity of reference coordinates
σ	contact parameter
ω	angular frequency (1/s)
$\omega_?$	angular velocity of a mass (1/s)
ω_n	natural frequency (1/s)
ω_m	minimum value frequency (1/s)
$\Omega_?$	angular velocity (1/s) of the inertia axes of a mass
$\xi, \bar{\xi}, \zeta, \bar{\zeta}$	minimum conicity derived from low speed instability
ξ_x	longitudinal creepage
ξ_y	lateral creepage
ξ_{sp}	spin creepage
ψ	yaw direction or yaw angle (rad)
$\bar{\Psi}_{bTL}$	relative yaw angle between leading bogie and carbody
$\bar{\Psi}_{bwo}$	relative yaw angle between outboard wheelset in leading bogie and carbody

Subscript:

b	carbody
bTL	between body and leading bogie
bw	between body and wheelset
e	effective
i	inboard
o	outboard
p	primary suspension
r	track
s	secondary suspension

T	bogie
TL	leading bogie
TR	trailing bogie
w	wheelset
x	longitudinal
y	lateral
z	vertical
ϕ	roll
θ	pitch
ψ	yaw

Chapter 1

INTRODUCTION

1.1 General Definitions

A bogie railway vehicle consists of several mass components such as wheelsets, bogies and a carbody that are connected by springs and dampers. Each mass component has six degrees of freedom, and the definitions and directions of the degrees of freedom are shown in Fig.1.1. If a bogie vehicle is fore-and-aft symmetric, the system can be decoupled into two sub-systems, one of which is used to study the dynamics of the vehicle in the vertical plane and the other is used to study its dynamics in the lateral plane. The dynamics of railway vehicles in the vertical plane is mainly used to study the vehicle strength and the dynamic loads on track as well as ride performance, whilst the dynamics in the lateral plane is used to investigate vehicle behaviour such as stability, ride performance and curving. In this research project, only the dynamics of railway bogie vehicles in the lateral plane is involved, and only three out of six degrees of freedom of each mass component are included in the dynamic equations of a fore-and-aft symmetric bogie vehicle in the lateral plane, which are lateral displacement, yaw angle and roll angle. One degree of freedom in wheelsets will disappear since wheelsets are assumed not to leave track, which is the roll angle of wheelset.

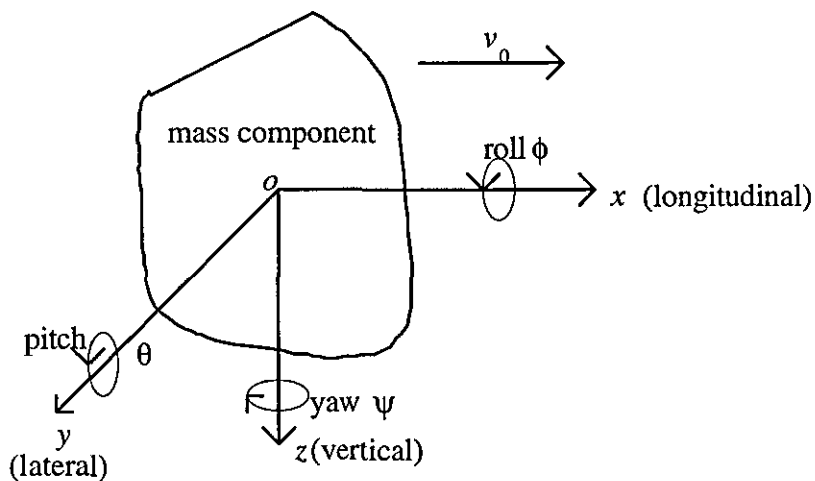


Figure 1.1 The definitions and directions of degrees of freedom

Usually, the bogies of railway vehicles can be divided into two axle bogies and three axle bogies, but only two axle bogies are discussed in this thesis. Commonly, a railway bogie vehicle possesses two bogies, and the general configuration of two-axle bogie vehicle is illustrated in Fig.1.2 where the mass components are connected by several springs and dampers. If the springs and dampers are considered as massless, there are seven mass components in a bogie vehicle, these being the four wheelsets, two bogie frames and carbody. Mass components are assumed as rigid bodies. The definitions of the springs are illustrated in Fig.1.2 in terms of stiffness while the dampers are defined in terms of damping and are parallel with the springs if they are applied. The connection between wheelset and bogie frame is called the primary suspension and the connection between carbody and bogie frame is called the secondary suspension, whilst the connection between wheelsets and carbody is defined as the steering linkage.

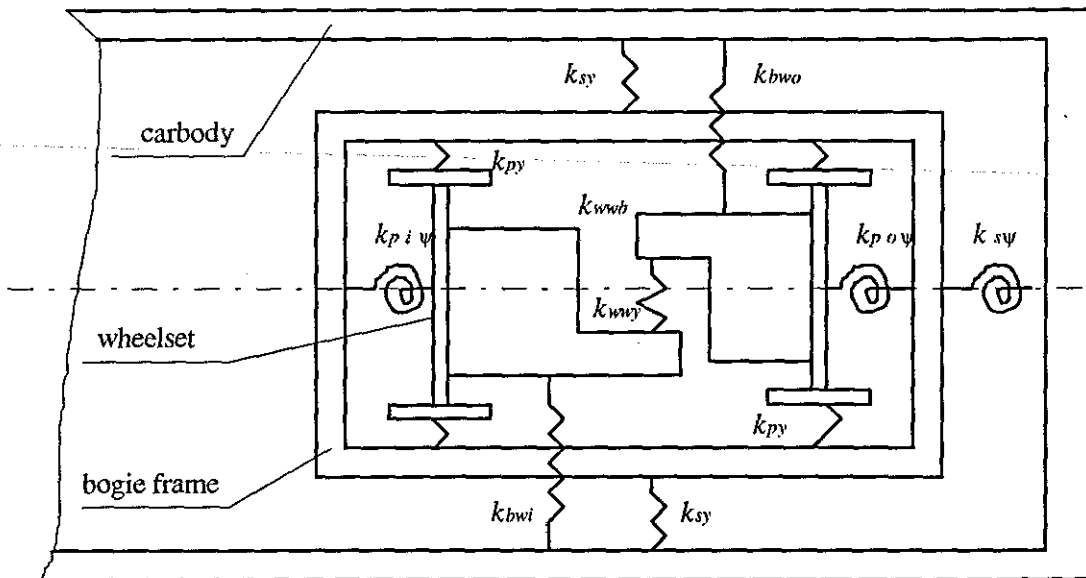


Figure 1.2 The definitions of the stiffnesses

A wheelset has two wheels that are connected firmly (conventional wheelset) or independently (independent wheelset) by an axle. The diagram in Fig.1.3 shows a conventional wheelset. Its wheels consist of a coned or profiled tread and a flange. The radius of the wheel on the contact point between the wheel and rail is called the rolling radius. When a wheelset moves out of its neutral (static stable) position, the rolling radii of two wheels of the wheelset are not equal to each other due to the profiles of these two wheel treads, as seen in Fig.3a, and the equivalent conicity (simplified as conicity λ) is defined:

$$\lambda_e = \frac{r_R - r_L}{2y_w} \tag{1-1}$$

For a coned wheel, as shown in Fig.1.3b, the conicity is the tangent of the contact angle δ between rail and wheel.

The difference in the rolling radii results in different forward speeds in each wheel and forces the wheelset to have a yaw angle such that the wheelset moves towards its neutral position. When the wheelset crosses its neutral position, the same action happens again and the wheelset is forced to move back, and the process goes on and on, as shown in Fig.1.4. This motion is called the '*kinematic oscillation*' of the wheelset or wheelset '*hunting*'.

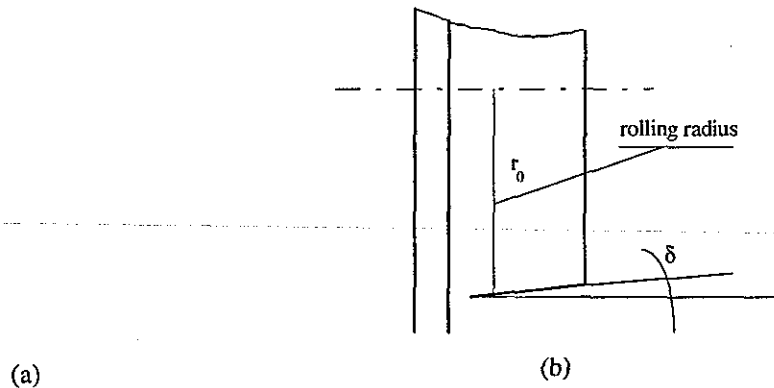


Figure 1-3 Wheelset (a) and wheel profile (b)

Figure 1-4 kinematic oscillation of wheelset

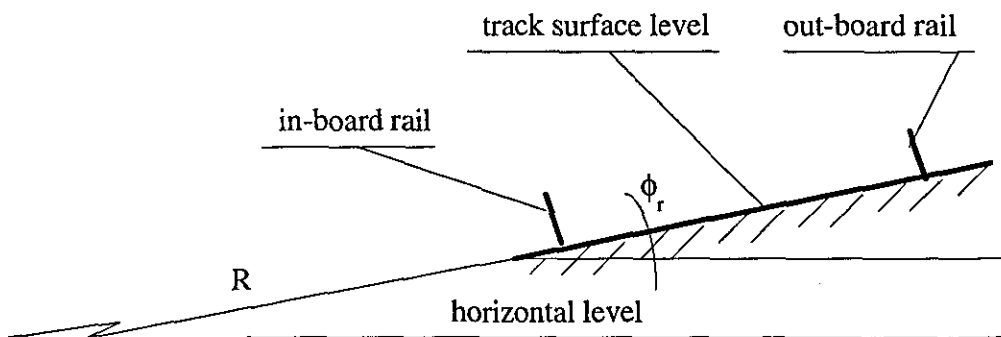


Figure 1.5 Curve definitions

A railway line consists of several sections: tangent tracks, uniform curves, spiral transitions (connecting tangent tracks with uniform curves), switches and reverse curves (two different direction curves connecting together). The positive direction of a curve is defined as that the circle centre is on the right side of the vehicle when it moves forward on the curve. The tracks on curves and spiral transitions are superelevated (or canted) to overcome the centrifugal force, as shown in Fig.1.5. The force produced by the cant deficiency is the unbalanced force between the centrifugal force and the component of gravity on the track surface. Thus, the cant deficiency is defined by:

$$\phi_d = -\left(\phi_r - \frac{v_0^2}{gR}\right) \quad (1-2)$$

There are three kinds of track irregularities: isolated variations, periodic geometry variations and random geometry variations. Strictly, the track random geometry variations are not stationary processes. They can however, be reasonably assumed as the stationary processes since the processes vary much slower than vehicle speed. Seven isolated variations are listed in the reference[1]. Only two of four random geometry variations affect the dynamic behaviour of railway vehicles in the lateral plane. They are defined as:

$$\text{cross-level irregularity:} \quad z_c = (z_{rR} - z_{rL})/2 \quad (1-3)$$

$$\text{alignment irregularity:} \quad y_a = (y_{rR} + y_{rL})/2$$

The forces between a rail and a wheel on the contact patch in the horizontal plane come from the creep between wheel and rail due to the material elasticity. The creep between rail and wheel is measured by the non-dimensional term creepage that is defined by:

longitudinal creepage:

$$\xi_x = \frac{\text{actual forward velocity} - \text{pure rolling forward velocity}}{\text{forward velocity due to rolling}} \quad (1-4a)$$

lateral creepage:

$$\xi_y = \frac{\text{actual lateral velocity} - \text{pure rolling lateral velocity}}{\text{forward velocity due to rolling}} \quad (1-4b)$$

spin creep:

$$\xi_{sp} = \frac{\text{angular velocity of upper body} - \text{angular velocity of lower body}}{\text{forward velocity due to rolling}} \quad (1-4c)$$

The forces caused by creep between rails and wheels are called creepage forces, which govern the dynamic characteristics of wheelset motion. There are several mathematical approaches to describe the relationships between the creepages and creepage forces. Carter[2] first set up the mathematical model for the creepage forces and applied it to railway vehicle system dynamics. The most significant and accurate solution of the creepage forces was developed by Kalker[3-4]. Strictly, the creepage forces are nonlinear function of the creepages, however, the linear theory of Kalker is now widely applied in railway vehicle dynamics because the creepage force can be considered as a linear function of creepage when creepage is small, and then:

longitudinal creepage force:

$$F_x = -f_{11}\xi_x \quad (1-5a)$$

lateral creepage force:

$$F_y = -f_{22}\xi_y - f_{23}\xi_{sp} \quad (1-5b)$$

spin creep moment:

$$M_z = f_{23}\xi_y - f_{33}\xi_{sp} \quad (1-5c)$$

The full review of creepage theories is not included here, and the reader is referred to [1].

1.2 The Fundamental Conflicts in Railway Vehicle Dynamics

When an unconstrained wheelset enters a curve, it tends to align itself. The simplest case of an unconstrained wheelset moving on curves is that it moves on a uniform curve without tangent acceleration and with zero cant deficiency. If it is considered as rigid, the forward speed difference in the two wheels caused by the conicity aligns

the wheelset to a radial position (in which the wheelset axle is perpendicular to the tangent direction of curve), and the wheelset will move laterally toward the outboard rail when the wheelset moves on a curve. The flange clearance (i.e. the distance between wheel flange and rail side) will become zero and flange contact (which often results in double point contact) occurs as the lateral displacement of the wheelset increases. The flange contact results in severe wear of both wheel and rail and increases the tendency of derailment. The lateral movement of the wheelset increases as the conicity decreases, and high conicity therefore is useful in reducing the lateral displacement of the wheelset when it is on curves. On the other hand, the '*kinematic oscillation*' will become unstable as the wheelset forward speed increases. The critical speed v_c is defined as the maximum speed at which a rigid body (wheelsets, bogies or vehicles) is stable. Wickens[5] fully demonstrated the dynamic characteristics of single wheelset, and found that the critical speed of single wheelset will reduce when its conicity becomes higher. One of the fundamental conflicts of railway vehicle dynamics is thus the trade-off between the stability and curve negotiation of railway vehicle with regard to wheelset conicity.

When wheelsets are mounted on a railway vehicle, the vehicle suspensions are able to constrain the wheelset motions, and the wheelset stability is improved by the suspensions. The most important parameters in the suspensions constraining wheelset motions are the primary lateral stiffness k_{py} (mainly constraining wheelset lateral motion) and the primary yaw stiffness k_{pw} (mainly constraining wheelset yaw motion). The stiffnesses between the outboard wheelset and the inboard wheelset are defined as the shear stiffness k_s and the bending stiffness k_b , and are schematically explained in Fig.1.6[6]. Similar definitions can apply to the stiffnesses between the bogies. If there is no direct connection between the wheelsets, only the primary yaw stiffness contributes to the wheelset bending stiffness. Similarly, only the secondary yaw stiffness contributes to the bending stiffness between the bogies (this stiffness is in fact the rotational stiffness, this thesis uses the term 'bending stiffness' instead of the term 'rotational stiffness') if there is no direct connection between the bogies. Generally, the critical speed of vehicle can be increased when the stiffnesses, especially the yaw stiffnesses, in the suspensions are high. In the other hand, the ideal alignment direction for each rigid body of a railway vehicle to take on curves is its own radial position, and an angle thus exists between the radial positions of each pair of the rigid bodies when the vehicle is on curves. This angle is a relative yaw between the pair of rigid bodies and can cause a moment between them, which forces the pair of rigid bodies to leave their radial positions, if there is a bending stiffness between them. It is obvious that soft bending stiffness causes less moment

such that the rigid bodies can take more radial alignment. Vehicle curving therefore requires soft bending stiffnesses that can reduce the critical speed. This contradiction between the stability and curving of railway vehicles with regard to vehicle suspensions represents another fundamental conflict in railway vehicle dynamics.

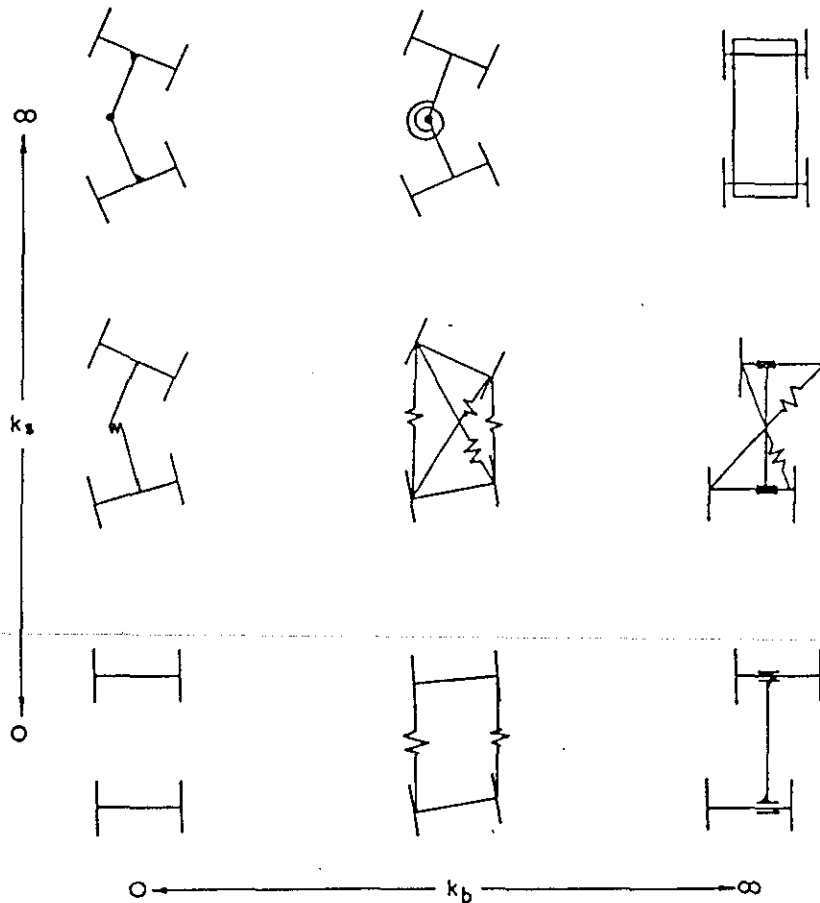


Figure 1.6, The schematic demonstration for the shear stiffness k_s and bending stiffness k_b between wheelsets[6]

The other fundamental conflict in railway vehicle dynamics comes from the trade-off between vehicle stability and ride performance. Track disturbances are transferred into vehicle body through its suspensions. Although soft suspensions can reduce the system responses, they degrade the vehicle stability. These fundamental conflicts mainly dominate railway vehicle suspension design.

1.3 A Review of Bogie Configuration

The most important part of a railway bogie vehicle is its bogies, and the dynamic behaviour of vehicles is mainly determined by their bogie configurations. Not only

do bogies constrain wheelset motions, but they also support carbody and accommodate traction motors. Although strength is an important factor that needs to be considered in bogie design, it is not within the scope of this research. A comprehensive review of bogie configurations related to vehicle performance has been contributed by Wickens in 1991[8]. This section briefly reviews two main kinds of bogie configurations (conventional and steerable) in connection with their dynamic characteristics. The main difference between them is that the stiffnesses (k_{bwo} & k_{bwi}) between the wheelsets and carbody, as seen in Fig.1.2, are equal to zero in a conventional bogie vehicle while they are not equal to zero for a steerable bogie vehicle.

In conventional bogie vehicles, bogie frames are mounted on wheelsets. There are springs (and sometimes dampers) between them that provide stiffnesses in vertical, longitudinal and lateral directions. Bogie frames are usually rigid and the carbody freely pivots on bogie frames or is connected to the bogie frames by secondary suspension. The critical speed of this class of vehicle can be made very high by optimally choosing longitudinal (equivalent to yaw stiffness) and lateral stiffnesses. Even for the British Railways B4 bogie[8] developed empirically without either stability or curving calculation in 1960, its critical speed reached 160km/h with low conicity. This class of vehicle has been widely used in high speed railways with various modifications because of the advantage in vehicle stability. However, conventional vehicles cannot solve the conflict between stability and curving even for well optimised conventional bogie vehicles. On one hand, it is necessary to have enough longitudinal (yaw) stiffnesses to stabilise the vehicle; whilst on the other hand, it is expected to have soft bending stiffness to achieve good curving. The main task for vehicle designers is to look for an equilibrium point between these two requirements under specified circumstances.

In order to improve the alignment ability, wheelset inter-connection bogie vehicles and steerable vehicles have been proposed and applied. There is a mechanism to assist wheelsets taking up radial alignment in steerable vehicles, and body-steered bogie vehicles and active-steering bogie vehicles are two basic forms of steerable vehicles. In a wheelset inter-connection bogie vehicle, the outboard wheelsets is directly connected to the inboard wheelset by springs or radial arms. The connection between wheelsets usually adds two additional stiffnesses between wheelsets (the shear stiffness k_{wyy} and the bending stiffness k_{wwb}). There are four parameters that can be optimised such that the overall lateral stiffness of wheelset can be increased beyond the limit for conventional bogies, and the overall yaw

stiffness of wheelset can be reduced. This brings two benefits: *'firstly, the reduction of overall bending stiffness improves curving and, secondly, under certain conditions dynamic stability is improved as the destabilizing effect of the coupling of inertia of the frame through the longitudinal stiffness is ameliorated'*[8]. Cross-bracing proposed by Scheffel[9], shown in Fig.1.7, is the most popular form of this class of vehicle. Scales[10] and List[11] designed separately two other configurations. These classes of vehicle were named as *'radial bogie vehicles'* and *'self-steering vehicles'*. These terms are however, not accurate terms with regard to the curving features of this class of vehicle because their wheelsets cannot take radial alignment neither can they steer themselves. The real mechanism is that they use wheelset inter-connection to increase the wheelset lateral stiffness and to reduce the yaw stiffness between the wheelsets and bogie frames.

Body-steered bogie vehicles have a linkage between wheelsets and carbody, which has three effects in vehicle dynamic behaviour. Firstly, the relative displacements between the carbody and wheelsets produce a moment in the linkage to force the wheelsets to align more radially when the vehicle moves on curves and, secondly, the linkage can be considered as another suspension for the vehicle so that the system stability is affected by the linkage and, finally, the track disturbances can transfer into the carbody through the linkage so that the vehicle ride quality is also affected. The first two effects have been noted and comprehensively investigated [12-20], but the last one has not been well studied.

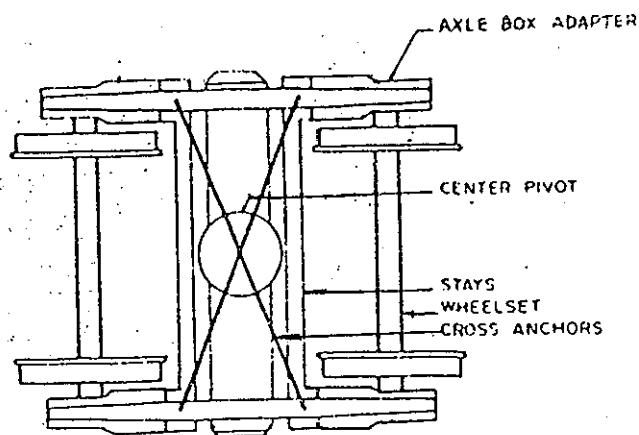


Figure 1.7 Scheffel radial bogie[9]

The application of linkage between wheelsets and carbody can be dated back to the last century[8], however, significant engineering progress was developed by Liechty [21-22] in 1930's. In 1974, Schwanck[23] published the results of a body-steered bogie vehicle experimented in DB, and reported that its basic advantages were in

reducing wheel and rail wear, reducing traction resistance in curves and increasing safety against derailment. The theoretical research and engineering development of body-steered bogie vehicles became active in the 1980's. The most significant theoretical research was independently contributed by Bell and Hedrick [12] and by Smith, Anderson and Fortin[13-16,19-20], which will be reviewed in the following paragraphs. Several other cases were reported individually: Weeks [17] reported the development of a cross-bracing type of body-steered bogie vehicle that was intended for use in the Central line of the London Underground system; Shen[18] investigated the improvement of dynamic behaviour of a three-piece bogie vehicle with a linkage between its wheelsets and carbody, and demonstrated the benefits in curving, stability and dynamic response, which promotes opportunities to extend the application for three-piece bogie.

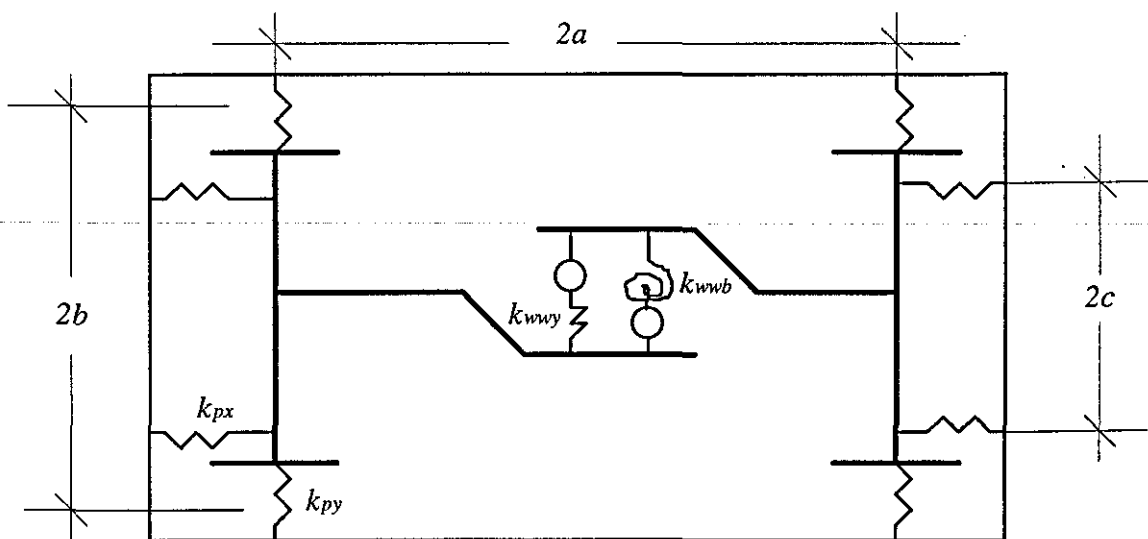


Figure 1.8 Bell & Hedrick's Model[12]

Actually, the steering mechanism of a body-steered bogie makes use of the relative orientation between carbody and bogie or between carbody and wheelsets, which develops when the vehicle moves on curves. Bell and Hedrick[12] studied the curving and stability of *forced-steering bogie vehicles*, as shown in Fig.1.8, and suggested that *'the steady state yaw angle that develops between the carbody and the truck can be used as an indication of curve radius being traversed, and linkage between the carbody and the wheelsets can be used to force the wheelsets into a more radial alignment. Likewise the lateral displacement that occurs between the carbody and truck can be used as an indication of cant deficiency, and linkages can be designed to produce forces on the wheelsets as a function of the cant deficiency'*[12]. On the basis of their findings, they defined the fundamental

difference between a *forced-steering bogie* and both the conventional and self-steering bogies as the presence of forces on the wheelsets of the forced-steering bogie being a function of the relative yaw and lateral displacement between the carbody and bogie.

Smith and Anderson[18] investigated the dynamic behaviour of a *guided steering bogie*, as shown in Fig.1.9, and their results led to the invention of the UTDC Floating Frame bogie[20]. The elementary distinctions of the model in Fig.1.9 from the model in Fig.1.8 are that: firstly, the wheelsets are pivoted on the bogie frame and, secondly, each wheelset is separately connected to the carbody. They reported that '*the only valid technique for positively steering the axles of two axle trucks is through an input from the yaw of the truck relative to the carbody*'[17].

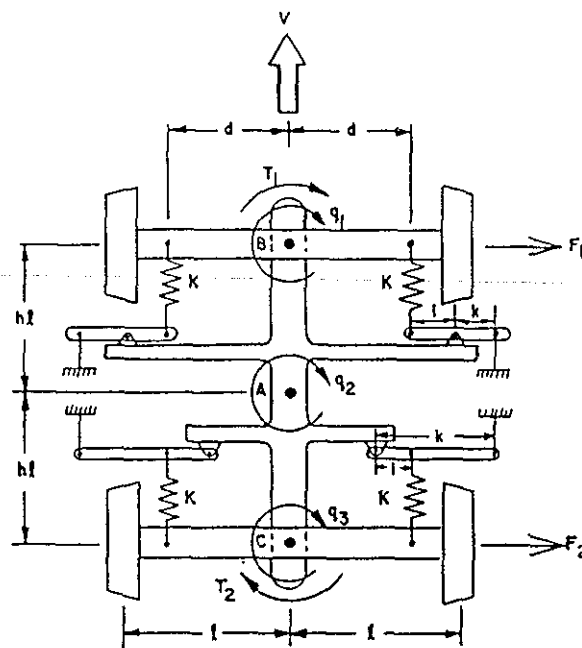


Figure 1.9 Smith & Anderson's Model[19]

The linkage between the wheelsets and the carbody increases the system coupling and therefore introduces new modes of instability. The most interesting mode of instabilities in a body-steered bogie vehicle is low conicity instability, as seen in Fig.1.10. Several papers[12,15,19] were published and analysed the mechanism of low conicity instability. Bell and Hedrick[12] gave a simple physical explanation that the longitudinal creepage reduces as conicity decreases so that there is not sufficient longitudinal creepage force to balance the force produced by the steering mechanism, thus the system become divergently unstable. This standpoint was also supported by the results of Anderson and Fortin[15].

Compared with both conventional and wheelset inter-connection bogie vehicles, the basic advantage of body-steered bogie vehicles is that the steering ability of body-steered bogie vehicles is greatly improved, which can reduce the conflict between vehicle stability and curving. Most of the researches in this field have thus led to successful practical implementation. The main drawback of body-steered bogies is however, the low conicity instability as has been identified by most of the researchers in this field.

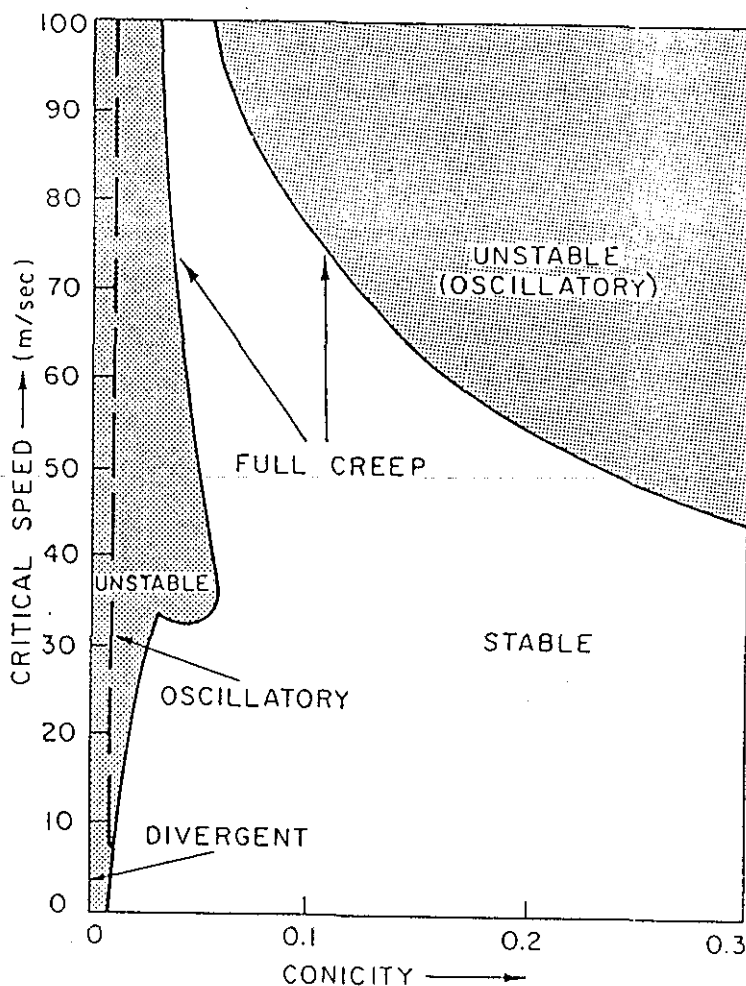


Figure 1.10 Stability against conicity of body-steered bogie vehicle[20]

It seems that most of the researchers in body-steered bogies have concentrated their efforts on exploring the advantages of body-steered bogies in stability and curving and on revealing the mechanism of steering and instabilities. Several other aspects of dynamic behaviour seem to have been investigated only in a limited manner. The effect of the linkage between wheelsets and carbody on ride performance, the influence of secondary suspension on stability, the effect of the bending stiffness

between two bogies on curving and the mechanisms of oscillatory unstable modes in low conicity are examples of this under researched work.

The concept of perfect steering was first proposed by Wickens[24] as without generating creep between wheelset and rail on a uniform curve with zero cant deficiency. First of all, he investigated the stability of asymmetric two-axle vehicle possessing perfect steering[25], and then studied stability of a multi-axle vehicle possessing perfect steering[26]. Recently, Wickens[27] has identified the necessary conditions of perfect steering and stability for railway bogie vehicles, and theoretically demonstrated that it is possible for a railway bogie vehicle with four wheelsets to achieve perfect steering and to have a non-zero critical speed. He schematically demonstrated several possible configurations for perfect steering bogies and investigated the stability of one of these configurations[28]. His work in this area provides a greater innovative freedom for both researchers and designers to utilise. A perfect steering bogie vehicle has a similar steering linkage between the wheelsets and carbody with other body-steered bogie vehicles. The fundamental difference between a perfect steering bogie and other body-steered bogies is that all bending stiffnesses (k_b 's) in the suspensions of a perfect steering vehicle are zero, and the stiffnesses in the steering linkages of a perfect steering vehicle do not contribute any bending stiffnesses. The wheelsets in a perfect steering bogie vehicle can therefore freely take their radial positions on a uniform curve with zero cant deficiency. It is important to understand that "perfect steering" is a useful abstraction, for there are many small effects which are present in reality but which can be ignored for practical design purposes.

The dynamic characteristics of perfect steering bogie vehicles have not been studied well although the feasibility of this class of vehicle has been theoretically proved by Wickens[27]. The following aspects of the dynamic behaviour of perfect steering bogie vehicles should therefore be carefully investigated before any practical implementation occurs.

1. The conditions of perfect steering with regard to track are a uniform curve and zero cant deficiency. The curvature of a uniform curve is a constant, but the curvatures are not a constant along a spiral transition that connect a straight line to a uniform curve. Moreover, most of uniform curves have cant deficiency. The capability of negotiating a spiral transition curve and the ability versus cant deficiency for each configuration of perfect steering bogie vehicle must be considered.

2. The linkage between wheelsets and carbody and zero yaw stiffness in primary and secondary suspension affects vehicle stability. The stability analysis has two objectives: firstly, to reveal the mechanism of instability and, secondly, to find an acceptable approach to stabilise the system. Some analyses for the stability have been contributed by Wickens[27], however, the optimisation of the suspensions and steering linkages of perfect steering bogie vehicles with regard to their stability is one of the subjects that need to be investigated further.

3. Track disturbances can be transferred into the carbody by the steering linkage in a perfect steering bogie vehicle, which means that the linkage has a negative effect on the ride performance. This area, as yet, has not been studied well even for other kinds of body-steered bogie vehicles.

4. Since there are many possible configurations for perfect steering bogies, the research in optimising the configurations for perfect steering bogies is very desirable.

1.4 Controlled Suspension Systems in Railway Vehicles

All components in the vehicle suspensions reviewed in the last section are passive. *'A very fundamental limitation of passive elements is that its static deflection varies as the inverse square of frequency: this limits the lower natural frequency to approximately 1 Hz with a corresponding static deflection of order of 250 mm and causes large dynamic deflections when external loads of the same frequency are applied'*[29]. The conflict between ride quality and rattle space is enhanced by this limitation. There are other two principal limitations of passive systems[30], firstly, passive systems by definition do not require any external power source, and therefore can only store (e.g. springs) or dissipate (e.g. dampers) energy and, secondly, passive systems are restricted to generating forces in response to local relative motion. As the railway vehicle speed increases, the passive only suspension systems face more challenge. It seems that passive systems reach their limitations and hardly satisfy all requirements in some circumstances even though nonlinear components (often air springs) are used.

Controlled suspensions to isolate body from disturbance were first conceived by Panzer[31] in 1960's, however, their application in vehicles did not appear until the

1970's when the cost of electronic components, especially '*Microchips*', became acceptable for non-military engineering. The definition of '*controlled suspension*' here is any suspension that has mechatronic components to control the suspension output, and usually, a controlled suspension unit consists of actuators, a measurement and sensor unit and a controller. Controlled suspensions are classified as active, semi-active, semi-passive and adaptive suspensions. Active suspension system can continuously supply and modulate the flow of energy while semi-active suspensions can only continually modulate the flow of energy. Semi-passive systems switch between passive and active states, this concept being used to minimise transient responses due to sudden changes. The forces generated in an adaptive system are modulated by a mechanical device and are independent of local variables, for example, the passive sequential hydraulic damper[32] and the vibrator-controlled adaptive damper[33]. Physically, adaptive systems are passive systems. Several control strategies (PID controller[34], LQR controller[35-36], LQG controller [37] and VSS controller[38]) have been applied to controlled suspensions. Preview control was first suggested by Bender[39] and was further developed by several researchers[40-41]. Neural network control[42] has also recently been used in controlled suspensions.

Of all controlled suspension systems, the active suspension form is the most powerful systems with regard to improving the dynamic behaviour of railway vehicles. Their potential advantages cited in[29] are derived from two basic features[30]. Active suspensions can continually supply and modulate the flow of energy and thus, forces can be generated which do not depend upon energy previously stored by the suspension and, an active system may generate forces that are functions of many variables, some of which may be remotely measured. The former feature of active suspension is not available in a semi-active system because there is no device that can store and release energy without any loss, while the latter can be achieved in semi-active suspensions only when the whole system is in dissipative state.

Some of the disadvantages of controlled suspensions are their complexity, difficult installation, maintenance costs and their robustness and reliability. The applications of controlled suspensions may depend on the balance between the economic factors and the requirements for vehicle dynamic performance.

A very fundamental feature of controlled suspensions is that the components of the (springs and dampers) suspension are the objects to be controlled. This is what

distinguishes between a controlled suspension and a reconfigurable mechanism that will be discussed in Chapter 7.

The applications and developments of controlled suspensions in road vehicles are not discussed in this thesis. The reader who is interested in this area is referred to [43]. Before the 1990's, the applications of controlled suspensions to railway vehicles were concentrated on developing active systems in secondary suspension [44-52] and tilting systems [53-58] to improve vehicle ride performance. Three papers [29-30, 46] have been published which review the developments of controlled suspensions in that period. Recently, Goodall [59] published another paper reviewing the recent development in active suspensions for railway vehicles. This section gives a brief review only.

In the 1970's, the feasibility of active suspension was studied widely and experimented in several countries. Very valuable work was carried out in the British Railway Technical Centre [49-51]. They theoretically and experimentally investigated various actuator configurations with regard to their cost, performance, reliability and maintenance, as shown in Table 1 [46].

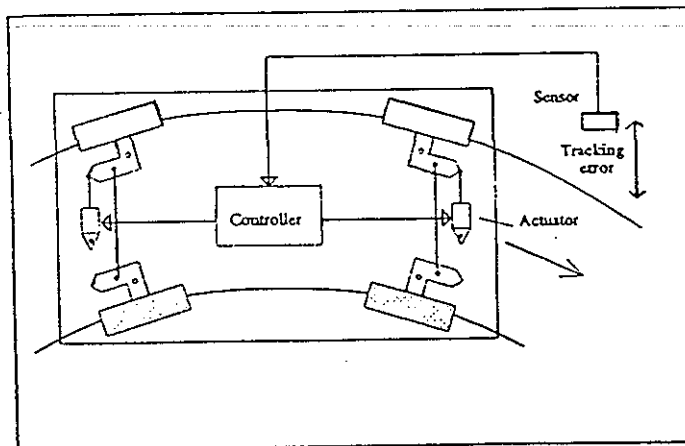


Figure 1.11 Actively-guided bogie [60]

In recent years, the strategies of controlled suspensions have been developed in applying controlled systems to improve vehicle curving performance. In 1992, Wickens and Goodall [60] proposed the strategy of the *actively-guided bogie*, as shown in Fig. 1.11, which is one kind of active-steering bogie vehicles. The principal feature of an *actively-guided bogie* is that wheelsets are steered in response to a control system. The deviation of the vehicle from a track reference line, or the relative yaw angles among the rigid bodies are used as feedback signals. The actively-guided system however, only needs to work when the vehicle negotiates a

curve. The concept seems as if a robot is planted into the wheelsets to steer them through curves, and the conflict between stability and curving is therefore well decoupled. The feasibility of practical implementation is discussed in[60]. Steering action, tracking error and control system accuracy, however, affect the dynamic performance. Further investigation in the area has been carried out at Loughborough University of Technology[61].

Suda[62] investigated the stability and curving of longitudinally asymmetric bogies with semi-active strategy. A new bogie was built up based on his research results. His research can be divided into two phases: firstly, he investigated the dynamic behaviour of asymmetric bogies having an independent trailing wheelset and, secondly, he developed a semi-active system. The bogie, as shown in Fig.1.12, is a very complex implementation. Firstly, the wheelset needs to be switched from a conventional wheelset into an independent wheelset when it is on the trailing position, whilst the wheelset is changed back to a conventional wheelset when it is on the leading position. Secondly, the dampers are switched on to provide a hard longitudinal stiffness for the trailing wheelset and a soft longitudinal stiffness for the leading wheelset. This control strategy is more like the reconfigurable mechanism (which will be defined and discussed in Chapter 7) because the bogie works like two different passive systems according to its moving direction.

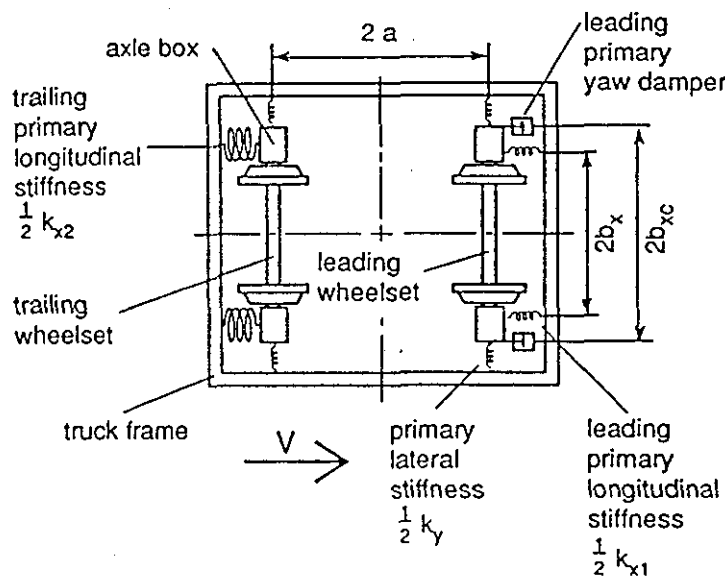


Figure 1.12 Suda's bogie[62]

Allen[63] reported the active bumpstop hold-off device developed by ABB Transportation Ltd UK and applied it to the BR MK III coach with BT10 bogie. The purpose of the device is to solve the conflict between ride quality and curving.

Soft suspensions lead a good ride quality in straight track, but cause a large lateral movement of the carbody on curves which results in the carbody contacting the lateral bumpstops at high speed. Only the primary suspension plays a role in isolating track disturbance when the carbody contacts the bumpstops, and the ride quality is therefore reduces. With the active bumpstop hold-off device, the most significant improvement in vehicle performance is that the ride quality can be much improved upon when the vehicle is subjected to large track irregularities at high cant deficiency. Allen also claimed that the device can be applied to most passenger vehicles, however, he did not give specific data related to the device.

Table 1 The active suspension systems of railway vehicles[46]

Load Carrying Element	Control Element	Advantages	Disadvantages
1. Airspring with pneumatic levelling valve (low rate integrator control)		Simple and well developed Ride independent of load	Passive response only Difficult to modify transfer function bulky
2. Airspring with pneumatic servo-valve (high rate integrator control)		Easily added to existing suspensions Relatively simple Tilt possible	Large air consumption (except for tilt alone) Suitable servo-valve not available
3. Airspring with displacement air pump		Can be added to existing suspension Low energy consumption Tilt possible	Moderately complicated Bulky for tilting
4. Airspring	Pneumatic actuator	Can be added to existing suspensions Tilt possible	Moderately high air consumption Moderately complicated
5. Electromagnet		High bandwidth Easy to control Mechanically simple & rugged	High power consumption Limited displacement (no tilt)
6. Mechanical Spring	Electromagnet	High bandwidth Easy to control Mechanically simple & rugged	Moderately high power consumption Limited displacement (no tilt)
7. Airspring	Electromagnet	High bandwidth, easy to control Mechanically simple & rugged Acceptable power consumption	Limited displacement (no tilt)
8. Servo-hydraulic jack		High bandwidth Easy to control. Tilt possible	Fairly expensive High maintenance Bulky power pack
9. Mechanical or airspring hydraulic jack	Servo-hydraulic	High bandwidth Easy to control Tilt possible	Fairly expensive High maintenance
10. Electro-mechanical actuator (electric motor & ball screw)		High bandwidth Easy to control Tilt possible	Mechanically bulky Moderately high maintenance
11. Mechanical or airspring	Electro-mechanical actuator	High bandwidth Easy to control Tilt possible	Moderately high maintenance

1.5 Research into Railway Vehicle Dynamics

It has been demonstrated that a railway bogie vehicle is a multi-body system with nonlinear factors (creepages, nonlinear components) and stochastic disturbances, and the elements in the suspensions can be passive, active, semi-active or a combination of them. Railway vehicles are, therefore, one of most complex systems in engineering. Even though it is impossible to analyse the dynamic behaviour of this system comprehensively and precisely without computer technology, some theoretical work explaining some physical phenomena had been done before the computer became the obvious answer. Carter[2] first set up a creepage model for the contact between wheel and rail, and also applied stability theorems to railway vehicle dynamics. Combined with his creepage theory, he theoretically identified the instability of a locomotive in the lateral plane[64]. In the 1950's, the newly formed Office Research and Experiments (ORE) of the International Union of Railways held a competition for the best analysis of the stability of a two-axle railway vehicle. The three prize winning papers (de Possel, Boutefoy and Matsudaira) in fact all gave linearized analyses. In his paper, Matsudaira first introduced into the mathematical model both longitudinal and lateral suspension flexibilities between wheelset and bogie frame and his results indicated their potential importance.

The most important part of railway vehicle dynamics is the wheelset dynamics. Wickens[5] fully investigated the dynamics of a single wheelset. A more accurate solution to the motion of a single wheelset was given by de Pater[65]. In order to study the contact problems between rails and wheels, Yang[66] made some contribution based on a nonlinear solution for wheelset motion.

The hunting instability is the major instability mode for railway bogie vehicles. In the 60's and 70's, a comprehensive investigation on the hunting instability of railway bogie vehicles was carried out by Matsudaira[67], British Railway[68-70] and Association of American Railroads[71-74] independently.

To simplify the complication, several models have been proposed to investigate the curving performance of railway vehicles[1]:

- i) Steady State[75-77] ---- Curving is assumed to continue indefinitely at a constant radius curve with constant speed where all components of a vehicle traverse perfect circular paths;

- ii) Quasi-Steady (kinematic)[78] ---- A general curve is negotiated, but, acceleration is ignored. The response of a vehicle is determined at discrete locations along the curved track by applying the kinematic constraints;
- iii) Dynamic State[79] ---- The complete equations of motion for the vehicle system are developed to account for arbitrary track curvature, speed and track input.

The first models are usually used to investigate the capability of a railway vehicle when negotiating curves while the last model is mainly applied to predict the dynamic responses when a vehicle moves on a curve.

The effects of track irregularities on the vehicle dynamic responses were theoretically and experimentally studied in the 70's[80-83]. The theory of railway vehicle dynamics has been summarised by Wickens and Gilchrist[84] and the dynamic equations have been documented by ORE[85]. Wickens has been studying the solution for the conflict between vehicle lateral stability and steering ability since the 70's[86-87]. Hedrick et al[88-89] extensively studied the performance limits of railway bogie vehicles.

"The objective of research in this field has been twofold: firstly, the development of sufficiently detailed and validated mathematical models that permit the simulation of actual motion on a specified stretch of track so that the performance of a specific design can be analysed, or a particular incident recreated (thus, by simulation the overall performance of a vehicle can be checked) and, secondly, analytical studies in which the description of the mechanism of various phenomena by the simplest model possible can be used to explore new suspension and vehicle design concepts and to develop a basis for understanding and physical insight. Ideally, though this is still largely in the future, the subject of vehicle dynamics should not only deal with analysis but also methods of synthesis in which the various possibilities for design are exposed." by Wickens[8]

Computer simulation has been playing an important role in the research of rail vehicle dynamics since the 1970's. The purpose of computer simulation is twofold: firstly, to explore the mechanism of various physical phenomena relating to new vehicle configuration and, secondly, to predict or analyse the dynamic behaviour of a specific vehicle in a specific environment. The former is best suited to a simple model in order to reveal fundamental physical features, whereas the latter considers

detail that results in very complex computer models. Various software packages investigating the dynamic behaviour of railway vehicles have been developed since the 70's, for example, VAMPIRE[90] and MEDYNA[91]. VAMPIRE is one of the most successful computer software packages in railway vehicle dynamics, and has been developed by British Railway Research since the 1960's. Garg and Dukkipati[1] published a book that systematically introduced the dynamics of railway vehicles in 1984. Dukkipati[92] later published another book summarising the techniques and the considerations in computer simulation. The application of software packages is often restricted by their complex and cost.

1.6 The Objectives of This Research

It has been shown that the railway vehicle system is very complex. It is impossible to simulate the system completely and precisely even with the most complex computer simulation models. Simplifications are necessary and mainly depend on the research objectives.

The objectives of this research project can be divided into parts:

1. to investigate further the dynamic behaviour of perfect steering bogie vehicles and to explore their advantages as well as to expose their weaknesses and;
2. to study the improvement of the dynamic performance of perfect steering bogie vehicles by applying the reconfigurable mechanism.

Several configurations of perfect steering bogie vehicles will be investigated. The research interests here are to expose various phenomena in the dynamic behaviour of these perfect steering bogie vehicles and to reveal the physical mechanism behind the phenomena. The results will have general and important significance to guide railway vehicle engineers in their practice. Without doubt, perfect steering bogies have their disadvantages, and several strategies can be employed to overcome, or at least to improve, these weaknesses. One of the strategies is the reconfigurable mechanism which will be presented in the thesis. Its feasibility and advantages will also be discussed and the improvement in the dynamic behaviour of perfect steering vehicles by applying reconfigurable mechanism will be presented.

To simplify the system complexity, several assumptions with the coincidence of the research objectives are made in the simulation models: firstly, it is assumed that all mass components are rigid bodies and, secondly, all springs and dampers are considered as massless and linear and, thirdly, the effects of flange contact are not taken into account and, finally, Kalker's linear creepage theory is used for calculating creepage forces. The whole vehicle system is therefore linearised, and the advantages of linear models are that the system complexity can be simplified so that the physical phenomena in the dynamic performance of perfect steering vehicles can be revealed. It can also be used to evaluate the dynamic behaviour of systems.

Chapter 2 will deal with the fundamental equations of railway vehicle dynamics. The dynamic behaviour of perfect steering bogie vehicles will be discussed in Chapter 3 (steering ability), Chapter 4 (stability) and Chapter 5 (ride performance). Chapter 6 will summarise the advantages and disadvantages of perfect steering bogie vehicles. The features and feasibility of the reconfigurable mechanism will be presented in Chapter 7, and the improvements in the dynamic behaviour will also be included in this chapter when the reconfigurable mechanism is applied to the perfect steering bogie vehicles. The last chapter will conclude the achievements and findings, and will illustrate the applications of the research results.

Chapter 2

DYNAMIC EQUATIONS

This chapter will deal with the essential dynamic equations of railway vehicles. Some of the processes used to derive the equations are excluded because they are well documented in several references[1,5,84-85], however, it should be noted that every equation presented in this chapter has been deduced by the author independently.

2.1 Coordinate Systems And Accelerations

Three basic coordinate systems are used to defined the motions of a rigid body in railway vehicle dynamics, and all three coordinate systems will move with the vehicle. The coordinate system $(oxyz)_r$ is the reference while the system $(oxyz)_o$ is the local coordinate system and is on the track nominal centre but takes the radial direction of a rigid body, and the reference $(oxyz)_r$ is equal to the local $(oxyz)_o$ if only one mass moves along a track. These two systems are illustrated in Fig.2.1. The other coordinate system is the inertia axes of the rigid body, which is not illustrated in Fig.2.1. In this thesis, the reference $(oxyz)_r$ is chosen to be at the centre of gravity of carbody in its radial position. The transform relation between two coordinate systems is defined by Eq.(2-1) if $\mathbf{R} = 0$ and θ, ϕ and ψ are small.

$$\begin{pmatrix} \vec{i} \\ \vec{j} \\ \vec{k} \end{pmatrix}_{(oxyz)_r} = \begin{pmatrix} 1 & -\psi & -\theta \\ \psi & 1 & -\phi \\ \theta & \phi & 1 \end{pmatrix} \begin{pmatrix} \vec{i} \\ \vec{j} \\ \vec{k} \end{pmatrix}_{(oxyz)_o} \quad \begin{pmatrix} \vec{i} \\ \vec{j} \\ \vec{k} \end{pmatrix}_{(oxyz)_o} = \begin{pmatrix} 1 & \psi & \theta \\ -\psi & 1 & \phi \\ -\theta & -\phi & 1 \end{pmatrix} \begin{pmatrix} \vec{i} \\ \vec{j} \\ \vec{k} \end{pmatrix}_{(oxyz)_r} \quad (2-1)$$

The inertial acceleration of a rigid body is defined by the expression:

$$\bar{a}_{xyz} = \bar{a}_r + \dot{\Theta} \times \bar{R}_w + \bar{\Theta} \times (\bar{\Theta} \times \bar{R}_w) + 2\bar{\Theta} \times \dot{\bar{R}}_w + \ddot{\bar{R}}_w \quad (2-2)$$

where, Θ is the angular velocity of the reference coordinate $(oxyz)_r$.

The angular accelerations of a mass can be found by applying the Euler Equation[93]:

$$\begin{aligned}
 I_x \dot{\omega}_x - I_y \Omega_z \omega_y + I_z \Omega_y \omega_z &= \sum M_x \\
 I_y \dot{\omega}_y - I_z \Omega_x \omega_z + I_x \Omega_z \omega_x &= \sum M_y \\
 I_z \dot{\omega}_z - I_x \Omega_y \omega_x + I_y \Omega_x \omega_y &= \sum M_z
 \end{aligned}
 \tag{2-3}$$

where, Ω is the angular velocity of the weight centre of a rigid body and, ω is the angular velocity of the rigid body.

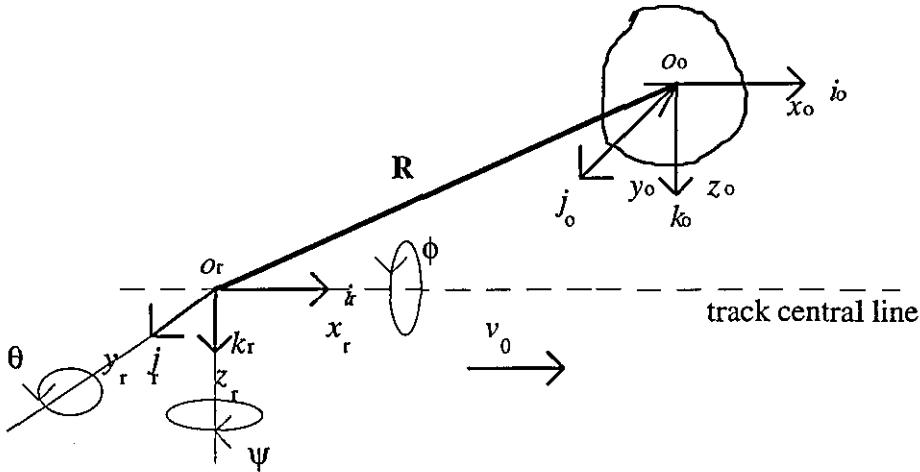


Figure. 2.1 Coordinate Systems

For a wheelset moving along a straight railway line, $(oxyz)_r = (oxyz)_o$, they can be considered as the absolute reference if its forward speed v_0 is a constant. If the coordinate system $(oxyz)_w$ represents the inertia axes of the wheelset, the terms in Eq.(2-2) and Eq.(2-3) for the wheelset become:

$$\begin{aligned}
 \bar{a}_r &= 0 \\
 \bar{R}_w &= x\bar{i}_r + y\bar{j}_r + z\bar{k}_r \\
 \bar{\Theta} &= 0 \\
 \bar{\Omega} &= \dot{\phi}_w \bar{i}_w + \dot{\psi}_w \bar{k}_w \\
 \bar{\omega} &= \dot{\phi}_w \bar{i}_w - \frac{v_0}{r_0} \bar{j}_w + \dot{\psi}_w \bar{k}_w
 \end{aligned}
 \tag{2-4}$$

For a wheelset moving along a curve, $(oxyz)_r = (oxyz)_o$, they possess the angular velocity v_0/R and the centripetal acceleration v_0^2/R even when $v_0 = \text{constant}$. If the coordinate system $(oxyz)_w$ still represents the inertia axes of the wheelset, the terms in Eq.(2-2) and Eq.(2-3) for the wheelset are:

$$\begin{aligned}
 \bar{a}_r &= R \frac{d}{dt} \left(\frac{v_0}{R} \right) \bar{i}_r + \left(\frac{v_0^2}{R} + r_0 \ddot{\phi}_r \right) \bar{j}_r - a_0 \ddot{\phi}_r \bar{k}_r \\
 \bar{R}_w &= x \bar{i}_r + y \bar{j}_r + (z - a \phi_w) \bar{k}_r \\
 \bar{\Theta} &= \dot{\phi}_r \bar{i}_r + \frac{v_0}{R} \bar{k}_r \\
 \bar{\Omega} &= (\dot{\phi}_r \bar{i}_r + \dot{\phi}_w \bar{i}_w) + \left(\frac{v_0}{R} \bar{k}_r + \dot{\psi}_w \bar{k}_w \right) \\
 &= (\dot{\phi}_r + \dot{\phi}_w + \frac{v_0}{R} \theta_r) \bar{i}_w + \frac{v_0}{R} \psi_r \bar{j}_w + \left(\frac{v_0}{R} + \dot{\psi}_w \right) \bar{k}_w \\
 \bar{\omega} &= (\dot{\phi}_r \bar{i}_r + \dot{\phi}_w \bar{i}_w) - \frac{v_0}{r_0} \bar{j}_w + \left(\frac{v_0}{R} \bar{k}_r + \dot{\psi}_w \bar{k}_w \right) \\
 &= (\dot{\phi}_r + \dot{\phi}_w + \frac{v_0}{R} \theta_r) \bar{i}_w + \left(\frac{v_0}{R} \psi_r - \frac{v_0}{r_0} \right) \bar{j}_w + \left(\frac{v_0}{R} + \dot{\psi}_w \right) \bar{k}_w
 \end{aligned} \tag{2-5a}$$

Since $\theta_r = \psi_r = 0$, we have

$$\begin{aligned}
 \bar{\Omega} &= (\dot{\phi}_r + \dot{\phi}_w) \bar{i}_w + \left(\frac{v_0}{R} + \dot{\psi}_w \right) \bar{k}_w \\
 \bar{\omega} &= (\dot{\phi}_r + \dot{\phi}_w) \bar{i}_w - \frac{v_0}{r_0} \bar{j}_w + \left(\frac{v_0}{R} + \dot{\psi}_w \right) \bar{k}_w
 \end{aligned} \tag{2-5b}$$

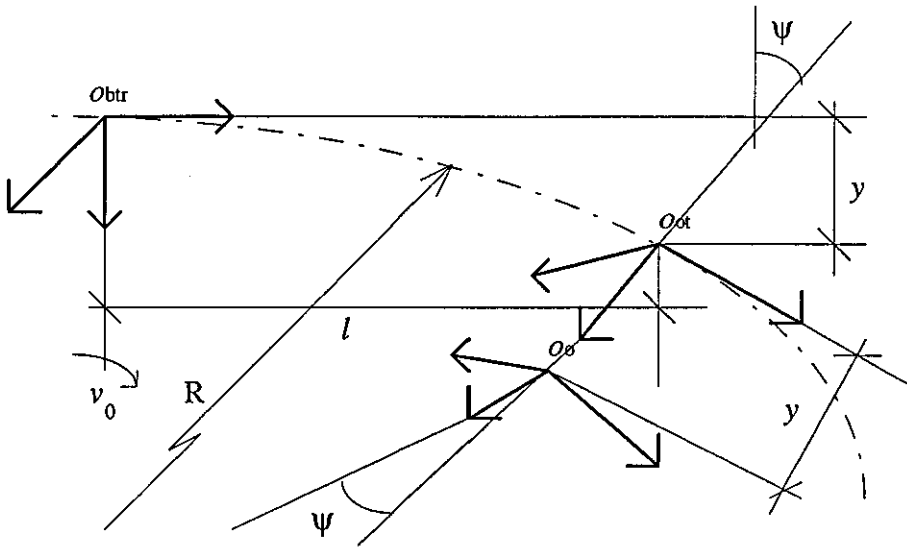


Figure 2.2 curve coordinate

When a railway vehicle is on a straight line, the radial directions of all rigid bodies are identical, and only difference between the two local coordinate systems is in x direction and is a constant, and therefore any of local coordinate systems can be considered as the reference $(oxyz)_r$, which is the absolute reference if the vehicle forward speed v_0 is a constant. When a vehicle is on a curve, there is a relative yaw angle between the radial positions of two rigid bodies since the track central line changes its direction on the curve, which results in a yaw angle and a lateral shift between the two local coordinate systems, i.e. $(oxyz)_r \neq (oxyz)_o$, as shown in

Fig.2.2. \bar{q} is defined as the general displacement of a local $(oxyz)_o$ in the reference $(oxyz)_r$ and the general relative displacement between two \bar{q} 's is defined as Δq , i.e. $\Delta q = \bar{q}_i - \bar{q}_j$, while \hat{q} is defined as the general displacement of the inertia axes of a rigid body in its local $(oxyz)_o$ and the general relative displacement between two \hat{q} 's is defined by δq , i.e. $\delta q = \hat{q}_i - \hat{q}_j$.

2.2 Track Definitions

A transition curve that is an example of a spiral in mathematical terms is used to connect a straight line and a uniform curve. Several spirals can be used for the purpose, and one example is the Clothoid spiral. A cubic parabola is used as a close approximation to the Clothoid spiral in BR[94] because of the difficulties in measuring and re-setting Clothoid spiral. In the thesis, a cubic parabola, as shown in Fig.2.3, is used as the transition curve and is defined by:

$$y = -\frac{y_L}{L^3} x^3 \quad (2-6)$$

The length of the cubic parabola is calculated by[94]:

$$L = \frac{V_{\max}^3}{33.5R} \quad (2-7)$$

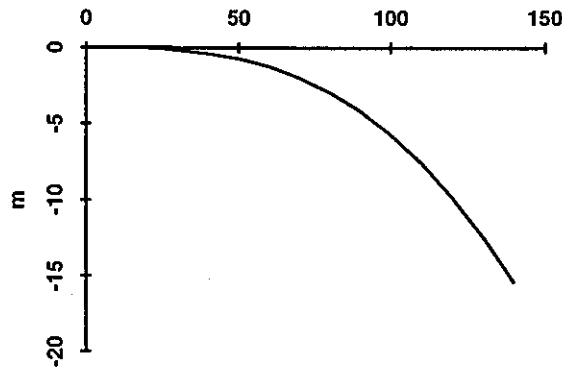


Figure 2.3 cubic parabola transition and circle.

We have $L = 100\text{m}$ and $y_L = 5.7\text{m}$ when $V_{\max} = 100\text{ km/h}$ and $R = 305\text{m}$. The tangent angle of the cubic parabola is the radial position of the rigid bodies and is the negative derivative of Eq.(2-6), i.e.

$$\psi_r = -\frac{dy}{dx} = \frac{3y_L}{L^3} x^2 \quad (2-8)$$

The curvature of the cubic parabola is defined by:

$$\frac{1}{R} = \frac{6y_L}{L^3} \frac{x}{(1+9y_L^2 x^4/L^6)^{3/2}} \quad (2-9)$$

2.3 Dynamic Equations Of Unconstrained Wheelset[5,65-66]

The diagram in Fig.2.4 shows the forces acting on an unconstrained wheelset when it moves on a curve. Applying the Newton's second law and the Euler Equation, the dynamic equations of the wheelset are:

$$m_w a_y = F_{yL} + F_{yR} \quad \text{and} \quad I_{wz} \dot{\omega}_z - I_{wx} \Omega_y \omega_x + I_{wy} \Omega_x \omega_y = \sum M_z \quad (2-10)$$

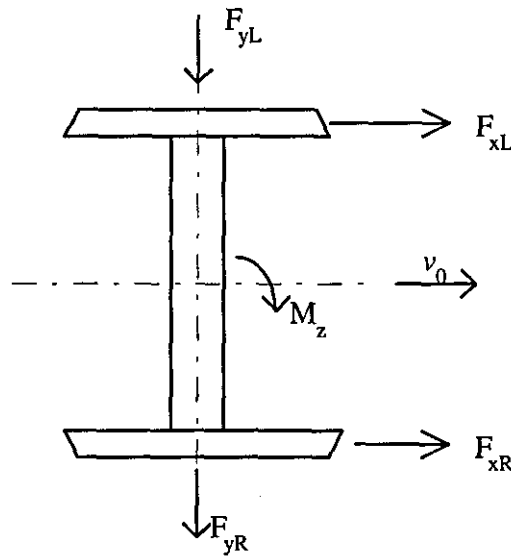


Figure 2.4 The force diagram of a wheelset

Applying Eq.(2-5) to Eq.(2-2) and Eq.(2-3), we have:

$$a_y = \ddot{y}_w + \frac{v_0^2}{R} + r_0 \ddot{\phi}_r$$

and

$$I_{wz} \dot{\omega}_z - I_{wx} \Omega_y \omega_x + I_{wy} \Omega_x \omega_y = I_{wz} \left[\frac{d}{dt} \left(\frac{v_0}{R} \right) + \ddot{\psi}_w \right] - I_{wy} \frac{v_0}{r_0} (\dot{\phi}_r + \dot{\phi}_w) \quad (2-11)$$

if neglecting the small high order components. Since $\phi_w = -\sigma y / a_0$ where $\sigma \ll 1$, the above equation can be simplified as follows:

$$I_{wz}\dot{\omega}_z - I_{wx}\Omega_y\omega_x + I_{wy}\Omega_x\omega_y = I_{wz}\left[\frac{d}{dt}\left(\frac{v_0}{R}\right) + \ddot{\psi}_w\right] - I_{wy}\frac{v_0}{r_0}\dot{\phi}_r$$

For an unconstrained wheelset, the forces acting in the horizontal plane are due to creepages. Referring to Eqs.(2-1)--(2-5), the creepage forces without considering track irregularities are obtained from:

$$\begin{aligned} F_{yL} + F_{yR} &= -\left(\frac{2f_{22}}{v_0}\dot{y}_w - 2f_{22}\psi_w\right) \\ \sum M_z &= -\left(\frac{2a_0^2 f_{11}}{v_0}\dot{\psi}_w + \frac{2a_0 f_{11}\lambda}{r_0}y_w + \frac{2a_0^2 f_{11}}{R}\right) \end{aligned} \quad (2-12a)$$

if Kalker's linear theory Eq.(1-5) is applied. If there are alignment and cross-level irregularities on track, the creepage forces for a straight line can be found as:

$$\begin{aligned} F_{yL} + F_{yR} &= -\left(\frac{2f_{22}}{v_0}\dot{y}_w - 2f_{22}\psi_w\right) \\ \sum M_z &= -\left(\frac{2a_0^2 f_{11}}{v_0}\dot{\psi}_w + \frac{2a_0 f_{11}\lambda}{r_0}y_w - \frac{2a_0 f_{11}\lambda}{r_0}y_a - 2a_0 f_{11}\lambda\frac{z_c}{2a_0}\right) \end{aligned} \quad (2-12b)$$

since $r_R - r_L = 2\lambda(y_w - y_a - r_0\phi_r)$ from Eq.(1-1).

Thus, the dynamic equations of an unconstrained wheelset can be simplified as:

$$\begin{aligned} m_w\ddot{y}_w + \frac{2f_{22}}{v_0}\dot{y}_w - 2f_{22}\psi_w &= -W_w\phi_d - mr_0\ddot{\phi}_r \\ I_{wz}\ddot{\psi}_w + \frac{2a_0^2 f_{11}}{v_0}\dot{\psi}_w + \frac{2a_0 f_{11}\lambda_e}{r_0}y_w &= -\frac{2a_0^2 f_{11}}{R} + \frac{v_0}{R^2}\dot{R}I_{wz} + \frac{v_0}{r_0}I_{wy}\dot{\phi}_r \end{aligned} \quad (2-13a)$$

if the track irregularities are not taken into account. For straight track without track irregularities, they become:

$$\begin{aligned} m_w\ddot{y}_w + \frac{2f_{22}}{v_0}\dot{y}_w - 2f_{22}\psi_w &= 0 \\ I_{wz}\ddot{\psi}_w + \frac{2a_0^2 f_{11}}{v_0}\dot{\psi}_w + \frac{2a_0 f_{11}\lambda_e}{r_0}y_w &= 0 \end{aligned} \quad (2-13b)$$

For straight lines with the track alignment and cross-level irregularities, they become:

$$m_w \ddot{y}_w + \frac{2f_{22}}{v_0} \dot{y}_w - 2f_{22} \Psi_w = 0$$

$$I_{wz} \ddot{\Psi}_w + \frac{2a_0^2 f_{11}}{v_0} \dot{\Psi}_w + \frac{2a_0 f_{11} \lambda_e}{r_0} y_w = \frac{2a_0 f_{11} \lambda_e}{r_0} y_a + 2a_0 f_{11} \lambda_e \frac{z_c}{2a_0} \quad (2-13c)$$

For the steady state, Eq.(2-13a) becomes:

$$2f_{22} \Psi_w = W_w \phi_d \quad \frac{2a_0 f_{11} \lambda_e}{r_0} y_w = - \frac{2a_0^2 f_{11}}{R} \quad (2-14)$$

Since $\frac{dq}{dt} = \frac{dq}{dx} \frac{dx}{dt} = v_0 \frac{dq}{dx} = v_0 q'$, Eq.(2-13a) becomes:

$$\frac{2f_{22}}{v_0} y_w' - 2f_{22} \Psi_w = -W_w \phi_d$$

$$\frac{2a_0^2 f_{11}}{v_0} \Psi_w' + \frac{2a_0 f_{11} \lambda_e}{r_0} y_w = - \frac{2a_0^2 f_{11}}{R} \quad (2-15)$$

when $v_0 = 0$. This state is called the kinematic state.

In steady state, the lateral displacement of an unconstrained wheelset can be obtained from Eq.(2-14), which is:

$$y = - \frac{a_0 r_0}{\lambda_e R} \quad (2-16)$$

This is the distance between the track central line and the wheelset pure rolling line, and is inversely proportional to both the wheelset equivalent conicity and the curve radius. If the limitation y of flange contact is 5mm, 7mm or 10mm respectively, the minimum radii R_{\min} to let an unconstrained wheelset move on its pure rolling line are listed Table 2-1 versus wheelset conicities. The yaw angle of wheelset related to its radial position is called the attack angle, which will be zero when the wheelset rolls on the pure rolling line if the cant deficiency is zero, as shown in Eq.(2-14).

Table 2-1 Minimum radius (m) to possess the pure rolling line

λ	.025	.05	.075	.1	.125	.15	.2	.3
R_{\min} when $y = 5$ mm	2592	1296	864	648	518	432	324	216
R_{\min} when $y = 7$ mm	1851	926	617	463	370	309	231	154
R_{\min} when $y = 10$ mm	1296	648	432	324	259	216	162	108

2.4 Dynamic Equations of a Railway Bogie Vehicle

Applying the assumptions listed in section 1.6, the dynamic equations of a railway vehicle with n degrees of freedom, m stiffnesses and m viscous dampings can be found as:

$$\mathbf{M}\ddot{\mathbf{q}} + (\mathbf{G} + \mathbf{C})\dot{\mathbf{q}} + (\mathbf{N} + \mathbf{E})\mathbf{q} = \mathbf{Q} \quad (2-17)$$

where, \mathbf{M} is the inertial matrix and is diagonal,

\mathbf{G} is the creepage damping matrix,

\mathbf{N} is the creepage stiffness matrix,

\mathbf{C} is the viscous damping matrix of the vehicle dampers,

\mathbf{E} is the system elastic matrix,

\mathbf{Q} is the force vector.

\mathbf{G} and \mathbf{N} can be found easily based on the dynamic equations Eq.(2-13) of an unconstrained wheelset. Applying the compatibility matrix method suggested by Wickens[27], the elastic matrix \mathbf{E} and the viscous damping matrix \mathbf{C} can be expressed as:

$$\mathbf{E} = \mathbf{a}^T[\mathbf{k}]\mathbf{a} \quad \mathbf{C} = \mathbf{a}^T[\mathbf{c}]\mathbf{a} \quad (2-18)$$

where, \mathbf{a} is called the $m \times n$ compatibility matrix, in which the column represents the deformations of each spring k_{ij} caused by an unit displacement of q_i (i.e. deformation vector $\delta = \mathbf{a}\mathbf{q}$); $[\mathbf{k}]$ and $[\mathbf{c}]$ are $m \times m$ diagonal matrixes and k_{ij} (or c_{ij}) is the stiffness (or the damping) corresponding to the strains (or the strain rates) represented by the i 'th row of \mathbf{a} .

Without considering track irregularities, the dynamic equation Eq.(2-18) becomes:

$$\text{For steady state:} \quad (\mathbf{N} + \mathbf{E})\mathbf{q} = \mathbf{F}_{\text{cant}} + \mathbf{F}_{\text{creep}} + \mathbf{F}_{\text{E}} \quad (2-19)$$

For kinematic state:
$$\mathbf{G}\mathbf{q}' + (\mathbf{N} + \mathbf{E})\mathbf{q} = \mathbf{F}_{\text{cant}} + \mathbf{F}_{\text{creep}} + \mathbf{F}_E \quad (2-20)$$

where, \mathbf{F}_{cant} is the force vector caused by cant deficiency,

$\mathbf{F}_{\text{creep}}$ is the extra creepage force vector due to curve,

\mathbf{F}_E is the extra elastic force vector in the suspensions due to curve.

\mathbf{F}_{cant} and $\mathbf{F}_{\text{creep}}$ can also be found from the dynamic equations Eq.(2-13) of an unconstrained wheelset. Since $\{\bar{q}_i\}$ represents the vector of the displacements between the local coordinates and the reference, and referring to Fig.2.5, the force produced by stiffness k_i due to $\{\bar{q}_i\}$ is:

$$\mathbf{F}_{Ei} = -\mathbf{a}^T [k_i] \mathbf{a} \{\bar{q}_i\} \quad (2-21)$$

It can be proved that:

$$\mathbf{a}^T [k_i] \mathbf{a} = k_i \{a_{in}\}^T \{a_{in}\} \quad (2-22)$$

if $[k_i]$ is diagonal, and thus the elastic forces in the system caused by curvature are:

$$\mathbf{F}_E = -\sum_{i=1}^m k_i \{a_{in}\}^T \{a_{in}\} \{\bar{q}_i\} \quad (2-23)$$

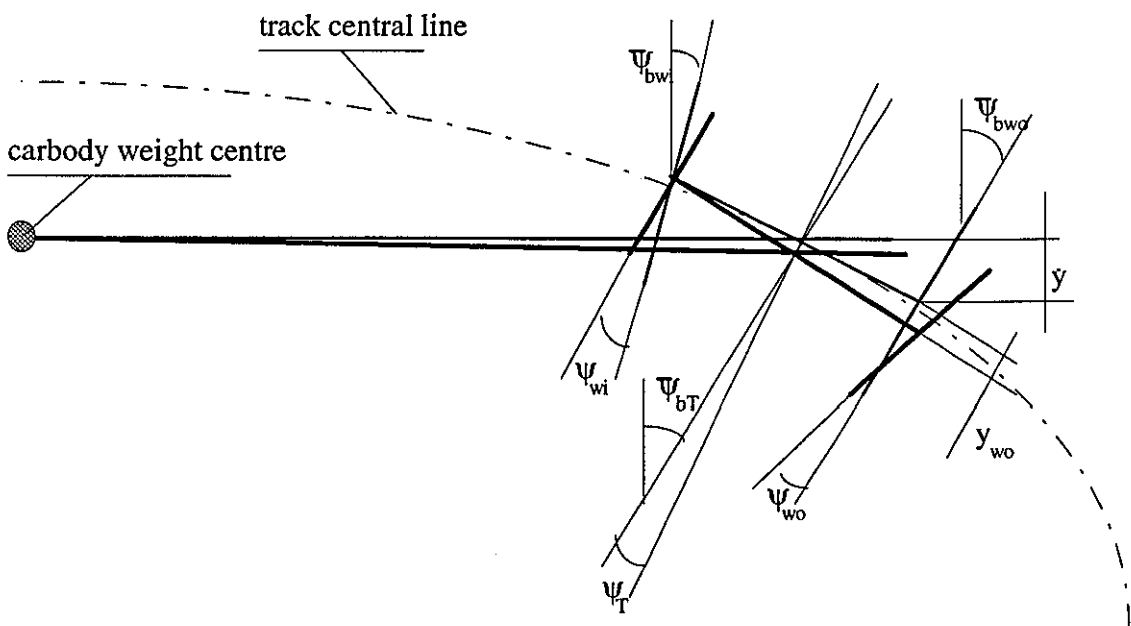


Figure 2.5 Geometric layout of vehicle rigid bodies on curves

Eq.(2-19) is a linear equation and can be solved easily while Eq.(2-20) is a differential equation and will be solved with numerical integration techniques. Since two important factors, those being curvature and system elasticity, are both included in Eq.(2-20), the solutions of the equations can explore the relationship between the suspension elasticity and curvature, and the results can therefore be used to evaluate the effects of the system elasticity on the vehicle's capability of negotiating curves when curvature varies.

Since only the elements, which are associated with wheelset displacements in the vector $\{q'\}$, exist in Eq.(2-20), this equation is split into two sub-equations:

$$\begin{aligned} \mathbf{G}\{q'\}_{[1:2j]} + (\mathbf{N} + \mathbf{E})_{[1:2j, 1:n]}\{q\}_{[1:n]} &= (\mathbf{F}_{\text{cant}} + \mathbf{F}_{\text{creep}} + \mathbf{F}_{\text{E}})_{[1:2j]} \\ (\mathbf{N} + \mathbf{E})_{[2j+1:n, 1:n]}\{q\}_{[1:n]} &= (\mathbf{F}_{\text{cant}} + \mathbf{F}_{\text{creep}} + \mathbf{F}_{\text{E}})_{[2j+1:n]} \end{aligned} \quad (2-24)$$

where, j is the number of wheelsets.

2.5 Perfect Steering Conditions

Perfect steering occurs when a curve can be negotiated without creep. All wheelsets must take up a radial position and move outwards to the pure rolling line, which without any elastic restraint would generate creep forces. It follows that there must be a further degeneracy in the elastic stiffness matrix corresponding to this bending mode. Wickens[27] proved that the necessary condition for a railway vehicle to possess the capability of perfect steering with non-zero critical speed is:

$$3 \leq P \leq j \quad (2-25)$$

where, P is the degeneracy of the elastic matrix \mathbf{E} and j is the number of wheelsets. The first ' \leq ' in Eq.(2-25) is the necessary condition for a railway bogie vehicle capable of perfect steering. The physical explanation for this is that firstly, the whole vehicle can move laterally and can yaw as one rigid body without causing any elastic deformation, (the degeneracy of the matrix \mathbf{E} must be at least two) and secondly, perfect steering results in no elastic deformation in the vehicle and produces another degeneracy, and thus the necessary condition for a railway bogie vehicle capable of perfect steering is that the degeneracy of the elastic matrix \mathbf{E} must be at least equal to or bigger than 3. The second ' \leq ' in Eq.(2-25) is the necessary condition for a railway bogie vehicle to be stable. The reason for this is

that the kinematic equation Eq.(2-20) has a solution if $P > j$, which means that undamped kinematic oscillation modes occur in the system.

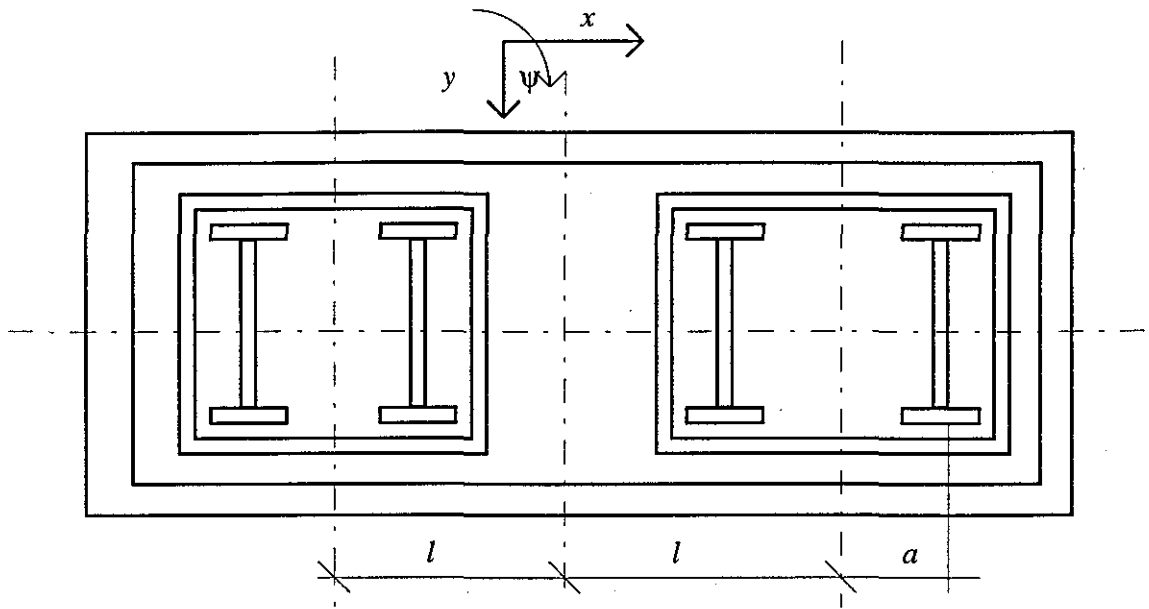
If $\phi_d = 0$, Eq.(2-19) becomes $(N + E) \mathbf{q} = \mathbf{F}_{creep} + \mathbf{F}_E$, and the equation becomes $(N + E) \mathbf{q} = \mathbf{F}_{creep}$ if $\mathbf{F}_E = 0$. If each wheelset moves on its own pure rolling line, $(N + E) \mathbf{q}_{pure} = 0$ and $\mathbf{q}_{pure} = 0$ are obtained, and perfect steering is realised. The sufficient condition for a railway vehicle capable of perfect steering is therefore that the elastic force vector \mathbf{F}_E caused by curvature must be zero, i.e.

$$\mathbf{F}_E = 0 \quad (2-26)$$

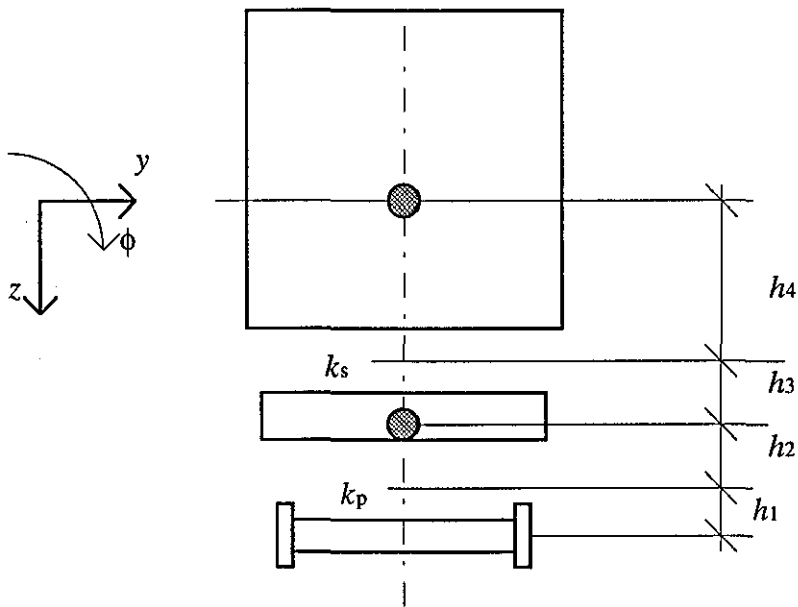
The sufficient condition Eq.(2-26) for bogie vehicles capable of perfect steering means that all bending stiffnesses in the vehicle must be eliminated. This is easily explained by referring to Fig.2.5. All rigid bodies of the vehicle should take their own radial positions when perfect steering is required. The relative yaw angles ($\Delta\psi$) among the rigid bodies are not equal to zero when the vehicle is on a uniform curve even with zero cant deficiency. If there is a yaw stiffness between any pair of rigid bodies, the moment produced due to the relative yaw angles ($\Delta\psi$) will force this pair of rigid bodies to move away from their radial position and perfect steering no longer exists. For example, if the secondary bending stiffness exists, the moment between the leading bogie frame and the carbody will resist the leading bogie frame in taking up its radial position. The leading bogie frame thus has an anticlockwise yaw related to its radial position. This yaw will be transferred to the wheelsets through the primary lateral stiffness and force the wheelsets to leave their pure rolling line, and a similar analysis can be applied to the trailing bogie. Perfect steering cannot, therefore, be achieved if any bending stiffnesses exists in the vehicle.

2.6 Displacement Vector

The essential configuration of the bogie vehicle models that are investigated in this thesis is schematically illustrated in Fig.2.6. As shown there are two bogies each with two wheelsets, each wheelset having two degrees of freedom (lateral and yaw), each bogie frame and carbody having three degrees of freedom (lateral, yaw and roll). There are a total of seventeen degrees of freedom in the system.



(a) x-y plane view



(b) y-z plane view

Figure 2.6 Schematic diagram of a bogie vehicle

The general displacement vector \mathbf{q} is arranged as:

$$\mathbf{q}^T = \{ y_{w1} \ \psi_{w1} \ y_{w2} \ \psi_{w2} \ y_{w3} \ \psi_{w3} \ y_{w4} \ \psi_{w4} \mid y_{TL} \ \psi_{TL} \ \phi_{TL} \ y_{TR} \ \psi_{TR} \ \phi_{TR} \mid y_b \ \psi_b \ \phi_b \} \quad (2-27)$$

The inertia parameters and some of the geometric parameters which have been used in the simulation are listed in Table 2.2.

2.7 Ride Performance

Two approaches can be applied to evaluate the ride performance of vehicles, one of which being to simulate the system response in the time domain, and another to find the response in the frequency domain. The former is often applied to study the transient response of the system while the latter is employed to estimate the overall response. In this chapter, only the latter is of concern. The theories used to analyse the frequency response of linear systems are well developed. The chapter only gives out the necessary definitions and their equations, and the reader is advised to view references[95-99] for more details.

2.7.1 Power Spectral Density (PSD) and Root Mean Square (rms)

If $y(t)$ is one of the responses of a linear system and $x(t)$ is one of the system inputs, the power spectral density **PSD** of $y(t)$ is defined by:

$$s_y(\omega) = H(\omega)s_x(\omega)H^*(\omega) \quad (2-28)$$

where, $s_x(\omega)$ is **PSD** of $x(t)$,

$H(\omega)$ is the transfer function of $x(t)$ to $y(t)$,

$H^*(\omega)$ is the conjugate of $H(\omega)$.

If $\{y(t)\}$ represents the response vector of a linear system and $\{x(t)\}$ is the system input vector, the power spectral density **PSD** of $\{y(t)\}$ is given by:

$$S_y(\omega) = H(\omega)S_x(\omega)(H^*(\omega)) \quad (2-29)$$

where, $S_x(\omega)$ is the **PSD** of the system input vector $\{x(t)\}$,

$H(\omega)$ is the system transfer function,

$H^*(\omega)$ is the conjugate of $H(\omega)$.

The power spectral density **PSD** has the following properties:

Property 1: if $\dot{x} = dx/dt$ and $\ddot{x} = d^2x/dt^2$, **PSD**'s of \dot{x} and \ddot{x} are:

$$S_{\dot{x}}(\omega) = \omega^2 S_x(\omega) \quad \text{and} \quad S_{\ddot{x}}(\omega) = \omega^4 S_x(\omega) \quad (2-30)$$

Property 2: if $\omega = 2\pi f$, the single side **PSD** is:

$$W(f) = 4\pi S_x(\omega = 2\pi f) \quad (2-31)$$

Property 3: if $E[x^2]$ represents the Mean Square of $x(t)$, it is found from:

$$E[x^2] = \int_{-\infty}^{\infty} s_x(\omega) d\omega = \int_0^{\infty} W(f) df \quad (2-32)$$

Property 4: the cross-power spectral density satisfies:

$$S_{x_i x_j}(\omega) = S_{x_j x_i}^*(\omega) \quad (2-33)$$

Property 5: the cross-power spectral density between $x(t)$ and $x(t-t_k)$ satisfies:

$$S_{x(t)x(t-t_k)}(\omega) = S_x(\omega) e^{-i\omega t_k} \quad (2-34)$$

2.7.2 PSD of Track Irregularities

Track irregularities are random processes depending on track situations such as the track maintenance, sleepers and rails. The parameters of the American Track Standard[1] are used to define the power spectral density of track irregularities in the simulation. They are defined by:

$$\text{Cross-level} \quad S_c(\phi) = \frac{A_c \phi_{2c}^2}{(\phi^2 + \phi_{1c}^2)(\phi + \phi_{2c}^2)} \quad (2-35)$$

$$\text{Alignment} \quad S_a(\phi) = \frac{A_a \phi_{2a}^2 (\phi^2 + \phi_{1a}^2)}{\phi^4 (\phi^2 + \phi_{2a}^2)} \quad (2-36)$$

where, ϕ is space frequency ($\phi = f/v_0$), and v_0 is the vehicle forward speed and f is time frequency (Hz). In the simulation, the values in Table 2.3 are used.

Table 2.3 Values of the parameters in Eq.(2-35) and Eq.(2-36)

A_c	$0.3 \times 10^{-4} \text{ in}^2/\text{cpf}$		A_a	$0.3 \times 10^{-4} \text{ in}^2/\text{cpf}$
ϕ_{1c}	$7.1 \times 10^{-3} \text{ cpf}$		ϕ_{1a}	$10.0 \times 10^{-3} \text{ cpf}$
ϕ_{2c}	$4.0 \times 10^{-2} \text{ cpf}$		ϕ_{2a}	$5.6 \times 10^{-2} \text{ cpf}$

For time frequency f , Eq.(5-8) and Eq.(5-9) become:

$$\text{Cross-level} \quad S_c(f) = \frac{1}{v_0} S_c\left(\frac{f}{v_0}\right) \quad (2-37)$$

$$\text{Alignment} \quad S_a(f) = \frac{1}{v_0} S_a\left(\frac{f}{v_0}\right) \quad (2-38)$$

If there is no correlation between *Cross-level* and *Alignment* irregularities and the vehicle has four wheelsets, the PSD's of track irregularities can be expressed as:

$$S_x(\omega) = \begin{bmatrix} s_{x_{a11}} & 0 & s_{x_{a12}} & 0 & s_{x_{a13}} & 0 & s_{x_{a14}} & 0 \\ 0 & s_{x_{c11}} & 0 & s_{x_{c12}} & 0 & s_{x_{c13}} & 0 & s_{x_{c14}} \\ s_{x_{a21}} & 0 & s_{x_{a22}} & 0 & s_{x_{a23}} & 0 & s_{x_{a24}} & 0 \\ 0 & s_{x_{c21}} & 0 & s_{x_{c22}} & 0 & s_{x_{c23}} & 0 & s_{x_{c24}} \\ s_{x_{a31}} & 0 & s_{x_{a32}} & 0 & s_{x_{a33}} & 0 & s_{x_{a34}} & 0 \\ 0 & s_{x_{c31}} & 0 & s_{x_{c32}} & 0 & s_{x_{c33}} & 0 & s_{x_{c34}} \\ s_{x_{a41}} & 0 & s_{x_{a42}} & 0 & s_{x_{a43}} & 0 & s_{x_{a44}} & 0 \\ 0 & s_{x_{c41}} & 0 & s_{x_{c42}} & 0 & s_{x_{c43}} & 0 & s_{x_{c44}} \end{bmatrix} \quad (2-39)$$

where,

$$s_{x_{cij}}(\omega) = s_{x_{cii}}(\omega)e^{-i\omega t_k} \quad \text{and} \quad s_{x_{aij}}(\omega) = s_{x_{aii}}(\omega)e^{-i\omega t_k} \quad (2-40)$$

For the same railway, if the track is a stiff body, we have

$$s_{x_{cij}}(\omega) = s_{x_{cjj}}(\omega) \quad \text{and} \quad s_{x_{aij}}(\omega) = s_{x_{aij}}(\omega) \quad (2-41)$$

Letting

$$s_x = (s_a \ s_c \ s_a \ s_c \ s_a \ s_c \ s_a \ s_c)^T$$

and

$$\bar{s}(\omega) = \begin{bmatrix} 1 & 0 & e^{-i\omega t_1} & 0 & e^{-i\omega t_2} & 0 & e^{-i\omega t_3} & 0 \\ 0 & 1 & 0 & e^{-i\omega t_1} & 0 & e^{-i\omega t_2} & 0 & e^{-i\omega t_3} \\ e^{i\omega t_1} & 0 & 1 & 0 & e^{-i\omega t_4} & 0 & e^{-i\omega t_2} & 0 \\ 0 & e^{i\omega t_1} & 0 & 1 & 0 & e^{-i\omega t_4} & 0 & e^{-i\omega t_2} \\ e^{i\omega t_2} & 0 & e^{i\omega t_4} & 0 & 1 & 0 & e^{-i\omega t_1} & 0 \\ 0 & e^{i\omega t_2} & 0 & e^{i\omega t_4} & 0 & 1 & 0 & e^{-i\omega t_1} \\ e^{i\omega t_3} & 0 & e^{i\omega t_2} & 0 & e^{i\omega t_1} & 0 & 1 & 0 \\ 0 & e^{i\omega t_3} & 0 & e^{i\omega t_2} & 0 & e^{i\omega t_1} & 0 & 1 \end{bmatrix}$$

the PSD of track irregularities is:

$$S_x(\omega) = \bar{s}(\omega)s_x(\omega) \quad (2-42)$$

where,

$$\begin{aligned} t_1 &= 2a/v_0 & t_2 &= 2l/v_0 \\ t_3 &= (2l+2a)/v_0 & t_4 &= (2l-2a)/v_0 \end{aligned}$$

2.7.3 The Transfer Function of a Railway Bogie Vehicle

If the track irregularities are the only disturbances of a railway vehicle, Eq.(2-18) becomes:

$$(Ms^2 + Ds + Ks)q(s) = A X(s) \quad (2-43)$$

after applying the Laplace transform to Eq.(2-18), where A is a constant matrix and $D = G + C$ and $K = N + E$.

There are only eight inputs on the right side of Eq.(2-43). It is therefore necessary to rearrange Eq.(2-43) before finding the transfer function between the track irregularities and the system responses.

Letting

$$\begin{aligned} P(\omega) &= K - M\omega^2 + iD\omega \\ \{q\} &= \{q_w \mid q_T \mid q_b\} \end{aligned} \quad (2-44)$$

and dividing Eq.(2-44) into three groups of equations; the first group being the wheelset dynamic equations in which there are eight equations, the second being the bogie dynamic equations in which there are six equations, and the last group being the body dynamic equation in which there are three equations, Eq.(2-43) becomes:

$$\begin{aligned} P_1(\omega)q_w(\omega) + P_2(\omega)q_T(\omega) + P_3(\omega)q_b(\omega) &= A_{11,81}X(\omega) \\ P_4(\omega)q_w(\omega) + P_5(\omega)q_T(\omega) + P_6(\omega)q_b(\omega) &= 0 \\ P_7(\omega)q_w(\omega) + P_8(\omega)q_T(\omega) + P_9(\omega)q_b(\omega) &= 0 \end{aligned} \quad (2-45)$$

where,

$$\begin{aligned} P_1(\omega) &\text{ is a } 8 \times 8 \text{ matrix,} & P_2(\omega) &\text{ is a } 8 \times 6 \text{ matrix,} \\ P_3(\omega) &\text{ is a } 8 \times 3 \text{ matrix,} & P_4(\omega) &\text{ is a } 6 \times 8 \text{ matrix,} \end{aligned}$$

$\mathbf{P}_5(\omega)$ is a 6×6 matrix, $\mathbf{P}_6(\omega)$ is a 6×3 matrix,
 $\mathbf{P}_7(\omega)$ is a 3×8 matrix, $\mathbf{P}_8(\omega)$ is a 3×6 matrix,
 $\mathbf{P}_9(\omega)$ is a 3×3 matrix, $\mathbf{X}(\omega)$ is the vector of the wheelset inputs,
 $\mathbf{A}_{[1,8]}$ is the sub-matrix of \mathbf{A} with 8×8 elements

and then we have

$$\begin{aligned} \mathbf{q}_w(\omega) + \mathbf{H}_{\%w}(\omega)\mathbf{q}_T(\omega) + \mathbf{H}_{\%b}(\omega)\mathbf{q}_b(\omega) &= \mathbf{H}_{\%w}(\omega)\mathbf{X}(\omega) \\ \mathbf{H}_{\%T}(\omega)\mathbf{q}_w(\omega) + \mathbf{q}_T(\omega) + \mathbf{H}_{\%T}(\omega)\mathbf{q}_b(\omega) &= 0 \\ \mathbf{H}_{\%b}(\omega)\mathbf{q}_w(\omega) + \mathbf{H}_{\%b}(\omega)\mathbf{q}_T(\omega) + \mathbf{q}_b(\omega) &= 0 \end{aligned} \quad (2-46)$$

where,

$$\begin{aligned} \mathbf{H}_{\%w}(\omega) &= \mathbf{P}_1^{-1}(\omega)\mathbf{F}(\omega) & \mathbf{H}_{\%b}(\omega) &= \mathbf{P}_1^{-1}(\omega)\mathbf{P}_2(\omega) \\ \mathbf{H}_{\%T}(\omega) &= \mathbf{P}_1^{-1}(\omega)\mathbf{P}_3(\omega) & \mathbf{H}_{\%T}(\omega) &= \mathbf{P}_5^{-1}(\omega)\mathbf{P}_4(\omega) \\ \mathbf{H}_{\%T}(\omega) &= \mathbf{P}_5^{-1}(\omega)\mathbf{P}_6(\omega) & \mathbf{H}_{\%b}(\omega) &= \mathbf{P}_9^{-1}(\omega)\mathbf{P}_7(\omega) \\ \mathbf{H}_{\%b}(\omega) &= \mathbf{P}_9^{-1}(\omega)\mathbf{P}_8(\omega) \end{aligned} \quad (2-47)$$

The transfer functions of wheelsets, bogies and carbody with track irregularities are therefore:

$$\begin{aligned} \mathbf{q}_w(\omega) &= \mathbf{H}_1(\omega)\mathbf{X}(\omega) \\ \mathbf{q}_T(\omega) &= \mathbf{H}_2(\omega)\mathbf{X}(\omega) \\ \mathbf{q}_b(\omega) &= \mathbf{H}_3(\omega)\mathbf{X}(\omega) \end{aligned} \quad (2-48)$$

where,

$$\begin{aligned} \mathbf{H}_1(\omega) &= \Delta_3^{-1}(\omega)\mathbf{H}_{\%w}(\omega) \\ \mathbf{H}_2(\omega) &= \Delta_1\Delta_3^{-1}(\omega)\mathbf{H}_{\%w}(\omega) \\ \mathbf{H}_3(\omega) &= \Delta_2\Delta_3^{-1}(\omega)\mathbf{H}_{\%w}(\omega) \end{aligned} \quad (2-49)$$

and

$$\begin{aligned} \Delta_1(\omega) &= [\mathbf{I} - \mathbf{H}_{\%T}(\omega)\mathbf{H}_{\%b}(\omega)]^{-1}[\mathbf{H}_{\%T}(\omega)\mathbf{H}_{\%w}(\omega) - \mathbf{H}_{\%T}(\omega)] \\ \Delta_2(\omega) &= -\mathbf{H}_{\%b}(\omega)\Delta_1(\omega) - \mathbf{H}_{\%b}(\omega) \\ \Delta_3(\omega) &= \mathbf{I} + \mathbf{H}_{\%w}(\omega)\Delta_1(\omega) + \mathbf{H}_{\%w}(\omega)\Delta_2(\omega) \end{aligned} \quad (2-50)$$

The auto-power spectral density PSD's of system responses are:

$$\begin{aligned}
\mathbf{S}_w(\omega) &= \mathbf{H}_1(\omega)\mathbf{S}_x(\omega)(\mathbf{H}_1^*(\omega))^T \\
\mathbf{S}_T(\omega) &= \mathbf{H}_2(\omega)\mathbf{S}_x(\omega)(\mathbf{H}_2^*(\omega))^T \\
\mathbf{S}_b(\omega) &= \mathbf{H}_3(\omega)\mathbf{S}_x(\omega)(\mathbf{H}_3^*(\omega))^T
\end{aligned}
\tag{2-51}$$

and their Cross-PSD's are:

$$\begin{aligned}
\mathbf{S}_{wT}(\omega) &= \mathbf{H}_1(\omega)\mathbf{S}_x(\omega)(\mathbf{H}_2^*(\omega))^T & \mathbf{S}_{Tw}(\omega) &= \mathbf{H}_2(\omega)\mathbf{S}_x(\omega)(\mathbf{H}_1^*(\omega))^T \\
\mathbf{S}_{Tb}(\omega) &= \mathbf{H}_2(\omega)\mathbf{S}_x(\omega)(\mathbf{H}_3^*(\omega))^T & \mathbf{S}_{bT}(\omega) &= \mathbf{H}_3(\omega)\mathbf{S}_x(\omega)(\mathbf{H}_2^*(\omega))^T \\
\mathbf{S}_{wb}(\omega) &= \mathbf{H}_1(\omega)\mathbf{S}_x(\omega)(\mathbf{H}_3^*(\omega))^T & \mathbf{S}_{bw}(\omega) &= \mathbf{H}_3(\omega)\mathbf{S}_x(\omega)(\mathbf{H}_1^*(\omega))^T
\end{aligned}
\tag{2-52}$$

2.8 Computer Programming

All the simulation results have been produced by the computer program developed by the author. The strategy and block diagrams of the computer program have been published and are included in Appendix C while the instructions of the computer program are listed in Appendix D. The relevant theory on Matrix and Numerical Mathematics can be found in references[100-101]. The computer program needs to be linked with NAG Library[102].

Table 2.2 The inertia parameters and some of geometric parameters of vehicle

Inertia Parameters:	kg or kg-m ²
wheelset mass m_w	1250
wheelset inertia in x axis I_{wx}	700
wheelset inertia in z axis I_{wz}	700
bogie frame mass m_T	2500
bogie frame inertia in x axis I_{Tx}	1000
bogie frame inertia in z axis I_{Tz}	3500
carbody mass m_b	25000
carbody inertia in x axis I_{bx}	30000
carbody inertia in z axis I_{bz}	1000000
Geometric Parameters:	m
wheel radius	0.45
wheelset base a	1.25
half of bogie pivot distance l	8.75
half of full vehicle body length l_0	11.5
height from wheelset to primary suspension h_1	0.0
height from primary suspension to bogie frame h_2	0.2
height from bogie frame to secondary suspension h_3	0.4
height from secondary suspension to carbody weight centre h_4	1.0

Chapter 3

PERFECT STEERING BOGIE VEHICLE MODELS AND THEIR CAPABILITY IN NEGOTIATING CURVES

This chapter presents three vehicle configurations capable of perfect steering, considering their capability in negotiating a cubic parabola transition curve and their ability to accommodate cant deficiency. The steering mechanism of the models is analysed and the effects of the geometric errors in the steering linkages on the vehicle curving are investigated. The Arabic numerals in the figures of this chapter stand for the following wheelset sequence: 1--the outboard wheelset in the leading bogie, 2--the inboard wheelset in the leading bogie, 3--the inboard wheelset in the trailing bogie and 4--the outboard wheelset in the trailing bogie.

3.1 Perfect Steering Bogie Vehicles

Most of the researchers in the field have noticed that a reduction in primary yaw stiffness would lead to better curving, but reduce stability. In order to decrease the conflict between stability and curving, wheelset inter-connected bogie vehicles and body-steered bogie vehicles have been invented and applied, which have been reviewed in Chapter 1. A wheelset inter-connected bogie vehicle uses the inter wheelset stiffnesses to reduce the primary yaw stiffness and thereby achieve stability and improve steering ability; while a body-steered bogie vehicle shifts some of the primary yaw stiffness to the stiffnesses in steering linkages to achieve the same goal. The steering linkages in body-steered bogie vehicles can, however, be designed such that the moment produced by the steering linkages achieves some equilibrium with the moment produced by the yaw stiffnesses in the suspensions. The steering ability of body-steered bogie vehicles can, therefore, be much better than that of wheelset inter-connected bogie vehicles.

There are not many references discussing the effect of secondary yaw stiffness on curving. There are two reasons that may be used to explain this fact: firstly, secondary yaw stiffness is much softer than primary yaw stiffness such that the influence of secondary yaw stiffness on curving is sheltered if primary yaw stiffness exists in

vehicles and, secondly, some bogie vehicles are freight vehicles that do not have secondary yaw stiffness.

3.1.1 Configurations

Referring to Eq.(2-15), a railway vehicle with two bogies and four wheelsets will be kinematically unstable if the degeneracy P of the elastic matrix \mathbf{E} is greater than 4. A conventional bogie vehicle will therefore be unstable if both the primary and secondary yaw stiffnesses are equal to zero because the degeneracy P of its elastic matrix \mathbf{E} is equal to 8. At least two more independent stiffnesses need to be applied into each bogie to stabilise the vehicle. These two stiffnesses should not make any contribution to vehicle bending stiffnesses if perfect steering is required. There are many forms in which the combination of two independent stiffnesses can be added to a bogie. This chapter demonstrates three kinds of configurations, as illustrated in Fig.3.1, Fig.3.2 and Fig.3.3, in which two independent stiffnesses are applied into each bogie when primary and secondary yaw stiffnesses are eliminated from conventional bogie vehicles.

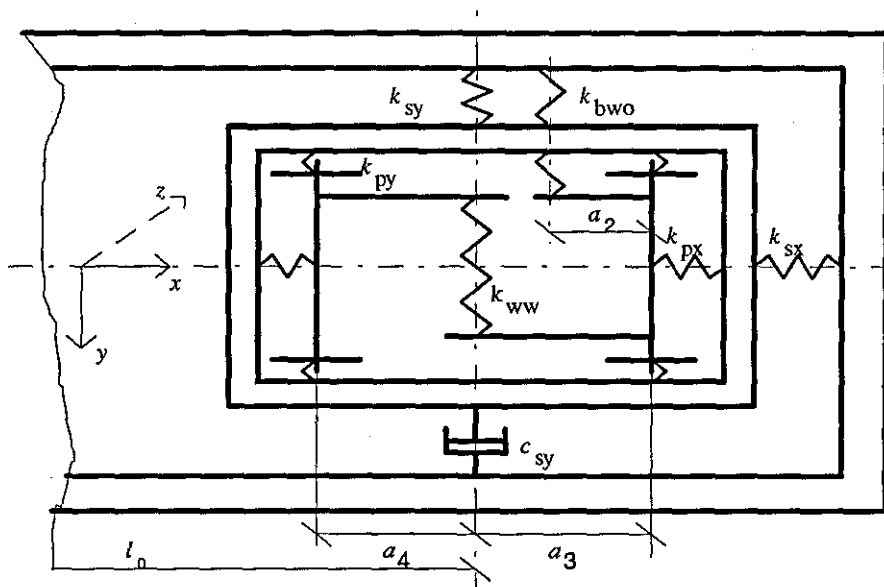
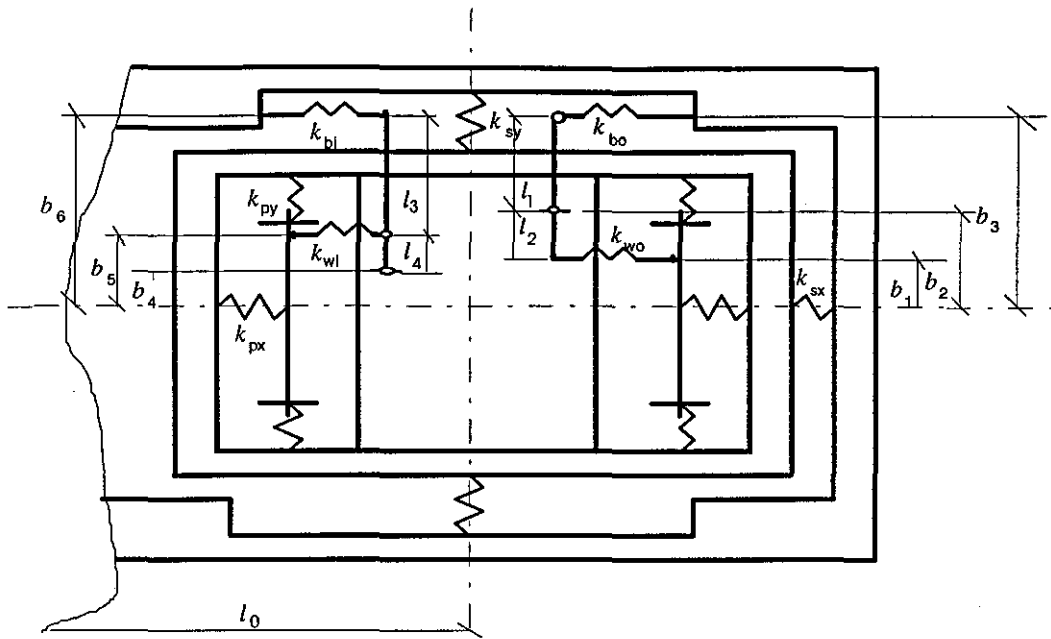
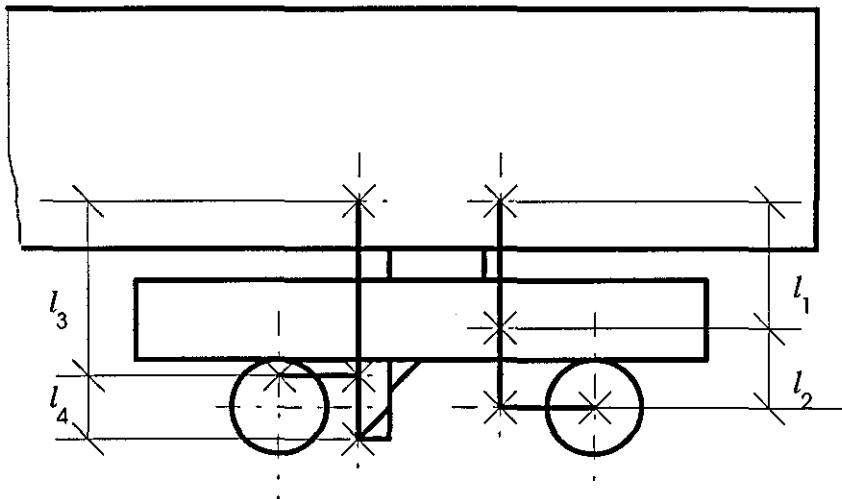


Figure 3.1 Configuration of a perfect steering bogie

In Fig.3.1, the outboard wheelsets are directly connected to the carbody by spring k_{bwo} and the wheelsets in the same bogie are connected by k_{ww} . Since these two stiffnesses are independent, the degeneracy of \mathbf{E} reduces from 8 to 4 and the necessary condition of stability is then satisfied. A feature of this kind of steering linkage is that two wheelset motion modes (yaw and lateral) are directly coupled with all carbody motions (yaw, roll and lateral) by the linkage. The dynamic behaviour of the vehicle is going to be published and is listed in Appendix A.



(a) horizontal type



(b) vertical type

Figure 3.2 The configuration of perfect steering bogie vehicle (Model I).

For the configuration given in Fig.3.2, the outboard and inboard wheelsets are independently connected with a linkage to the carbody and bogie frame, and there is no inter wheelset stiffness such that the outboard and inboard wheelsets are steered by each linkage separately. This configuration is called Model I to simplify further description. Each linkage creates an independent effective stiffness so that the degeneracy of \mathbf{E} reduces from 8 to 4 and the necessary condition of stability is then satisfied. These two effective stiffnesses created by the linkages in one of bogies are given by:

$$k_{e1} = \frac{k_{bo} k_{wo}}{l_1^2 k_{bo} + l_2^2 k_{wo}}; \quad k_{e2} = \frac{k_{hi} k_{wi}}{(l_3 + l_4)^2 k_{hi} + l_4^2 k_{wi}} \quad (3-1)$$

The full form of the compatibility matrix **a** for this model is listed at Table 3.1 with the diagonal elements of the system stiffness matrix [**k**] being defined by:

$$\{k_{ii}\} = \text{diag}\{k_{py} \ k_{p\psi} \ k_{p\phi} \ k_{py} \ k_{p\psi} \ k_{p\phi} \ k_{py} \ k_{p\psi} \ k_{p\phi} \ k_{py} \ k_{p\psi} \ k_{p\phi} \ | \ k_{sy} \ k_{s\psi} \ k_{s\phi} \ k_{sy} \ k_{s\psi} \ k_{s\phi} \ | \ k_{e1} \ k_{e2} \ k_{e2} \ k_{e1} \} \quad (3-2)$$

Let $\mathbf{a}^T = [\mathbf{a}_p \ | \ \mathbf{a}_s \ | \ \mathbf{a}_{LL} \ | \ \mathbf{a}_{LT}]^T$, where the subscripts p and s stand for the primary and secondary suspensions; the subscript LL stands for the steering linkage in the leading bogie and the subscript LT for the steering linkage in the trailing bogie, the sub-compatibility \mathbf{a}_{LL} for the leading bogie can be simplified as:

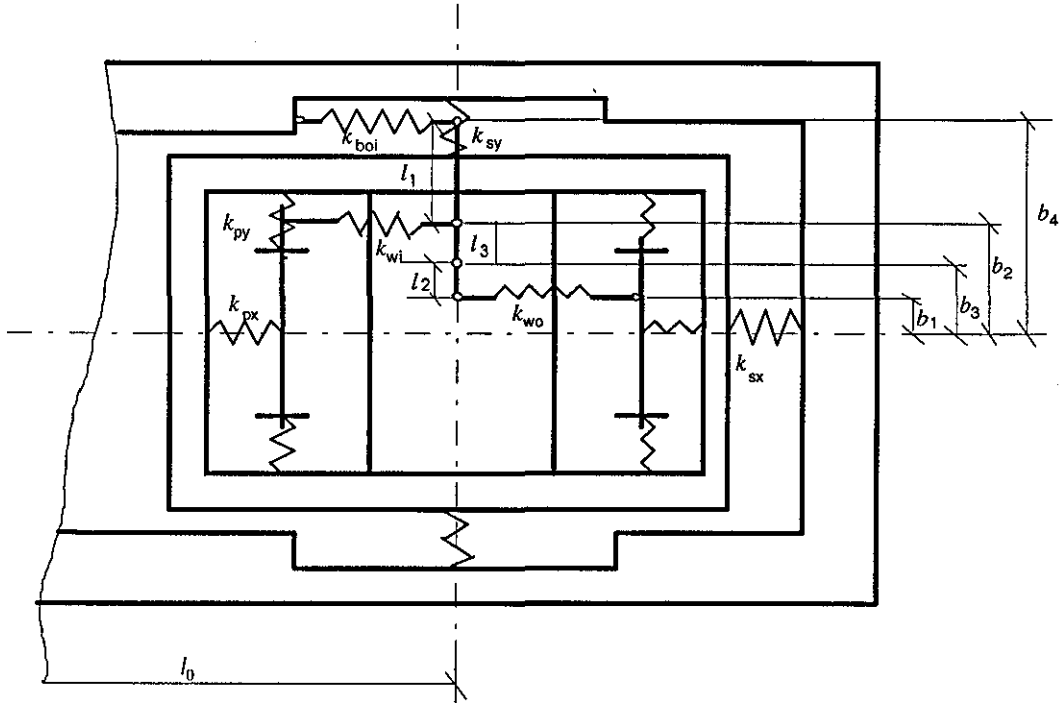
$$\mathbf{a}_{LL} = \begin{bmatrix} \Psi_{wo} & \Psi_{wi} & \Psi_{TL} & \Psi_b \\ -b_1 l_1 & 0 & b_2 (l_1 + l_2) & -b_3 l_2 \\ 0 & b_5 (l_3 + l_4) & -b_4 l_3 & -b_6 l_4 \end{bmatrix} = \begin{bmatrix} \Psi_{wo} & \Psi_{wi} & \Psi_{TL} & \Psi_b \\ -g_1 & 0 & g_2 & -g_3 \\ 0 & g_4 & -g_5 & -g_6 \end{bmatrix} \quad (3-23)$$

since the effective stiffnesses of Eq.(3-1) in one of bogies only affect the elasticity of four degrees of freedom (Ψ_{wo} , Ψ_{wi} , Ψ_{TL} and Ψ_b), and the elastic sub-matrix \mathbf{E}_L that is only associated with the effective stiffnesses in the leading bogie is:

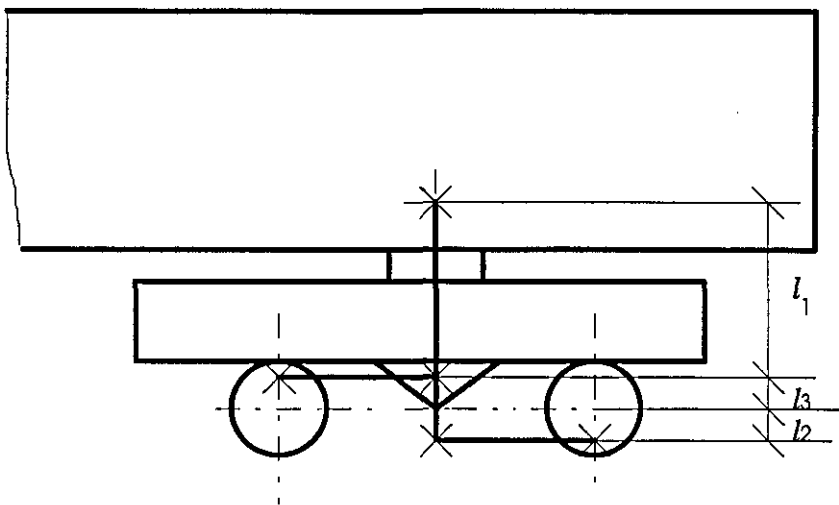
$$\mathbf{E}_L = \mathbf{a}_{LL}^T \begin{bmatrix} k_{e1} & 0 \\ 0 & k_{e2} \end{bmatrix} \mathbf{a}_{LL} = \begin{bmatrix} g_1^2 k_{e1} & 0 & -g_1 g_2 k_{e1} & g_1 g_3 k_{e1} \\ 0 & g_4^2 k_{e2} & -g_4 g_5 k_{e2} & -g_4 g_6 k_{e2} \\ -g_1 g_2 k_{e1} & -g_4 g_5 k_{e2} & g_2^2 k_{e1} + g_5^2 k_{e2} & -g_2 g_3 k_{e1} + g_5 g_6 k_{e2} \\ g_1 g_3 k_{e1} & -g_4 g_6 k_{e2} & -g_2 g_3 k_{e1} + g_5 g_6 k_{e2} & g_3^2 k_{e1} + g_6^2 k_{e2} \end{bmatrix} \quad (3-2b)$$

The outboard and inboard wheelsets are connected by the same lever to the carbody and bogie frame in the model given in Fig.3.3. This model will be referred to as Model II. Three stiffnesses are added to each bogie by this linkage and are given by:

$$\begin{aligned}
 k_{e1} &= \frac{k_{boi} k_{wo}}{(l_1 + l_3)^2 k_{boi} + l_3^2 k_{wi} + l_2^2 k_{wo}} \\
 k_{e2} &= \frac{k_{boi} k_{wi}}{(l_1 + l_3)^2 k_{boi} + l_3^2 k_{wi} + l_2^2 k_{wo}} \\
 k_{e3} &= \frac{k_{wo} k_{wi}}{(l_1 + l_3)^2 k_{boi} + l_3^2 k_{wi} + l_2^2 k_{wo}}
 \end{aligned}
 \tag{3-4}$$



(a) horizontal type



(b) vertical type

Figure 3.3 The configuration of perfect steering bogie vehicle (Model II).

It can be proved, however, that only two of them are independent; for example, k_{e3} can be formed from k_{e1} and k_{e2} , and thus the degeneracy of \mathbf{E} is 4 such that the necessary condition of stability is then satisfied. Inter wheelset stiffness k_{e3} exists in this model and the full form of the compatibility matrix \mathbf{a} for this model is listed in Table 3.2 with the diagonal elements of the system stiffness matrix $[\mathbf{k}]$ being defined by:

$$\{k_{ii}\} = \text{diag}\{k_{py} \ k_{pb} \ k_{p\phi} \ k_{py} \ k_{pb} \ k_{p\phi} \ k_{py} \ k_{pb} \ k_{p\phi} \ k_{py} \ k_{pb} \ k_{p\phi} \ | \ k_{sy} \ k_{sb} \ k_{s\phi} \ k_{sy} \ k_{sb} \ k_{s\phi} \ | \ k_{e1} \ k_{e2} \ k_{e3} \ k_{e2} \ k_{e1} \ k_{e3}\} \quad (3-5)$$

The sub-matrix of the compatibility matrix \mathbf{a}_{LL} is given by:

$$\mathbf{a}_{LL} = \begin{bmatrix} \Psi_{wo} & \Psi_{wi} & \Psi_{TL} & \Psi_b \\ -b_1(l_1 + l_3) & 0 & b_3(l_1 + l_2 + l_3) & -b_4 l_2 \\ 0 & -b_2(l_1 + l_3) & b_3 l_1 & b_4 l_3 \\ b_1 l_3 & b_2 l_2 & -b_3(l_2 + l_3) & 0 \end{bmatrix} = \begin{bmatrix} \Psi_{wo} & \Psi_{wi} & \Psi_{TL} & \Psi_b \\ -g_1 & 0 & g_2 & -g_3 \\ 0 & -g_4 & g_5 & g_6 \\ g_7 & g_8 & -g_9 & 0 \end{bmatrix} \quad (3-6a)$$

and the elastic sub-matrix \mathbf{E}_L that is associated with the effective stiffnesses in the leading bogie is given by:

$$\mathbf{E}_L = \mathbf{a}_{LL}^T \begin{bmatrix} k_{e1} & 0 & 0 \\ 0 & k_{e2} & 0 \\ 0 & 0 & k_{e3} \end{bmatrix} \mathbf{a}_{LT} = \begin{bmatrix} g_1^2 k_{e1} + g_7^2 k_{e3} & g_7 g_8 k_{e3} & -(g_1 g_2 k_{e1} + g_7 g_9 k_{e3}) & g_1 g_3 k_{e1} \\ g_7 g_8 k_{e3} & g_4^2 k_{e2} + g_8^2 k_{e3} & -(g_4 g_5 k_{e2} + g_8 g_9 k_{e3}) & -g_4 g_6 k_{e2} \\ -(g_1 g_2 k_{e1} + g_7 g_9 k_{e3}) & -(g_4 g_5 k_{e2} + g_8 g_9 k_{e3}) & g_2^2 k_{e1} + g_5^2 k_{e2} + g_9^2 k_{e3} & -g_2 g_3 k_{e1} + g_5 g_6 k_{e2} \\ g_1 g_3 k_{e1} & -g_4 g_6 k_{e2} & -g_2 g_3 k_{e1} + g_5 g_6 k_{e2} & g_3^2 k_{e1} + g_6^2 k_{e2} \end{bmatrix} \quad (3-6b)$$

All effective stiffnesses in these two configurations are merely yaw stiffnesses because they only associate to the yaw motions of rigid bodies. Indeed, the steering linkages of Model I have a similar form to the *guided bogie vehicle* suggested by Smith and Anderson[19] while the steering linkage of Model II closes to the form of the *forced*

bogie vehicle proposed by Bell and Hedrick[12]. In their configurations, however, the steering linkages provide the bending stiffness.

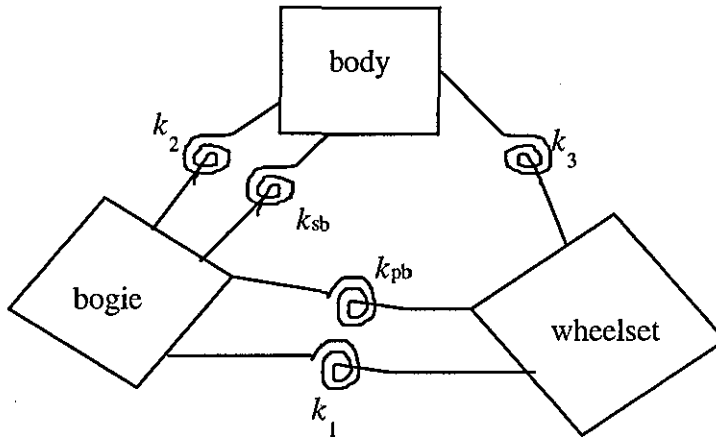


Figure 3.4 The simplified bogie vehicle

A body-steered bogie vehicle can be simplified according to the system in Fig.3.4, where the stiffnesses k_1 , k_2 and k_3 are the yaw stiffnesses and come from the steering linkages while the bending stiffnesses k_{pb} and k_{sb} come from the suspension yaw stiffnesses and are independent of the stiffnesses in the steering linkages. In perfect steering vehicles, we have $k_{pb} = k_{sb} = 0$. If the ratio of the absolute displacements between the carbody (q_b), bogie frame (q_T) and wheelset (q_w) is a constant, it is possible to set up the ratio for the stiffnesses k_1 , k_2 and k_3 letting the moments act on each rigid body be equal to zero whenever the displacements take place. For example, if the ratio of the displacements between the carbody, bogie frame and wheelset is $(q_b : q_T : q_w) = (0 : -1 : 2)$, the moments acting on each rigid body can be equal to zero when the ratio of stiffnesses k_1 , k_2 and k_3 satisfies $(k_1 : k_2 : k_3) = (1 : 2 : 1)$. In conventional bogie vehicles, we have $k_1 = k_2 = k_3 = 0$. It is impossible to set up the relationship between the bending stiffnesses k_{pb} and k_{sb} to let the moments acting on each rigid body be zero when their displacements are non-zero. In other body-steered bogie vehicles, both the bending stiffnesses and the stiffnesses in the steering linkages are not equal to zero. Since the bending stiffnesses in suspensions are independent of the stiffnesses k_1 , k_2 and k_3 in the steering linkages while the stiffnesses k_1 , k_2 and k_3 are dependent of each other, it is impossible to establish a relationship between the bending stiffnesses and the stiffnesses in the steering linkages which will permit the forces acting on each rigid body to be zero, for any particular relationship between the displacements among the rigid bodies, if both the bending stiffnesses and the steering linkages exist.

In steady state, the relationship of the displacements $\{\bar{q}\}$ depends on the curvature and some of the geometric parameters of vehicles. For example, the displacements $\{\bar{q}\}$ of the outboard wheelset, the leading bogie and the carbody are $(l_0 + a)/R$, l_0/R and 0, the relationship between them being $(l_0 + a) : l_0 : 0$. Fortunately, this relationship is governed only by the vehicle geometry and it can be easily proven that the ratio between any pair of the elements in $\{\bar{q}\}$ is a constant and is determined only by the vehicle geometry in steady state. It is therefore possible to set up the relationships between the stiffnesses k_1 , k_2 and k_3 to give $\mathbf{E}\{\Delta\bar{q}\} = 0$ for perfect steering vehicles. The most important fact is that the relationship $\mathbf{E}\{\Delta\bar{q}\} = 0$ is only decided by the vehicle geometry. The next sub-section concentrates on finding the relationships for Model I and Model II.

3.1.2 Perfect Steering Linkages

Since there is no yaw stiffness in the suspension of a perfect steering vehicle, one of the functions of the steering linkages in perfect steering vehicles is to provide the constraints for the yaw motions of the vehicle rigid bodies, but not to cause any bending stiffness. In satisfying the sufficient condition for perfect steering Eq.(2-26), the force vector \mathbf{F}_E defined in Eq.(2-23) should be zero. The sufficient conditions for the configurations of Model I and Model II to possess perfect steering capability are that the geometric parameters of their steering linkages must satisfy the following:

For Model I:

$$\frac{b_1(b_3 - b_2)}{b_2(b_3 - b_1)} = \frac{l_0}{l_0 + a}; \quad \frac{b_5(b_6 - b_4)}{b_4(b_6 - b_5)} = \frac{l_0}{l_0 - a} \quad (3-7)$$

and for Model II:

$$\frac{b_1(b_4 - b_3)}{b_3(b_4 - b_1)} = \frac{l_0}{l_0 + a}; \quad \frac{b_2(b_4 - b_3)}{b_3(b_4 - b_2)} = \frac{l_0}{l_0 - a} \quad (3-8)$$

If the steering linkages are horizontally mounted, the following relationships can be derived from Eq.(3-7):

$$b_3 = \frac{ab_1b_2}{ab_1 - (b_2 - b_1)l_0}; \quad b_6 = \frac{ab_4b_5}{ab_5 - (b_5 - b_4)l_0} \quad (3-9)$$

Because of $b_3 > 0$ and $b_6 > 0$, we have:

$$\frac{b_1}{b_2 - b_1} > \frac{l_0}{a}; \quad \frac{b_5}{b_5 - b_4} > \frac{l_0}{a} \quad (3-10)$$

Using the parameters listed in Table 2.2, $l_0 / a = 7$. In order to have enough space to fit the levers of the steering linkages, letting $b_2 - b_1 = 0.1m$ and $b_5 - b_4 = 0.1m$, we have $b_1 = 0.75m$ and $b_5 = 0.75m$ such that $b_2 = 0.85m$, $b_3 = 12.75m$, $b_4 = 0.65m$ and $b_6 = 9.75m$ are obtained. It appears that b_3 and b_6 are too large to be realised in practical applications.

A similar situation to that above occurs in Model II if the steering linkages are horizontally mounted. Eq.(3-8) can be transformed into:

$$b_4 = \frac{ab_1b_3}{ab_1 - (b_3 - b_1)l_0} \quad \text{or} \quad b_4 = \frac{ab_2b_3}{(b_2 - b_3)l_0 - ab_2} \quad (3-11)$$

and because of $b_4 > 0$, we have:

$$\frac{b_1}{b_3 - b_1} > \frac{l_0}{a}; \quad \frac{b_2}{b_2 - b_3} < \frac{l_0}{a} \quad (3-12)$$

Letting $b_3 - b_1 = 0.1m$, $b_2 - b_3 = 0.15m$ and $b_1 = 0.75m$, we have $b_2 \approx 1.00m$, $b_3 = 0.85m$ and $b_4 \approx 12.75m$. The above analysis shows that it is impossible to mount the steering linkages horizontally in practical situations if perfect steering is required.

If the linkages are vertically fitted, we have $b_3 - b_2 = l_1$, $b_2 - b_1 = l_2$ and $b_6 - b_5 = l_3$, $b_5 - b_4 = l_4$ for Model I. The sufficient condition for perfect steering can be derived from Eq.(3-7) whereby:

$$\frac{b_1 l_1}{b_2 (l_1 + l_2)} = \frac{l_0}{l_0 + a}; \quad \frac{b_5 (l_4 + l_3)}{b_4 l_3} = \frac{l_0}{l_0 - a} \quad (3-13)$$

In Model II, for the sufficient condition of perfect steering, Eq.(3-8) becomes:

$$\frac{b_1 (l_1 + l_3)}{b_3 (l_1 + l_2 + l_3)} = \frac{l_0}{l_0 + a}; \quad \frac{b_2 (l_1 + l_3)}{b_3 l_1} = \frac{l_0}{l_0 - a} \quad (3-14)$$

Letting $b_1 = b_2 = b_3 = b_4 = b_5 = b_6$, the geometric relationship for the linkage levers in Model I is:

$$l_2 = \frac{a}{l_0} l_1; \quad l_4 = \frac{a}{l_0 - a} l_3 \quad (3-15)$$

The geometric relationship for the linkage lever in Model II is:

$$l_1 = \frac{l_0 - a}{a} l_3; \quad l_2 = l_3 \quad (3-16)$$

In this research, we have:

In Model I: $l_1 = 1.05m$, $l_2 = 0.15m$, $l_3 = 0.9m$ and $l_4 = 0.15m$;

In Model II: $l_1 = 0.9m$ and $l_2 = l_3 = 0.15m$.

The interesting thing is that the conditions {Eq.(3-15) and Eq.(3-16)} for Model I and Model II capable of perfect steering are independent of curvature and the stiffnesses in the steering linkages. The steering linkages are called the perfect steering linkages if the geometric parameters of the levers in the steering linkages satisfy Eq.(3-15) for Model I or Eq.(3-16) for Model II.

In order to explore the dynamic behaviour of Model I and Model II, two sets of stiffnesses and dampings for each model are used in this research. They are listed in Table 3.3 (for Model I) and Table 3.4 (for Model II). The parameters in Set 1 represent a 'soft' steering linkage system and those in Set 2 stand for a 'stiff' steering linkage system. The parameters listed in Table 3.5 are of a conventional bogie vehicle.

3.2 Perfect Steering And Flange Clearance

The angle between the wheelset rolling direction and the track tangent direction is called the attack angle. If the conditions in Eq.(3-15) and Eq.(3-16) exist, all rigid bodies of Model I and Model II take their radial positions and the attack angle of each wheelset is equal to zero when the vehicles are on a uniform curve with zero cant deficiency; perfect steering being achieved. These occurrences are independent of the vehicle suspension elasticity and steering linkage stiffness, and of the degrees of track curvatures. When these conditions prevail, the wheelsets will laterally move to their pure rolling line, realising perfect steering. If the distance between the wheelset pure rolling line and the track central line is not big enough, flange clearance disappears and flange contact occurs. Perfect steering does not exist if flange contact occurs. Another condition for perfect steering is therefore that the distance between the pure rolling line of the wheelsets and the track central line must be less than the maximum flange clearance. In Eq.(2-16), the distance between the pure rolling line and the track central line is proportional to $1/\lambda_c$ so that high equivalent conicity can be used to avoid

flange contact if other parameters are fixed. The minimum conicity that can avoid flange contact is called the necessary conicity λ_n in the thesis. In the figures of this chapter, Minimum conicity stands for the necessary conicity λ_n .

The lateral displacements \hat{y}_w 's of wheelsets from the track central line along their radial directions are shown in Fig.3.5 where the flange clearance is set to 5mm. The lateral displacements of the perfect steering vehicle wheelsets are much smaller than those of the conventional bogie vehicle. From the results in Fig.3.5, the reduction in the lateral displacements of the perfect steering vehicles allows Model I and Model II to achieve perfect steering without causing flange contact if the radii of curves $R \geq 200\text{m}$, since an equivalent conicity of around 0.3 has been measured by BR researchers [103] in practical cases. If the radii of curves become $R < 200\text{m}$, it is necessary to increase the equivalent conicities of wheelsets or/and to extend the flange clearance to prevent flange contact. Further increment in wheelset conicity may cause the problems with regard to stability and ride quality, and will be investigated in the subsequent chapters. The extension of track gauge can increase the flange clearance, but if extended too much, the equivalent conicity may be reduced[66]. It is therefore unlikely that perfect steering vehicles will achieve perfect steering on sharp curves.

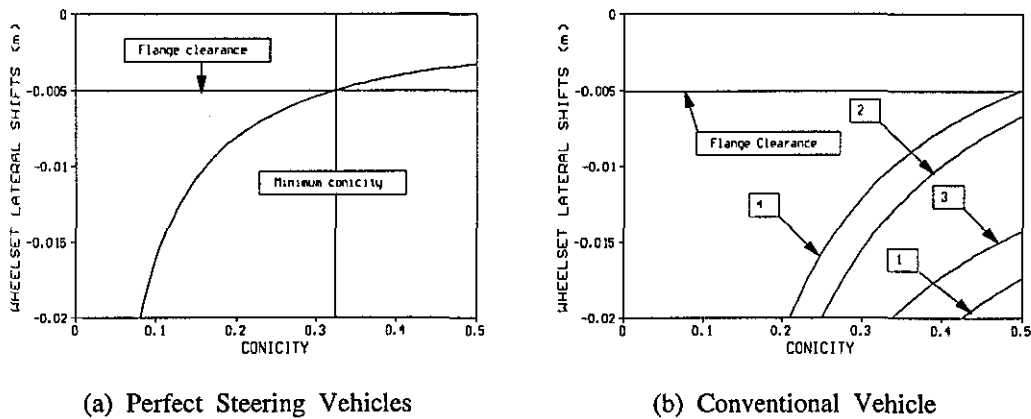


Figure 3.5 The lateral displacements of wheelsets when $R = 200\text{ m}$, $\phi_d = 0$

Compared with the conventional vehicle, Model I and Model II have two advantages in curving: firstly, they dramatically reduce the lateral displacements of wheelsets and, secondly, the wheelsets can take on their radial position if perfect steering is realised. These advantages can greatly decrease the forces that act on track, and therefore, two benefits arise: firstly, the wear between wheels and rails can be greatly reduced so that the maintenance of both tracks and wheelsets is cut down and, secondly, the potential of derailment is reduced, giving improved vehicle safety.

3.3 Geometric Errors in the Steering Linkages

The geometric parameters of the perfect steering linkages are theoretically defined by Eq.(3-15) for Model I and Eq.(3-16) for Model II. In practical applications, however, the real products are unlikely to match the theoretical design precisely, and the discrepancies exist with the geometric parameters. The geometric errors in the steering linkages will break the sufficient conditions for bogie vehicles capable of perfect steering, and thus cause the elastic forces $F_E \neq 0$ even on steady state. The effects of geometric errors in the steering linkages on the dynamic behaviour of the perfect steering vehicles will be investigated in several chapters of this thesis. This section studies the effects of geometric errors on the curving of Model I and Model II. There are many possible combinations of geometric errors, one form being defined in Fig.3.6. The percentage alterations of the effective stiffnesses of the steering linkages are listed in Table 3.6 (Model I) and in Table 3.7 (Model II) separately when the stiffnesses of Set 2 are used. The geometric errors framed in bold in Table 3.6 and Table 3.7 are used in the section, and the elastic forces F_E caused by these geometric errors are listed in Table 3.8, where the curve radius is $R = 200\text{m}$.

The steering mechanism of Model I and Model II is similar to that of the *forced steering vehicle*[12] and the *guided bogie vehicle*[19] when the geometric errors exist in the steering linkages of Model I and Model II. When the geometric errors in the steering linkages occur, the results in Table 3.8 show that the effective stiffnesses in the steering linkages of Model I and Model II will contribute to the bending stiffnesses. The essential difference between perfect steering vehicles and other body-steered bogie vehicles is that there are neither primary nor secondary yaw stiffnesses in perfect steering vehicles. The steering linkages in the *forced steering vehicle*[12] and the *guided bogie vehicle*[19] are designed to reduce the forces produced by the bending stiffnesses and to assist in the wheelsets taking more radial alignment. In Model I and Model II, the bending stiffnesses caused by the geometric errors in the steering linkages will result in the wheelsets moving away from their radial positions rather than assisting in them taking radial alignment because there is no any bending stiffness in the suspensions of Model I and Model II. Each wheelset will therefore move away from its radial position and its attack angle will no longer equal zero when the geometric errors exist in the steering linkages. Both the attack angle of wheelset and the lateral displacement away from its pure rolling line result in the creepage between wheels and rails. The attack angles, lateral displacements away from the track central line and resultant creepages of the wheelsets are illustrated in Fig.3.7 (Model I) and Fig.3.8

(Model II) as the functions of conicity when the elastic force F_E caused by the geometric errors (listed in Table 3.8) is used.

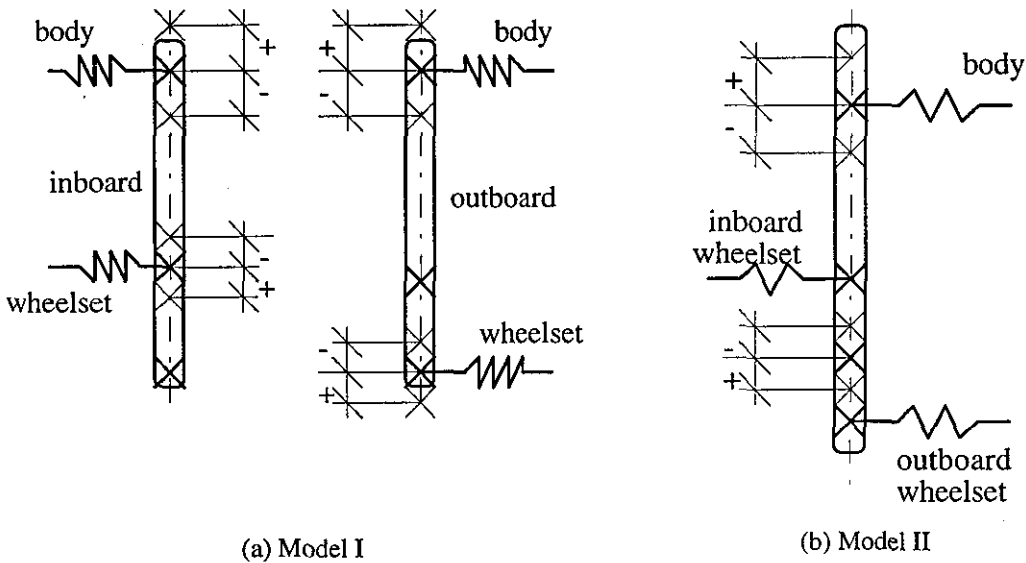
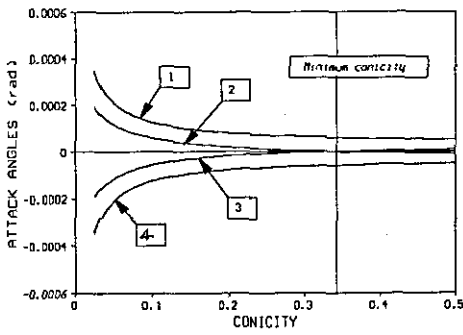
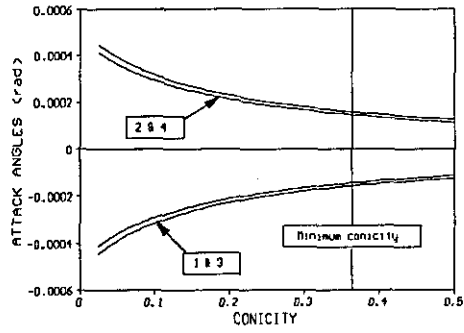


Figure 3.6 Schematic demonstration of geometric errors in steering linkages

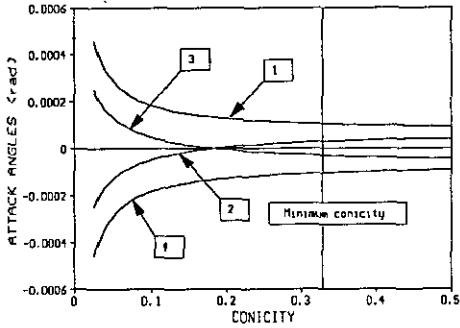
The effects of the geometric errors in the steering linkages on the wheelset attack angles obviously depend on the configuration and elasticity of the steering linkages. Stiff steering linkages result in large elastic forces F_E , as is shown in Table 3.8, and thus the attack angles will increase as the steering linkages become stiff. The resultant creepages also rise as the steering linkages become stiff because they are in proportion to the attack angles. When the steering linkages are soft, the attack angles and resultant creepages of Model I are larger than those of Model II when the geometric errors exist. Conversely, the differences in the attack angles and resultant creepages between Model I and Model II are not so obvious when their steering linkages are stiff. This means that the attack angles and resultant creepages are not sensitive to the configurations of steering linkages when they are stiff. The lateral displacements of the wheelsets are also illustrated in Fig.3.7 (Model I) and Fig.3.8 (Model II). Since the steering linkages only produce yaw moments when geometric errors exist, the influence of the geometric errors on the wheelset lateral displacements is much less than on the attack angles. Although the geometric errors have little influence on the lateral displacements of wheelset, this influence may still be vital in some cases because of flange contact. The results in Fig.3.9 show that the necessary conicity in avoiding flange contact increases when the geometric errors exist. Moreover, the necessary conicity becomes larger as soon as the geometric errors exist regardless of whether the steering levers become longer or shorter or whether the steering linkages are stiff or soft.



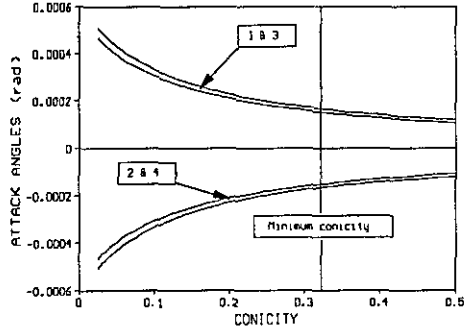
(a) wheelset attack angles of Model I when $l_1 = 1.155m$ and $l_3 = 0.99m$ (soft linkage)



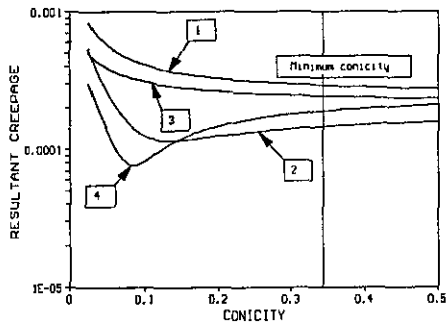
(b) wheelset attack angles of Model I when $l_1 = 1.155m$ and $l_3 = 0.99m$ (stiff linkage)



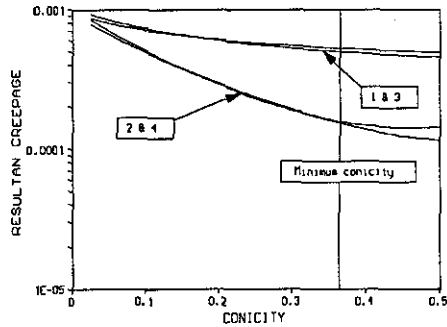
(c) wheelset attack angles of Model I when $l_1 = 0.945m$ and $l_3 = 0.81m$ (soft linkage)



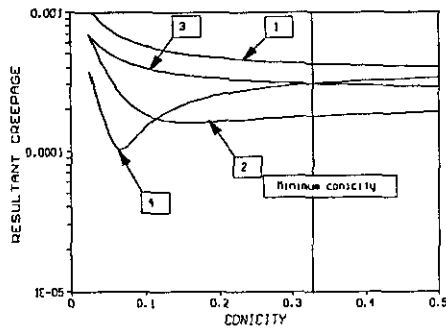
(d) wheelset attack angles of Model I when $l_1 = 0.945m$ and $l_3 = 0.81m$ (stiff linkage)



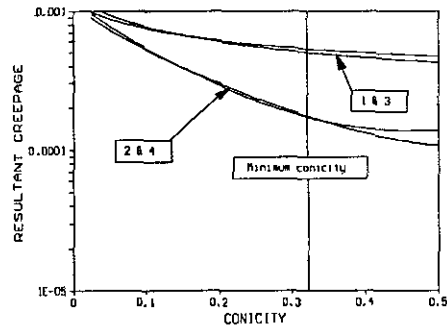
(e) resultant creepages of Model I when $l_1 = 1.155m$ and $l_3 = 0.99m$ (soft linkage)



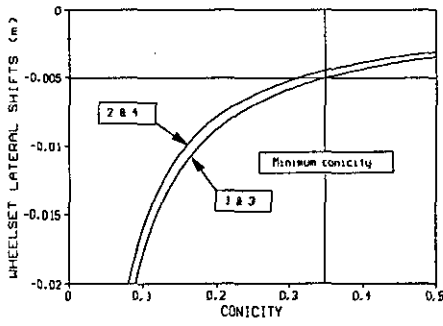
(f) resultant creepages of Model I when $l_1 = 1.155m$ and $l_3 = 0.99m$ (stiff linkage)



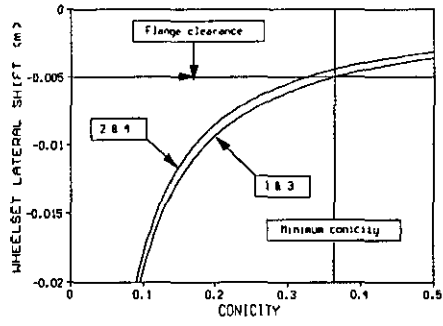
(g) resultant creepages of Model I when $l_1 = 0.945m$ and $l_3 = 0.81m$ (soft linkage)



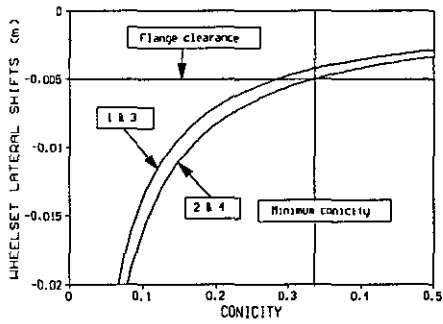
(h) resultant creepages of Model I when $l_1 = 0.945m$ and $l_3 = 0.81m$ (stiff linkage)



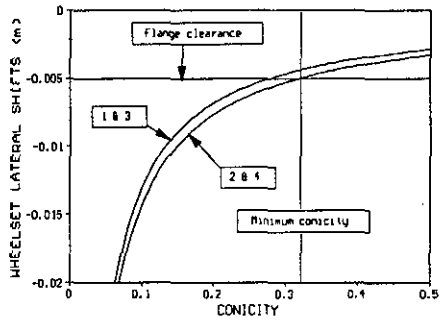
(i) wheelset lateral shifts of Model I when $l_1 = 1.155m$ and $l_3 = 0.99m$ (soft linkage)



(j) wheelset lateral shifts of Model I when $l_1 = 1.155m$ and $l_3 = 0.99m$ (stiff linkage)

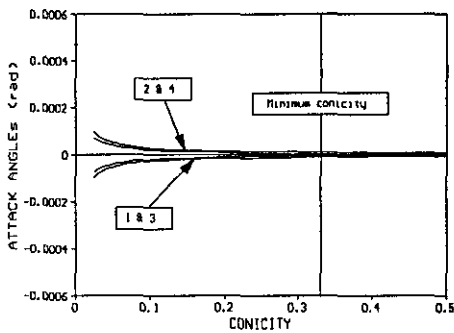


(k) wheelset lateral shifts of Model I when $l_1 = 0.945m$ and $l_3 = 0.81m$ (soft linkage)

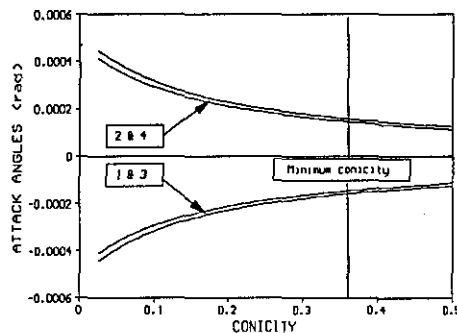


(l) wheelset lateral shifts of Model I when $l_1 = 0.945m$ and $l_3 = 0.81m$ (stiff linkage)

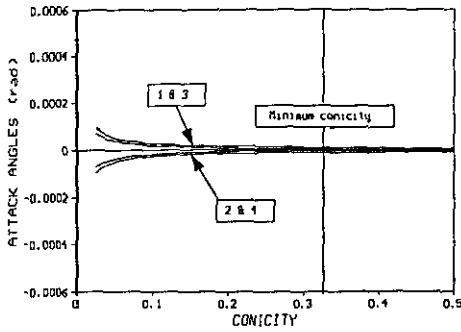
Figure 3.7 The wheelset attack angles, resultant creepages and lateral shifts of Model I when the geometric errors exist and $R = 200m$



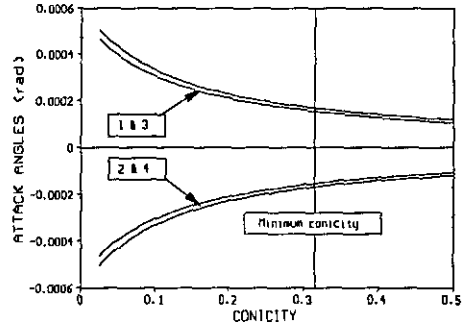
(a) wheelset attack angles of Model II when $l_1 = 0.99m$ (soft linkage)



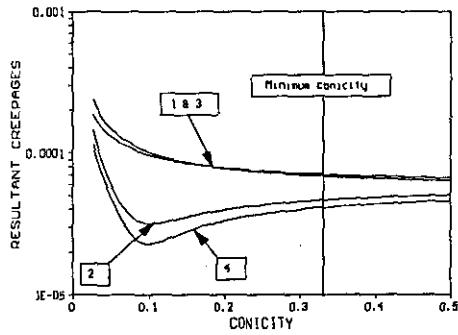
(b) wheelset attack angles of Model II when $l_1 = 0.99m$ (stiff linkage)



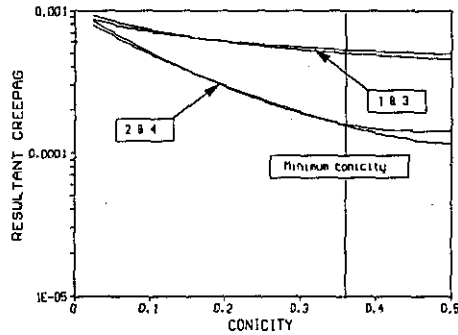
(c) wheelset attack angles of Model II when $l_1 = 0.845m$ (soft linkage)



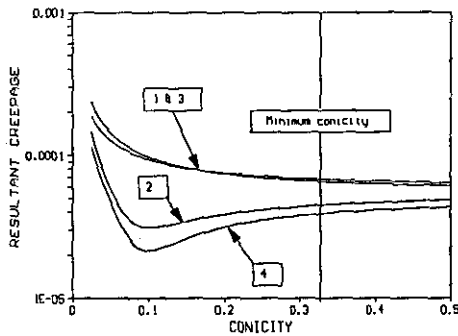
(d) attack angles of Model II when $l_1 = 0.845m$ (stiff linkage)



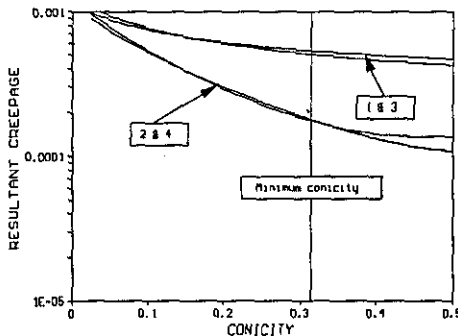
(e) resultant creepages of Model II when $l_1 = 0.99m$ (soft linkage)



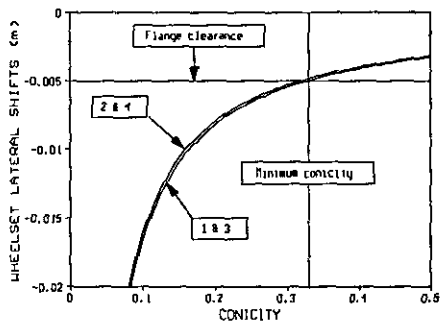
(f) resultant creepages of Model II when $l_1 = 0.99m$ (stiff linkage)



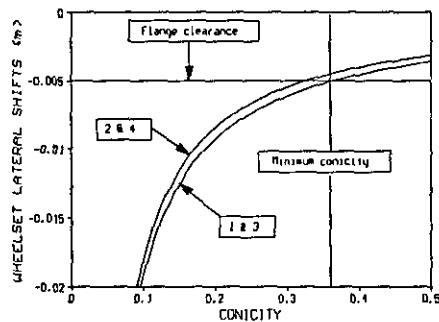
(g) resultant creepages of Model II when $l_1 = 0.845m$ (soft linkage)



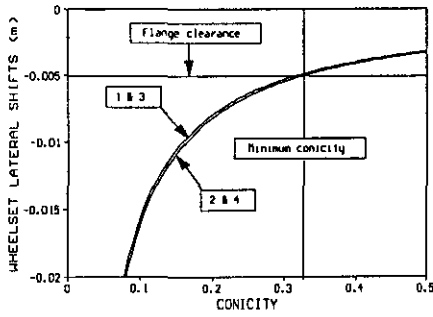
(h) resultant creepages of Model II when $l_1 = 0.845m$ (stiff linkage)



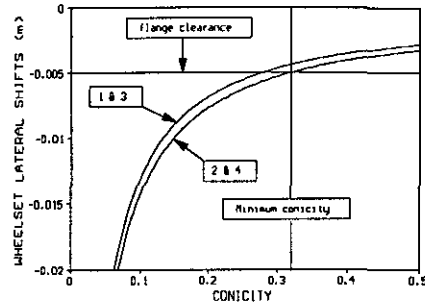
(i) wheelset lateral shifts of Model II when $l_1 = 0.99m$ (soft linkage)



(j) wheelset lateral shifts of Model II when $l_1 = 0.99m$ (stiff linkage)



(k) wheelset lateral shifts of Model II when $l_1 = 0.845m$ (soft linkage)



(l) wheelset lateral shifts of Model II when $l_1 = 0.845m$ (stiff linkage)

Figure 3.8 The wheelset attack angles, resultant creepages and lateral shifts of Model II when the geometric errors exist and $R = 200m$

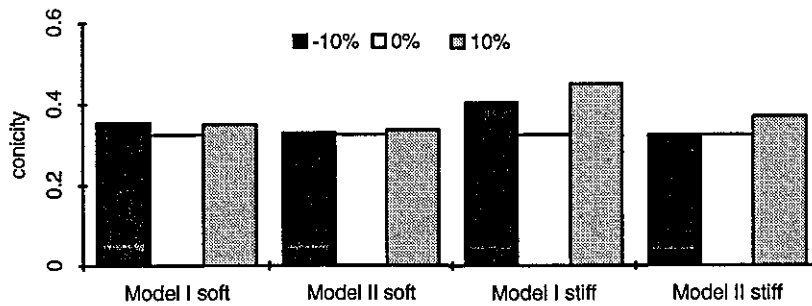


Figure 3.9 The necessary conicity to avoid flange contact

The steering linkage of Model II is roughly demonstrated in Fig.3.10 and is used to analyse the influence of geometric error on the wheelset attack angles. The dark solid lines in Fig.3.10 show the equilibrium positions of rigid bodies when there is no geometric error whilst the dash lines shows the equilibrium positions of rigid bodies when there is a geometric error. When there is no geometric error, each rigid body takes up its own radial position (a linear displacement a_1 for joint A, b_1 for joint B and c_1 for joint C), and then the linkage lever has an angle α_1 . When there is a geometric error ($l_1 = l_{10} + \Delta l_1$) in the lever, the relationships $a_2 = a_1$ and $\alpha_2 < \alpha_1$ are set up if the carbody is assumed as the motionless reference. The equations of $b_2 < b_1$ and $c_2 < c_1$ can be obtained. These equations mean that the elastic deformations of the springs connected to the wheelsets with the steering linkage lever become smaller when the geometric error exists. The forces caused by the elastic deformations of the springs are therefore reduced. To reach to the new equilibrium position, the outboard wheelset must have a negative (anticlockwise) attack angle while the inboard wheelset must have a positive (clockwise) attack angle, which is consistent with the simulation results in Fig.3.8b. It is easy to apply the analysis to other cases.

The above analyses about the effects of the geometric errors in the steering linkages on the vehicle curving also have a practical significance for other body-steered bogie vehicles. In body-steered bogie vehicles, the steering linkages are designed to reduce the forces produced by the bending stiffnesses in the suspensions due to curvature. The stiffness and geometry of the steering linkage will affect the steering mechanism. The analyses and results in this section can be applied to guide the design of the steering linkages for body-steered bogie vehicles.

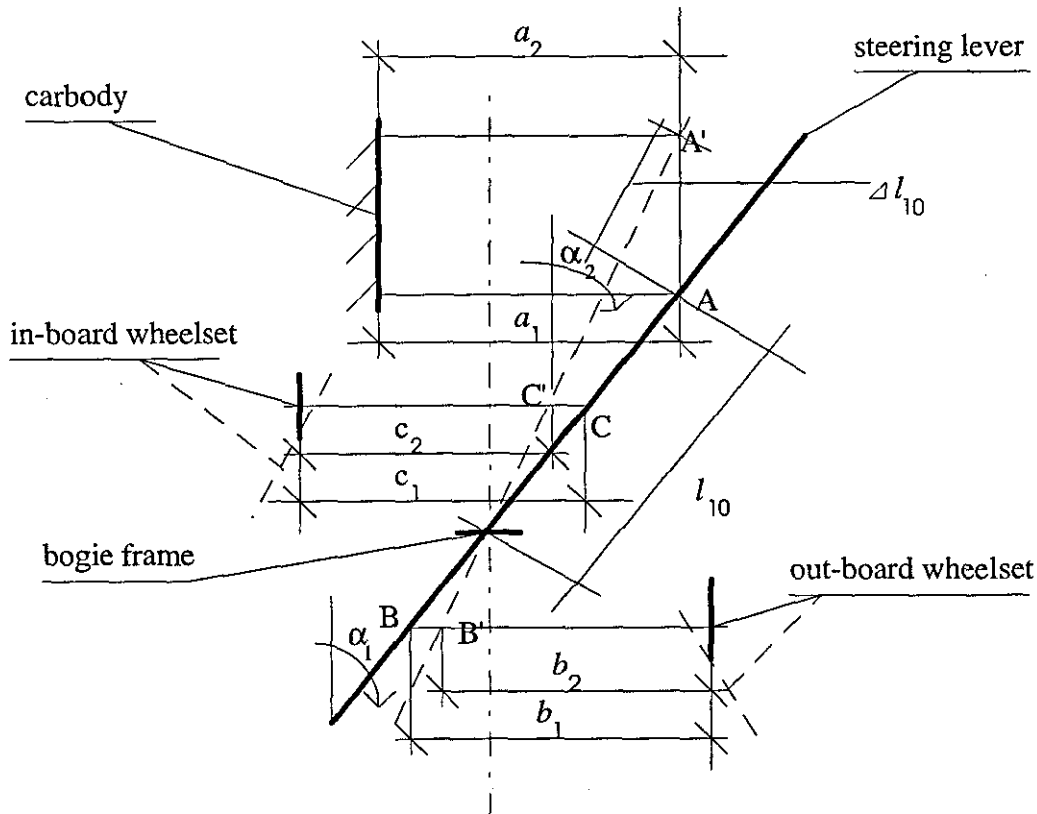


Figure 3.10 Diagram of the rigid bodies positions for the leading bogie of Model II when $l_1 = l_{10} + \Delta l_{10}$

3.4 Effects of Cant Deficiency

Eq.(2-15) shows that an unconstrained wheelset will have a yaw angle related to its radial position when cant deficiency exists ($\phi_d \neq 0$). For a whole vehicle, this movement will be transferred to other rigid bodies by its suspensions and/or steering linkages. Other rigid bodies may no longer take their radial alignment, and thus the relative yaw vector $\{\delta\psi\} \neq 0$ produces. Since the cant deficiency acts on every rigid body, the carbody and the bogie frames will move laterally, which may also cause the suspensions and linkages to deform, i.e. the relative displacement vector $\{\delta y\} \neq 0$.

The vehicle will finally reach to an equilibrium state and each rigid body of the vehicle will now be on a new position that corresponds to the cant deficiency. Perfect steering cannot be achieved if cant deficiency is non-zero.

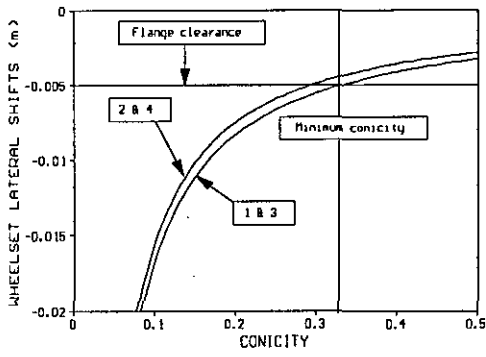
The effect of cant deficiency acts on any class of railway vehicles. The question that arises is whether perfect steering vehicles still have the advantages on accommodating cant deficiency over other classes of bogie vehicles. The most important point is whether perfect steering vehicles can still avoid flange contact when $\phi_d \neq 0$. Two extreme situations are considered in evaluating the capability of perfect steering vehicles with regard to accommodating cant deficiency, these being $\phi_d \neq -0.11\text{rad}$ (inboard cant deficiency) and $\phi_d \neq 0.053\text{rad}$ (outboard cant deficiency). The lateral displacements of the wheelsets are displayed in Fig.3.11 when the cant deficiencies are utilised in the calculation. Comparing these results with Fig.3.5, the alterations of the lateral movements of the wheelsets are not obvious and the alteration in the necessary conicity (in Fig.3.12) to avoid flange contact is very small, and it is thus possible for both models to avoid flange contact even if cant deficiency exists.

Although the wheelset attack angles of Model I and Model II become non-zero when cant deficiency exists, as shown in Fig.3.13, they are quite small. The following analysis can be used to explain this fact. When cant deficiency exists, the yaw angle of an unconstrained wheelset can be obtained from Eq.(2-15). We have

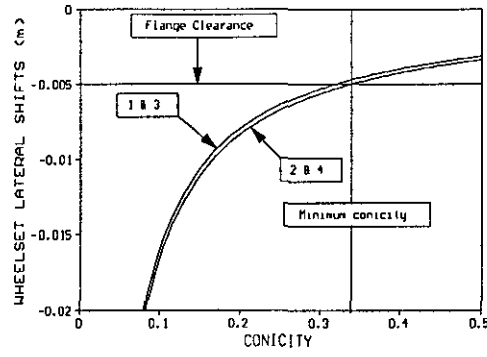
$$\hat{\psi}_w \approx -6.875 \times 10^{-5} \text{ when } \phi_d \neq -0.11\text{rad} \text{ and, } \hat{\psi}_w \approx 3.313 \times 10^{-5} \text{ when } \phi_d \neq 0.053\text{rad}$$

If the bogie frame is assumed as the reference, the relative yaw angle between the wheelset and bogie frame is $(\delta\psi + \Delta\psi)$, where $\delta\psi = \hat{\psi}_w$ and $\Delta\psi = a/R = 6.25 \times 10^{-3}$. It is obvious that $\Delta\psi \gg \delta\psi$. For the whole vehicle, the relative displacement vector that is $\{\Delta q + \delta q\}$ will cause the deformations in the suspensions and steering linkages and produce the elastic forces $\mathbf{E}\{\Delta q + \delta q\}$. In perfect steering vehicles, $\mathbf{F}_E = \mathbf{E}\{\Delta q\} = 0$, the displacements of the rigid bodies are produced only by the force $\mathbf{E}\{\delta q\}$ and thus are small even if cant deficiency is non-zero.

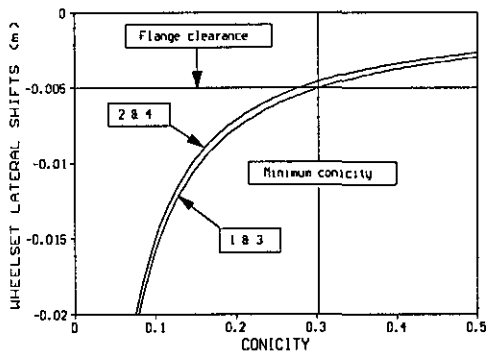
Since Model II has the inter wheelset stiffness k_{e3} , the differences between the wheelset attack angles of Model II are more sensitive to the system elasticity than those associated with Model I, as seen in Fig.3.13, which means that the equilibrium positions of perfect steering vehicles depend on the vehicle configuration and the system elasticity when $\phi_d \neq 0$.



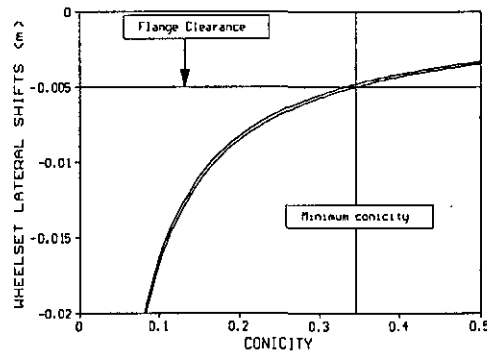
(a) Model I $\phi_d = -0.11$



(b) Model I $\phi_d = 0.053$



(c) Model II $\phi_d = -0.11$



(d) Model II $\phi_d = 0.053$

Figure 3.11 The lateral displacements of wheelsets when cant deficiency exists, stiff linkages, and $R = 200$ m

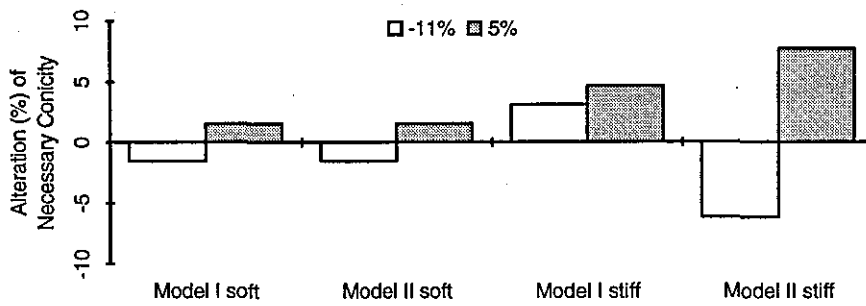
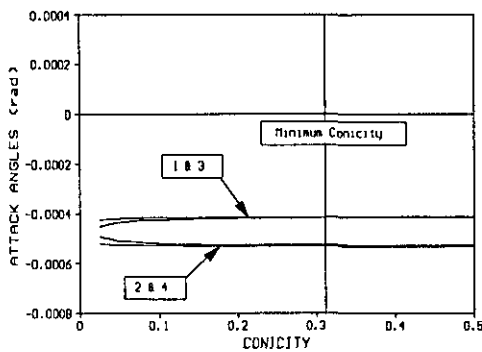
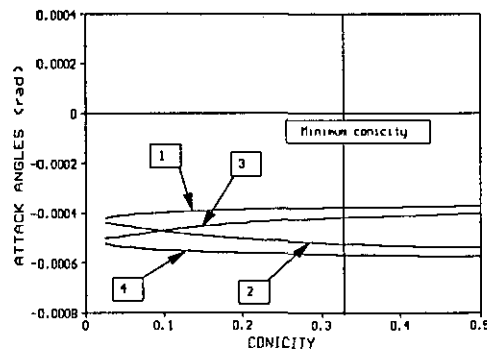


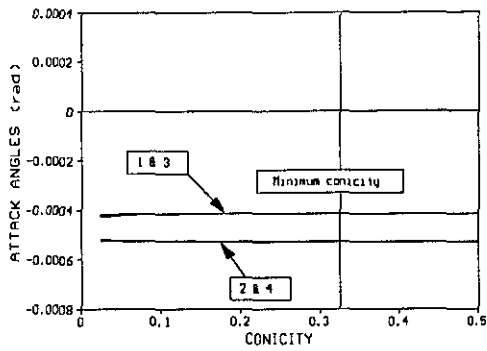
Figure 3.12 The alteration (%) of the necessary conicity when $\phi_d \neq -0.11$ and $\phi_d \neq 0.053$, $R = 200$ m



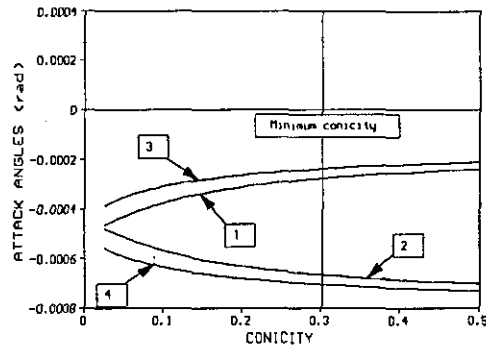
(a) Model I, soft linkage



(b) Model I, stiff linkage



(c) Model II, Soft linkage



(d) Model II, stiff linkage

Figure 3.13. The wheelset attack angles when $R = 200$ m, $\phi_d = -0.11$

3.5 Kinematic State of Perfect Steering Vehicles on a Cubic Parabola Transition

Since the curvature of the transition is not a constant, the relative displacement vector $\{\Delta q\}$ caused by the curvature is not constant, i.e. $\{\Delta q\} \neq \text{constant}$. The elastic force vector F_E defined by Eq.(2-23) cannot be zero on any transition curve even for perfect steering vehicles. To explore the effect of system elasticity on the steering ability associated with transition curves, the kinematic state is applied. The transition curve defined in Fig.2.3 is used in the calculation. In other words, the problem becomes finding the solution to solve the differential equation Eq.(2-24) along the transition. To simplify the matter, the cant deficiency on the transition is assumed to be zero. The solutions of Eq.(2-24) therefore reveal the influence of the curvature difference and the vehicle elasticity on the steering ability of perfect steering vehicles. The basic interest is the same as before, i.e. whether the perfect steering vehicles have flange contact in the transition.

Two values of conicity are used, these being $\lambda = 0.1$ and $\lambda = 0.3$. The lateral displacements and attack angles of the wheelsets are illustrated in Fig.3.14 (Model I) & Fig.3.15 (Model II) when Model I and Model II are on the transition. Flange contact certainly occurs in both perfect steering vehicles when the conicity $\lambda = 0.1$, whilst it can be avoided when $\lambda = 0.3$. If the conicity can rise as the wheelsets laterally move, it is possible for the perfect steering vehicles to avoid flange contact on the transition. In practice, the equivalent conicity usually rises as wheelsets laterally move[103].

The lateral displacements and the attack angles of the perfect steering vehicles on the transition are much smaller than those of the conventional bogie vehicle (as shown in Fig.3.16). The reason for this is that the curvature difference produces the relative

displacements $\{\Delta q\}$, but one of the functions of the steering linkages is to reduce the elastic forces caused by $\{\Delta q\}$. This function of the steering linkages is still effective whenever the relative displacements $\{\Delta q\}$ exist. Consider now the moments acting on the outboard wheelset in the leading bogie due to $\{\Delta q\}$ if the carbody is considered as the inertia reference. For Model I, this is:

$$M_{w\psi_0} = b^2 l_1 [(l_1 + l_2) \bar{\psi}_{bTL} - l_1 \bar{\psi}_{bwo}] k_{el}$$

and for the conventional bogie vehicle,

$$M_{w\psi_0} = (\bar{\psi}_{bTL} - \bar{\psi}_{bwo}) k_{pb}$$

where, the subscript b represents displacement related to the carbody. Since there are:

$$(l_1 + l_2) > l_1 \text{ and } \bar{\psi}_{bTL} < \bar{\psi}_{bwo}$$

we have

$$|(\bar{\psi}_{bTL} - \bar{\psi}_{bwo})| > |(l_1 + l_2) \bar{\psi}_{bTL} - l_1 \bar{\psi}_{bwo}|$$

The difference between $|(\bar{\psi}_{bTL} - \bar{\psi}_{bwo})|$ and $|(l_1 + l_2) \bar{\psi}_{bTL} - l_1 \bar{\psi}_{bwo}|$ can be very big. For example, when this outboard wheelset is 50m away from the curve starting point, i.e. $x = 50\text{m}$, referring to Fig.2.3, from Eq.(2-8), we have

$$\bar{\psi}_{bTL} = 0.0140531 \text{ and } \bar{\psi}_{bwo} = 0.0119498$$

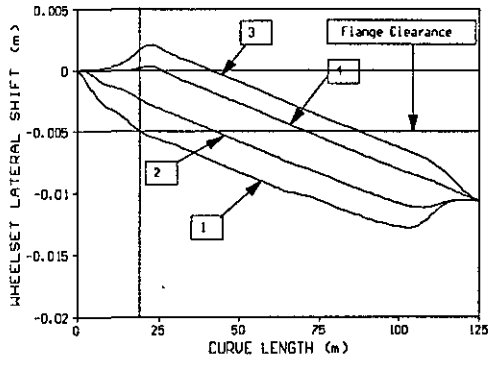
So,

$$|(\bar{\psi}_{bTL} - \bar{\psi}_{bwo})| = 2.1033 \times 10^{-3}$$

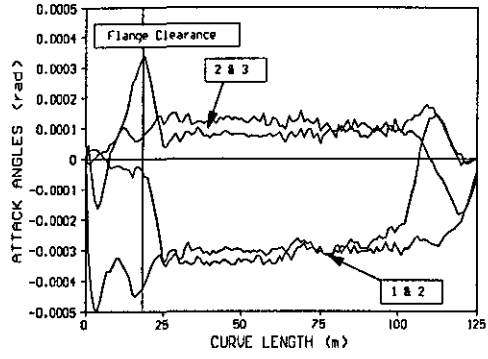
but,

$$|(l_1 + l_2) \bar{\psi}_{bTL} - l_1 \bar{\psi}_{bwo}| = 4.15995 \times 10^{-4}$$

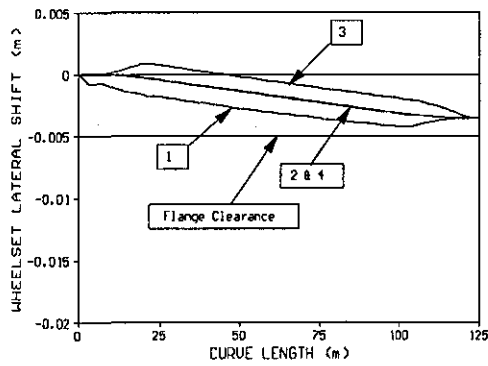
The analysis above shows that the moment acting on the outboard wheelset in the leading bogie of the conventional bogie vehicle is much greater than that of the perfect steering vehicles even if $k_{pb} = b^2 l_1 k_{el}$. The similar analysis can be applied to other rigid bodies and to Model II, and it can be found that the elastic force F_E caused by the curvature variation in transition curves in the perfect steering vehicles are much smaller than those in conventional bogie vehicles, and their capability of negotiating transitions is therefore better than that of conventional bogie vehicles.



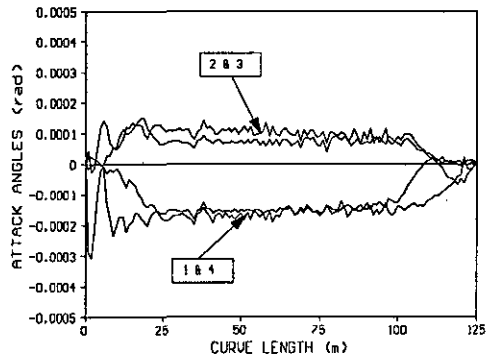
(a) wheelset lateral displacements, $\lambda = 0.1$



(b) attack angles, $\lambda = 0.1$

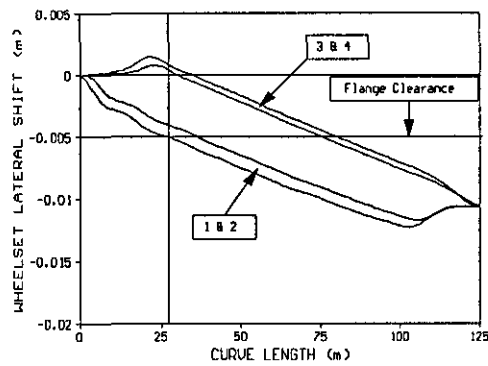


(c) wheelset lateral displacements, $\lambda = 0.3$

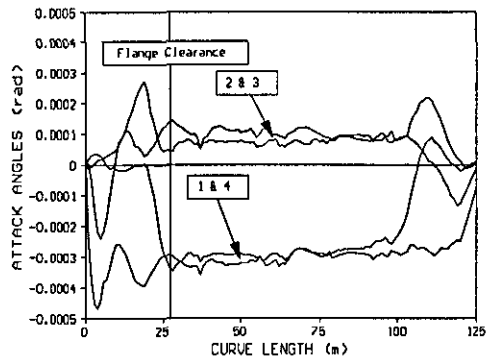


(d) attack angles, $\lambda = 0.3$

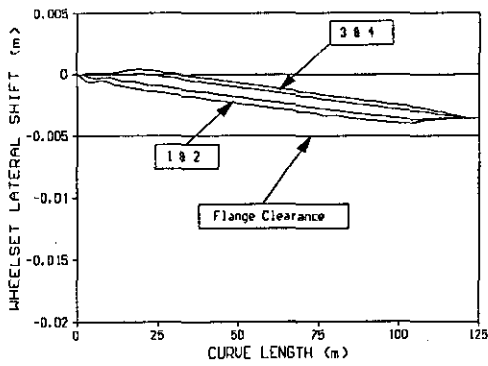
Figure 3.14 The lateral displacements and attack angles of the wheelsets when Model I is on the transition curve



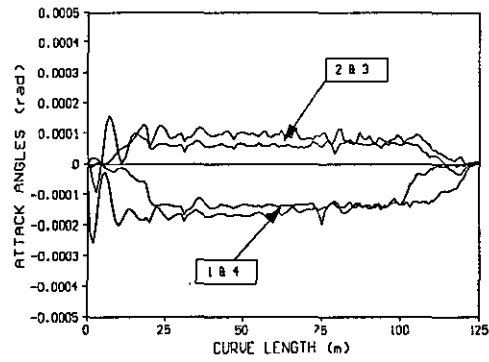
(a) wheelset lateral displacements, $\lambda = 0.1$



(b) attack angles, $\lambda = 0.1$

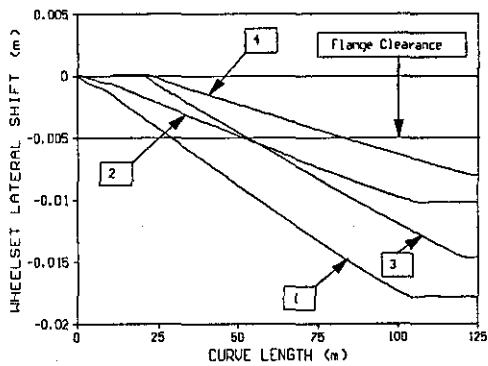


(c) wheelset lateral displacements, $\lambda = 0.3$

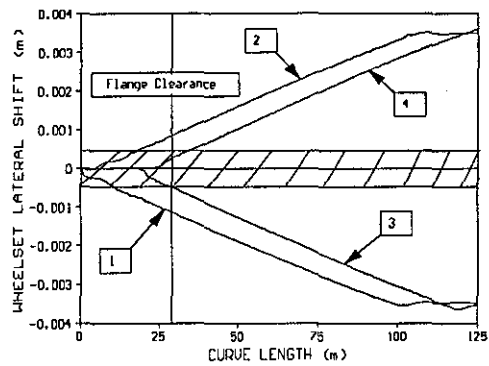


(d) attack angles, $\lambda = 0.3$

Figure 3.15 The lateral displacements and attack angles of the wheelsets when Model II is on the transition curve



(a) wheelset lateral displacements



(b) attack angles

Figure 3.16 The lateral displacements and attack angles of the wheelsets when the conventional vehicle is on the transition curve and $\lambda = 0.3$.

3.6 Summary

Several conclusions can be derived from the analysis and results above.

Since the curvature of a uniform curve is a constant, the relative displacement vector $\{\Delta q\} = \text{constant}$ is true. It is possible to design a linkage to eliminate the elastic forces in the vehicles caused by the curvature if there is no bending stiffness in their suspensions. To achieve this, all stiffnesses in the suspensions and linkages should not make any contribution to the bending stiffnesses.

The wheelsets of the perfect steering vehicles negotiate uniform curves as unconstrained wheelsets if the elastic force $F_E = 0$ and $\phi_d = 0$. This means that the wheelsets should be free as much as possible rather than input some steering mechanism to steer them. This conclusion has a very general significance for the

practice of body-steered bogie vehicles in which the steering linkages should be designed to minimise the elastic force vector F_E .

The wheelsets of the perfect steering vehicles roll on their pure rolling lines as soon as perfect steering is realised no matter what the vehicle configuration is and what the elasticity of the suspensions and steering linkages is. One of the conditions allowing perfect steering vehicles to achieve perfect steering is therefore to let the wheelsets roll on their pure rolling line. This distance between the pure rolling line and the track central line is determined by the curvature and the equivalent conicity, and should be smaller than the maximum flange clearance. In order to achieve perfect steering, the equivalent conicity of the perfect steering vehicles should be increased as the curvatures become larger, and thus a special design for wheel profile would be required for the applications of perfect steering vehicles in sharp curves (such as in underground railways and light railways).

The effects of cant deficiency and curvature variation on the steering ability of the perfect steering vehicles are much less than those of conventional bogie vehicles. Although cant deficiency and curvature variation will cause the attack angles in perfect steering vehicles, they do not much affect the lateral displacements of the wheelsets from the pure rolling lines. This advantage of perfect steering vehicles can much reduce the possibility of flange contact.

The advantages of Model I and Model II on curving over the conventional bogie vehicle are obvious. The capabilities of both perfect steering vehicles with regard to cant deficiencies and alignment on transitions are much better than those of the conventional bogie vehicle. The vehicle safety with regard to derailment and the reduction in the wear for both rails and wheels are therefore much improved upon.

The most significant factor affecting the steering ability of Model I and Model II is the geometric errors in their steering linkages, and thus the accuracy in the geometric parameters of the steering linkages is very important.

It should be noted again that the perfect steering linkages are unlikely to be arranged in the horizontal plane in practical applications.

These conclusions are based on the results and analyses in this chapter. They can be used to estimate the influences of the system elasticity on the curving of perfect steering vehicles, but the full understanding on the curving behaviour of perfect

steering vehicles depends on the dynamic responses of perfect steering vehicles on curves, which is a candidate for future research projects.

Table 3.1 The compatibility matrix of Model I

y_{w1}	Ψ_{w1}	y_{w2}	Ψ_{w2}	y_{w3}	Ψ_{w3}	y_{w4}	Ψ_{w4}	y_{TL}	Ψ_{TL}	ϕ_{TL}	y_{TR}	Ψ_{TR}	ϕ_{TR}	y_b	Ψ_b	ϕ_b
1	0	0	0	0	0	0	0	-1	$-a_1$	h_1	0	0	0	0	0	0
0	1	0	0	0	0	0	0	0	-1	0	0	0	0	0	0	0
0	0	0	0	0	0	0	0	0	0	-1	0	0	0	0	0	0
0	0	1	0	0	0	0	0	-1	a_2	h_1	0	0	0	0	0	0
0	0	0	1	0	0	0	0	0	-1	0	0	0	0	0	0	0
0	0	0	0	0	0	0	0	0	0	-1	0	0	0	0	0	0
0	0	0	0	1	0	0	0	0	0	0	-1	$-a_2$	h_1	0	0	0
0	0	0	0	0	1	0	0	0	0	0	0	-1	0	0	0	0
0	0	0	0	0	0	0	0	0	0	0	0	0	-1	0	0	0
0	0	0	0	0	0	1	0	0	0	0	-1	a_1	h_1	0	0	0
0	0	0	0	0	0	0	1	0	0	0	0	-1	0	0	0	0
0	0	0	0	0	0	0	0	0	0	0	0	0	-1	0	0	0
0	0	0	0	0	0	0	0	1	0	h_4	0	0	0	-1	$-l_1$	h_5
0	0	0	0	0	0	0	0	0	1	0	0	0	0	0	-1	0
0	0	0	0	0	0	0	0	0	0	1	0	0	0	0	0	-1
0	0	0	0	0	0	0	0	0	0	0	1	0	h_4	-1	l_2	h_5
0	0	0	0	0	0	0	0	0	0	0	0	1	0	0	-1	0
0	0	0	0	0	0	0	0	0	0	0	0	0	1	0	0	-1
0	$-g_1$	0	0	0	0	0	0	0	g_2	0	0	0	0	0	$-g_3$	0
0	0	0	g_4	0	0	0	0	0	$-g_5$	0	0	0	0	0	$-g_6$	0
0	0	0	0	0	g_4	0	0	0	0	0	0	$-g_5$	0	0	$-g_6$	0
0	0	0	0	0	0	0	$-g_1$	0	0	0	0	g_2	0	0	$-g_3$	0

Table 3.2 The compatibility matrix of Model II

y_{w1}	Ψ_{w1}	y_{w2}	Ψ_{w2}	y_{w3}	Ψ_{w3}	y_{w4}	Ψ_{w4}	y_{TL}	Ψ_{TL}	Φ_{TL}	y_{TR}	Ψ_{TR}	Φ_{TR}	y_b	Ψ_b	Φ_b
1	0	0	0	0	0	0	0	-1	$-a_1$	h_1	0	0	0	0	0	0
0	1	0	0	0	0	0	0	0	-1	0	0	0	0	0	0	0
0	0	0	0	0	0	0	0	0	0	-1	0	0	0	0	0	0
0	0	1	0	0	0	0	0	-1	a_2	h_1	0	0	0	0	0	0
0	0	0	1	0	0	0	0	0	-1	0	0	0	0	0	0	0
0	0	0	0	0	0	0	0	0	0	-1	0	0	0	0	0	0
0	0	0	0	1	0	0	0	0	0	0	-1	$-a_2$	h_1	0	0	0
0	0	0	0	0	1	0	0	0	0	0	0	-1	0	0	0	0
0	0	0	0	0	0	0	0	0	0	0	0	0	-1	0	0	0
0	0	0	0	0	0	1	0	0	0	0	-1	a_1	h_1	0	0	0
0	0	0	0	0	0	0	1	0	0	0	0	-1	0	0	0	0
0	0	0	0	0	0	0	0	0	0	0	0	0	-1	0	0	0
0	0	0	0	0	0	0	0	1	0	h_4	0	0	0	-1	$-l_1$	h_5
0	0	0	0	0	0	0	0	0	1	0	0	0	0	0	-1	0
0	0	0	0	0	0	0	0	0	0	1	0	0	0	0	0	0
0	0	0	0	0	0	0	0	0	0	0	1	0	h_4	-1	l_2	h_5
0	0	0	0	0	0	0	0	0	0	0	0	1	0	0	-1	0
0	0	0	0	0	0	0	0	0	0	0	0	0	1	0	0	0
0	$-g_1$	0	0	0	0	0	0	0	g_2	0	0	0	0	0	$-g_3$	0
0	0	0	g_4	0	0	0	0	0	$-g_5$	0	0	0	0	0	$-g_6$	0
0	g_7	0	g_8	0	0	0	0	0	$-g_9$	0	0	0	0	0	0	0
0	0	0	0	0	g_4	0	0	0	0	0	0	$-g_5$	0	0	$-g_6$	0
0	0	0	0	0	0	0	$-g_1$	0	0	0	0	g_2	0	0	$-g_3$	0
0	0	0	0	0	g_7	0	g_8	0	0	0	0	$-g_9$	0	0	0	0

Table 3.3 Stiffnesses and dampings of Model I

Stiffnesses:	Set 1	Set 2
primary lateral stiffness k_{py}	6 MN/m	5 MN/m
primary rolling stiffness $k_{p\phi}$	1 MN-m	1 MN-m
secondary lateral stiffness k_{sy}	0.1 MN/m	0.1 MN/m
secondary rolling stiffness $k_{s\phi}$	1 MN-m	1 MN-m
linkage stiffness k_{b1}	0.4 MN/m	2 MN/m
linkage stiffness k_{b2}	0.4 MN/m	2 MN/m
linkage stiffness k_{w1}	8.5 MN/m	60 MN/m
linkage stiffness k_{w2}	8.5 MN/m	60 MN/m
other stiffnesses	0	0
Dampings:		
primary rolling damping $c_{p\phi}$	10 KN-m-s	10 KN-m-s
secondary lateral damping c_{sy}	60 KN-s/m	60 KN-s/m
secondary rolling damping $c_{s\phi}$	60 KN-m-s	60 KN-m-s
other dampings	0	0

Table 3.4 Stiffnesses and dampings of Model II

Stiffnesses:	Set 1	Set 2
primary lateral stiffness k_{py}	8 MN/m	15 MN/m
primary rolling stiffness $k_{p\phi}$	1 MN-m	1 MN-m
secondary lateral stiffness k_{sy}	0.6 MN/m	0.3 MN/m
secondary rolling stiffness $k_{s\phi}$	1 MN-m	1 MN-m
linkage stiffness k_{b1}	0.12 MN/m	0.5 MN/m
linkage stiffness k_{w1}	5 MN/m	70 MN/m
linkage stiffness k_{w2}	5 MN/m	70 MN/m
other stiffnesses	0	0
Dampings:		
primary rolling damping $c_{p\phi}$	10 KN-m-s	10 KN-m-s
secondary lateral damping c_{sy}	60 KN-s/m	60 KN-s/m
secondary rolling damping $c_{s\phi}$	60 KN-m-s	60 KN-m-s
other dampings	0	0

Table 3.5 Stiffnesses and dampings of the conventional bogie vehicle

Stiffnesses:	
primary lateral stiffness k_{py}	40 MN/m
primary bending stiffness k_{pb}	60 MN-m
primary rolling stiffness $k_{p\phi}$	1 MN-m
secondary lateral stiffness k_{sy}	0.1 MN/m
secondary bending stiffness k_{pb}	1 MN-m
secondary rolling stiffness $k_{p\phi}$	1 MN-m
other stiffnesses	0
Dampings	
primary rolling damping $c_{p\phi}$	10 KN-m-s
secondary lateral damping c_{sy}	60 KN-s/m
secondary rolling damping $c_{s\phi}$	60 KN-m-s
other dampings	0

Table 3.6a Alteration (%) of k_{e1} when geometric errors exist in Model I

	-10%	-5%	0%	5%	10%
-10%	40.99	15.29	7.78	.86	-1.92
-5%	34.33	10.8	3.85	-2.59	-5.19
0%	27.97	6.44	0	-5.98	-9.98
5%	24.47	2.2	-3.75	-9.3	-13.75
10%	16.12	-1.89	-7.39	-12.55	-17.36

Table 3.6b Alteration (%) of k_{e2} when geometric errors exist in Model I

	-10%	-5%	0%	5%	10%
-10%	23.46	16.42	9.86	3.76	-1.92
-5%	17.22	10.8	4.81	-.8	-5.19
0%	11.33	5.49	0	-5.15	-9.98
5%	5.79	.46	-4.56	-9.3	-13.75
10%	0.57	-4.26	-8.89	-13.24	-17.36

Table 3.7 Alteration (%) of k_{e1} when geometric errors exist in Model II

	-10%	-5%	0%	5%	10%
-10%	2.02	0.81	-0.43	-1.07	-2.96
-5%	2.49	1.22	0	-1.28	-2.58
0%	2.51	1.27	0	-1.29	-2.59
5%	2.08	0.84	-0.43	-1.71	-3.0
10%	1.22	-0.01	-1.26	-2.54	-3.83

Table 3.8 Elastic forces F_E caused by geometric errors in the steering linkages

	Model I $l_1 = 1.155, l_3 = 0.99$	Model I $l_1 = 0.945, l_3 = 0.81$	Model II $l_1 = 0.99$	Model II $l_1 = 0.81$
$M_{\psi w1}$	- 10.9576 KN	19.2213 KN	- 4.7843 KN	4.2398 KN
$M_{\psi w2}$	15.7828 KN	- 16.4374 KN	4.7843 KN	- 4.2398 KN
$M_{\psi w3}$	- 15.7828 KN	16.4374 KN	- 4.7843 KN	4.2398 KN
$M_{\psi w4}$	10.9576 KN	- 19.2213 KN	4.7843 KN	- 4.2398 KN
$M_{\psi TL}$	- 1.2743 KN	- 8.4033 KN	- 1.0362 KN	1.3249 KN
$M_{\psi TR}$	1.2743 KN	8.4033 KN	1.0362 KN	- 1.3249 KN
$M_{\psi b}$	0	0	0	0

STABILITY OF PERFECT STEERING BOGIE VEHICLES

The steering mechanisms of Model I and Model II as well as their advantages in curving over conventional bogie vehicles were studied in the previous chapter. In order to achieve perfect steering, not only must the bending stiffnesses of perfect steering vehicles be eliminated, but also their steering linkages ought to satisfy certain conditions. These factors will promote some new problems with regard to stability that do not occur in other classes of bogie vehicles. This chapter will investigate the stability of Model I and Model II with special regard to the instabilities, and the effects of system elasticity and damping on the stability.

4.1 Stability Criteria [104-105]

By applying the Laplace transform to a linear system, its *Eigen-Equation* can be expressed as:

$$\sum_{i=0}^n p_i s^i = 0 \quad (4-1)$$

where, $n/2$ is the number of degrees of freedom.

If the system's number of degrees of freedom is not beyond a manageable quantity, the system stability can be analysed by theoretical criteria expressed via equations. The criterion of Routh[104] is used in this chapter to decide upon system stability, which is that when $n = 3$, the necessary and sufficient conditions for a stable system are:

$$p_2 > 0, p_1 > 0, p_0 > 0, \Delta_2 = p_1 p_2 - p_3 p_0 > 0 \quad \text{if } p_3 > 0 \quad (4-2a)$$

and when $n = 4$, the necessary and sufficient conditions for a stable system are:

$$p_3 > 0, p_2 > 0, p_1 > 0, p_0 > 0, \Delta_3 = p_1 p_2 p_3 - p_1^2 p_4 - p_3^2 p_0 > 0 \quad (4-2b) \\ \text{if } p_4 > 0$$

If the Eigen-Equation Eq.(4-1) is a real equation, there are three ways in which a transition from stability to instability can occur[104]:

- 1) A real root can cross from the left to the right half of the s -plane by moving along the real axis and passing through the origin;
- 2) A root can cross from the left to the right half-plane as a result of its real part jumping from $-\infty$ to $+\infty$;
- 3) A pair of conjugate complex roots having negative real parts can become conjugate imaginary roots and then move into the right half-plane as conjugate complex roots having positive real parts.

A system is on a stability boundary of the first kind if $p_0 = 0$ and all the remaining stability conditions are satisfied; for when $p_0 = 0$, $s = 0$ is obviously a root of Eq.(4-1). A system is on a stability boundary of the second kind if $p_n = 0$ and all the remaining stability conditions are satisfied; for when $p_n = 0$, it is obvious that one root of Eq.(4-1) tends to infinity. It can be proved[104] that a system is on a stability boundary of third kind if $\Delta_{n-1} = 0$, where Δ_{n-1} is the Routh's array, and all the remaining stability conditions are satisfied.

If $p_0 < 0$ and all the remaining stability conditions are satisfied, there is at least one positive real root for Eq.(4-1), and thus the system will be divergent unstable, whilst the system is going to be unstable in an oscillatory manner if $\Delta_{n-1} > 0$ becomes $\Delta_{n-1} < 0$ and all the remaining stability conditions are satisfied. The condition $p_0 > 0$ is therefore used to examine the divergent instability of a system, while the condition $\Delta_{n-1} > 0$ is used to inspect its oscillatory instability if all other stability conditions are satisfied.

When the system's number of degrees of freedom is too large, it is impossible to apply theoretical criteria as defined by equations in order to determine the system stability. The most convenient method of studying the system stability is to apply a numerical method in finding the eigenvalues of Eq.(4-1). The modes of stability and instability are defined by Table 4.1, where the impulse response correspondent to eigenvalue is illustrated. Only asymptotically stable modes are considered as stable in this thesis because it is difficult to decide marginally stable modes in the numerical calculation due to the accuracy of numerical solutions. Indeed, marginally unstable modes are not real cases in a railway vehicle system because of nonlinear factors, and therefore, the necessary and sufficient conditions for a railway vehicle to be stable in numerical solutions are:

$$\text{Real } (\lambda) < 0 \tag{4-3}$$

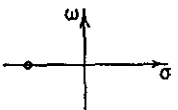
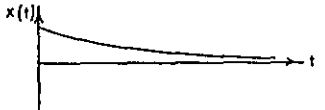
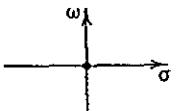
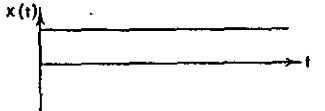
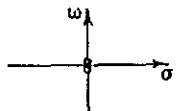
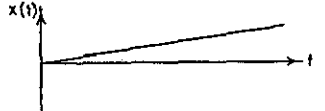
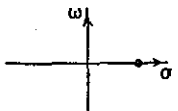
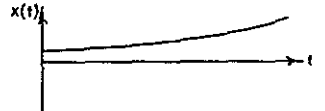
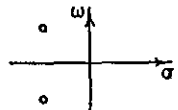
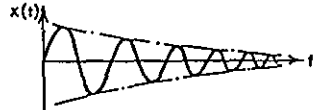
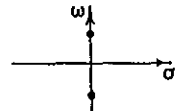
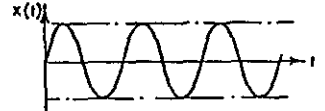
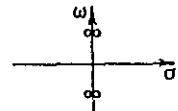
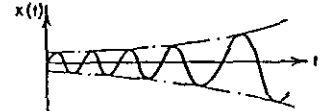

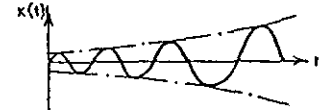
Referring to Eq.(2-17), the Eigen-Equation of a railway vehicle is defined by:

$$|\lambda I - J| = 0 \tag{4-4}$$

where,

$$J = \begin{bmatrix} 0 & I \\ -M^{-1}(G+C) & -M^{-1}(N+E) \end{bmatrix} \tag{4-5}$$

Table 4.1 The definitions of stable and unstable modes[104]

	Location of characteristic roots in s-plane	Impulse response	
1			ASYMPTOTICALLY STABLE
2			MARGINALLY STABLE
3			UNSTABLE
4			UNSTABLE
5			ASYMPTOTICALLY STABLE
6			MARGINALLY STABLE
7			UNSTABLE
8			UNSTABLE

4.2 Eigenvalues of Bogie Vehicles

For a bogie vehicle defined by Eq.(2-17), Eq.(4-4) produces seventeen pairs of eigenvalues that are illustrated in Fig.4.1 as functions of vehicle speed. Each eigenvalue is represented by two curves (one for real part and another for imaginary part) with the same mark in the same diagram. The unit of imaginary parts of eigenvalues in Fig.4.1 is frequency f (1/s).

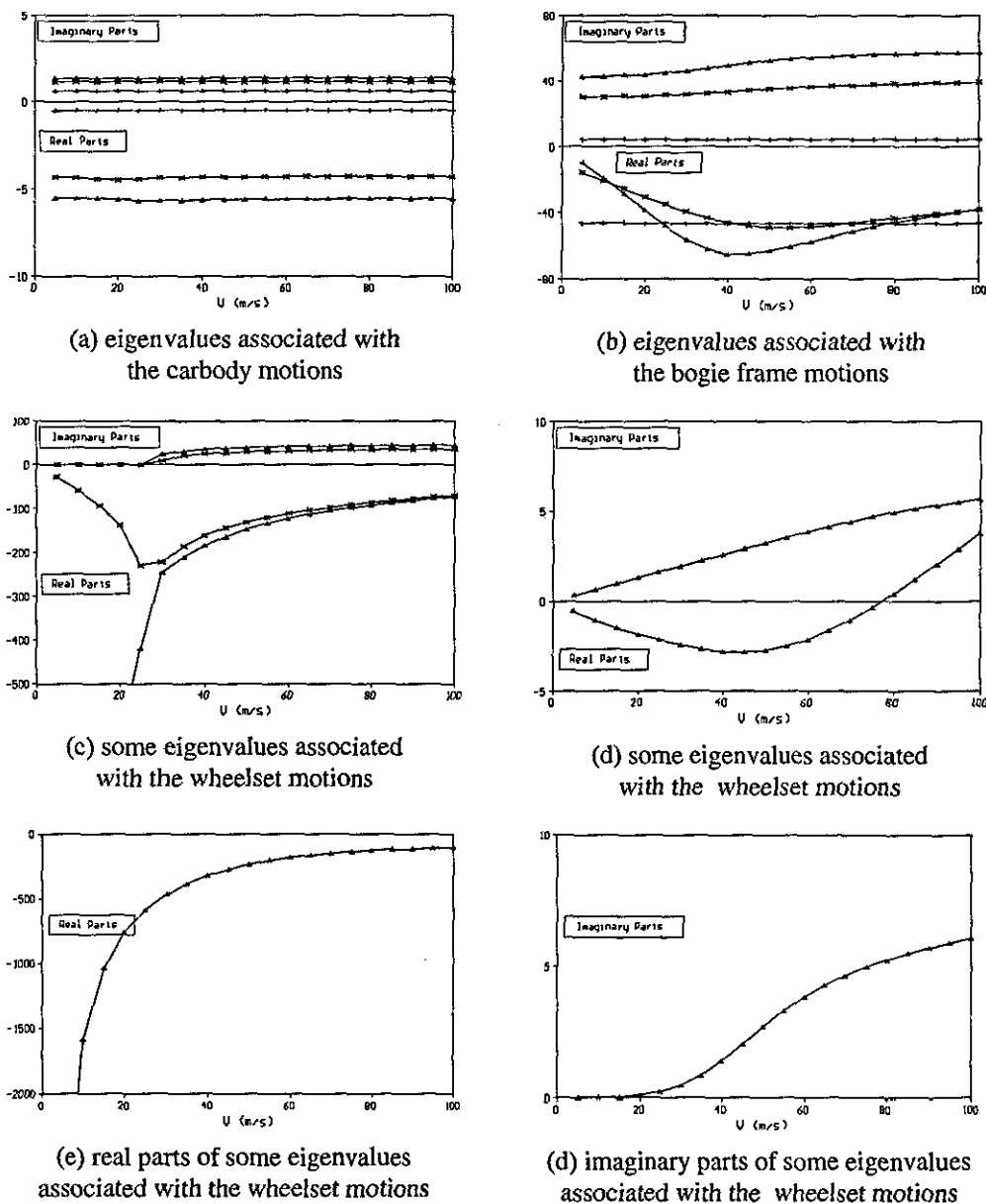


Figure 4.1 Eigenvalues of the conventional bogie vehicle as function of speed, $\lambda = 0.2$

Three pairs of eigenvalues with small frequencies and small absolute real parts have a little alteration versus the vehicle speed. These three eigenvalues are mainly

associated with the carbody motions, as illustrated in Fig.4.1a. Since this conventional bogie vehicle is fore-and-aft symmetric with regard to elasticity, the performance of the leading bogie and the trailing bogie with regard to stability should be very similar. The eigenvalues mainly linked with the bogie motions are illustrated in Fig.4.1b, where each pair of curves stands for two eigenvalues, giving six pairs of the eigenvalues in this diagram. Another eight eigenvalues mainly associated with wheelset motions are displayed in Fig.4.1c-f where each pair of curves represents two eigenvalues. Four of the eight eigenvalues as displayed in Fig.4.1c have very large negative real parts and their imaginary parts are zero when the vehicle speed is low, while other four of the eight eigenvalues associated with the wheelset motions have the frequencies that are close to the kinematic frequency $\omega = 2\pi f = v_0 \sqrt{\lambda/a_0 r_0}$ [5] of unconstrained wheelset, as shown in Fig.4.1d&f. Two of the eigenvalues with frequencies close to the kinematic frequency have the real parts that become positive as the vehicle velocity increases, as seen in Fig.4.1d, and other two eigenvalues of which real parts and imaginary parts are separately displayed in Fig.4.1e&f have the big negative real parts as seen in Fig.4.1e. The results in Fig.4.1 indicate that the instabilities of this vehicle are mainly associated with the wheelset motions.

If the inter wheelset shear stiffness is zero, the sub-elasticity matrix E_T of a bogie can be written as:

$$E_T = \begin{bmatrix} y_{w1} & \Psi_{w1} & y_{w2} & \Psi_{w2} & y_T & \Psi_T & \phi_T \\ \times & 0 & 0 & 0 & \times & \times & \times \\ 0 & k_1 & 0 & k_2 & 0 & -k_1 & 0 \\ 0 & 0 & \times & 0 & \times & \times & \times \\ 0 & k_2 & 0 & k_3 & 0 & -k_3 & 0 \\ \times & 0 & \times & 0 & \times & \times & \times \\ \times & -k_1 & \times & -k_3 & 0 & (k_1 + k_3 + \times) & 0 \\ \times & 0 & \times & 0 & 0 & 0 & 0 \end{bmatrix} \quad (4-6)$$

where, \times presents non-zero elements.

For a conventional bogie vehicle, $k_1 = k_3 = k_{pw}$ and $k_2 = 0$ if there is no direct connection between the outboard and inboard wheelsets. For Model I and Model II, k_1 , k_2 ($=0$ for Model I) and k_3 are contributed by the steering linkages. This indicates that the effective stiffnesses of the steering linkages are at the positions of the primary yaw stiffness of the conventional bogie in the elastic sub-matrix E_T , which means that the steering linkages provide the constraints for wheelset and

bogie yaw motions. From this point, the effects of the effective stiffnesses in the linkages on the stability can be considered equivalent to those of the primary yaw stiffness in conventional bogie vehicle.

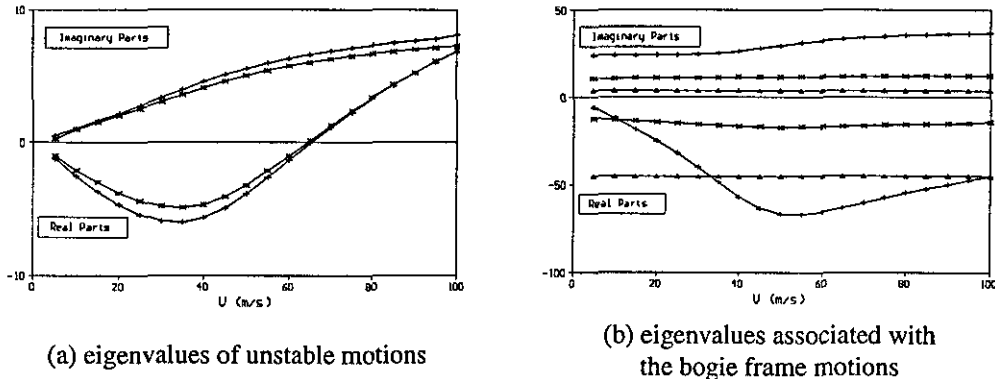


Figure 4.2 Some of eigenvalues of Model I as function of speed, $\lambda = 0.2$, stiff linkage

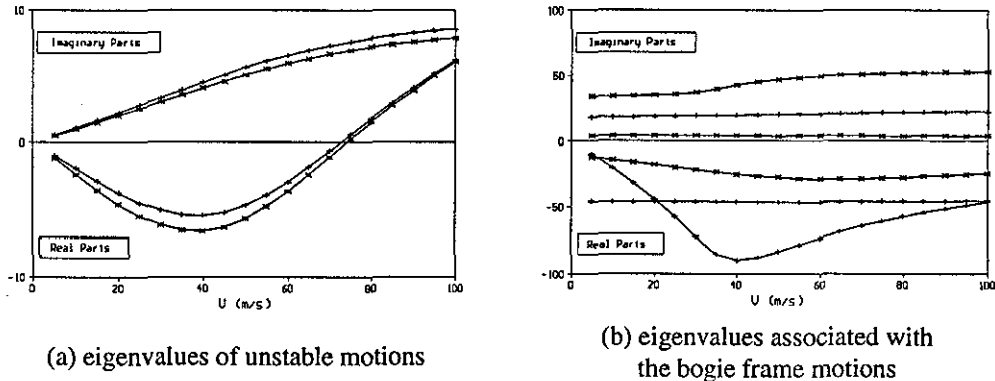


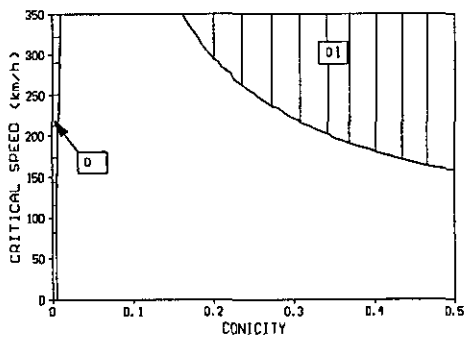
Figure 4.3 Some of eigenvalues of Model II as function of speed, $\lambda = 0.2$ and stiff linkage

Some of the eigenvalues of perfect steering vehicles are displayed in Fig.4.2 (Model I) and in Fig.4.3 (Model II) separately when the wheelset conicity $\lambda = 0.2$ (the parameters of Set 2 in Table 3.3 and Table 3.4 being used in these figures). The eigenvalues in Fig.4.2a and Fig.4.3a are associated with the wheelset motions since their frequencies close to the kinematic frequency of wheelset. The tendency of the eigenvalues of wheelset in Fig.4.2a and Fig.4.3a is similar to that in Fig.4.1d while the eigenvalues of the bogie motions in Fig.4.2b and Fig.4.3b are consistent with the results in Fig.4.1b. This indicates that the stability of the perfect steering vehicles well matches that of conventional bogie vehicles when conicity $\lambda = 0.2$. The eigenvalues associated with the kinematic frequency of wheelset in Model I and Model II are slightly different from those of the conventional bogie vehicle. These two eigenvalues in Model I and Model II are slightly split, which implies that one of the bogies is more stable than the other. The reason for this is that the bogies are

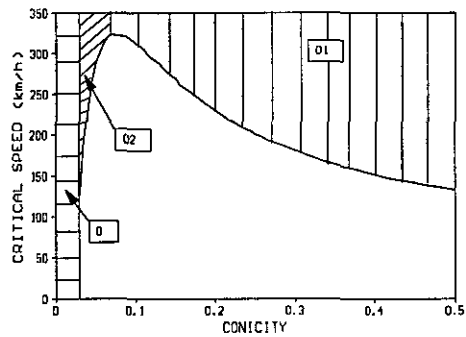
not symmetric with regard to elasticity due to elasticity of the outboard wheelset not being equal to that of the inboard wheelset when the steering linkages exist. The difference of stability between the leading bogie and the trailing bogie has been noted and explained by Wickens[7,25] when the elasticity of the bogie is asymmetric, and this fact will be studied further in this chapter.

4.3 Instability Modes of the Perfect Steering Vehicles

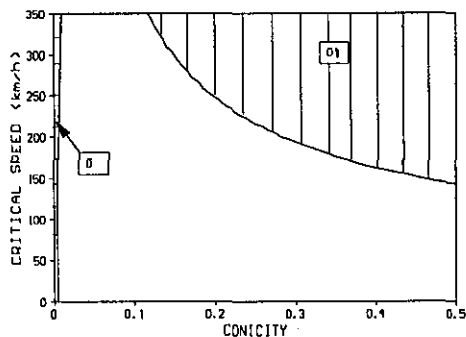
The various instabilities of Model I and Model II are shown in Fig.4.4 where the critical speed is a function of conicity. Both Model I and Model II will be unstable if the conicity is less than a certain value, as is seen in Fig.4.4, and this physical phenomenon is called low conicity instability. There are two instabilities associated with low conicity: when the conicity is very low, the critical speed is close to zero, and thus this instability is called low speed instability that is labelled by D in Fig.4.4; and then the critical speed will increase as the conicity rises when the conicity is in the range indicated by O2 in Fig.4.4, and the instability in O2 is called dynamic instability in low conicity since the critical speed is much greater than zero. The critical speed in the area marked by O1 in Fig.4.4 decreases as the conicity increases, and the instability in O1 is called conventional instability that also occurs in conventional bogie vehicles.



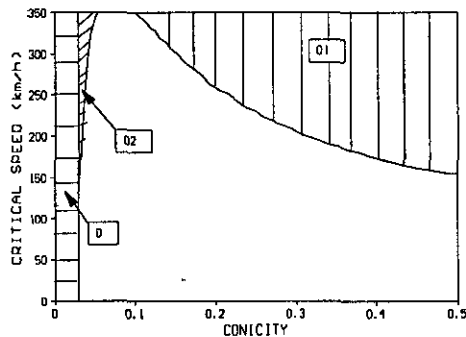
(a) Model I, soft linkage



(b) Model I, stiff linkage



(c) Model II, soft linkage

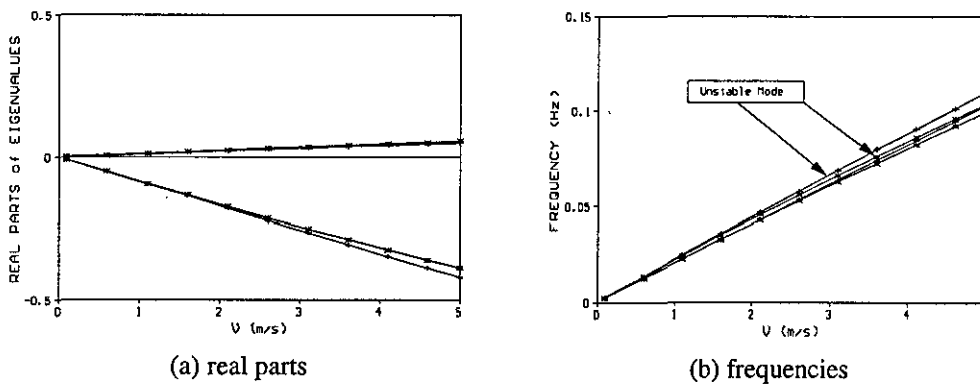


(d) Model II, stiff linkage

Figure 4.4 The critical speed (as function of conicity) of perfect steering vehicles

4.3.1 Low Speed Instability in Low Conicity

When the conicity is very low, instability occurs and the critical speed is very low, as is shown in Fig.4.5. The results in Fig.4.5 show that the frequencies of low speed instability are very close to the kinematic frequency $\omega = 2\pi f = v_0 \sqrt{\lambda/a_0 r_0}$ of unconstrained wheelset, which indicates that the low speed instability of Model I and Model II is associated with the wheelset motions. Low speed instability can be either static (divergent) or oscillatory since the wave length $\frac{v_0}{\omega} = \sqrt{a_0 r_0 / \lambda}$ of this motion is not zero even when $\omega \rightarrow 0$ and $v_0 \rightarrow 0$. Another feature of low speed instability is that only one of these eigenvalues throughout each perfect steering vehicle has a positive real part, which implies that low speed instability only occurs in one of the bogies.



(a) real parts
 (b) frequencies
 Figure 4.5 The wheelset eigenvalues as function of speed when conicity $\lambda = 0.02$, * -- Model I, + -- Model II

4.3.2 Dynamic Instability in Low Conicity

The eigenvalues of unstable motions are illustrated in Fig.4.6 when $\lambda = 0.04$. The frequencies of these motions in each perfect steering vehicle are very close to those illustrated in Fig.4.1, which means that the motions represented by the eigenvalues are the same in both types of vehicle. Since the frequencies of these motions are close to the kinematic frequency of wheelset, the unstable motions are associated with the wheelset motions. The difference between each perfect steering vehicle and the conventional bogie vehicle exists in the real parts of the associated eigenvalues. In the conventional bogie vehicle (Fig.4.6a), the real parts of the two eigenvalues are very close, which means that the performance in stability of both the leading and trailing bogies is very similar. In each perfect steering vehicle (Fig.4.6c), the real parts of the two eigenvalues split as the speed increases, which

means that one of the bogies turns unstable while another becomes more stable. It has also found that dynamic instability in low conicity disappears if the steering linkages are too stiff or too soft, which will be studied further in section 4.5. Since low speed instability and dynamic instability in low conicity both happen in low conicity, the term low conicity instability includes both of them.

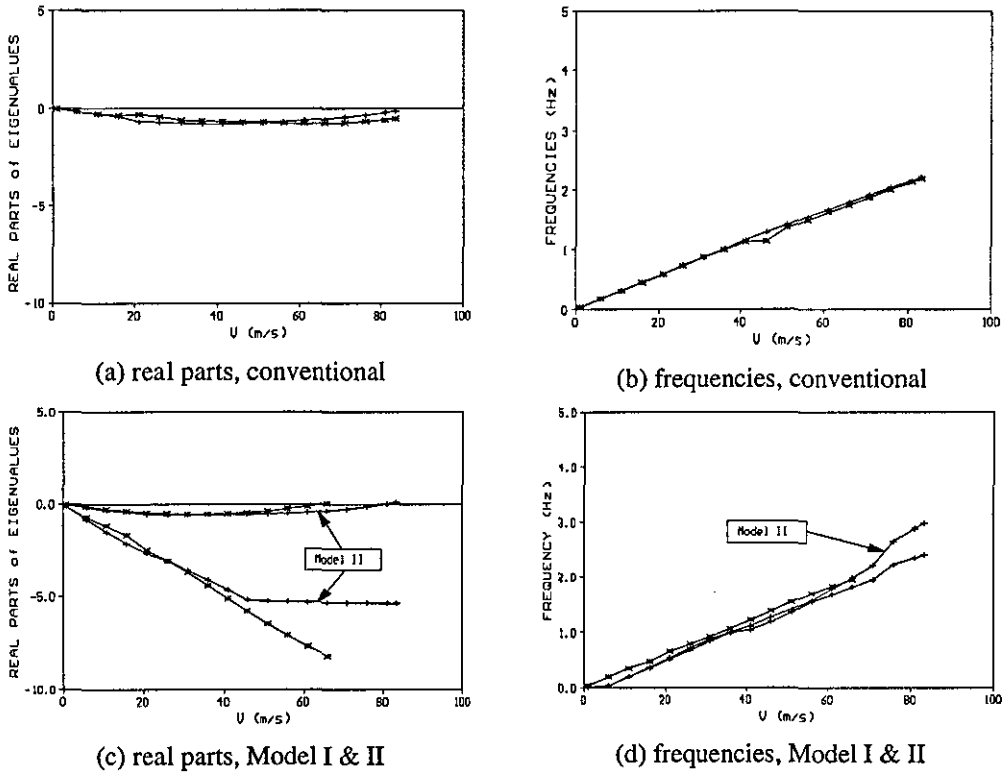


Figure 4.6 The eigenvalues (as function of speed) associated with the wheelset motions when $\lambda = 0.04$

4.3.3 Conventional Instability

The critical speed of the perfect steering vehicles decreases as the conicity increases in conventional instability, as seen in Fig.4.4. The eigenvalues of the unstable motions are displayed in Fig.4.2a (for Model I) and Fig.4.3a (for Model II) when conicity $\lambda = 0.2$. Since the frequencies of the motions approximate to the kinematic frequency of wheelset, the unstable modes are related to the wheelset motions. The real parts of the two pairs of eigenvalues are very close, which means that the performance of the leading bogie in conventional stability is similar to that of the trailing bogie in Model I and Model II. The fundamental difference between dynamic instability in low conicity and conventional instability, therefore, is that only one of the bogies is unstable in dynamic instability in low conicity whilst both bogies are unstable in conventional instability. The conventionally unstable mode occurs in

any class of bogie vehicle and has been well studied[67-74]. In this chapter, the mechanism of conventional instability is, therefore, not included, but the influences of steering linkage elasticity on the conventional instability of Model I and Model II will be investigated in section 4.5.

4.4 Theoretical Analysis of Low Conicity Instability

Bell and Hedrick[12] as well as Smith, Anderson and Fortin[15-16,19] have studied low conicity instability of body-steered bogie vehicles in 1980's, and more recent contribution has been made by Wickens[28] when he investigated the stability of one kind of perfect steering vehicle. This section applies the stability criteria on bogie sub-systems and theoretically explores the mechanism of low conicity instability for perfect steering vehicles.

4.4.1 Bogie Sub-Systems

When the vehicle forward speed is low, the carbody can be considered as the inertia reference. Since the primary suspension is stiff, the wheelsets can be assumed to be pinned to the bogie frames. It is also assumed that the roll motions are very small and can be ignored. Using these assumptions, the bogies of Model I and Model II can be simplified to those as shown in Fig.4.7. Smith, Anderson and Fortin[15,19] assumed that the bogie frames were pinned to the carbody, and thus there were only three degrees of freedom in their bogie sub-system, these being the wheelset yaws (Ψ_{wo}, Ψ_{wi}) and bogie frame yaw (Ψ_T). For most bogie vehicles, however, the secondary suspension exists and is very soft, and the bogie frames can thus have a large lateral movement related to the carbody as compared with its yaw motion. Wickens[28] has considered this lateral motion (y_T) of the bogie frame in his bogie sub-system, and thus there are four degrees of freedom in his model. In this sub-section, both the bogie sub-systems are used to study low conicity instability of Model I and Model II.

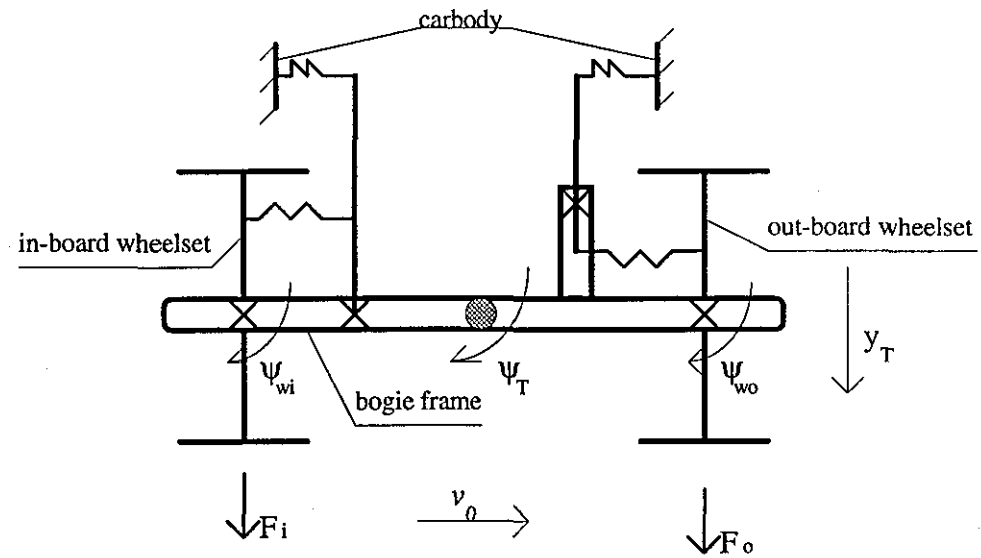
Referring to Fig.4.7, the lateral displacements of the wheelsets in the models are defined by:

For the bogie sub-system with three degrees of freedom

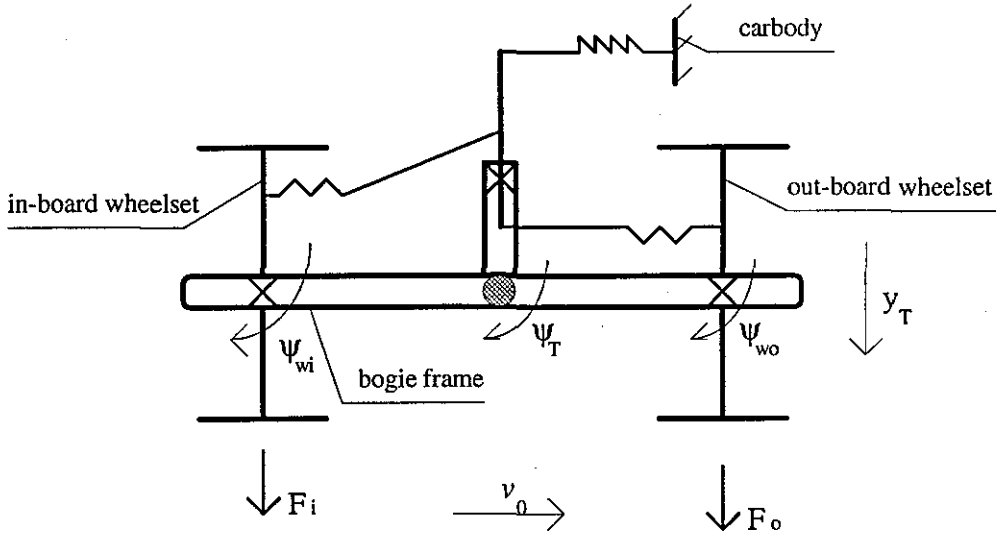
$$y_{wo} = a \Psi_T \quad \text{and} \quad y_{wi} = -a \Psi_T \quad (4-7a)$$

For the bogie sub-system with four degrees of freedom

$$y_{wo} = a \Psi_T + y_T \quad \text{and} \quad y_{wi} = -a \Psi_T + y_T \quad (4-7b)$$



(a) simplified bogie model for Model I



(b) simplified bogie model for Model II

Figure 4.7 Simplified bogie models

The lateral creepage forces F_o and F_i are therefore determined by:

For the bogie sub-system with three degrees of freedom

$$\begin{aligned}
 F_{wo} &= -\left(\frac{2f_{22}}{v_0} \dot{y}_{wo} - 2f_{22} \psi_{wo}\right) = -\left(\frac{2f_{22}}{v_0} a \dot{\psi}_T - 2f_{22} \psi_{wo}\right) \\
 F_{wi} &= -\left(\frac{2f_{22}}{v_0} \dot{y}_{wi} - 2f_{22} \psi_{wi}\right) = -\left[\frac{2f_{22}}{v_0} (-a \dot{\psi}_T) - 2f_{22} \psi_{wi}\right] \quad (4-8a)
 \end{aligned}$$

For the bogie sub-system with four degrees of freedom

$$\begin{aligned} F_{w_o} &= -\left[\frac{2f_{22}}{v_0} (a\dot{\Psi}_T + y_T) - 2f_{22} \Psi_{w_o}\right] \\ F_{w_i} &= -\left[\frac{2f_{22}}{v_0} (-a\dot{\Psi}_T + y_T) - 2f_{22} \Psi_{w_i}\right] \end{aligned} \quad (4-8b)$$

For Model I, the dynamic equations of the bogie sub-system with four degrees of freedom are:

$$\begin{aligned} I_w \ddot{\Psi}_{w_o} + \frac{2a_0^2 f_{11}}{v_0} \dot{\Psi}_{w_o} + \frac{2a_0 f_{11} \lambda}{r_0} y_{w_o} + k_1 \Psi_{w_o} - k_2 \Psi_T &= 0 \\ I_w \ddot{\Psi}_{w_i} + \frac{2a_0^2 f_{11}}{v_0} \dot{\Psi}_{w_i} + \frac{2a_0 f_{11} \lambda}{r_0} y_{w_i} + k_3 \Psi_{w_i} - k_4 \Psi_T &= 0 \\ I_T \ddot{\Psi}_T + k_5 \Psi_T - k_2 \Psi_{w_o} - k_4 \Psi_{w_i} &= aF_{w_o} - aF_{w_i} \\ m_T \ddot{y}_T &= F_{w_o} + F_{w_i} \end{aligned} \quad (4-9)$$

where, the definition of each stiffness k_i can be found in Eq.(3-2). For Model II, the dynamic equations for the bogie sub-system with four degrees of freedom can be derived as:

$$\begin{aligned} I_w \ddot{\Psi}_{w_o} + \frac{2a_0^2 f_{11}}{v_0} \dot{\Psi}_{w_o} + \frac{2a_0 f_{11} \lambda}{r_0} y_{w_o} + k_1 \Psi_{w_o} + k_2 \Psi_{w_i} - k_3 \Psi_T &= 0 \\ I_w \ddot{\Psi}_{w_i} + \frac{2a_0^2 f_{11}}{v_0} \dot{\Psi}_{w_i} + \frac{2a_0 f_{11} \lambda}{r_0} y_{w_i} + k_2 \Psi_{w_o} + k_4 \Psi_{w_i} - k_5 \Psi_T &= 0 \\ I_T \ddot{\Psi}_T + k_6 \Psi_T - k_3 \Psi_{w_o} - k_5 \Psi_{w_i} &= aF_{w_o} - aF_{w_i} \\ m_T \ddot{y}_T &= F_{w_o} + F_{w_i} \end{aligned} \quad (4-10)$$

where, each k_i can be found from Eq.(3-5). For the bogie sub-systems with three degrees of freedom, only the first three equations in Eq.(4-9) (Model I) and in Eq.(4-10) (Model II) are of concern.

4.4.2 Instability at Low Speed

By letting $\frac{d}{dt} = \frac{dx}{dt} \frac{d}{dx} = v_0 \frac{d}{dx}$, replacing F_o and F_i by Eq.(4-8b), using $v_0 \rightarrow 0$ and then by applying the Laplace transform, the dynamic equations of the bogie sub-system with four degrees of freedom for Model I become:

$$(2a_0^2 f_{11} s + k_1) \bar{\Psi}_{w_o}(s) + \left(\frac{2a_0 f_{11} \lambda}{r_0} a - k_2\right) \bar{\Psi}_T(s) + \frac{2a_0 f_{11} \lambda}{r_0} \bar{y}_T(s) = 0$$

$$\begin{aligned}
 (2a_0^2 f_{11} s + k_3) \bar{\Psi}_{wi}(s) - \left(\frac{2a_0 f_{11} \lambda}{r_0} a + k_4 \right) \bar{\Psi}_T(s) + \frac{2a_0 f_{11} \lambda}{r_0} \bar{y}_T(s) &= 0 \\
 (4a^2 f_{22} s + k_5) \bar{\Psi}_T(s) - (2af_{22} + k_2) \bar{\Psi}_{wo}(s) + (2af_{22} - k_4) \bar{\Psi}_{wi}(s) &= 0 \\
 2s \bar{y}_T(s) - \bar{\Psi}_{wo}(s) - \bar{\Psi}_{wi}(s) &= 0
 \end{aligned} \tag{4-11}$$

For the system with three degrees of freedom, only the first three equations above and $y_T = 0$ are of concern. The *Eigen-Equation* of the bogie sub-system is defined by:

For the bogie sub-system with three degrees of freedom:

$$p_3 s^3 + p_2 s^2 + p_1 s + p_0 = 0 \tag{4-12a}$$

For the bogie sub-system with four degrees of freedom:

$$p_4 s^4 + p_3 s^3 + p_2 s^2 + p_1 s + p_0 = 0 \tag{4-12b}$$

where, for Eq.(4-12a),

$$\begin{aligned}
 p_3 &= 4a_0^4 f_{11}^2 \times 4a^2 f_{22} \\
 p_2 &= 2a_0^2 f_{11} \times 4a^2 f_{22} (k_1 + k_3) + 4a_0^4 f_{11}^2 k_5 \\
 p_1 &= 2a_0^2 f_{11} (k_1 + k_3) k_5 + 4a^2 f_{22} k_1 k_3 + 2a_0^2 f_{11} (\alpha_1 \beta_1 - \alpha_2 \beta_2) \\
 p_0 &= k_1 k_3 k_5 - k_1 \alpha_2 \beta_2 + k_3 \alpha_1 \beta_1
 \end{aligned} \tag{4-13a}$$

and for Eq.(4-12b),

$$\begin{aligned}
 p_4 &= 4a_0^4 f_{11}^2 \times 4a^2 f_{22} \\
 p_3 &= 2a_0^2 f_{11} \times 4a^2 f_{22} (k_1 + k_3) + 4a_0^4 f_{11}^2 k_5 \\
 p_2 &= [2a_0^2 f_{11} (k_1 + k_3) k_5 + 4a^2 f_{22} k_1 k_3 + 2a_0^2 f_{11} (\alpha_1 \beta_1 - \alpha_2 \beta_2)] \\
 &\quad + \frac{8a_0^3 a^2 f_{11}^2 f_{22} \lambda}{r_0} \\
 p_1 &= [k_1 k_3 k_5 - k_1 \alpha_2 \beta_2 + k_3 \alpha_1 \beta_1] + \\
 &\quad + \frac{2a_0 f_{11} \lambda}{r_0} [2a^2 f_{22} (k_1 + k_3) + a_0^2 f_{11} k_5] \\
 p_0 &= \frac{a_0 f_{11} \lambda}{r_0} [(k_1 + k_3) k_5 + (\alpha_1 + \alpha_2) (\beta_1 - \beta_2)]
 \end{aligned} \tag{4-13b}$$

and

$$\begin{aligned}
 \alpha_1 &= \left(\frac{2a_0 a f_{11} \lambda}{r_0} - k_2 \right) & \alpha_2 &= \left(\frac{2a_0 a f_{11} \lambda}{r_0} + k_4 \right) \\
 \beta_1 &= (2af_{22} + k_2) & \beta_2 &= (k_4 - 2af_{22})
 \end{aligned}$$

The system with three degrees of freedom will be discussed first. To satisfy the necessary and sufficient conditions of stability in Eq.(4-2), all the coefficients in the *Eigen-Equation* must be greater than zero, i.e. $p_i > 0$. It is obvious that $p_3 > 0$ and $p_2 > 0$, and it can be easily proved that $p_1 > 0$ if $\lambda > 0$. From $p_0 > 0$, it can be proved that the wheelset conicity must satisfy the following condition:

$$\lambda > \frac{r_0}{2a_0 f_{11} a} \frac{(k_1 k_4^2 + k_3 k_2^2 - k_1 k_3 k_5) + 2af_{22}(k_2 k_3 - k_1 k_4)}{2af_{22}(k_1 + k_3) + k_2 k_3 - k_1 k_4} \quad (4-14)$$

For a conventional bogie vehicle with fore-and-aft symmetric configuration, we have $k_1 = k_2 = k_3 = k_4 = k_5/2$, and thus it is divergent stable if $\lambda > 0$.

For Model I, referring to Eq.(3-2), k_i 's in Eq.(4-14) are defined by:

$$\begin{aligned} k_1 &= g_1^2 k_{e1}, \quad k_2 = g_1 g_2 k_{e1}, \quad k_3 = g_4^2 k_{e2}, \\ k_4 &= g_4 g_5 k_{e2}, \quad k_5 = g_2^2 k_{e1} + g_5^2 k_{e2}, \quad g_1 = g_4 \end{aligned}$$

So, we have

$$k_1 k_4^2 + k_3 k_2^2 - k_1 k_3 k_5 = 0.$$

and

$$k_2 k_3 - k_1 k_4 = g_1^3 (g_2 - g_5) k_{e1} k_{e2}$$

Thus, Eq.(4-14) becomes:

$$\lambda > \frac{r_0 f_{22}}{a_0 f_{11}} \frac{g_1 (g_2 - g_5)}{2af_{22}(1/k_{e1} + 1/k_{e2}) + g_1 (g_2 - g_5)} \quad (4-15a)$$

Since $g_1 = b l_1$, $g_2 = b(l_1 + l_2)$, $g_5 = b l_3$ and that the geometric parameters of the steering levers in Model I must satisfy Eq.(3-15) (the sufficient condition for Model I capable of perfect steering), we have

$$\lambda > \frac{r_0 f_{22}}{a_0 f_{11}} \frac{b^2 l_2^2 l_0}{a^2 f_{22}(1/k_{e1} + 1/k_{e2}) + b^2 l_2^2 l_0} = \xi \quad (4-15b)$$

If $k_{b1} = k_{b2}$ and $k_{w1} = k_{w2}$ in Eq.(3-1), we have $k_{e1} = k_{e2}$ and Eq.(4-15b) becomes:

$$\lambda > \frac{r_0 f_{22}}{a_0 f_{11}} \frac{l_0 l_2^2 b^2 k_e}{2a^2 f_{22} + l_0 l_2^2 b^2 k_e} = \xi \quad (4-15c)$$

Since Eq.(4-14) and Eq.(4-15) are deduced from $p_0 > 0$, the instability will be divergent if Eq.(4-15) does not exist. In other words, the bogie sub-system with three degrees of freedom is a divergent unstable system if $\lambda < \xi$. Indeed, the Eigen-Equation Eq.(4-12a) of the bogie sub-system with three degrees of freedom is a third order equation, and for a third order equation, at least one real root exists. This indicates that the bogie sub-system with three degrees of freedom has a non-oscillatory motion that will become divergent unstable when $\lambda < \xi$.

The oscillatory instability can be investigated by applying the condition $\Delta_2 = p_1 p_2 - p_3 p_0 > 0$. If $p_1 p_2 - p_3 p_0 > 0$ exists, the oscillatory motion of the system is stable, otherwise, it is unstable. From this condition, the following restriction for conicity can be derived:

$$\lambda > \frac{r_0 f_{22}}{a_0 f_{11}} \frac{(k_2 - k_4)}{4af_{22} + k_2 - k_4} - \Lambda_1 = \zeta \quad (4-16)$$

where,

$$\Lambda_1 = \frac{r_0 [4k_1^2 + 2a_0^2 k_1 k_5 / a^2 - k_2^2 - k_4^2]}{2a_0 a f_{11} (4af_{22} + k_2 - k_4)} > 0$$

For fore-and-aft symmetric conventional bogie vehicles, $k_2 = k_4$ and $\zeta < 0$, and thus, the oscillatory motion of the bogie sub-system of a conventional bogie vehicle with fore-and-aft symmetric configuration is stable if $\lambda > 0$.

For Model I, it is obvious that $\xi > \zeta$ is true if the same definitions of k_i 's as those in Eq.(4-15) are used. In order to let $\zeta > 0$ in Eq.(4-16), the effective stiffness k_e ($= k_{e1} = k_{e2}$) must satisfy the following equation:

$$k_e < \frac{f_{22}(g_2 - g_5)}{4a^2 g_1^2 - (a^2 - 2a_0^2)(g_2^2 + g_5^2)} \quad (4-17)$$

This means that oscillatory instability at low speed occurs when the steering linkage is soft and also implies that soft steering linkage promotes this instability. The physical cause of oscillatory instability at low speed is the constraint of wheelset in yaw motion being too weak to hold the wheelsets if the steering linkage is too soft. This is true as only the steering linkage provides the constraint for wheelset yaw motion in Model I and Model II.

Investigation of the bogie sub-system with three degrees of freedom identifies two instabilities at low speed: the divergent instability and the oscillatory instability. The system is both divergent and oscillatory unstable if $\lambda < \zeta$; divergent unstable but oscillatory stable if $\zeta < \lambda < \xi$ or; both divergent and oscillatory stable if $\lambda > \xi$. Stiff steering linkage will promote divergent instability and increase ξ while soft steering linkage will develop oscillatory instability and increase ζ . This bogie sub-system also demonstrates that low speed instabilities do not appear in fore-and-aft symmetric conventional bogie vehicles.

For the bogie sub-system with four degrees of freedom, we have $p_4 > 0$ and $p_3 > 0$, and since p_2 in Eq.(4-13b) is larger than p_1 in Eq.(4-13a) if $\lambda > 0$, we have $p_2 > 0$ if $\lambda > 0$. For divergent stability, the following relationship can be derived from $p_0 > 0$:

$$\lambda > 0$$

and

$$\lambda > \frac{r_0}{4a_0af_{11}} \frac{4af_{22}(k_2 - k_4) + (k_2 - k_4)^2 - (k_1 + k_3)k_5}{4af_{22} + k_2 - k_4} = \bar{\xi} \quad (4-18a)$$

For a fore-and-aft symmetric conventional bogie vehicle, the condition $p_0 > 0$ exists if $\lambda > 0$ due to $k_2 = k_4$. Using the definitions of k_i 's in Eq.(3-2), this relationship becomes:

$$\lambda > \frac{r_0}{4a_0af_{11}} \frac{[4af_{22}(g_2 - g_5) - g_1(g_2 + g_5)^2 k_e] k_e}{4af_{22} + (g_2 - g_5)k_e} = \bar{\xi} \quad (4-18b)$$

For $\bar{\xi} > 0$, we have

$$4af_{22}(g_2 - g_5) - g_1(g_2 + g_5)^2 k_e > 0$$

Thus, the conditions $p_0 > 0$ and $\lambda > 0$ can only be satisfied if

$$k_e < \frac{4af_{22}(g_2 - g_5)}{g_1(g_2 + g_5)^2} = \frac{4a(l_1 + l_2 - l_3)}{b(l_1 + l_2 + l_3)^2} f_{22} = \frac{2a^2}{bl_1l_0} f_{22} \approx 0.4 f_{22} \quad (4-18c)$$

The formulae in Eq.(4-18) indicate that the bogie sub-system can be divergent unstable if the steering linkage is too soft.

The condition of oscillatory stability can be obtained from:

$$\Delta_3 = p_1 p_2 p_3 - p_1^2 p_4 - p_3^2 p_0 > 0$$

which can be rewritten as:

$$p_1(p_2p_3 - p_1p_4 - p_3^2p_0 / p_1) > 0$$

This condition can be divided into two conditions:

- i) $p_1 > 0$ and $p_2p_3 - p_1p_4 - p_3^2p_0 / p_1 > 0$ or,
 ii) $p_1 < 0$ and $p_2p_3 - p_1p_4 - p_3^2p_0 / p_1 < 0$

The condition ii) cannot be true because the system would be unstable and $p_2p_3 - p_1p_4 - p_3^2p_0 / p_1 > 0$ if $p_1 < 0$, and thus only the condition i) is valid to decide the system stability. For $p_1 > 0$, the following condition is obtained:

$$\lambda > \frac{r_0}{2a_0f_{11}} \frac{(k_1k_4^2 + k_3k_2^2 - k_1k_3k_5) + 2af_{22}(k_2k_3 - k_1k_4)}{a[2af_{22}(k_1 + k_3) + k_2k_3 - k_1k_4] + [2a^2f_{22}(k_1 + k_3) + 2a_0^2f_{11}k_5]} = \bar{\zeta} \quad (4-19)$$

For a conventional bogie vehicle with fore-and-aft symmetric configuration, we have $k_1 = k_2 = k_3 = k_4 = k_5/2$, and thus it is oscillatory stable if $\lambda > 0$. Applying k_i 's defined by Eq.(3-2) to Eq.(4-19), we have:

$$\lambda > \frac{r_0f_{22}}{a_0f_{11}} \frac{g_1(g_2 - g_5)}{8af_{22}/k_e + g_1(g_2 - g_5) + 2a_0^2f_{11}(g_2^2 + g_5^2)/(ag_1^2k_e)} = \bar{\zeta} \quad (4-20a)$$

and by applying the condition Eq.(3-15) for Model I capable of perfect steering, the above expression becomes:

$$\lambda > \frac{r_0f_{22}}{a_0f_{11}} \frac{b^2l_2^2l_0}{4a^2f_{22}/k_e + b^2l_2^2l_0 + 2a_0^2(a^2 + l_0^2)f_{11}/(l_0^2k_e)} = \bar{\zeta} \quad (4-20b)$$

Another condition for stability can be derived from $p_2p_3 - p_1p_4 - p_3^2p_0 / p_1 > 0$, but the process in finding it is very complex and is not necessary to present here with regard to the purpose of this section.

The application of the bogie sub-system with four degrees of freedom can also identify two instabilities at low speed: the divergent instability and the oscillatory instability. Since $\bar{\zeta} > \bar{\xi}$ exists, the system is both divergent and oscillatory unstable if $\lambda < \bar{\xi}$; oscillatory unstable but divergent stable if $\bar{\xi} < \lambda < \bar{\zeta}$ or; both divergent and oscillatory stable if $\lambda > \bar{\zeta}$. Stiff steering linkage promotes the oscillatory

instability and increases $\bar{\zeta}$ while soft steering linkage develops divergent instability and increases $\bar{\xi}$. This bogie sub-system also demonstrates that low speed instabilities do not appear in fore-and-aft symmetric conventional bogie vehicles.

For the bogie sub-system with three degrees of freedom, there are two low speed instability modes: divergent and oscillatory. Oscillatory instability occurs in much lower value of conicity than does divergent instability. For the bogie sub-system with four degrees of freedom, there are also two low conicity instability modes: divergent and oscillatory, however here, divergent instability occurs in much lower value of conicity than does oscillatory instability. The low speed instabilities illustrated in Fig.4.5 are oscillatory because the frequencies are greater than zero and are associated with the kinematic frequencies of wheelset. In the development of Eq.(4-15), Eq.(4-16), Eq.(4-18) and Eq.(4-20) and in the results of Fig.4.5, the condition of $k_e = k_{e1} = k_{e2}$ is used. Referring to the results derived by Wickens[28], low speed instability is oscillatory when $k_e = k_{e1} = k_{e2}$.

Applying the parameters given in Table 3.3 to Eq.(4-15) and Eq.(4-19), we have:

$$\begin{aligned} \xi &= 0.0167 \text{ and } \bar{\zeta} = 0.0073 \text{ (for the soft steering linkage Set 1) and,} \\ \xi &= 0.092 \text{ and } \bar{\zeta} = 0.043 \text{ (for the stiff steering linkage Set 2).} \end{aligned}$$

From the results in Fig.4.4a&b, low speed instability occurs when the conicity is less than 0.01 for the soft steering linkage and less than 0.035 for the stiff steering linkage. The conditions derived from the bogie sub-system with four degrees of freedom are thus more close to the simulated results than those derived from the bogie sub-system with three degrees of freedom.

For divergent instability, the following explanation has been widely accepted [12,15,19,28]. Steering forces produced by steering linkages effectively reduce the longitudinal creepage force, and when the conicity is low, there is not enough longitudinal creepage force to restore the wheelsets back to their balance position as soon as the wheelsets have yaw motion, and thus divergent instability occurs.

ξ and $\bar{\zeta}$ are both called the minimum conicity, and Eq.(4-15) and Eq.(4-20) show that ξ or $\bar{\zeta}$ depend on the geometric parameters b and l of the levers of steering linkages as well as the vehicle geometric parameters a and l_0 . Obviously, any gain in b , l_2 and l_0 will increase the steering effect and promote low speed instability, whilst long wheelset base a will decrease the steering effect and thus stabilise the system.

Eq.(4-15) and Eq.(4-20) indicate that low speed instability will occur even in high conicity except when one of the effective stiffnesses k_{e1} and k_{e2} is zero. Unfortunately, the degeneracy P of the elastic matrix \mathbf{E} is greater than 4 if any of the effective stiffnesses is zero. The perfect steering vehicle cannot be stable at all because the necessary condition of stability Eq.(2-25) is no long satisfied. Low speed instability is thus unavoidable in the perfect steering vehicle if conicity is too low or if the steering linkage is too stiff. This is one of the basic features that distinguishes perfect steering vehicles from other body-steered bogie vehicles. Theoretically, if a body-steered bogie vehicle possesses primary and secondary yaw stiffnesses, it can have non-zero critical speed even if its effective stiffnesses in the steering linkages are zero because the degeneracy of its elastic matrix \mathbf{E} still equals or less than 4.

The minimum conicity (ξ & $\bar{\zeta}$) $\rightarrow \frac{r_0 f_{22}}{a_0 f_{11}}$ when $k_e \rightarrow \infty$, which means that the minimum conicity also depends on contact parameters. If $f_{11} > f_{22}$, the minimum conicity reduces, and the physical reason for this is that a larger longitudinal creepage coefficient produces a larger creepage yaw moment, which can resist the wheelset yaw motion promoted by the steering linkage, and that a smaller lateral creepage force yields a smaller moment that forces the bogie frame to have a yaw motion so that the minimum conicity is reduced. A larger gauge a_0 means that the arm of the longitudinal creepage moment becomes longer, and so increases the moment and reduces the minimum conicity.

By applying the similar analyses to Model II, the *Eigen-Equation* of Eq.(4-15) is:

For the bogie sub-system with three degrees of freedom:

$$p_3 s^3 + p_2 s^2 + p_1 s + p_0 = 0 \quad (4-21a)$$

For the bogie sub-system with four degrees of freedom:

$$p_4 s^4 + p_3 s^3 + p_2 s^2 + p_1 s + p_0 = 0 \quad (4-21b)$$

where, for Eq.(4-21a),

$$\begin{aligned} p_3 &= 4a_0^4 f_{11}^2 \times 4a^2 f_{22} \\ p_2 &= 2a_0^2 f_{11} \times 4a^2 f_{22} (k_1 + k_4) + 4a_0^4 f_{11}^2 k_6 \\ p_1 &= 2a_0^2 f_{11} (k_1 + k_4) k_6 + 4a^2 f_{22} k_1 k_4 + 2a_0^2 f_{11} (\alpha_1 \beta_1 - \alpha_2 \beta_2) - 4a^2 f_{22} k_2^2 \\ p_0 &= k_1 k_4 k_6 - k_1 \alpha_2 \beta_2 + k_4 \alpha_1 \beta_1 - k_2^2 k_6 + k_2 (\alpha_2 \beta_1 - \alpha_1 \beta_2) \end{aligned} \quad (4-22a)$$

and for Eq.(4-21b),

$$\begin{aligned}
 p_4 &= 4a_0^4 f_{11}^2 \times 4a^2 f_{22} \\
 p_3 &= 2a_0^2 f_{11} \times 4a^2 f_{22} (k_1 + k_4) + 4a_0^4 f_{11}^2 k_6 \\
 p_2 &= [2a_0^2 f_{11} (k_1 + k_4) k_6 + 4a^2 f_{22} k_1 k_4 + 2a_0^2 f_{11} (\alpha_1 \beta_1 - \alpha_2 \beta_2) - 4a^2 f_{22} k_2^2] \\
 &\quad + \frac{8a_0^3 a^2 f_{11}^2 f_{22}}{r_0} \lambda \\
 p_1 &= k_1 k_4 k_6 - k_1 \alpha_2 \beta_2 + k_4 \alpha_1 \beta_1 - k_2^2 k_6 + k_2 (\alpha_2 \beta_1 - \alpha_1 \beta_2) + \\
 &\quad + \frac{2a_0 f_{11} \lambda}{r_0} [2a^2 f_{22} (k_1 + k_4 - 2k_2) + 2a_0^2 f_{11} k_6] \\
 p_0 &= \frac{a_0 f_{11} \lambda}{r_0} [(k_1 + k_4 - 2k_2) k_6 + (\alpha_1 + \alpha_2) (\beta_1 - \beta_2)] \quad (4-22b)
 \end{aligned}$$

and

$$\begin{aligned}
 \alpha_1 &= \frac{2a_0^2 f_{11} \lambda}{r_0} a - k_3 & \alpha_2 &= \frac{2a_0^2 f_{11} \lambda}{r_0} a + k_5 \\
 \beta_1 &= 2f_{22} a + k_3 & \beta_2 &= k_5 - 2f_{22} a
 \end{aligned}$$

For the bogie sub-system with three degrees of freedom, divergent instability will occur if $p_0 > 0$ in Eq.(4-22a); so we have

$$\lambda > \frac{r_0}{a_0 f_{11}} \frac{f_{22} [k_3 (k_2 + k_4) - k_5 (k_1 + k_2)]}{2af_{22} (k_1 + 2k_2 + k_4) + k_3 (k_2 + k_4) - k_5 (k_1 + k_2)} + \Pi \quad (4-23)$$

where,

$$\Pi = \frac{r_0}{2a_0 f_{11} a} \frac{k_1 (k_3^2 + k_5^2) + k_6 k_2^2 - 2k_2 k_3 k_5 - k_6 k_1^2}{2af_{22} (k_1 + 2k_2 + k_4) + k_3 (k_2 + k_4) - k_5 (k_1 + k_2)}$$

For a conventional bogie vehicle with fore-and-aft symmetric configuration and without inter wheelset connection, we have $k_1 = k_3 = k_4 = k_5 = k_6/2$ and $k_2 = 0$, and thus it is static stable if $\lambda > 0$. For Model II, using the definitions of k_i 's in Eq.(3-5), it can be proved that $\Pi = 0$ and Eq.(4-23) becomes:

$$\lambda > \frac{r_0 f_{22}}{a_0 f_{11}} \frac{\Gamma}{2af_{22} [g_1^2 (1/k_{e1} + 1/k_{e2}) + 4g_7^2 k_{e3} / k_{e1} / k_{e2}] + \Gamma} = \xi \quad (4-24a)$$

where

$$\Gamma = g_1^3 (g_2 - g_5) + g_1 g_7^2 (g_2 / k_{e1} - g_5 / k_{e2}) k_{e3}$$

Eq.(4-24a) is different from Eq.(4-15a) since the effective stiffness k_{e3} exists. If $k_{w1} = k_{w2}$, $l_2 = l$ and $k_{e1} = k_{e2} = k_e$ and by applying the condition Eq.(3-16) for Model II capable of perfect steering, we have $k_1 = k_4$ and $(k_3 - k_5) = 2b^2 l_0 k_e l^2 / a$ and Eq.(4-24a) becomes:

$$\lambda > \frac{r_0 f_{22}}{a_0 f_{11}} \frac{b^2 l_0^2 k_e}{2a^2 f_{22} + b^2 l_0^2 k_e} \quad (4-24b)$$

Here, Eq.(4-24b) is exactly the same as Eq.(4-15c), which means that a bogie sub-system with three degrees of freedom cannot distinguish the divergent instability of Model I from that of Model II.

The condition of oscillatory instability for Model II can be derived from the condition $p_1 p_2 - p_3 p_0 > 0$, and is:

$$\lambda > \xi - \frac{r_0}{2aa_0 f_{11}} \frac{[4k_1(k_1 + a_0^2 k_6 / a^2 / 2) - k_3^2 - k_5^2](k_1 + a_0^2 k_6 / a^2 / 2) - 4a^2 k_1 k_2^2 / a_0^2 - 2k_2 k_3 k_5}{(4af_{22} + k_3 - k_4)(k_1 + a_0^2 k_6 / a^2 / 2 - k_2)} = \zeta \quad (4-25)$$

It can be also proved that $\xi > \zeta$ and that the effective stiffness k_e must be less than a certain value if $\zeta > 0$. Eq.(4-25) thus demonstrates that the perfect steering vehicle will be oscillatory unstable in low conicity if its steering linkage is too soft.

Since the bogie sub-system with four degrees of freedom will be divergent unstable if $p_0 > 0$ in Eq.(4-22b), we have:

$$\lambda > \frac{r_0}{4aa_0 f_{11}} \frac{(4af_{22} + k_3 - k_5)(k_3 - k_5) - k_6(k_1 + k_4 - 2k_2)}{4af_{22} + k_3 - k_5} = \bar{\xi}$$

To let $\bar{\xi} > 0$, the effective stiffnesses k_{e1} and k_{e3} must satisfy:

$$(g_2 + g_5)^2 k_{e1} + 2g_9^2 k_{e3} < 4af_{22}(g_2 - g_5) / g_1 \quad (4-26)$$

Oscillatory instability will not happen if $\Delta_3 = p_1 p_2 p_3 - p_1^2 p_4 - p_3^2 p_0 > 0$ which can turn into the conditions $p_1 > 0$ and $p_2 p_3 - p_1 p_4 - p_3^2 p_0 / p_1 > 0$, and thus the bogie sub-system with four degrees of freedom to be oscillatory unstable if $p_1 < 0$, the condition being:

$$\lambda > \frac{r_0 f_{22}}{a_0 f_{11}} \frac{(k_1 + k_2)(k_3 - k_5)}{8af_{22} k_1 + (k_1 + k_2)(k_3 - k_5) + 2a_0^2 f_{11} k_6 / a} = \bar{\zeta} \quad (4-27)$$

For a conventional bogie vehicle with fore-and-aft symmetric configuration and without inter wheelset connection, we have $k_1 = k_3 = k_4 = k_5 = k_6/2$ and $k_2 = 0$ such that $\lambda > 0$ exists, and thus it is oscillatory stable.

The effective stiffness k_{e3} is included in the condition Eq.(4-27) but disappears in the condition Eq.(4-24), which implies that the bogie sub-system with four degrees of freedom more closes to the physical system. Moreover, the condition Eq.(4-19) for Model I to be oscillatory stable at low speed is different from the condition Eq.(4-27) for Model II to be oscillatory stable at low speed, which means that the conditions obtained from the bogie sub-system with four degrees of freedom can distinguish the difference between Model I and Model II with regard to oscillatory instability at low speed, and thus the bogie sub-system with four degrees of freedom is more accurate than the sub-system with three degrees of freedom.

For Model II, from Eq.(4-24b) and Eq.(4-27), we have

$$\begin{aligned} \xi &= 0.0288 \text{ and } \bar{\xi} = 0.022 \text{ for the stiff steering linkage (Set 2) and,} \\ \xi &= 0.0053 \text{ and } \bar{\xi} = 0.0045 \text{ for the soft steering linkage (Set 1).} \end{aligned}$$

These results are very close to the simulated results in Fig.4.1b, where low speed instability does not happen even if the conicity is equal to 0.005 with soft steering linkage, but happens if the conicity is less than 0.03 for stiff steering linkage.

The above analysis can only be applied to the leading bogie. With regard to the trailing bogie, some of the elements in the matrix defined by Eq.(3-2b) and Eq.(3-5b) will change position. For the trailing bogie: k_2 becomes k_4 and k_4 becomes k_2 , and therefore, the minimum conicity ξ and $\bar{\xi}$ becomes negative for the trailing bogie, which means that the trailing bogie will be stable at low speed when the vehicles move forward, but it will be unstable at low speed when the vehicles move backward. Low speed instability in low conicity therefore only appears in one of the bogies and depends on the direction of the moving vehicles. The analysis in this sub-section can be applied to other body-steered bogie vehicles, since the bogie sub-systems in Fig.4.7 have the general features of body-steered bogies. The steering linkages of other body-steered bogie vehicles, however, do not need to satisfy perfect steering conditions .

From Eq.(4-15a) to Eq.(4-15b) and from Eq.(4-20a) to Eq.(4-20b), the condition Eq.(3-15) for Model I capable of perfect steering is used, which means that the low

speed stability of the perfect steering vehicle is also affected by the perfect steering condition. For other classes of body-steered bogie vehicle, however, perfect steering is not required and thus the minimum conicity can be zero, for example, $\xi = \bar{\zeta} = 0$ if $g_2 = g_5$ (i.e. $l_1 + l_2 = l_3$). This analysis implies that low speed instability can be eliminated for body-steered bogie vehicles if perfect steering is not required. The similar analysis can be applied to the configuration of Model II, in which condition eliminating low speed instability is $k_3 = k_5$. It should be noted that the condition $p_2 p_3 - p_1 p_4 - p_3^2 p_0 / p_1 > 0$ has not been discussed, and that primary and secondary yaw stiffnesses are not included in the above analysis, and thus low speed instability of other body-steered bogie vehicles may still occur even if $g_2 = g_5$ or $k_3 = k_5$.

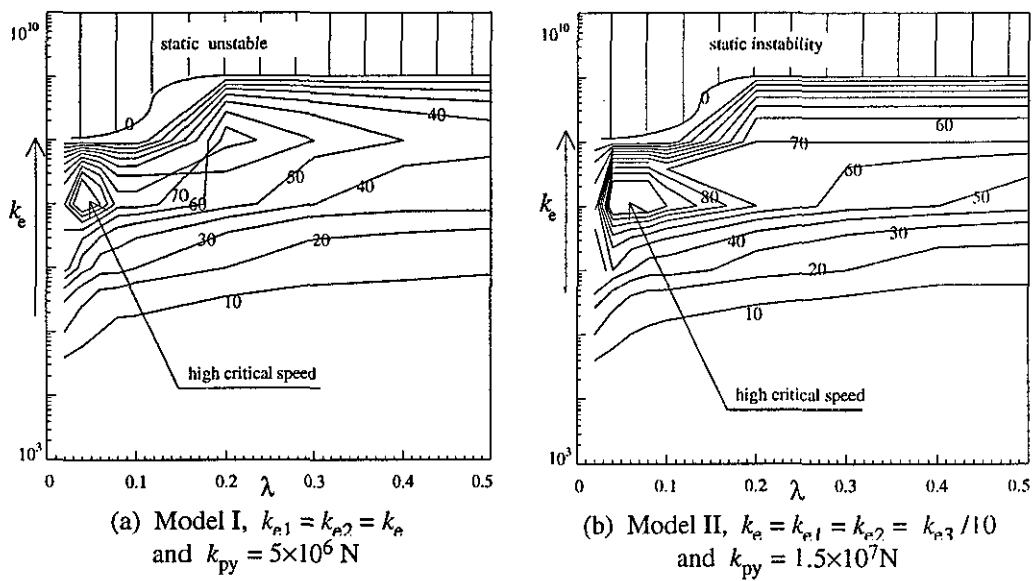


Figure 4.8 The critical speed contours as function of k_{e1} & k_{c2}

The results in Eq.(4-17), Eq.(4-20), Eq.(4-24) and Eq.(4-27) show that the minimum conicity will increase as any of the effective stiffness increases and that low speed instability not only occurs in low conicity, but also occurs in high conicity if the steering linkage is too stiff. The simulated results in Fig.4.8 illustrate the various situations: when the effective stiffness is approximately 10^7 , the critical speed can be very high if conicity is less than 0.1; when the effective stiffness increases to 10^8 , the high critical speed can be achieved only when conicity is greater than 0.15; when the effective stiffness is close to 10^9 , low speed instability occurs at any conicity.

4.4.3 Dynamic Instability in Low Conicity

If the inertia of the mass components is taken into account, by reviewing the models in Fig.4.5 and letting

$$S = D^2 + \frac{2a_0^2 f_{11}}{I_w v_0} D \quad \text{where, } D = \frac{d}{dt}$$

The dynamic equation Eq.(4-9) for the bogie sub-system with three degrees of freedom becomes:

$$\begin{aligned} (S + \frac{k_1}{I_w})\psi_{wo} + (\frac{2a_0 f_{11} \lambda}{I_w r_0} a - \frac{k_2}{I_w})\psi_T &= 0 \\ (S + \frac{k_3}{I_w})\psi_{wi} - (\frac{2a_0 f_{11} \lambda}{I_w r_0} a + \frac{k_4}{I_w})\psi_T &= 0 \\ (S + \frac{k_5}{I_T})\psi_T - \frac{2af_{22} + k_2}{I_T} \psi_{wo} + \frac{2af_{22} - k_4}{I_T} \psi_{wi} &= 0 \end{aligned} \quad (4-28)$$

If the difference between $2a^2/I_T$ and $2a_0^2/I_w$ is neglected, the *Eigen-Equation* is:

$$p_3 S^3 + p_2 S^2 + p_1 S + p_0 = 0$$

For the condition $p_0 > 0$, we have:

$$\lambda > \frac{r_0}{2a_0 f_{11} a} \frac{2af_{22}(k_2 k_3 - k_1 k_4) + (k_1 k_4^2 + k_3 k_2^2 - I_w k_1 k_3 k_5 / I_T)}{2af_{22}(k_1 + k_3) + k_2 k_3 - k_1 k_4} \quad (4-29a)$$

or

$$\lambda > \xi + \frac{r_0}{2a_0 f_{11} a} \frac{k_1 k_4^2 + k_3 k_2^2 - I_w k_1 k_3 k_5 / I_T}{2af_{22}(k_1 + k_3) + k_2 k_3 - k_1 k_4} = \xi_d \quad (4-29b)$$

It has been proved that $k_1 k_4^2 + k_3 k_2^2 - k_1 k_3 k_5 = 0$ if k_i 's come from Eq.(3-2). So, we obtain:

$$k_1 k_4^2 + k_3 k_2^2 - I_w k_1 k_3 k_5 / I_T > 0$$

Because of $I_w / I_T < 1$, we have $\xi_d > \xi$, which means that dynamic instability in low conicity happens at a higher conicity than that of low speed instability in low conicity. A similar result can also be obtained for Model II. These results cannot explain fully and precisely the physical reasons for dynamic instability in low conicity, since the carbody can no longer stand for the inertia reference when the critical speed is much greater than zero. These results, however, at least indicate two facts: dynamic instability in low conicity occurs in higher conicity than low

speed instability and, dynamic instability in low conicity only happens in one of the bogies.

The real reasons causing dynamic instability in low conicity may depend on the following factors. The damping produced by longitudinal creepage decreases as the vehicle speed rises, and in the leading bogie, the forces yielded by the steering mechanism always have the tendency to force the wheelsets to a yaw. When the forces generated by the longitudinal creepages reduce to such a level that they cannot eliminate this tendency as the vehicle speed increases, dynamic instability in low conicity occurs.

4.5 Influences of the Parameters in the Steering Linkages and Suspensions

The connection between the wheelsets and carbody has an effect on the increment of wheelset base, which can improve vehicle stability, while the elastic sub-matrix of bogie in Eq.(4-6) shows that the effective stiffnesses are on the positions of the primary yaw stiffness in the matrix, which means that the wheelset yaw motion is only constrained by the steering linkage in perfect steering vehicles. These two effects imply that a stiff steering linkage can increase the critical speed of the perfect steering vehicles. On the other hand, the last section demonstrated that the stiffness of the steering linkages is restricted by low conicity instability (low speed and dynamic), and cancellation of the primary and secondary yaw stiffnesses in perfect steering vehicles weakens their suspensions. All of these factors will affect the behaviour of vehicle stability, and thus it is necessary to investigate these factors in greater detail.

4.5.1 Conicity

When the conicity is low and the steering linkages are stiff, three kinds of instability (low speed instability, dynamic instability and conventional instability) are very obvious, as shown in Fig.4.4b&d, however, the results in Fig.4.8 show that low speed instability occurs for any conicity if the steering linkages are too stiff. Further investigation has been carried out to identify the modes of instability for various conicities, and has found that the dynamic instability zone O2 disappears as the stiffness of the steering linkages increases and that the unstable mode possesses the features of both conventional instability and dynamic instability in low conicity when the conicity is close to the minimum conicity, as seen in Fig.4.9 in which one of the bogies loses stability at much lower speed than the other, but the tendency of the

real parts of the two eigenvalues is similar. The tendency of the real parts seems to be a feature of conventional instability while the unequal critical speeds between two bogies are a feature of dynamic instability in low conicity.

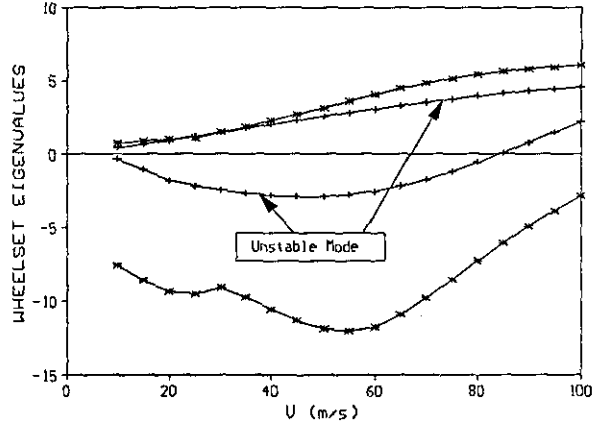
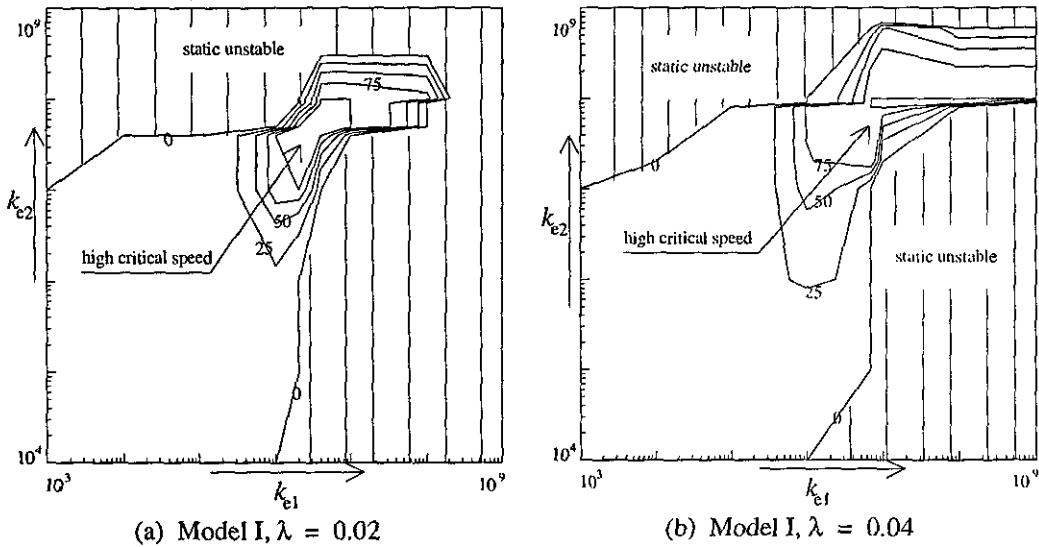
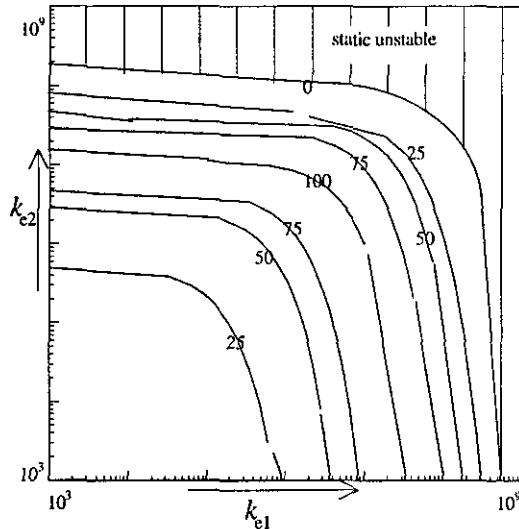


Figure 4.9 The eigenvalues of unstable modes of Model I as function of speed when $k_{e1} = k_{e2} = 10^8$ and $\lambda = 0.1$

Another interesting result is illustrated in Fig.4.10 where there is an optimal zone for the effective stiffnesses of Model I. The critical speed can be very high if the effective stiffnesses are in this zone, but the critical speed is very sensitive to both the effective stiffnesses in the zone; and as conicity increases, this zone becomes bigger. The phenomenon is not, however, observed in Model II.





(c) Model II, $\lambda = 0.04$

Figure 4.10 The critical speed contours as function of k_{e1} & k_{e2}

4.5.2 Effective Stiffnesses

It has been shown that only the effective stiffnesses in the steering linkages provide the constraint for wheelset yaw motion. The critical speed contours as functions of the effective stiffnesses k_{e1} & k_{e2} are illustrated in Fig.4.11 and can be seen that if effective stiffnesses are too soft, the steering linkages are not strong enough to hold the wheelsets and the critical speed is low, but low speed instability occurs if they are too hard; and that the critical speed gets higher as the steering linkages are stiffened in conventional stability, but further increment in the effective stiffnesses does not improve conventional stability after k_{e1} & k_{e2} are about 10^8 .

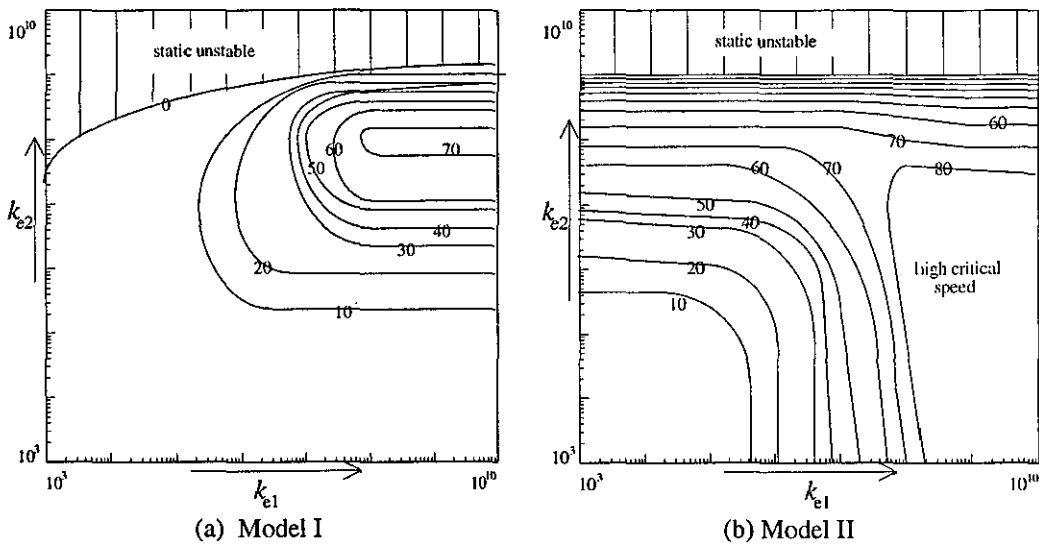


Figure 4.11 The critical speed contours as function of k_{e1} & k_{e2} , $\lambda = 0.2$

The steering effect and the constraint for wheelset yaw motion are both enhanced by hard effective stiffnesses. When the effective stiffnesses are very hard, the wheelsets are firmly held by the steering linkages. If the force produced by longitudinal creepage overcomes the steering effect, the wheelsets can be stable, but they are unstable at low speed if it is not. Dynamic instability in low conicity does therefore not happen with high effective stiffnesses, as is shown in Fig.4.12 (Model I) and in Fig.4.13 (Model II), in each of which the instabilities of each perfect steering vehicle are either unstable at low speed or conventionally unstable when $k_{e1} = k_{e2} = 2 \times 10^8$.

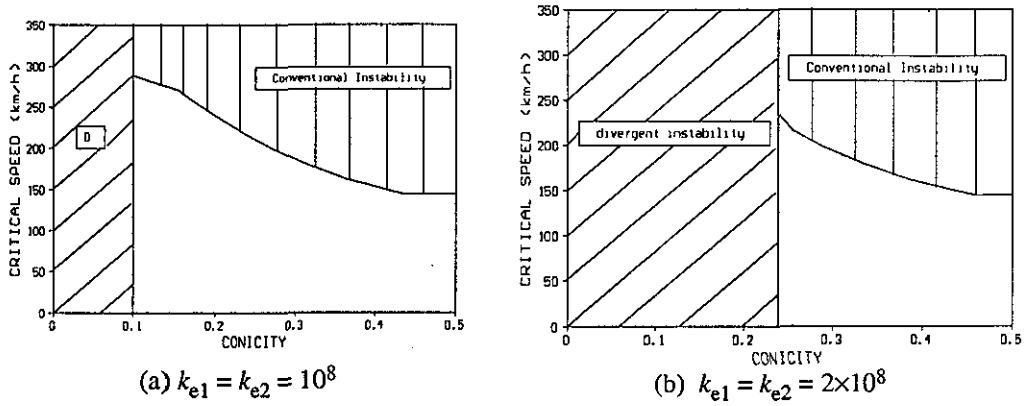


Figure 4.12 The critical speed of Model I as function of conicity, stiff linkage

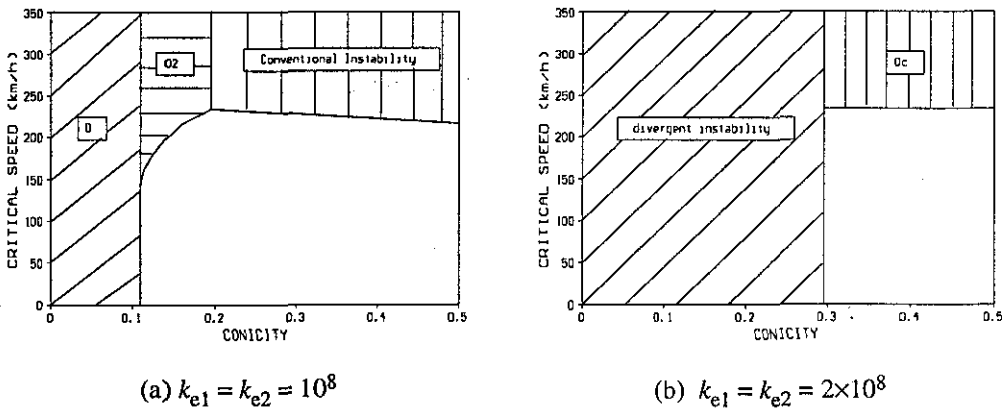


Figure 4.13 The critical speed of Model II as function of conicity, stiff linkage

In Model II, there is effective stiffness k_{e3} between the two wheelsets, and it has been found that this effective stiffness has little influence on the critical speed, as seen in Fig.4.14. Several advantages of Model II in stability over Model I can, however, be found from Fig.4.10 and Fig.4.11. Firstly, the high speed area of Model II is larger and, secondly, its critical speed is less sensitive to the effective stiffnesses k_{e1} & k_{e2} and, finally, the area of low speed instability is smaller. All of these benefits of Model II in stability are attributed to k_{e3} because it effectively increases the yaw inertia for the wheelsets.

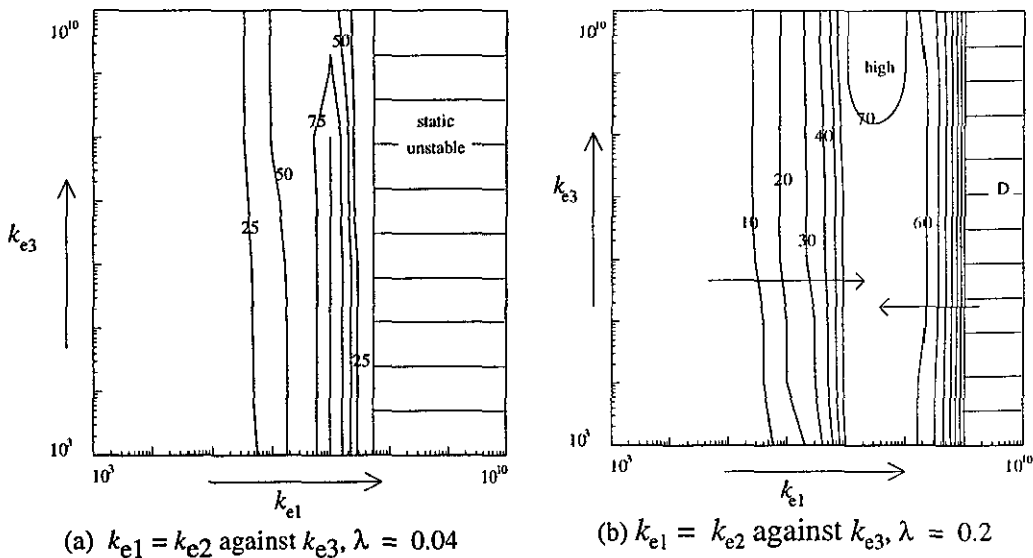


Figure 4.14 The critical speed contours of Model II as function of k_{e1} & k_{e3}

Further simulation has been carried out to identify whether instability could occur with other motions, but has found that the frequency of unstable motion always closes to the kinematic frequency of wheelset, which means that unstable mode is mainly associated with the wheelset motions. The reason for this is that the effective stiffnesses cannot be very hard because of the risk of low speed instability, and thus the wheelset constraints cannot be very strong and the modes associated with wheelset motion go to unstable first. This is another feature associated with the stability of perfect steering vehicles.

4.5.3 Primary Lateral Stiffness

In Model I and Model II, the primary lateral stiffness constrains wheelset lateral motion while the steering linkages provide the constraint for wheelset yaw motion. If any of them is too soft, the critical speed of the vehicles is very low. When both of the primary lateral stiffness and the effective stiffnesses are hard enough, the stability of each perfect steering vehicle is mainly governed by the effective stiffness, as shown in Fig.4.15. This indicates that the wheelset lateral motion is more easily stabilised than the wheelset yaw motion. The optimal value for the primary stiffness with regard to stability is around 10 MN/m.

The results in Fig.4.16 demonstrate that the stability of Model II is more sensitive to the primary lateral stiffness than that of Model I, especially in low conicity. It has been found that very hard primary lateral stiffness can promote the static instability of Model II when the effective stiffnesses are very high. It appears that the

combination of high primary lateral stiffness and high effective stiffness k_{e3} between the wheelsets increases minimum conicity.

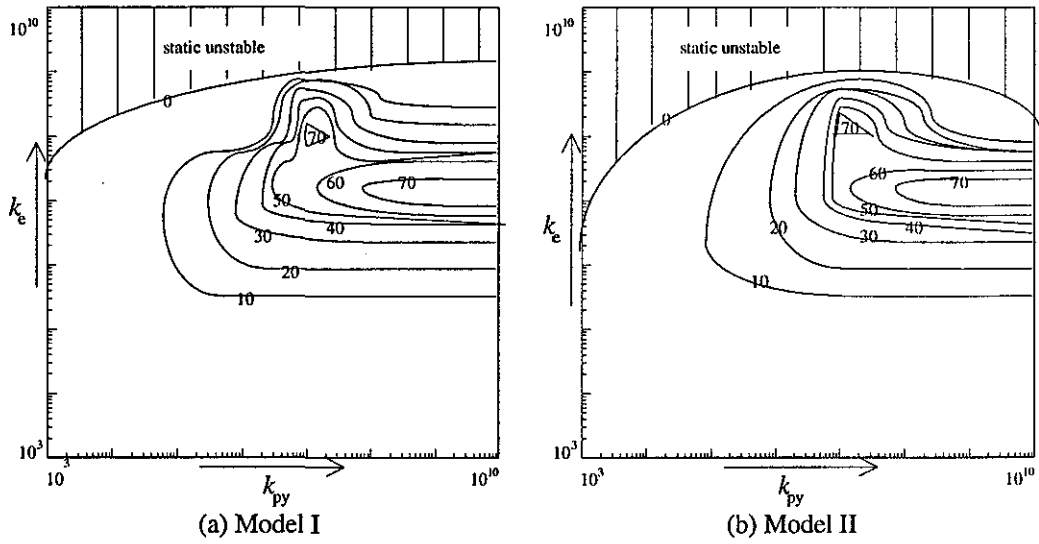


Figure 4.15 The critical speed contours as function of k_{e1} & k_{py} , $\lambda = 0.2$

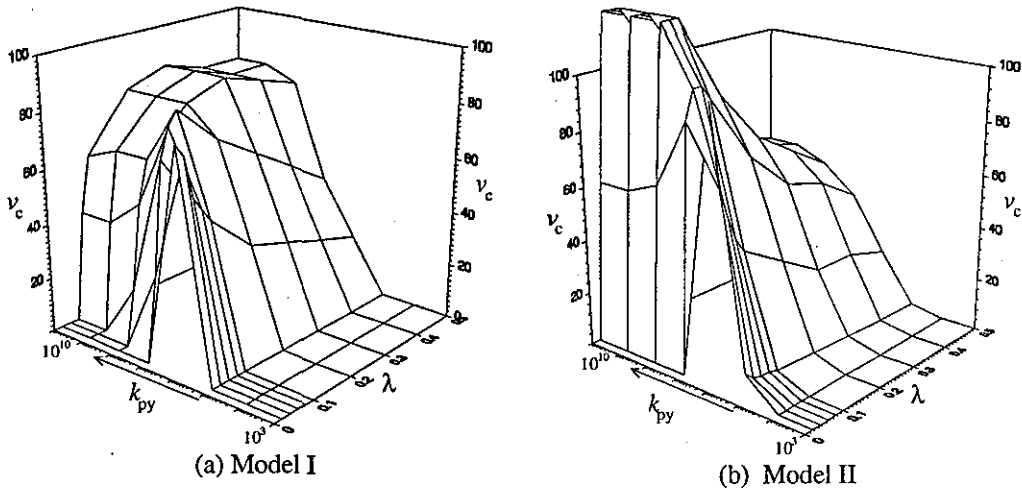


Figure 4.16 The critical speed (m/s) as function of λ & k_{py} , stiff linkages

4.5.4 Some Considerations

In Model II, there are three effective stiffnesses in the steering linkage, only two of which are independent, the third being governed by the first two. If the geometric parameters of steering levers are fixed, the effective stiffnesses are decided by k_{w0} , k_{wi} and k_b . By letting $k_{w0} = k_{wi} = k_w$, Eq.(3-5) becomes:

$$k_{e1} = \frac{k_b}{\Delta} \quad k_{e2} = \frac{k_b}{\Delta} \quad k_{e3} = \frac{k_w}{\Delta}$$

where,

$$\Delta = (l_1 + l_3)^2 k_b / k_w + 2l_3^2$$

We have

- i) $k_w = 1.154k_b$, $k_b = k_{e1}$ and $k_{e3} = 1.154k_{e1}$, when $\Delta = 1$;
- ii) $k_w = 10.023k_b$, $k_b = 0.155k_{e1}$ and $k_{e3} = 10k_{e1}$, when $\Delta = 0.155$;
- iii) $k_w = 100k_b$, $k_b = 0.056k_{e1}$ and $k_{e3} = 100k_{e1}$, when $\Delta = 0.056$.

Hard effective stiffness k_{e3} strengthens the connection between two wheelsets and thus improves stability, but if it is too hard, two wheelsets will become one inertia body, and system stability is reduced. From the results in Fig.4.17, the vehicle has the best stability when $\Delta = 0.155$.

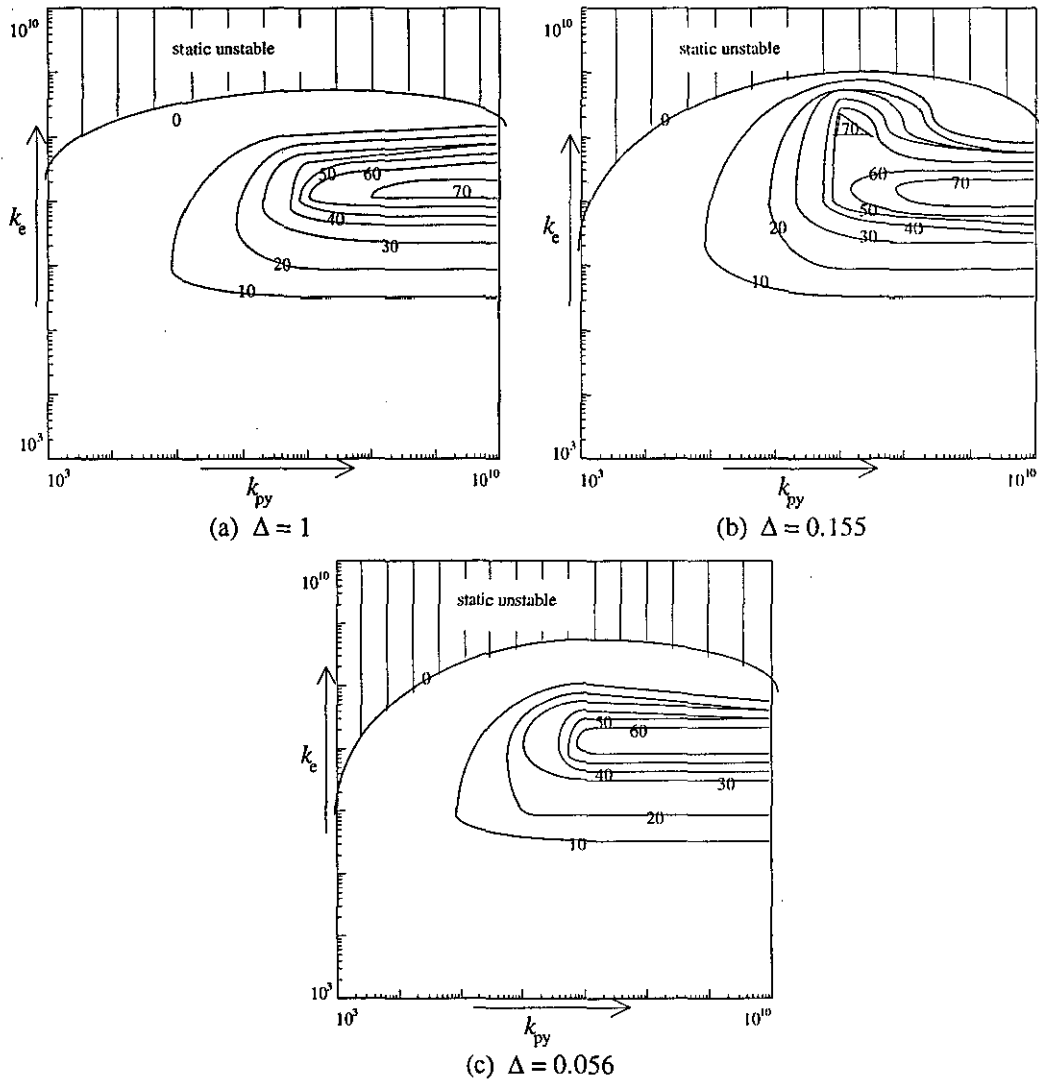


Figure 4.17 Critical speed contours as function of k_{e1} & k_{py} , Model II, $k_{e1} = k_{e2} = k_e$ and $\lambda = 0.2$

When the effective stiffnesses k_{e1} & k_{e2} are approximately 10^8 for both models, the critical speed is the highest, however, the critical speed is very sensitive to the effective stiffnesses k_{e1} & k_{e2} , and the minimum conicity becomes too high if the steering linkages are so stiff. On the other hand, the critical speed is very low when the effective stiffnesses k_{e1} & k_{e2} are less than 10^6 , and thus the optimal value for the effective stiffnesses k_{e1} & k_{e2} should be around 10^7 , but they can be less in Model II since it possesses the effective stiffness k_{e3} . The optimal value for the primary lateral stiffness is in the magnitude of 10MN/m .

4.5.5 Influence of the Secondary Suspension Parameters

Usually, secondary suspension is designed to improve the ride quality of vehicles rather than their stability since the effects of secondary suspension on the stability are limited. This principle also applies to Model I and Model II somewhat because the instability of each perfect steering vehicle is associated with wheelset motions. Although the results in Fig.4.18 seem to indicate that high values of the secondary suspension parameter improve the stability, their influences on the stability are not fundamental and the values resulting in higher critical speed are beyond the values that would be applied in practical applications. Out of three parameters in Fig.4.18, the secondary yaw damping has the most positive effect in increasing critical speed.

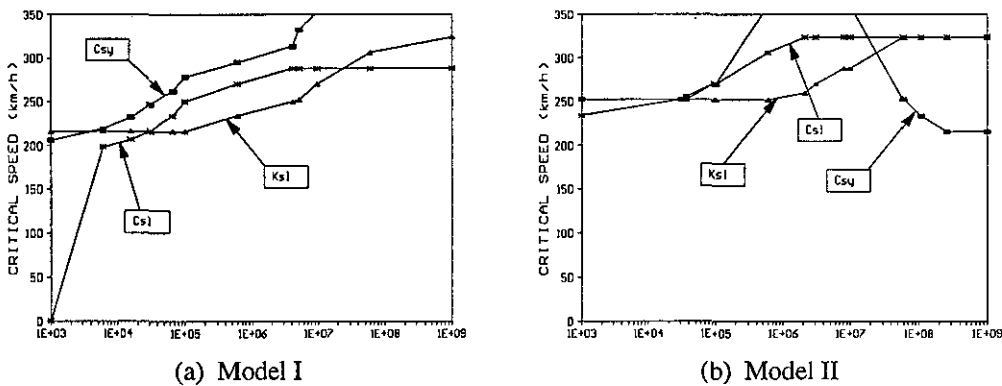


Figure 4.18 The critical speed as function of secondary suspension parameters, $\lambda = 0.2$, $K_{s1} = k_{sy}$, $C_{s1} = c_{sy}$ and $C_{sy} = c_{s\psi}$

Hard secondary suspension may promote instability in low conicity. For example, the critical speed of Model I without yaw secondary damping is slightly higher than that of Model I with yaw secondary damping, as seen in Fig.4.19. When secondary yaw damping is added, the connection between the carbody and bogie frames becomes more rigid, resulting in an increased steering effect. The unstable tendency of the wheelsets is thus increased, and the vehicle has less critical speed in low conicity. Actually, the bogies can be considered as pinned to the carbody when the

secondary suspension is very stiff, which is more close to the system with three degrees of freedom, and the analysis in the last section showed that the bogie sub-system with three degrees of freedom more easily occurs low speed instability in low conicity, and thus low conicity instability gets worse as secondary suspension gets stiffer.

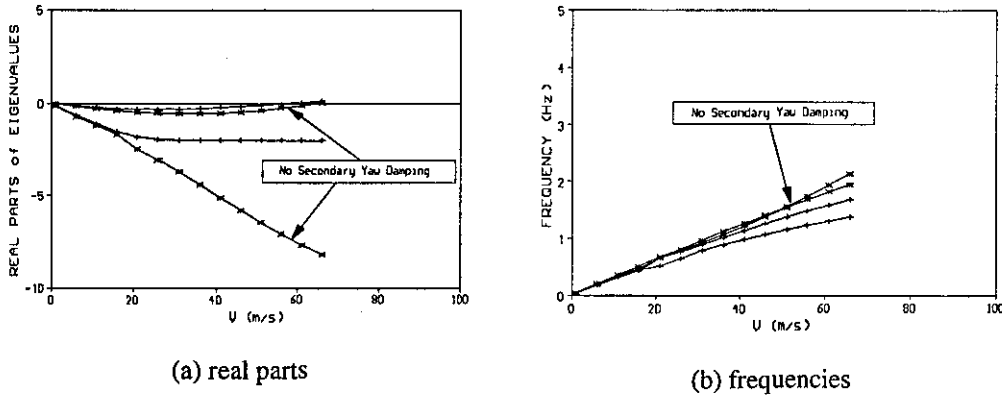


Figure 4.19 The eigenvalues of Model I (with or without secondary yaw damping) as function of vehicle speed when $\lambda = 0.04$

4.5.6 Influence of the Geometric Errors in the Steering Linkages

Since the geometric errors of steering levers will change the effective stiffnesses, their effects on stability can be evaluated by studying the alteration of the effective stiffnesses caused by these errors. The results in Table 3.6 and Table 3.7 show that the effective stiffnesses of Model I are dramatically varied by the geometric errors in the steering linkages whilst the alternation of the effective stiffnesses in Model II caused by the geometric errors in the steering linkage is very small. Since hard effective stiffnesses promote the potential of low speed instability, the particular attention is required with regard to the accuracy of the steering linkages in practical applications of Model I.

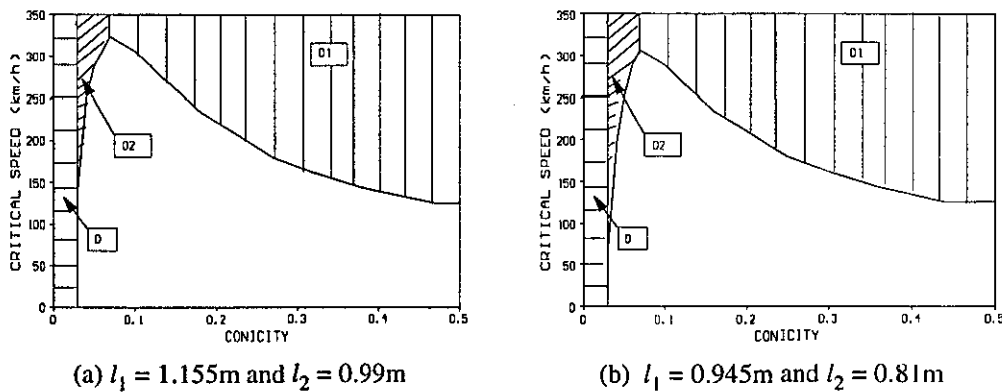


Figure 4.20 The critical speed as function of conicity when the geometric errors exist in Model I, stiff linkage

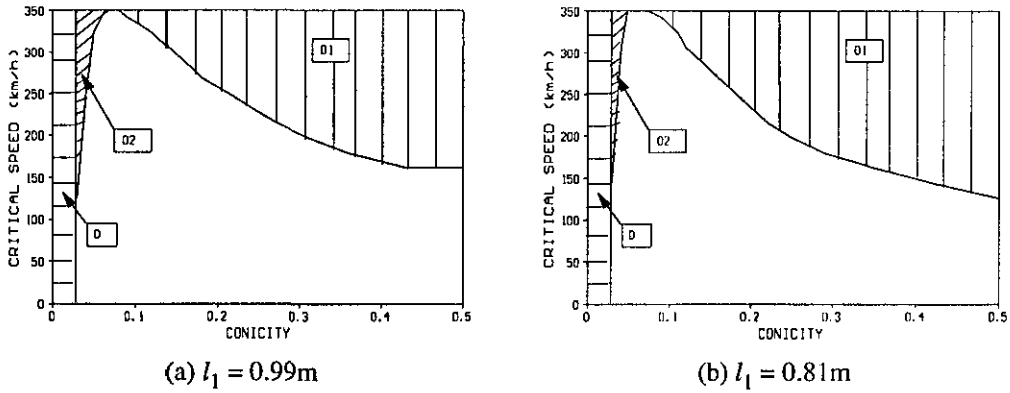


Figure 4.21 The critical speed as function of conicity when the geometric errors exist in Model II, stiff linkage

The geometric errors not only alter the effective stiffnesses, but also change the elements in the sub-compatibility matrices of Eq.(3-2a) and Eq.(3-5a), which bring in the asymmetric factor in the elastic matrices of Eq.(3-2b) and Eq.(3-5b) and the capacity for low speed instability is therefore increased. When the geometric errors (boldly framed in Table 3.6 and Table 3.7) are used in the simulation, the critical speed as a function of conicity is shown in Fig.4.20 and Fig.4.21. Comparing with the results in Fig.4.4, the noticeable variation of the critical speed in Fig.4.20 and Fig.4.21 is in zone O1 in which the critical speed in zone O1 rises when the geometric errors result in the increase of the effective stiffnesses whilst it decreases if the effective stiffnesses are reduced by geometric errors. This is consistent with the above analysis.

4.6 Summary

Although low conicity instability of body-steered bogie vehicles has been noted and studied by several researchers[12,15,19,28] since the 1980's, the contributions to this subject within this chapter are as follows:

This thesis forms the first investigation using both bogie sub-systems with 3 D.O.F (the bogie frame is assumed pinned to the carbody) and with 4 D.O.F (the bogie frame is freely connected to the carbody) in studying low speed instability of perfect steering vehicles. The results show that the bogie sub-system with four degrees of freedom more closely resembles to the physical system than does the bogie sub-system with three degrees of freedom. The conditions derived from the bogie sub-system with four degrees of freedom are more accurate than those from the three degrees of freedom system.

The instability modes of body-steered bogie vehicles have been studied in more detail. There are two major instability modes in body-steered bogie vehicles: low conicity instability and conventional instability. The low conicity instability of body-steered bogie vehicles can be divided into low speed instability and dynamic instability. Low speed instability has been well documented[12,15,19,28], however, dynamic instability in low conicity has not been well reported. Furthermore, a lot of researchers have only noticed divergent mode of low speed instability in low conicity. The theoretical and simulated results in this chapter indicate that low speed instability in low conicity can be oscillatory and may be divergent.

Bogies can be considered as being pinned to the carbody if the secondary suspension is very stiff. Since the minimum conicity derived from the bogie sub-system with three degrees of freedom is higher than that from the four degrees of freedom system, the difference between these two systems indicates that stiff secondary suspension also promotes low conicity instability. This has not been reported until now.

The effects of the parameters in the suspensions and the steering linkages on the instabilities of perfect steering vehicles have also been investigated in more details.

Besides the above contributions, some findings on the stability of perfect steering vehicles are summarised as follows:

- 1, The minimum conicity of low speed instability of perfect steering vehicles is associated with the conditions for bogie vehicle capable of perfect steering. Low speed instability is unavoidable in perfect steering vehicles once their conicity is very low or their steering linkages are too stiff.

- 2, Dynamic instability in low conicity disappears when the steering linkages are very stiff or very soft, however, low speed instability will occur in any conicity whenever the steering linkages are too stiff. The zero yaw stiffnesses in the suspensions are the reasons for this phenomenon because no forces balance the steering mechanism produced by the steering linkages except longitudinal creepage force.

- 3, The instabilities of the perfect steering vehicles are always associated with the wheelset motions. The reasons for this are that the stiffness of the steering linkages is restricted by low speed instability and that the wheelset yaw motions of perfect

steering vehicles are only constrained by their steering linkages. To guarantee the vehicles as being stable at low speed in a reasonable range of conicity, the steering linkages should not be so stiff such that the wheelset constraints become strong enough to promote other unstable motions. The instability, however, may appear in the bogies or the carbody since all motions are coupled.

4, A conflict exists in the requirement for the stiffness of the steering linkages. To cut down the potential of low speed instability, the steering linkages should be soft, whilst stiff steering linkages can improve conventional stability.

5, When the inter wheelset connection exists, some of the effective stiffnesses that promote low speed instability can be shifted to the inter wheelset effective stiffness. The potential of low speed instability is therefore reduced and stability is improved. This is the reason why Model II has better performance in stability than Model I, and this conclusion has general significance for other body-steered bogie vehicles.

6, The primary lateral stiffness does not affect the stability of perfect steering vehicles much as long as it is not too soft nor too hard.

7, The increase of the stiffness and damping of secondary suspension can only improve conventional stability, but, their influences are not too dramatic, especially with regard to the potential range of applications.

8, The geometric errors in the steering linkages can dramatically change the effective stiffnesses of Model I and affect stability. Their accuracy may become very important in practical applications.

RIDE PERFORMANCE OF PERFECT STEERING BOGIE VEHICLES

The comfort of a railway vehicle is one of the most important factors as far as its passengers are concerned, and thus the ride performance is another important index in evaluating the dynamic behaviour of railway vehicles. The ride performance is one form of system response and is decided by two factors: system inputs and system transmissibility. System transmissibility is decided by the system configuration while system inputs are mainly determined by the environment. In this chapter, only track irregularities (alignment and cross-level) are used as system inputs. Strictly, track irregularities are not stationary random process, but are approximated as being so because their variations are usually very slow as compared with vehicle speed. On the other hand, different countries have different standards and classifications for track irregularities, and in this chapter, the American Railroad Standard is used. The PSD's of track irregularities (alignment and cross-level) defined by this standard are shown in Fig.5.1, with their definitions as previously given in Eq.(2-35) and Eq.(2-36).

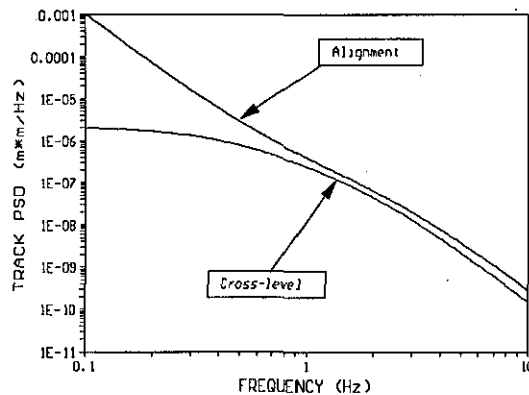


Figure 5.1 PSD's of track irregularities, $v_0 = 200\text{km/h}$

The transmissibility of a railway vehicle mainly depends on its suspensions. A body-steered bogie vehicle possesses linkages that connect the carbody with the wheelsets such that track irregularities can be transferred into the carbody through these linkages, and the ride quality of a body-steered bogie vehicle is thus potentially adversely affected with regard to conventional bogie vehicles. For perfect steering bogie vehicles, the constraints provided by the suspensions are weakened since there

are neither primary nor secondary yaw stiffnesses, which may produce a positive effect on vehicle ride quality. There are few investigations and explanations in this field so far, and thus, in this chapter, the ride performance of perfect steering vehicles will be studied and the influences of suspensions and steering linkages on the ride performance will be explored. Since only one kind of vehicle disturbance (track random irregularities) has been used in the simulation, the results and analyses in this chapter approximately reflect the effects of system transmissibility on ride performance of perfect steering vehicles, and the comprehensive understanding of the ride performance of perfect steering vehicles needs to be investigated further by applying various disturbances.

5.1 Indices of Ride Performance

Carbody accelerations, primary strokes (relative lateral displacements between wheelsets and bogie frames) and secondary strokes (relative lateral displacement between carbody and bogie frames) are well known to evaluate ride performance of railway bogie vehicles. The carbody accelerations calculated at five points on the floor level, as illustrated in Fig.5.2, are the index of ride quality while the strokes are the index of working spaces for suspensions.

The accelerations at these points are:

$$\begin{aligned}
 \text{at point A, } a_A &= \ddot{y}_b + l\ddot{\psi}_b + h_0\ddot{\phi}_b \\
 \text{at point B, } a_B &= \ddot{y}_b + l_0\ddot{\psi}_b + h_0\ddot{\phi}_b \\
 \text{at point C, } a_C &= \ddot{y}_b + h_0\ddot{\phi}_b \\
 \text{at point D, } a_D &= \ddot{y}_b - l_0\ddot{\psi}_b + h_0\ddot{\phi}_b \\
 \text{at point E, } a_E &= \ddot{y}_b - l\ddot{\psi}_b + h_0\ddot{\phi}_b
 \end{aligned} \tag{5-1}$$

and so, the auto-correlation functions of the accelerations at those points are:

$$\begin{aligned}
 R_{a_A}(\tau) &= \lim_{T \rightarrow \infty} \frac{1}{T} \int_0^T (\ddot{y}_b + l\ddot{\psi}_b + h_0\ddot{\phi}_b)_t (\ddot{y}_b + l\ddot{\psi}_b + h_0\ddot{\phi}_b)_{t+\tau} dt \\
 R_{a_B}(\tau) &= \lim_{T \rightarrow \infty} \frac{1}{T} \int_0^T (\ddot{y}_b + l_0\ddot{\psi}_b + h_0\ddot{\phi}_b)_t (\ddot{y}_b + l_0\ddot{\psi}_b + h_0\ddot{\phi}_b)_{t+\tau} dt \\
 R_{a_C}(\tau) &= \lim_{T \rightarrow \infty} \frac{1}{T} \int_0^T (\ddot{y}_b + h_0\ddot{\phi}_b)_t (\ddot{y}_b + h_0\ddot{\phi}_b)_{t+\tau} dt \\
 R_{a_D}(\tau) &= \lim_{T \rightarrow \infty} \frac{1}{T} \int_0^T (\ddot{y}_b - l_0\ddot{\psi}_b + h_0\ddot{\phi}_b)_t (\ddot{y}_b - l_0\ddot{\psi}_b + h_0\ddot{\phi}_b)_{t+\tau} dt \\
 R_{a_E}(\tau) &= \lim_{T \rightarrow \infty} \frac{1}{T} \int_0^T (\ddot{y}_b - l\ddot{\psi}_b + h_0\ddot{\phi}_b)_t (\ddot{y}_b - l\ddot{\psi}_b + h_0\ddot{\phi}_b)_{t+\tau} dt
 \end{aligned} \tag{5-2}$$

PSD's of the accelerations at these points are:

$$\begin{aligned}
 S_{a_A}(\omega) &= \omega^4 (s_{y_b} + l s_{y\psi_b} + h_0 s_{y\phi_b} + l s_{\psi y_b} + l^2 s_{\psi_b} + h_0 l s_{\psi\phi_b} + h_0 s_{\phi y_b} + l h_0 s_{\phi\psi_b} + h_0^2 s_{\phi_b}) \\
 S_{a_B}(\omega) &= \omega^4 (s_{y_b} + l_0 s_{y\psi_b} + h_0 s_{y\phi_b} + l_0 s_{\psi y_b} + l_0^2 s_{\psi_b} + h_0 l_0 s_{\psi\phi_b} + h_0 s_{\phi y_b} + l_0 h_0 s_{\phi\psi_b} + h_0^2 s_{\phi_b}) \\
 S_{a_C}(\omega) &= \omega^4 (s_{y_b} + h_0 s_{y\phi_b} + h_0 s_{\phi y_b} + h_0^2 s_{\phi_b}) \\
 S_{a_D}(\omega) &= \omega^4 (s_{y_b} - l s_{y\psi_b} + h_0 s_{y\phi_b} - l s_{\psi y_b} + l^2 s_{\psi_b} - h_0 l s_{\psi\phi_b} + h_0 s_{\phi y_b} - l h_0 s_{\phi\psi_b} + h_0^2 s_{\phi_b}) \\
 S_{a_E}(\omega) &= \omega^4 (s_{y_b} - l_0 s_{y\psi_b} + h_0 s_{y\phi_b} - l_0 s_{\psi y_b} + l_0^2 s_{\psi_b} - h_0 l_0 s_{\psi\phi_b} + h_0 s_{\phi y_b} - l_0 h_0 s_{\phi\psi_b} + h_0^2 s_{\phi_b})
 \end{aligned}
 \tag{5-3}$$

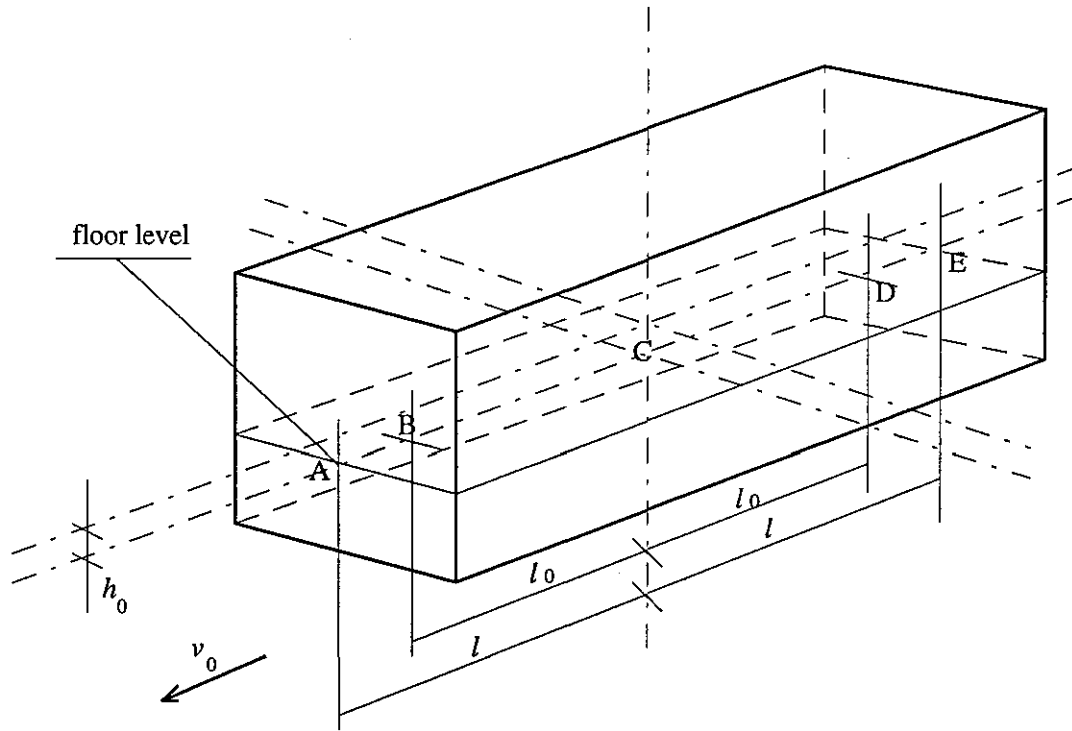


Figure 5.2 The five points at which accelerations are calculated

The secondary strokes are defined by:

$$\text{Front Secondary Stroke} = y_b + l_0 \psi_b - h_3 \phi_b - y_{T_L} - h_2 \phi_{T_L}$$

(relative lateral displacement between carbody and leading bogie frame)

$$\text{Rear Secondary Stroke} = y_b - l_0 \psi_b - h_3 \phi_b - y_{T_L} - h_2 \phi_{T_L}$$

(relative lateral displacement between carbody and trailing bogie frame)

and their PSD's are:

$$\begin{aligned}
 S_{FSS}(\omega) &= s_{y_b} + l_0 s_{y\psi_b} - h_3 s_{y\phi_b} - s_{y_b y_{TL}} - h_2 s_{y_b \phi_{TL}} + l_0 s_{y\psi_b} + l_0^2 s_{\psi_b} - l_0 h_3 s_{\psi\phi_b} - l_0 s_{\psi_b y_{TL}} - l_0 h_2 s_{\psi_b \phi_{TL}} \\
 &\quad - h_3 s_{\phi_{y_b}} - l_0 h_3 s_{\phi\psi_b} + h_3^2 s_{\phi_b} + h_3 s_{\phi_b y_{TL}} + h_3 h_2 s_{\phi_b \phi_{TL}} - s_{y_{TL} y_b} - l_0 s_{y_{TL} \psi_b} - h_3 s_{y_{TL} \phi_b} + s_{y_{TL}} \\
 &\quad + h_2 s_{y_{TL} \phi_{TL}} - h_2 s_{\phi_{TL} y_b} - h_2 l_0 s_{\phi_{TL} \psi_b} + h_2 h_3 s_{\phi_{TL} \phi_b} + h_2 s_{\phi_{TL} y_{TL}} + h_2^2 s_{\phi_{TL}} \\
 S_{RSS}(\omega) &= s_{y_b} - l_0 s_{y\psi_b} - h_3 s_{y\phi_b} - s_{y_b y_{TR}} - h_2 s_{y_b \phi_{TR}} - l_0 s_{y\psi_b} + l_0^2 s_{\psi_b} + l_0 h_3 s_{\psi\phi_b} + l_0 s_{\psi_b y_{TR}} + l_0 h_2 s_{\psi_b \phi_{TR}} \\
 &\quad - h_3 s_{\phi_{y_b}} + l_0 h_3 s_{\phi\psi_b} + h_3^2 s_{\phi_b} + h_3 s_{\phi_b y_{TR}} + h_3 h_2 s_{\phi_b \phi_{TR}} - s_{y_{TR} y_b} + l_0 s_{y_{TR} \psi_b} + h_3 s_{y_{TR} \phi_b} + s_{y_{TR}} \\
 &\quad + h_2 s_{y_{TR} \phi_{TR}} - h_2 s_{\phi_{TR} y_b} + h_2 l_0 s_{\phi_{TR} \psi_b} + h_2 h_3 s_{\phi_{TR} \phi_b} - h_2 s_{\phi_{TR} y_{TR}} + h_2^2 s_{\phi_{TR}}
 \end{aligned} \tag{5-4}$$

The primary strokes at the first and fourth wheelsets are:

$$\begin{aligned}
 \text{Primary Stroke of First Wheelset} &= y_{TL} - h_1 \phi_{TL} + a\psi_{TL} - y_{w_1} \\
 &\text{(relative lateral displacement between outboard wheelset and bogie frame in leading bogie)}
 \end{aligned}$$

$$\begin{aligned}
 \text{Primary Stroke of Fourth Wheelset} &= y_{TR} - h_1 \phi_{TR} - a\psi_{TR} - y_{w_4} \\
 &\text{(relative lateral displacement between outboard wheelset and bogie frame in trailing bogie)}
 \end{aligned}$$

So, their PSD's are:

$$\begin{aligned}
 S_{PSI}(\omega) &= s_{y_{TL}} - h_1 s_{y_{TL} \phi_{TL}} + a s_{y_{TL} \psi_{TL}} - s_{y_{TL} y_{w_1}} - h_1 s_{\phi_{TL} y_{TL}} + h_1^2 s_{\phi_{TL}} - a h_1 s_{\phi_{TL} \psi_{TL}} + h_1 s_{\phi_{TL} y_{w_1}} \\
 &\quad + a s_{\psi_{TL} y_{TL}} - a h_1 s_{\psi_{TL} \phi_{TL}} + a^2 s_{\psi_{TL}} - a s_{\psi_{TL} y_{w_1}} - s_{y_{w_1} y_{TL}} + h_1 s_{y_{w_1} \phi_{TL}} - a s_{y_{w_1} \psi_{TL}} + s_{y_{w_1}} \\
 S_{PSI}(\omega) &= s_{y_{TR}} - h_1 s_{y_{TR} \phi_{TR}} - a s_{y_{TR} \psi_{TR}} - s_{y_{TR} y_{w_4}} - h_1 s_{\phi_{TR} y_{TR}} + h_1^2 s_{\phi_{TR}} + a h_1 s_{\phi_{TR} \psi_{TR}} + h_1 s_{\phi_{TR} y_{w_4}} \\
 &\quad - a s_{\psi_{TR} y_{TR}} + a h_1 s_{\psi_{TR} \phi_{TR}} + a^2 s_{\psi_{TR}} + a s_{\psi_{TR} y_{w_4}} - s_{y_{w_4} y_{TR}} + h_1 s_{y_{w_4} \phi_{TR}} + a s_{y_{w_4} \psi_{TR}} + s_{y_{w_4}}
 \end{aligned} \tag{5-5}$$

The Root Mean Square (rms) of $\mathbf{x}(t)$ can be found from:

$$\text{rms} = \sqrt{E[x^2]} = \sqrt{\int_{-\infty}^{\infty} s_x(\omega) d\omega} = \sqrt{\int_0^{\infty} W_x(f) df} \tag{5-6}$$

Since human beings have different sensitivity to various band frequency accelerations, the weighted rms is usually used to evaluate the comfort of vehicles. In this research, the filter suggested by ISO/DIS 2631-1 (1994) [106] is applied to weight rms's of the accelerations at these chosen points. The weighted acceleration is defined by[106]:

$$a_w = \left[\sum_{23} (W_i a_i)^2 \right]^{1/2} \tag{5-7}$$

where, a_i is the rms acceleration in the i^{th} one-third octave band and,
 W_i is the weighting factor for the i^{th} one-third octave band as
 given in Table 5.1.

5.2 Coupling between Steering Linkages And Suspensions

By expanding $\Delta_2(\omega)$ in Eq.(2-50), it becomes:

$$\begin{aligned} \Delta_2(\omega) = & \mathbf{H}_{\gamma_b}(\omega)[\mathbf{I} - \mathbf{H}_{\gamma_r}(\omega)\mathbf{H}_{\gamma_b}(\omega)]^{-1}\mathbf{H}_{w_r}(\omega) - \mathbf{H}_{w_b}(\omega) \\ & - \mathbf{H}_{\gamma_b}(\omega)[\mathbf{I} - \mathbf{H}_{\gamma_r}(\omega)\mathbf{H}_{\gamma_b}(\omega)]^{-1}\mathbf{H}_{\gamma_r}(\omega)\mathbf{H}_{w_b}(\omega) \end{aligned} \quad (5-8a)$$

Since there is no direct connection between the carbody and wheelsets in a conventional bogie vehicle, we have $\mathbf{H}_{w/b}(\omega) = \mathbf{H}_{b/w}(\omega) = 0$ and

$$\Delta_2(\omega) = \mathbf{H}_{\gamma_b}(\omega)[\mathbf{I} - \mathbf{H}_{\gamma_r}(\omega)\mathbf{H}_{\gamma_b}(\omega)]^{-1}\mathbf{H}_{w_r}(\omega) \quad (5-8b)$$

The transfer function $\mathbf{H}_3(\omega)$ of body-steered bogie vehicles thus has two more terms than that of conventional bogie vehicles, as seen in Eq.(2-49). These two terms mean that a body-steered bogie vehicle has two extra channels that can transfer track irregularities to the carbody, i.e. they can be transferred into the carbody directly by the steering linkages $\mathbf{H}_{w/b}(\omega)$ and by the coupling of the steering linkage and secondary suspension, i.e. by $\mathbf{H}_{\gamma_b}(\omega)[\mathbf{I} - \mathbf{H}_{\gamma_r}(\omega)\mathbf{H}_{\gamma_b}(\omega)]^{-1}\mathbf{H}_{\gamma_r}(\omega)\mathbf{H}_{w_b}(\omega)$. System transmissibility is therefore potentially increased by the steering linkages in body-steered bogie vehicles. On the other hand, $\mathbf{H}_{w/b}(\omega)$ and $\mathbf{H}_{b/w}(\omega)$ are also included in $\Delta_1(\omega)$ and $\Delta_3(\omega)$ of Eq.(2-49), which means that the coupling of the suspensions is thus complicated by the steering linkages in body-steered bogie vehicles.

5.2.1 An Example

Before discussing further the transmissibility and suspension couplings of the perfect steering vehicles, a rather simple example is set up in Fig.5.3 to allow an understanding of i)the system transmissibility and ii)the effect of three suspensions on system transmissibility.

Supposing that all elements in Fig.5.3 are linear, the transmissibility of this linear system can be investigated by its transfer function. If the input remains unchanged, the output of this linear system is mainly governed by its transfer function.

The dynamic equation of the system in Fig.5.3 is:

$$\begin{aligned} m_1 \ddot{x}_1 + (k_1 + k_2)x_1 - k_2 x_2 &= k_1 x_0 \\ m_2 \ddot{x}_2 + (k_2 + k_3)x_2 - k_2 x_1 &= k_3 x_0 \end{aligned}$$

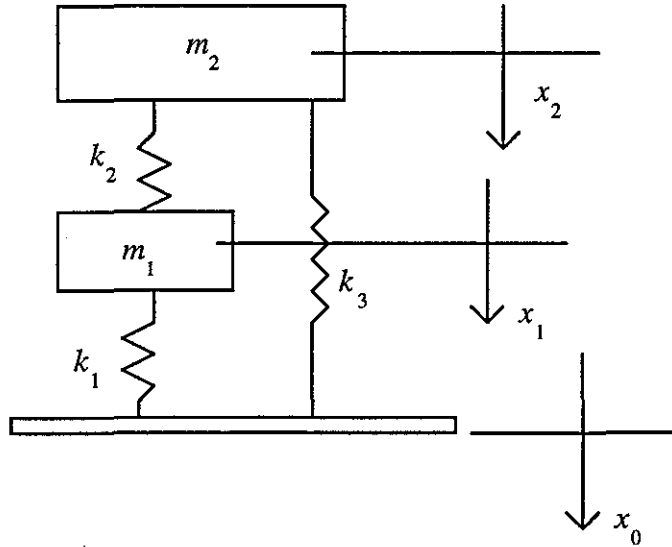


Figure 5.3 A system with two degrees of freedom and three suspensions

After applying the Laplace transform, it becomes:

$$\begin{aligned} X_1(s) &= \frac{(m_2 s^2 + k_2 + k_3)k_1 + k_2 k_3}{(m_1 s^2 + k_1 + k_2)(m_2 s^2 + k_2 + k_3) - k_2^2} X_0(s) \\ X_2(s) &= \frac{k_1 k_2 + (m_1 s^2 + k_1 + k_2)k_3}{(m_1 s^2 + k_1 + k_2)(m_2 s^2 + k_2 + k_3) - k_2^2} X_0(s) \end{aligned}$$

The transfer function from x_0 to x_2 is:

$$H_2(\omega) = \frac{k_1 k_2}{\Delta} + \frac{(k_1 + k_2)k_3}{\Delta} - \frac{m_1 k_3 \omega^2}{\Delta} \tag{5-9a}$$

$$H_2(\omega) = H_{21}(\omega) + H_{22}(\omega) - H_{23}(\omega) \tag{5-9b}$$

where,

$$\Delta = (k_1 + k_2 - m_1 \omega^2)(k_2 + k_3 - m_2 \omega^2) - k_2^2$$

The natural frequency ω_n is defined as the frequency at which the transfer function becomes infinite if there is no damping in the system; and the minimum value frequency ω_m is defined as the frequency at which $dH_2(\omega)/d\omega = 0$ if there is no damping in the system. When $\Delta \rightarrow 0$, we have $H_2(\omega) \rightarrow \infty$, and thus the natural frequencies can be found by letting $\Delta = 0$, i.e.

$$(k_1 + k_2 - m_1\omega^2)(k_2 + k_3 - m_2\omega^2) - k_2^2 = 0$$

If $k_3 = 0$, the natural frequencies of $H_2(\omega)$ are

$$\begin{aligned} \omega_{n_{1,2}}^2 &= \frac{1}{2}(\omega_{0_1}^2 + \frac{m_1 + m_2}{m_1}\omega_{0_2}^2) \\ &\pm \frac{1}{2}\left[\omega_{0_1}^4 + \frac{(m_1 + m_2)^2}{m_1^2}\omega_{0_2}^4 + \frac{m_2 - m_1}{m_1}2\omega_{0_1}^2\omega_{0_2}^2\right]^{1/2} \end{aligned} \quad (5-10)$$

where,

$$\omega_{n_2} > \omega_{n_1}, \quad \omega_{0_1}^2 = \frac{k_1}{m_1} \quad \text{and} \quad \omega_{0_2}^2 = \frac{k_2}{m_2}$$

and minimum value frequencies of $H_2(\omega)$ are:

$$\omega_{m_1}^2 = 0 \quad \text{and} \quad \omega_{m_2}^2 = \frac{1}{2}(\omega_{0_1}^2 + \frac{m_1 + m_2}{m_1}\omega_{0_2}^2) \quad (5-11)$$

So, the minimum values of $H_2(\omega)$ are

$$H_2(\omega_{m_1}) = 1 \quad \text{and} \quad |H_2(\omega_{m_2})| = \frac{4\omega_{0_1}^2\omega_{0_2}^2}{\omega_{0_1}^4 + (m_2 + m_1)^2\omega_{0_2}^4 / m_1^2} \quad (5-12)$$

When $k_3 \neq 0$, the natural frequencies of $H_2(\omega)$ are:

$$\begin{aligned} \tilde{\omega}_{n_{1,2}}^2 &= \frac{1}{2}(\omega_{0_1}^2 + \omega_{0_3}^2 + \frac{m_1 + m_2}{m_1}\omega_{0_2}^2) \\ &\pm \frac{1}{2}\left[(\omega_{0_1}^2 - \omega_{0_3}^2)(\omega_{0_1}^2 - \omega_{0_3}^2 + \frac{m_2 - m_1}{m_1}2\omega_{0_2}^2) + \frac{(m_1 + m_2)^2}{m_1^2}\omega_{0_2}^4\right]^{1/2} \end{aligned} \quad (5-13)$$

where, $\tilde{\omega}_{n_2} > \tilde{\omega}_{n_1}$ and $\omega_{0_3}^2 = \frac{k_3}{m_2}$.

Since

$$(\omega_{0_1}^2 + \omega_{0_3}^2 + \frac{m_1 + m_2}{m_1} \omega_{0_2}^2) > (\omega_{0_1}^2 + \frac{m_1 + m_2}{m_1} \omega_{0_2}^2)$$

and

$$\left[(\omega_{0_1}^2 - \omega_{0_3}^2)^2 + \frac{m_2 - m_1}{m_1} 2\omega_{0_2}^2 (\omega_{0_1}^2 - \omega_{0_3}^2) + \frac{(m_1 + m_2)^2}{m_1^2} \omega_{0_2}^4 \right] <$$

$$< \left[(\omega_{0_1}^4 + \frac{m_2 - m_1}{m_1} 2\omega_{0_2}^2 \omega_{0_1}^2 + \frac{(m_1 + m_2)^2}{m_1^2} \omega_{0_2}^4 \right]$$

we have:

$$\tilde{\omega}_{n_1} > \omega_{n_1} \quad \text{and} \quad \tilde{\omega}_{n_2} < \omega_{n_2}$$

Three effects on the natural frequencies are produced as a result of $k_3 \neq 0$:

- i) the first natural frequency gets bigger, i.e. $\tilde{\omega}_{n_1} > \omega_{n_1}$,
- ii) the second natural frequency get smaller, i.e. $\tilde{\omega}_{n_2} < \omega_{n_2}$ and thus,
- iii) the difference between the two natural frequencies is reduced, i.e.

$$(\tilde{\omega}_{n_2} - \tilde{\omega}_{n_1}) < (\omega_{n_2} - \omega_{n_1})$$

The minimum value frequencies of $H_2(\omega)$ are:

$$\tilde{\omega}_{m_1}^2 = 0$$

$$\tilde{\omega}_{m_2}^4 = \left(\frac{\omega_{0_2}^2 + \omega_{0_3}^2}{\omega_{0_3}^2} \omega_{0_1}^2 + \frac{m_2}{m_1} \omega_{0_2}^2 \right) \pm$$

$$\left[\left(\frac{\omega_{0_2}^2 + \omega_{0_3}^2}{\omega_{0_3}^2} \omega_{0_1}^2 + \frac{m_2}{m_1} \omega_{0_2}^2 \right) \left(\frac{\omega_{0_1}^2 - \omega_{0_3}^2}{\omega_{0_3}^2} \right) \omega_{0_2}^2 \right]^{\frac{1}{2}} \quad (5-14)$$

It is easy to show that $H_2(0) = 1$. The second minimum value frequency of $H_2(\omega)$ when $k_3 \neq 0$ can be either larger or smaller than that in Eq.(5-11) when $k_3 = 0$. It is difficult to compare theoretically the second minimum value of $H_2(\omega)$ directly from the result in Eq.(5-14). Suppose $\tilde{\omega}_{m_2} > \omega_{m_2}$, then we have:

$$\left| H_2(\tilde{\omega}_{m_2}) \right| = \frac{4\omega_{0_1}^2 \omega_{0_2}^2 + \omega_{0_1}^2 \omega_{0_3}^2 / 2 + (m_2 - m_1) \omega_{0_2}^2 \omega_{0_3}^2 / 2m_1}{\left| \omega_{0_1}^2 \omega_{0_3}^2 - (\omega_{0_1}^2 - \omega_{0_3}^2) [\omega_{0_1}^2 + 2(m_2 - m_1) \omega_{0_2}^2] - (m_2 + m_1)^2 \omega_{0_2}^4 / m_1^2 \right|} \quad (5-15)$$

Comparing Eq.(5-15) with Eq.(5-12), it can be found that:

The numerator of Eq.(5-15) > The numerator of Eq.(5-12) and,
 The denominator of Eq.(5-15) < The denominator of Eq(5-12)

So, we get $|H_2(\tilde{\omega}_{m_2})|$ (when $k_3 \neq 0$) > $|H_2(\omega_{m_2})|$ (when $k_3 = 0$).

For frequencies are in $\tilde{\omega}_{n_1} < \omega < \omega_{m_2}$, the amplitude of $H_2(\omega)$ when $k_3 \neq 0$ is larger than that when $k_3 = 0$. On the other hand, the values of H_{23} in low frequencies will be much lower than H_{21} and H_{22} while the values of H_2 are governed by H_{23} in high frequency because the numerator of H_{23} increases in proportion to ω^2 . Actually,

$$H_{23} > H_{21} + H_{22}$$

when

$$\omega^2 \geq \omega_{01}^2 + \frac{\omega_{01}^2}{\omega_{03}^2} \omega_{02}^2 + m_2 \omega_{02}^2 / m_1$$

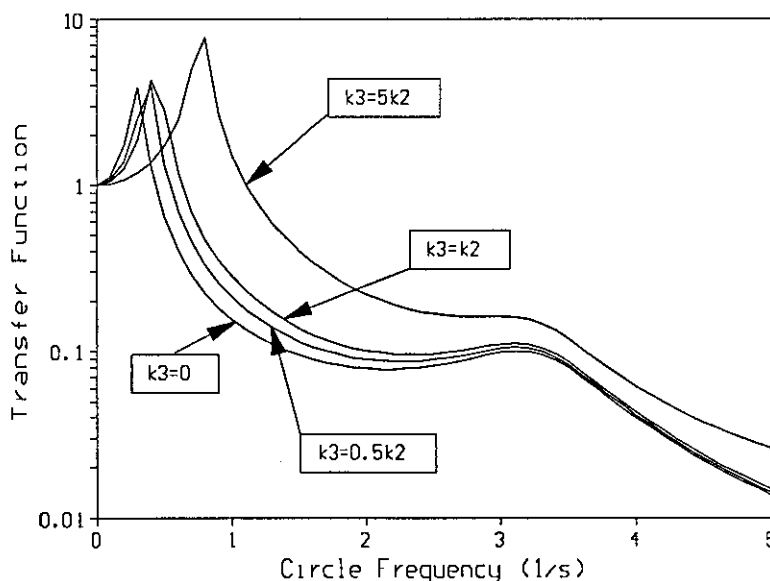


Figure 5.4 The transfer function $H_2(\omega)$, $\omega_{01}^2 = 5$ and $\omega_{02}^2 = 1$

In general, damping exists in a physical system, and thus transfer function $H_2(\omega)$ in a physical system cannot become infinite when frequency equals to the natural frequencies. Basing on the analysis above, the diagram in Fig.5.4 illustrates how the influence of the increment of k_3 on the transfer function $H_2(\omega)$ in the frequency domain when a damper is applied to the connection between m_1 and m_2 . Four

effects can be observed in Fig.5.4 when $k_3 \neq 0$: i) the first natural frequency increases and its variation is bigger than that of the second natural frequency; ii) the transfer function in the first natural frequency and between the two natural frequencies increases; iii) the transfer function reduces at very low frequencies and iv) the effects are strengthened as k_3 becomes stiff. The overall results show that the transmissibility increases as the stiffness k_3 becomes from zero to non-zero and harder, especially between two natural frequencies.

To evaluate ride quality, another two factors need to be considered, these being the distribution of system disturbances over the frequency range and the sensitivity of human beings to vibrations over the frequency range. For railway vehicles, the former is governed by track while the latter is a universal standard. In Fig.5.1, the amplitudes of the disturbances are high at the low frequencies and reduce as the frequency increases. Since $H_2(0) = 1$ and $H_2(\omega)$ increases as ω becomes larger until it reaches the first natural frequency, the first natural frequency should be as low as possible so as to decrease system responses. On the other hand, human beings are most sensitive to the acceleration in the lateral direction between 0.315Hz and 4.0Hz since the weighting factors in this frequency band are bigger than 0.5, as seen in Table 5.1. Any natural frequency should thus be designed outside this frequency band if it is possible, i.e. the first natural frequency should be lower than 0.315Hz and the second natural frequency should be higher than 4.0Hz.

In order to reduce the transfer function $H_2(\omega)$, therefore, several methods can be used. Increasing system damping to depress the responses over all frequencies will have the desired effect and increasing the difference between the two natural frequencies as to reduce the transmissibility between the two natural frequencies will also work and finally, minimising the first natural frequency will also help.

5.2.2 Complication Associated with Perfect Steering Vehicles

A body-steered bogie vehicle can be approximately considered as a system with three suspensions and two masses if the masses of the wheelsets are ignored, in which the carbody and the bogies can be considered as m_2 and m_1 respectively whilst the primary suspension, secondary suspension and steering linkage act as k_1 , k_2 and k_3 respectively, by referring to Fig.5.3. It seems that the steering linkages in body-steered bogie vehicles will deteriorate the ride quality of body-steered bogie vehicles. There are, however, neither primary nor secondary yaw stiffnesses in perfect steering vehicles, only the steering linkages providing the constraints for the

inertia bodies in their yaw motions, and thus the increment in the effective stiffnesses can strengthen these constraints, which may benefit ride performance, and therefore, the functions of the effective stiffnesses in the steering linkages on the ride performance are more complex.

Three approaches shown in the previous section can improve ride quality. Firstly, increasing the difference between the first two natural frequencies will filter out more of the disturbances between the natural frequencies. The other techniques involve softening the secondary suspension to decrease the responses of low frequencies, and applying more damping to minimise the responses over all frequencies. Soft suspension, however, will require more working space and thus has its limitation in any practical application, whilst the effective stiffnesses are restricted by low conicity instability in perfect steering vehicles, which may reduce the difference between first two natural frequencies, giving the potential for increasing transmissibility between the two natural frequencies. All of these factors will be therefore investigated in the next section.

5.3 Results of Simulation

In this section, the vehicle speed v_0 is 200km/h and the conicity λ is 0.1, and the suspension parameters and steering linkage parameters of Set 2 (stiff steering linkage) in Table 3.4 (Model I) and Table 3.5 (Model II) are used, and the secondary yaw damping (10^6 N-s-m) is applied to Model I.

5.3.1 Ride Quality

The PSD's of the accelerations at the five points defined in Fig.5.2 are very small when frequency $f > 10.0$ Hz, and thus only PSD's at points A and C in the band of $0.1\text{Hz} \leq f \leq 10.0\text{Hz}$ are displayed in Fig.5.5. The weighted rms's of the accelerations at the five points from 0.1Hz to 100.0Hz are:

	point A	point B	point C	point D	point E
Model I	8.85mg	7.58mg	5.97mg	9.02mg	10.47mg
Model II	10.19mg	9.07mg	6.57mg	7.01mg	7.77mg

The maximum rms of the acceleration of Model I is at the tail end (point E) while it is at the front end (point A) for Model II.

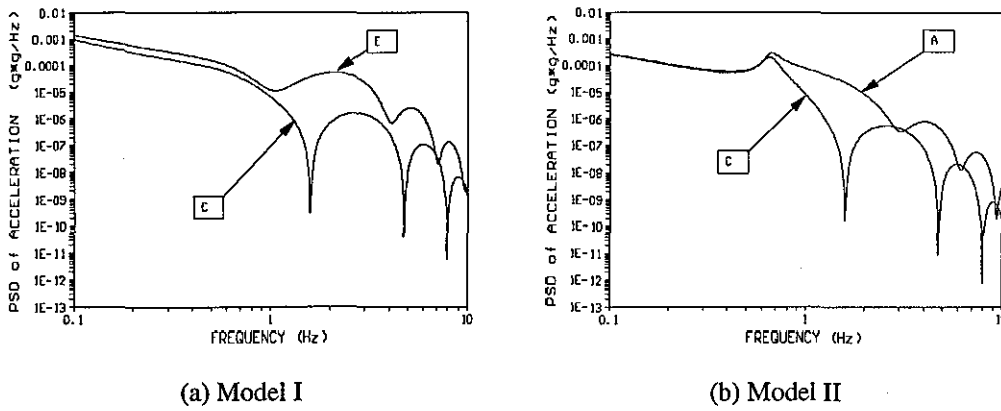


Figure 5.5 PSD's of Model I and Model II

The responses of Model I at low frequencies ($f < 0.5\text{Hz}$) are the highest, as shown in Fig.5.5a, while the highest responses of Model II are around 1.0Hz, as shown in Fig.5.5b. Since the amplitude of the transfer function is equal to or greater than 1 from the zero frequency to the first natural frequency, it is not difficult to understand the reasons why the system responses are very high at low frequencies when the track irregularities in Fig.5.1 are used. The results also imply that the first natural frequency is less than 1.0Hz for Model I and is around 1.0Hz for Model II. In the calculation, $h_0 = 0$ is used such that the accelerations at the points A, C and E are:

$$a_A = \ddot{y}_b + l\ddot{\psi}_b \quad a_C = \ddot{y}_b \quad a_E = \ddot{y}_b - l\ddot{\psi}_b$$

The acceleration of point C is, in fact, the lateral acceleration at the carbody weight centre. The difference between a_A and a_E is the sign of $l\ddot{\psi}_b$, and in Fig.5.5a, the phase of a_E is very close to the phase of a_C . In Fig.5.5b, the phase difference between a_A and a_C is nearly 180° , which indicates that the phase difference between the yaw acceleration and lateral acceleration of the carbodies is approximately 180° ,

The stiffness ratio between Model I and Model II are listed as follows:

	Model I		Model II
Primary lateral stiffness	1	:	3
Secondary lateral stiffness	1	:	3
Effective stiffness $k_e (= k_{e1} = k_{e2})$	3.5	:	1

If the vehicles are considered as the system of Fig.5.3, the primary suspension is k_1 , the secondary suspension is k_2 and the steering linkage is k_3 . Thus,

$$\begin{aligned} \omega_{01} \text{ (of Model I)} &< \omega_{01} \text{ (of Model II)} \\ \omega_{02} \text{ (of Model I)} &< \omega_{02} \text{ (of Model II)} \\ \omega_{03} \text{ (of Model I)} &> \omega_{03} \text{ (of Model II)}. \end{aligned}$$

From Eq.(5-13), the first natural frequency of Model I is lower than that of Model II, and thus the responses of Model I in low frequencies is higher than those of Model II while the responses of Model II around the first natural frequency are higher than those of Model I, as shown in Fig.5.5.

In Table 5.1, the weighting factors are less than 0.5 when $f < 0.315\text{Hz}$ and $f > 4.0\text{Hz}$, therefore, the reduction in the system responses between 0.315-4.0Hz can result in the most significant benefit with regard to vehicle ride quality. To simplify the analysis, the frequency range of interest is divided into three bands: 0.1-0.315 Hz, 0.315-4.0 Hz, and 4.0-10.0Hz. Since $\text{rms} = \sqrt{\int_0^{\infty} W_x(f)df}$, the proportions of unweighted rms's in each band are defined by:

$$\left[\left(\frac{\text{rms}_{0.1-0.315\text{Hz}}}{\text{rms}_{0.1-10.0\text{Hz}}} \right)^2 + \left(\frac{\text{rms}_{0.315-4.0\text{Hz}}}{\text{rms}_{0.1-10.0\text{Hz}}} \right)^2 + \left(\frac{\text{rms}_{4.0-10.0\text{Hz}}}{\text{rms}_{0.1-10.0\text{Hz}}} \right)^2 \right]^{1/2} = 1 \quad (5-16a)$$

or

$$[\vartheta_1^2 + \vartheta_2^2 + \vartheta_3^2] = 1 \quad (5-16b)$$

where, ϑ_1 is the proportion for the 0.1-0.315Hz band, ϑ_2 for the 0.315-4.0Hz band and ϑ_3 for the 4.0-10.0Hz band.

The mean ratio of unweighted rms at each frequency band is defined by:

$$\begin{aligned} \varphi_1 &= (\vartheta_{1A} + \vartheta_{1B} + \vartheta_{1C})/3; \quad \varphi_2 = (\vartheta_{2A} + \vartheta_{2B} + \vartheta_{2C})/3; \\ \varphi_3 &= (\vartheta_{3A} + \vartheta_{3B} + \vartheta_{3C})/3. \end{aligned} \quad (5-17)$$

where subscripts A, B and C represent the points A, B and C.

The results in Fig.5.6 show that the rms's of the accelerations of Model I are almost equally distributed in the 0.1-0.315Hz and 0.315-4.0Hz bands while they are mainly

concentrated on the 0.315-4.0Hz band for Model II, which indicates that the first natural frequency of Model I is lower than that of Model II.

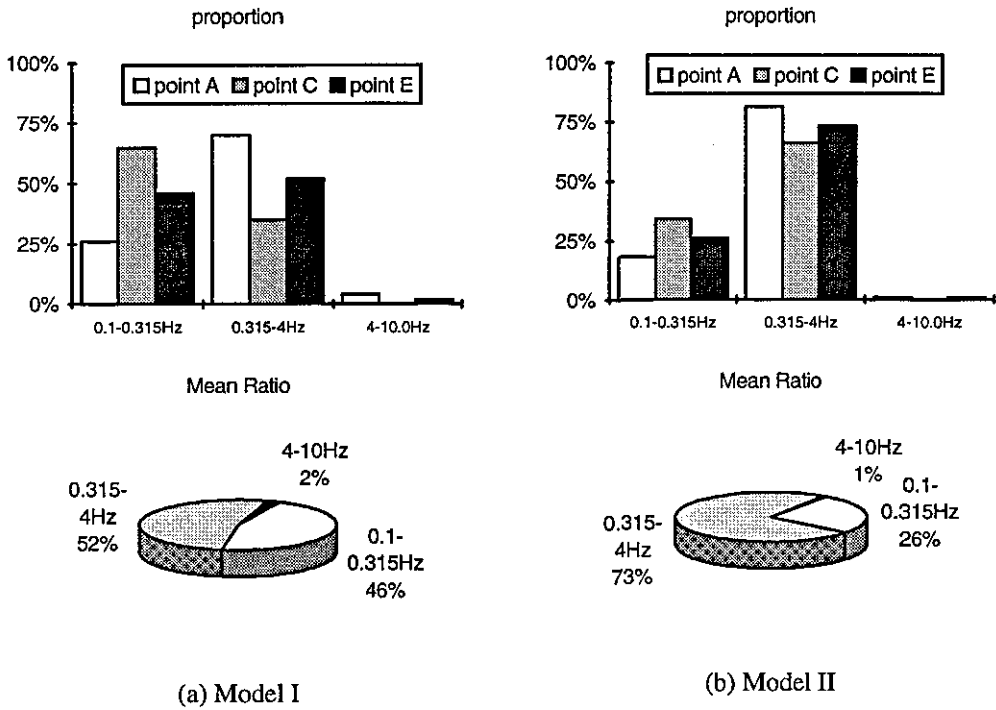


Figure 5.6 The proportions and mean ratios of unweighted rms's of accelerations

If the proportion of the weighted rms in each band is defined as: $\frac{\text{rms}_{\text{weighted}}}{\sum \text{rms}_{\text{weighted}}}$.

the mean ratios of the weighted rms's at points A, C and E over the frequency bands are illustrated in Fig.5.7, and the average reductions of rms's by weighting factors over the three points are listed as follows:

	0.1-0.315Hz	0.315-4.0Hz	4.0-10.0Hz
Model I	70.8%	18.21%	66.67%
Model II	66.09%	8.5%	66.09%

It can be seen that almost two thirds of the unweighted acceleration rms's are depressed by the weighting factors on both 0.1-0.315Hz and 4.0-10.0Hz. If the unweighted rms is a constant, the ride quality can be improved by moving the PSD's of the accelerations from the 0.315-4.0Hz band into either the 0.1-0.315Hz or 4-10.0Hz bands. Referring to Fig.5.4, it is implied that the first natural frequency should be reduced and the second natural frequency increased. From Eq.(5-10), this can be achieved by adding up the difference between ω_{01} and ω_{02} , which means either increasing the inertia difference between the two masses (carbody and bogie)

or enlarging the stiffness difference between the two suspensions (primary and secondary).

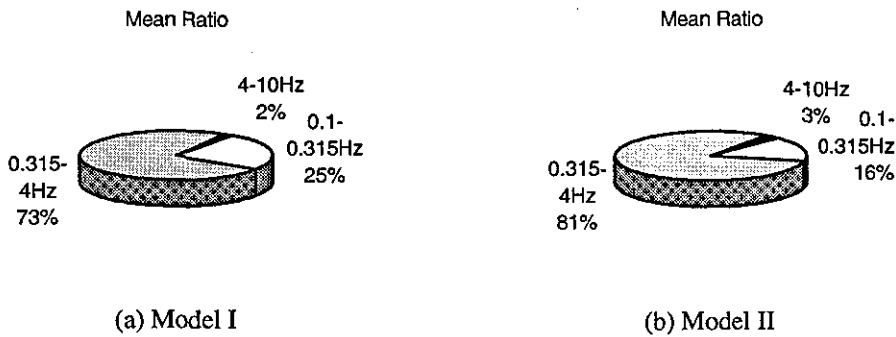


Figure 5.7 The mean ratio of weighted rms of acceleration

5.3.2 Strokes

PSD's of the strokes are displayed in Fig.5.8 (primary strokes) and in Fig.5.9 (secondary strokes). For the strokes, it is only considered the unweighted rms's and they are listed below:

	primary stroke at the first wheelset	primary stroke at the first wheelset	secondary stroke at the leading bogie	secondary stroke at the trailing bogie
Model I	2.43mm	2.04mm	16.68mm	26.67mm
Model II	0.85mm	0.81mm	2.0mm	4.87mm

Since the suspensions of Model I are softer than Model II, the strokes of Model I are certainly larger than those of Model II.

The proportions of the stroke rms's defined by Eq.(5-16) are shown in Fig.5.10 (primary strokes) and Fig.5.11 (secondary strokes) respectively. Since the magnitudes of the PSD's of the track irregularities in Fig.5.1 with low frequencies are much higher than those associated with high frequencies, the deformations of suspensions occur mainly at low frequencies. Since viscous damping does not affect system responses in low frequency effectively, the best way to reduce the working space of suspensions is to increase the stiffnesses of suspensions, which contradicts to the requirement for better ride quality.

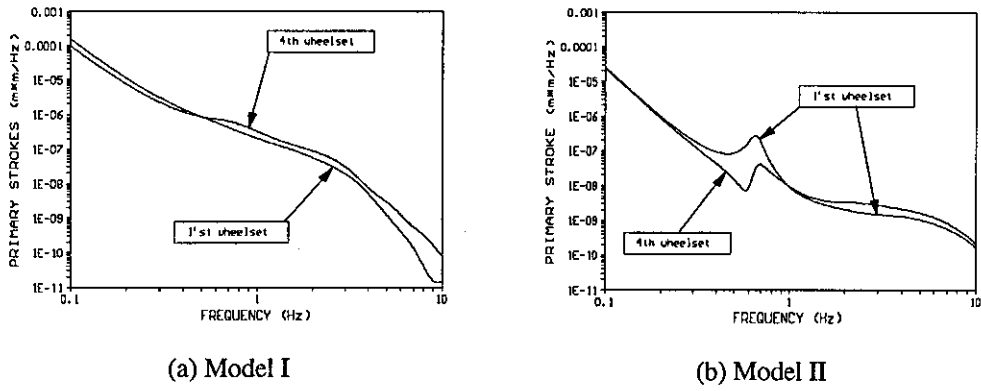


Figure 5.8 PSD's of primary strokes

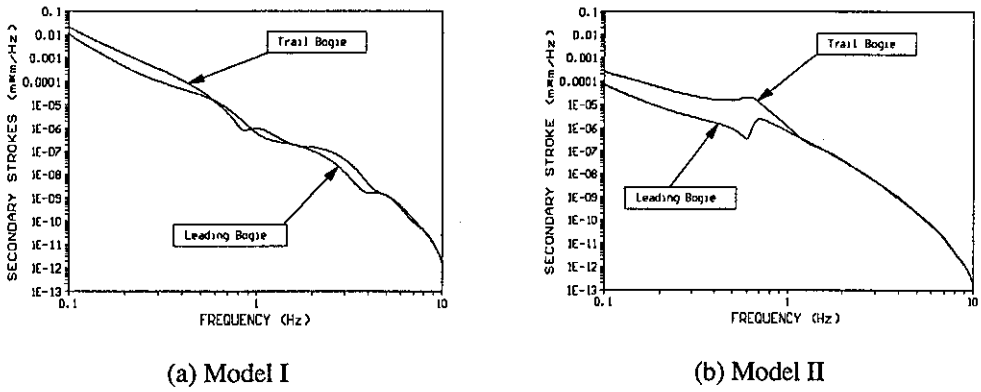


Figure 5.9 PSD's of secondary strokes

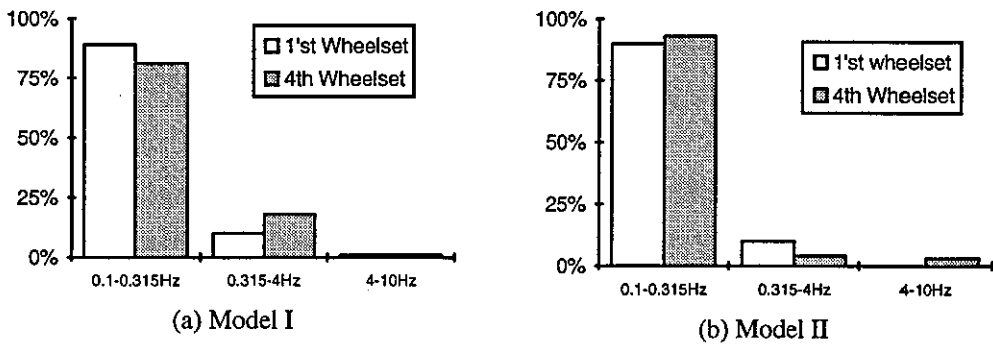


Figure 5.10 The proportion of primary stroke rms

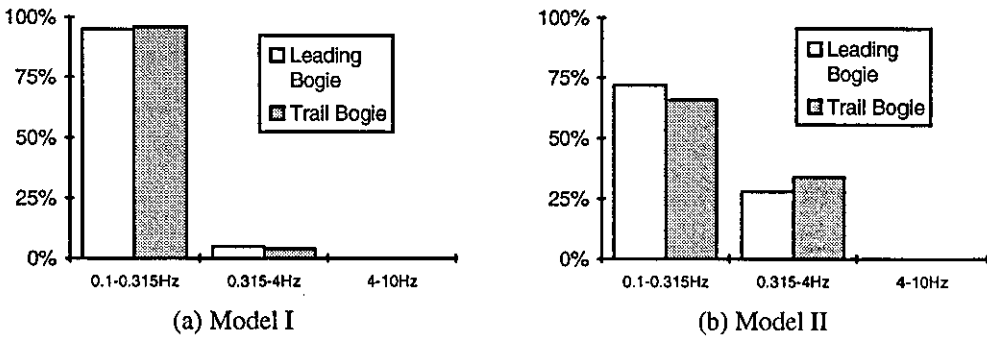


Figure 5.11 The proportion of secondary stroke rms

5.3.3 Influences of the Parameters in Suspensions and Steering Linkages

It has been pointed out in Eq.(5-8) that track irregularities can be transferred to the carbody through three channels in body-steered bogie vehicles: the primary and secondary suspensions, the steering linkage, and the steering linkage and secondary suspensions. The effective stiffnesses in perfect steering vehicles only provide the stiffnesses for the inertia components in their yaw motions, but the lateral stiffnesses and dampings in the suspensions provide the constraints for both lateral and yaw motions of the rigid bodies. For example, the primary lateral stiffness not only provides the stiffness for the lateral motion of the wheelsets and bogie frames, but also provides the stiffness for the yaw motion of the bogie frames. These channels are thus not independent such that the alteration of the parameters in suspensions or steering linkages may reduce the transmissibility of one channel but increase the transmissibility of others. The influence of the parameters on the ride quality can be very complex.

To explore this subject in more details, each parameter in the suspensions and steering linkages is investigated independently. For the ride quality, two situations are considered: the alteration (%) of the maximum unweighted **rms** among the five points in two frequency bands (0.1-0.315Hz and 0.315-4.0Hz), and the alterations (%) of the unweighted **rms**'s at the points A, C and E over 0.1-100.0Hz, when the parameter in suspensions and steering linkages changes (in %). For the strokes, it is only worthwhile discussing the **rms**'s on the band between 0.1Hz to 0.315 Hz since the proportions of the stroke **rms**'s in this band are over 70% total of the whole frequency band.

Lateral Stiffnesses

The primary lateral stiffness connects the bogie frames and wheelsets, which not only provides the stiffness for the wheelsets and bogie frames in their lateral motion, but it also provides the stiffness for the bogie frames in yaw motion, and the secondary lateral stiffness has a similar effect to the primary lateral stiffness, providing the constraints to the carbody and bogie frames in their lateral motions and constraining the carbody in its yaw motion, whilst the steering linkages in Model I and Model II only constrain the yaw motions of rigid bodies. Model I and Model II can be therefore approximately considered as a system with three

suspensions associated with yaw motion, and two suspensions associated with lateral motion.

With regard to lateral motion, the primary lateral stiffness can be considered as being k_1 and the secondary lateral stiffness as k_2 in the system in Fig.5.3, and thus the natural frequencies rise and the transfer function shifts towards the right in the frequency domain as the lateral stiffnesses increase. Referring to Fig.5.4, the transmissibility will be intensified over the whole frequency range, (especially between the two natural frequencies) when the lateral stiffnesses rise. The responses in the lateral motions will thus be enhanced whenever the lateral stiffnesses become harder, as is shown by observing the rms's at point C in Fig.5.12a-b and in Fig.5.13a-b.

With regard to yaw motion, the steering linkages in each perfect steering vehicle perform as a double suspension system alone because they not only provide the yaw constraint between wheelsets and bogie frames, but also the constraint between carbody and bogie frames, and thus the steering linkages contribute two stiffnesses k_1 (between wheelsets and bogie frames) and k_2 (between carbody and bogie frames) for yaw motion. Their effects on ride performance will be analysed later. Since the primary lateral stiffness only provides yaw constraint for the bogie frames while the secondary lateral stiffness only provides yaw constraint for the carbody, their function for yaw motion more closes to k_3 in Fig.5.3. In yaw motion, therefore, the first natural frequency becomes larger and the second natural frequency becomes smaller when the primary lateral stiffness gets harder while the natural frequencies increase as the secondary lateral stiffness becomes harder, and thus the transmissibility in yaw motion is amplified by the increment in the lateral stiffnesses. Since the phase difference between the yaw motion and lateral motion of the carbody is approximately 180° , the rms's at the point A (the front end) may be reduced as the primary lateral stiffness gets harder, however, if the primary lateral stiffness is very hard, the rms's at point A also becomes larger. Since the first natural frequency is raised as the lateral stiffnesses are hardened, the transmissibility on low frequencies may be reduced, as seen in Fig.5.12d and Fig.5.13c-d.

Since the lateral stiffnesses of Model II are higher than those of Model I, for the same percentage increment in lateral stiffnesses, the increment in the values of lateral stiffnesses of Model II is larger than that in Model I, and thus the increases of the natural frequencies of Model II are higher than those of Model I for the same

percentage increment in the lateral stiffnesses. This is the reason why Model II seems more sensitive to lateral stiffness than Model I.

The strokes are more complicated to analyse than the ride quality since the strokes are relative movements. Usually, the relative movement of two inertia bodies decreases as the elasticity between them rises. There are however three groups of inertia (carbody, bogie frames and wheelsets) and three suspensions in each perfect steering vehicle, and therefore the relative motions not only depend on local elasticity, but are also affected by the whole elasticity.

The primary strokes

If the secondary suspension is hard enough and can hold the carbody and bogie frames, the increment in the primary lateral stiffness will strengthen the constraint between the bogie frames and wheelsets. The relative motion between the wheelsets and the bogie frames is reduced as the primary lateral stiffness rises. If the secondary suspension is soft, the increment in the primary lateral stiffness will result in a larger lateral shift of both the wheelsets and bogie frames, which may amplify the primary strokes. The results in Fig.5.12 show that the former case occurs in Model II (Fig.5.12f) and the latter in Model I (Fig.5.12e).

If the secondary lateral stiffness increases, the connections between the bogie frames and the carbody are strengthened and the bogie frames are held more firmly by the carbody. The relative movements (primary strokes) between the wheelsets and bogie frames are thus increased as the secondary lateral stiffness is hardened.

The secondary strokes

If the secondary suspensions (Model II) are hard enough to hold the carbody and bogie frames, an increment in the primary lateral stiffness strengthens the constraints between the bogie frames and wheelsets. All mass components are held more firmly, and thus the secondary strokes can be reduced as the primary lateral stiffness increases, as shown in Fig.5.12h. If the secondary suspension (Model I) is soft, the increment in the primary lateral stiffness will relatively reduce the connection between the carbody and bogie frames and will lead to the higher secondary strokes, as shown in Fig.5.12g. An increment in the secondary lateral stiffness always cut down the secondary strokes, as shown in Fig.5.13g-h because it directly strengthens the connect between the carbody and the bogie frames.

In practical applications, the working space of the primary suspension is very restricted. To reduce the working spaces of primary suspension, the simulation results in Fig.5.12 & Fig.5.13 and the above analysis demonstrate that not only the primary suspension should be hardened, but also the secondary suspension should be stiffened.

Effective Stiffnesses

It has been described that Model I and Model II can be approximated as a system with three suspensions in yaw motion. It seems that the reduction in effective stiffnesses can improve ride performance, however, the results of Fig.5.15 and Fig.5.16 show opposite effects. To explain the results, reconsider the model in Fig.5.3. If the yaw stiffness between the wheelset and bogie frame is considered as k_1 , the yaw stiffness between the bogie frame and carbody as k_2 , and the yaw stiffness provided by the effective stiffnesses as k_3 , it can be seen that the function of effective stiffnesses in each perfect steering vehicle is not the same as k_3 in Fig.5.3. In Fig.5.3, k_1 and k_2 are independent of k_3 , however, the effective stiffnesses in Mode I and Model II affect the all yaw constraints of the wheelsets, bogie frames and carbody, and thus the steering linkages of each perfect steering vehicle work more like a double suspension system.

The yaw stiffnesses provided by the effective stiffnesses to the wheelset, bogie frame and carbody are:

	wheelset	bogie frame	carbody
For Model I	30.15 MN-m	61.52 MN-m	2.46 MN-m
For Model II	32.57 MN-m	113.75 MN-m	0.69 MN-m

and the yaw stiffness provided by the lateral stiffnesses to the wheelset, bogie frame and carbody are:

		k_{py}	k_{sy}
	wheelset	bogie frame	carbody
For Model I	0	15.63 MN-m	15.31 MN-m
For Model II	0	46.88 MN-m	45.95 MN-m

It can be seen that the yaw stiffness provided by the effective stiffnesses plays a major part in the yaw constraints for the wheelsets and bogie frames, whilst the effective stiffnesses only contribute a small portion of the yaw stiffness for the

carbodies. The increment in the effective stiffnesses can strengthen the yaw constraints (k_1 in Fig.5.3) between the wheelsets and bogie frames, but has little influence on the yaw constraints (k_2 in Fig.5.3) between the bogie frames and carbodies. The first natural frequency will change a little while the second natural frequency will obviously increase, and thus the system transmissibility between the first two natural frequencies is reduced, as the effective stiffnesses increase. In Model II, $k_{e3} \gg k_{e1} = k_{e2}$ (about 100:1), the ride performance of Model II is more sensitive to k_{e3} than $k_{e1}(= k_{e2})$.

The analysis above shows that the steering linkages act more like a double suspension system: hard primary stiffness and soft secondary stiffness, and therefore the increment in the effective stiffnesses can bring out a positive effect on the ride performance. The increment in steering linkage stiffness can however deteriorate the ride performance, as shown in Appendix A, which implies that the effect of the effective stiffnesses on the ride performance depends on the steering linkage configurations.

It has been demonstrated in Chapter 4 that the critical speed of the perfect steering vehicles increases as the effective stiffnesses rise, with the condition that they are not hard enough to promote static instability. The ride quality may also benefit from the stability improvement as the effective stiffnesses become harder.

The strokes always benefit from the increment of effective stiffnesses because both the connections between the wheelsets and bogie frames and between the bogie frames and carbody in yaw motion are strengthened by the gain in the effective stiffnesses.

Dampings

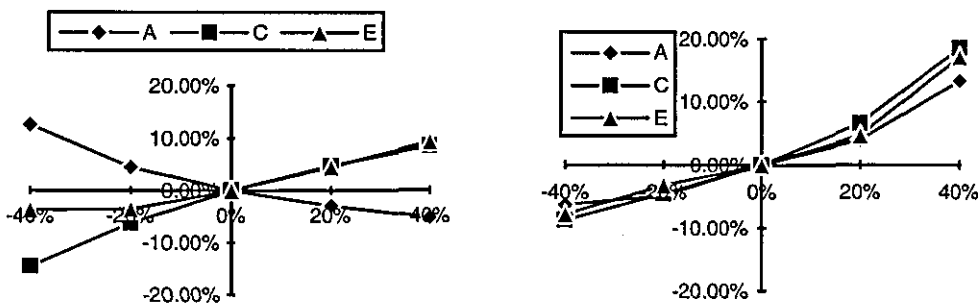
The secondary lateral damping mainly compresses the responses in the lateral motion of the carbody, as shown in Fig.5.17. The ride quality will be improved as lateral secondary damping increases, as seen in Fig.5.17a-b. The acceleration rms's may rise at the front end (point A), as seen in Fig.5.17a, when the lateral secondary damping increases because of the phase difference between the lateral motion and yaw motion of the carbody. Both ride quality and strokes in Model II are improved when the secondary lateral damping increases, but the secondary stroke is more sensitive to the secondary lateral damping than the primary stroke because the damping can reduce the movements of both the carbody and bogie frames. The

results in Fig.5.17 also indicate that the secondary lateral damping in Model II must be high enough in order to obtain reasonable ride performance.

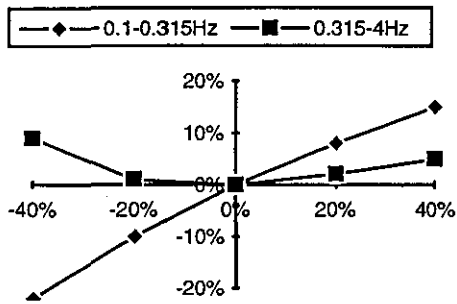
Secondary yaw damping, which has been applied to Model I in order to study its effect on ride performance, can damp yaw motion, but has little effect on lateral motion, as seen in Fig.5.18a (point C). Its increment will lead to reducing the acceleration at one end of the vehicle but raising it at the other end due to the phase difference between the yaw motion and lateral motion of the carbody, as shown in Fig.5.18a-b.

Since the relative motions (secondary stroke) at the pivots between the carbody and bogie frames depend on the relative lateral motions between the carbody and bogie frames and the yaw motion of the carbody, and since the secondary yaw damping only reduces the lateral movement at the pivots caused the carbody yaw motion, the relative motions (secondary strokes) may be increased when the secondary yaw damping is applied, as seen in Fig.5.17d. This can also be applied to explain the reason why the primary strokes rise as the secondary yaw damping increases.

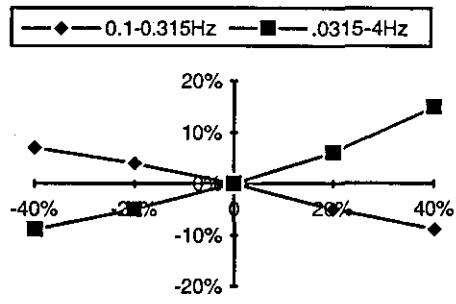
The alteration in the responses caused by damping mainly distributes around the carbody natural frequencies. The carbody natural frequency in lateral motion is about 1.0Hz for Model II and about 0.57Hz for Model I, and thus the changes in the carbody's responses caused by the secondary lateral damping are mainly between 0.315-4.0Hz, as seen in Fig.5.17. The natural frequency of the carbody in yaw motion is about 0.24Hz for Model I, and therefore the changes in the carbody's responses caused by the secondary yaw damping are mainly on 0.1-0.315Hz, as shown in Fig.5.18



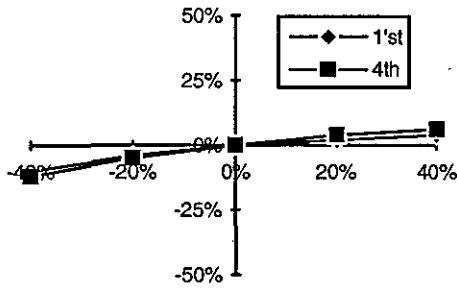
(a) acceleration rms's on 0.1-100Hz, Model I (b) acceleration rms's on 0.1-100Hz, Model II



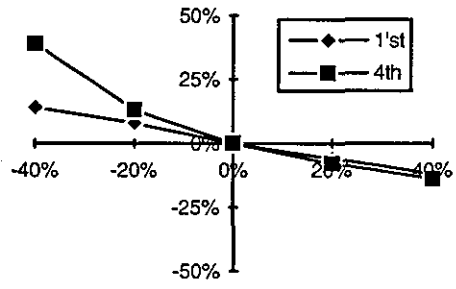
(c) acceleration rms's, Model I



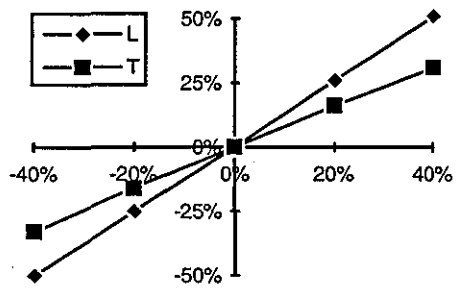
(d) acceleration rms's, Model II



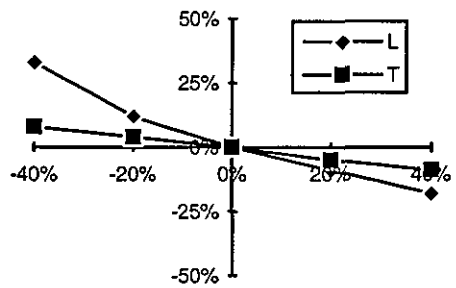
(e) primary stroke rms's on 0.1-0.315Hz, Model I



(f) primary stroke rms's on 0.1-0.315Hz, Model II

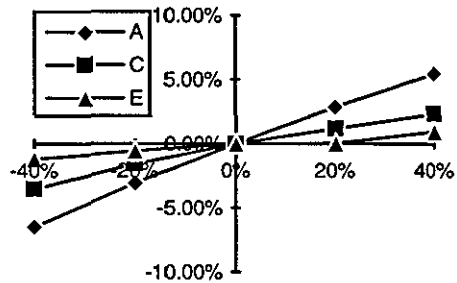


(g) secondary stroke rms's on 0.1-0.315Hz, Model I

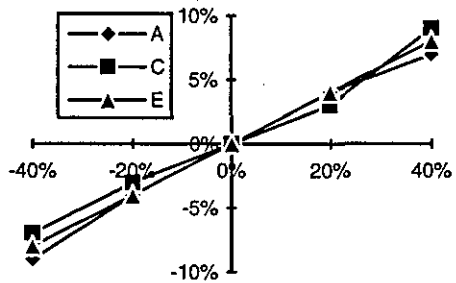


(h) secondary stroke rms's on 0.1-0.315Hz, Model II

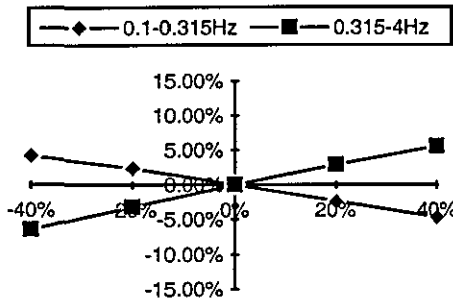
Figure 5.13 Influence of primary lateral stiffness on ride performance, A-- point A, C--point C and E--point E; L--leading bogie and T--trail Bogie



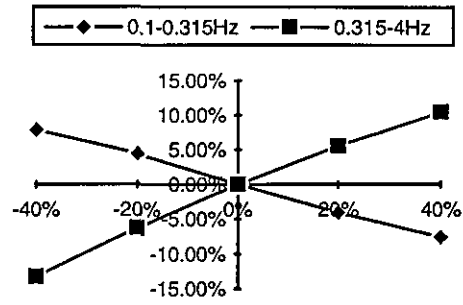
(a) acceleration rms's on 0.1-100Hz, Model I



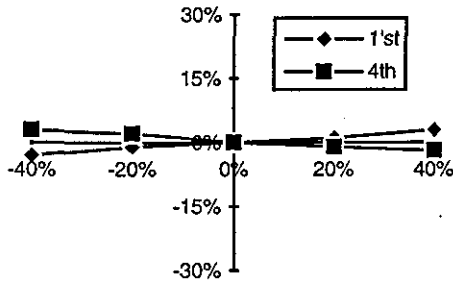
(b) acceleration rms's on 0.1-100Hz, Model II



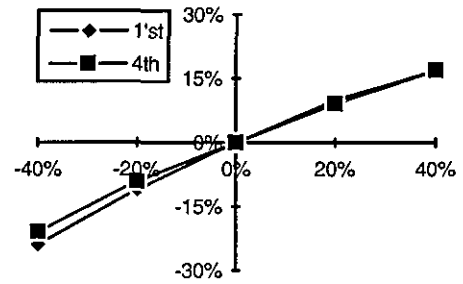
(c) acceleration rms's, Model I



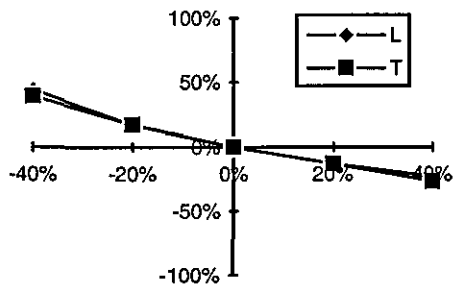
(d) acceleration rms's, Model II



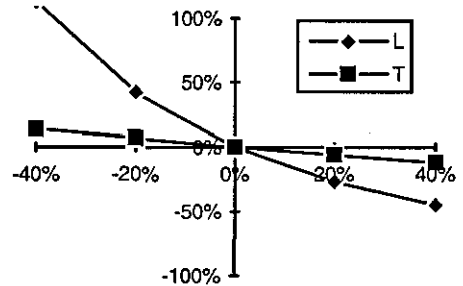
(e) primary stroke rms's on 0.1-0.315Hz, Model I



(f) primary stroke rms's on 0.1-0.315Hz, Model II

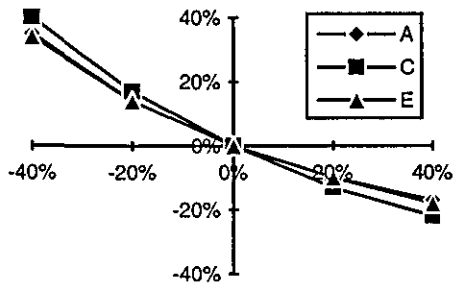


(g) secondary stroke rms's on 0.1-0.315Hz, Model I

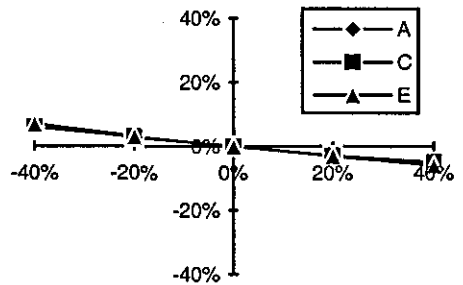


(f) secondary stroke rms's on 0.1-0.315Hz, Model II

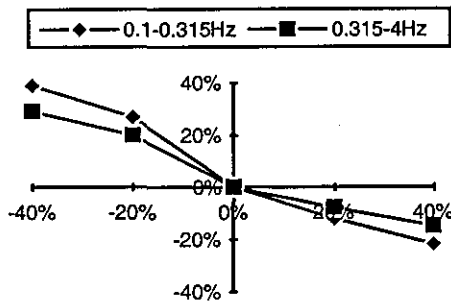
Figure 5.14 Influence of secondary lateral stiffness on ride performance, A-- point A, C--point C and E--point E; L--leading bogie and T--trail Bogie



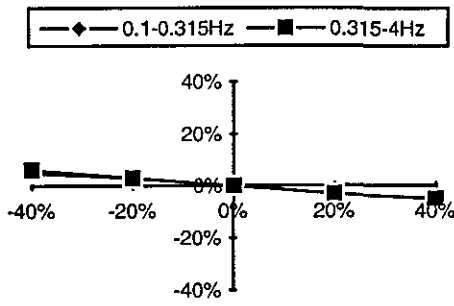
(a) acceleration rms's on 0.1-100Hz, Model I



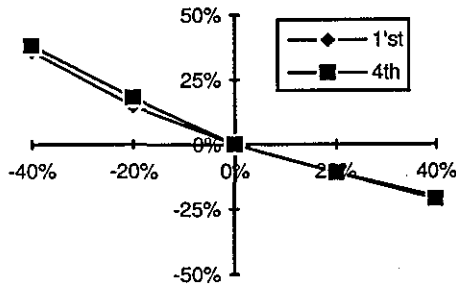
(b) acceleration rms's on 0.1-100Hz, Model II



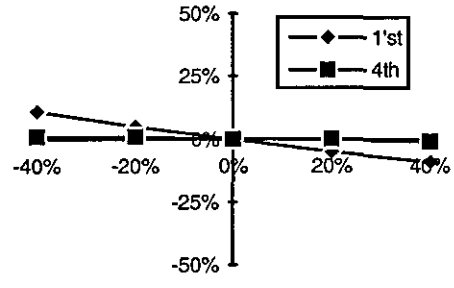
(c) acceleration rms's, Model I



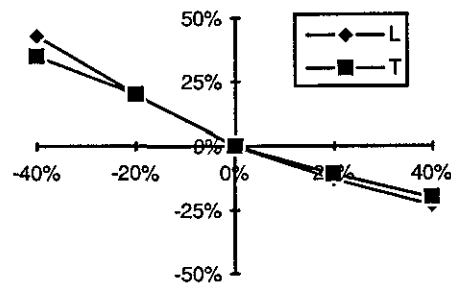
(d) acceleration rms's Model II



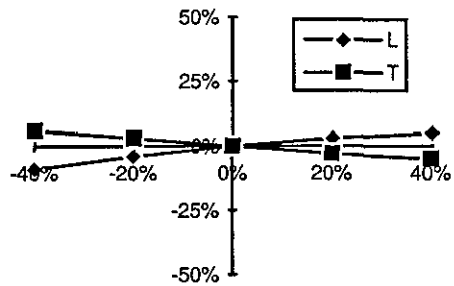
(e) primary stroke rms's on 0.1-0.315Hz, Model I



f0 primary stroke rms's on 0.1-0.315Hz, Model II



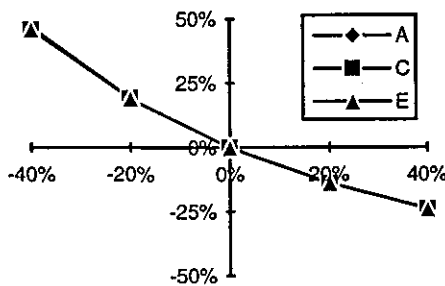
(g) secondary stroke rms's on 0.1-0.315Hz, Model I



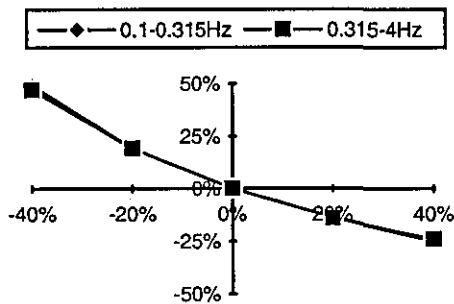
(h) secondary stroke rms's on 0.1-0.315Hz, Model II

Figure 5.15 Influence of effective stiffness $k_e = k_{e1} = k_{e2}$ on ride performance, A-- point A, C--point C and E--point E; L--leading bogie and T--trail Bogie

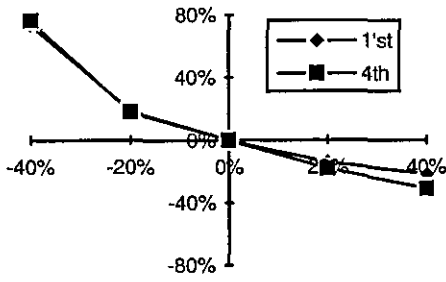
Effective Stiffness k_{e3}



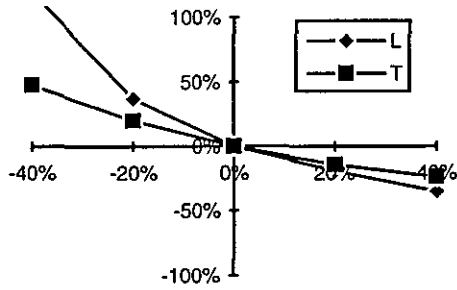
(a) acceleration rms's on 0.1-100Hz



(b) acceleration rms's



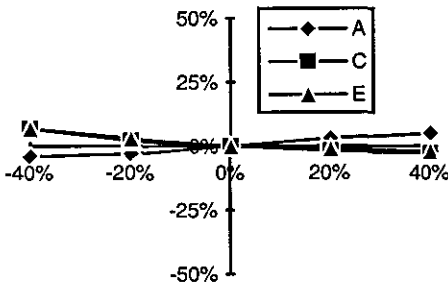
(c) primary stroke rms's on 0.1-0.315Hz



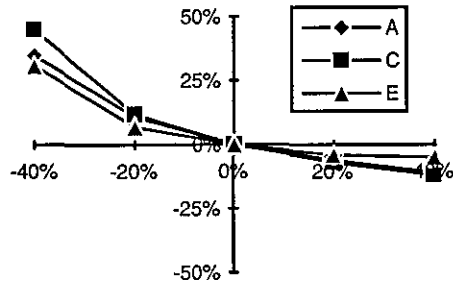
(d) secondary stroke rms's on 0.1-0.315Hz

Figure 5.16 Influence of effective stiffness k_{e3} on ride performance, A-- point A, C--point C and E--point E; L--leading bogie and T--trail Bogie

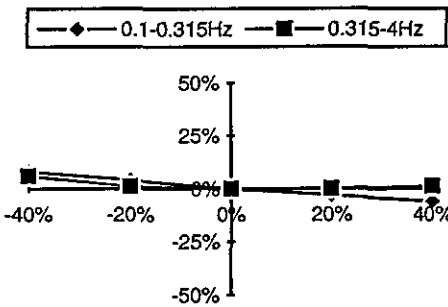
Secondary Lateral Damping



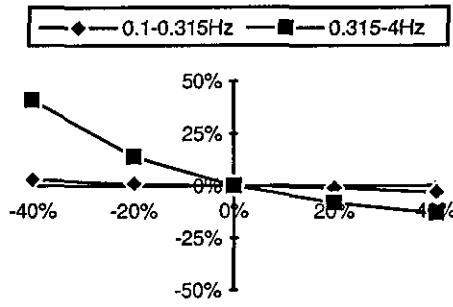
(a) acceleration rms's on 0.1-100Hz, Model I



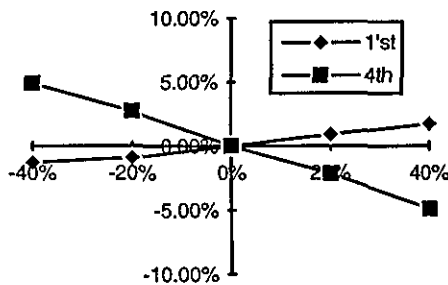
(b) acceleration rms's on 0.1-100Hz, Model II



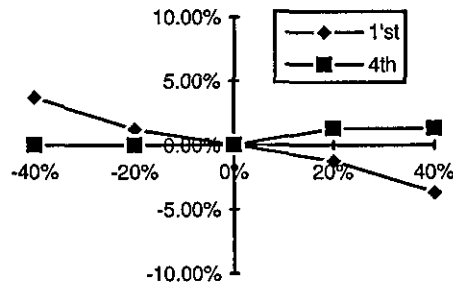
(c) acceleration rms, Model I



(d) acceleration rms, Model II



(e) primary stroke rms's on 0.1-0.315Hz, Model I



(f) primary stroke rms's on 0.1-0.315Hz, Model II

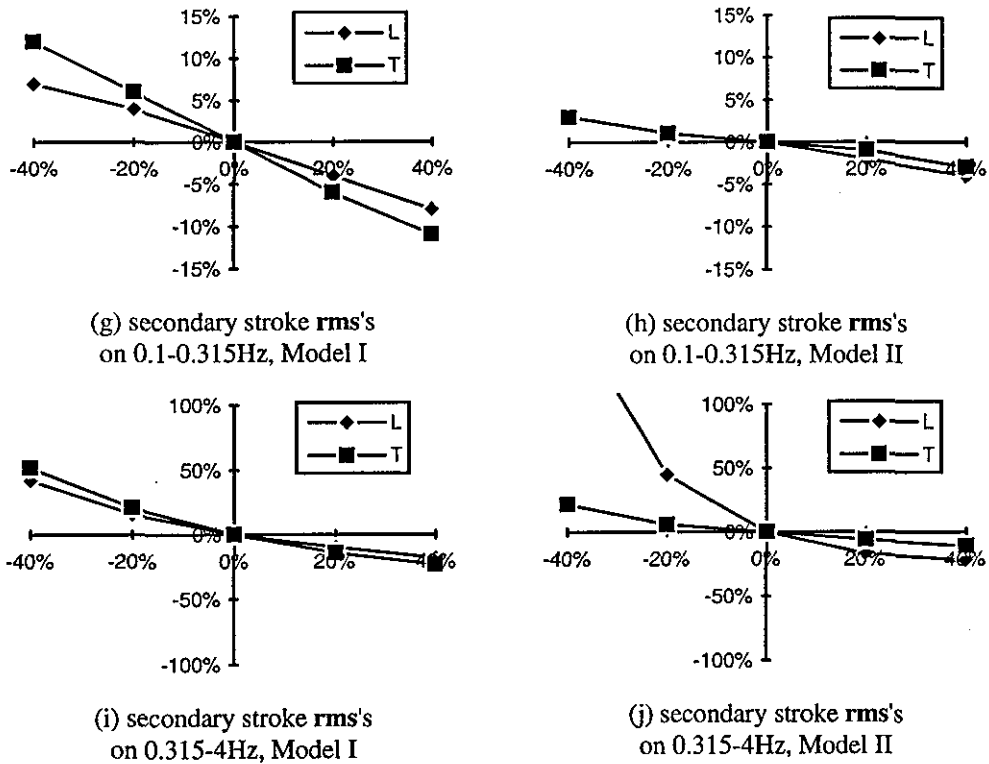


Figure 5.17 Influence of secondary lateral damping on ride performance, A-- point A, C--point C and E--point E; L--leading bogie and T--trail Bogie

Secondary Yaw Damping

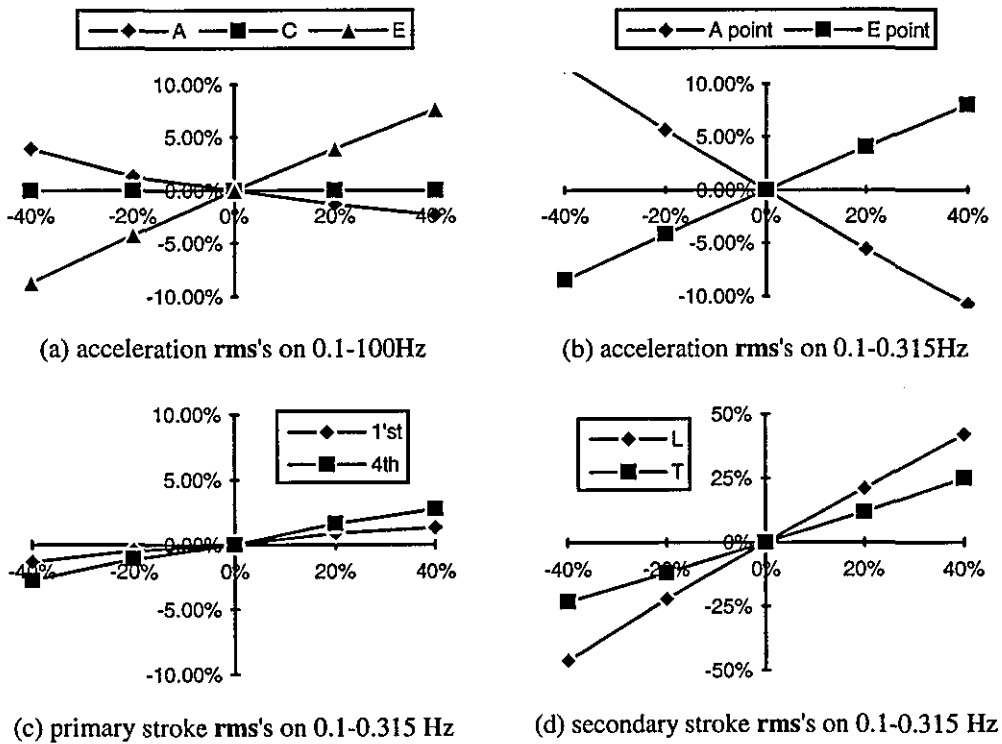


Figure 5.18 Influence of secondary yaw damping on ride performance, A-- point A, C--point C and E--point E; L--leading bogie and T--trail Bogie

5.3.4 Geometric Errors

Geometric error in the steering linkages will change the effective stiffnesses and thus affect the ride performance. The influence of effective stiffnesses on ride performance has already been discussed in the previous sections and so a repeat of the analysis is unnecessary.

5.4 Summary

There are three channels which transfer track disturbances to the carbody in body-steered bogie vehicles: the coupling between the primary and secondary suspensions, the steering linkages and the coupling between the secondary suspension and steering linkages. Since the three channels are not independent, coupling among the suspensions is complicated when steering linkages are applied. The complexity of the suspension coupling is, however, simplified in perfect steering vehicles because there is neither the primary yaw stiffness nor the secondary yaw stiffness in their suspensions. In lateral motions, Model I and Model II can be considered as double suspension systems, while they work as three suspension systems with regard to yaw motion.

Since the transmissibility around the first natural frequency is high, the low first natural frequency is always preferred. The large difference between the first and second natural frequencies is also useful with regard to cutting down the system transmissibility. This is a basic principle for vehicle suspension designs with regard to ride performance.

The rms's of the body accelerations mainly comes from two low frequency bands (0.1-0.315Hz & 0.315-4.0Hz). More rms's of the carbody accelerations will shift from the 0.1-0.315Hz band to the 0.315-4.0Hz band as system elasticity increases. Since the human beings are more sensitive to vibration in the 0.315-4.0Hz range, the main task in improving ride quality is to reduce the responses in this band. The proper approach in reducing carbody responses is therefore to let the first natural frequency be less than 0.315Hz and the secondary natural frequency be greater than 4.0Hz.

The effective stiffnesses unequally contribute to the yaw constraints for the wheelsets, the bogie frames and the carbodies in Model I and Model II. They dominate the yaw constraints of wheelsets and bogie frames while their contribution to the yaw constraint of carbodies only occupies a small proportion. The gain in the effective stiffnesses can much strengthen the yaw constraint between the wheelsets and bogie frames, but only increase the yaw stiffnesses between the carbody and bogie frames a little, and thus the steering linkages of Model I and Model II work as a double suspension system with stiff primary suspension and soft secondary suspensions. The increment in the steering linkages can therefore not only improve the ride quality, but also reduce the strokes.

In Chapter 4, it was demonstrated that the conventional stability of Model I and Model II is improved upon by hard effective stiffnesses, and thus stiff steering linkages in Model I and Model II not only improve ride performance, but also conventional stability. The coincidence of the effects of the effective stiffnesses on the ride performance and conventional stability of Model I and Model II means that the configurations such as Model I and Model II can decouple the conflict between conventional stability and ride performance.

The effects of the effective stiffnesses in Model I and Model II on ride performance can also be applied to other body-steered bogie vehicles if their steering linkages have similar configuration to those of Model I or Model II. For the different configurations, steering linkages of body-steered bogie vehicles may, however, produce the negative effects on ride performance, as seen in Appendix A. This implies that the effects of steering linkages on ride performance depend on their configurations.

An increment in lateral stiffnesses deteriorates ride quality, and the influence of the lateral stiffnesses on the strokes depends on the secondary suspension. If a secondary suspension is hard, the increment in the lateral stiffnesses can cut down the strokes, whereas conversely, a soft secondary suspension may lead to an increase in strokes when the lateral stiffnesses increases. This means that in order to minimise the strokes, not only is a stiff primary suspension required, but also a stiff secondary suspension.

Secondary lateral damping is necessary for the ride quality of perfect steering vehicles, while secondary yaw damping is not necessary although it has a positive effect on ride quality.

The phase difference between the lateral and yaw motion of the carbody is about 180°. This phase difference can be used to improve the ride quality in some cases.

Since the stroke rms's mainly (over 70%) come from the low frequency band (0.1-0.315Hz), and the viscous dampings are inactive in low frequencies, the only approach in cutting down the strokes is to increase system stiffness, especially to increase the primary lateral stiffness to reduce the primary stroke because wheelset constraint in lateral motion mainly depends on the primary lateral stiffness, however this will bring out a negative effect on ride quality. A conflict between the ride quality and strokes therefore exists.

Table 5.1 Weighted Factor W_i [106]

f (Hz)	W_i (dB)	f (Hz)	W_i (dB)	f (Hz)	W_i (dB)
0.100	0.0624	1.250	1.0100	20.00	0.1270
0.125	0.0987	1.600	0.9710	25.00	0.1000
0.160	0.1550	2.000	0.8910	25.00	0.0796
0.200	0.2420	2.500	0.7730	31.50	0.0630
0.250	0.3680	3.150	0.6400	40.00	0.0496
0.315	0.5330	4.000	0.5140	50.00	0.0387
0.400	0.7100	5.000	0.4080	63.00	0.0295
0.500	0.8540	6.300	0.3230	80.00	0.0213
0.630	0.9440	8.000	0.2550	100.0	0.0141
0.800	0.9910	10.00	0.2020		
1.000	1.0100	12.50	0.160		

Chapter 6

SUMMARY OF THE DYNAMIC BEHAVIOUR OF PERFECT STEERING BOGIE VEHICLES

In the last three chapters, the dynamic characteristics of perfect steering vehicles on curving, stability and ride performance has been investigated. On the basis of the results and analyses in the previous chapters, this chapter will summarise the main features of dynamic performance of perfect steering vehicles.

It has been shown that the displacement vector $\{q\}$ of the rigid bodies in a railway vehicle has two components $\{\bar{q}\}$ and $\{\hat{q}\}$, i.e.

$$\{q\} = \{\bar{q}\} + \{\hat{q}\}$$

where, $\{\bar{q}\}$ is the displacement vector of the local coordinates of rigid bodies related to a uniform reference and,
 $\{\hat{q}\}$ is the displacement vector of rigid bodies related to their local coordinates.

The origin of the local coordinate system of a rigid body is usually defined as the nominal position of its weight centre on the track central line, and thus the elements of $\{\bar{q}\}$ are determined only by curvatures, wheelset base $2a$ and distance $2l_0$ for a fore-and-aft symmetric bogie vehicle. The uniform reference is usually defined on the nominal position of carbody weight centre in the radial direction of carbody such that all local coordinate systems are equal to each other except in x -direction in straight track, and thus we have $\{\bar{q}\} = 0$ and $\{q\} = \{\hat{q}\}$ in straight track since the differences between rigid bodies in x -direction can be ignored if the vehicle speed is constant, while on a curve, the track central line changes its direction, and a displacement between a local coordinate and the uniform reference exists so that $\{\bar{q}\} \neq 0$.

If $\{\Delta q\}$ represents the relative displacement vector between the elements of $\{\bar{q}\}$, the elements of the elastic force vector $\mathbf{F}_E = \mathbf{E}\{\Delta q\}$ (where \mathbf{E} is the elastic matrix of the system) become larger as the corresponding elements of $\{\Delta q\}$ increase, which

results in increasing the elements of $\{\hat{q}\}$. The increments in the elements of $\{\hat{q}\}$ mean that the distances between the track central line and the weight centres of rigid bodies, such as attack angles and lateral displacements of wheelsets, are increased. The main task in reducing $\{\hat{q}\}$ and improving vehicle curving is therefore to minimise the elastic forces F_E caused by $\{\Delta q\}$. If $\{\delta q\}$ represents the relative displacement vector between the elements of $\{\hat{q}\}$, it can usually be reduced as $\{\Delta q\}$ decreases since the reduction in $\{\Delta q\}$ can reduce $\{\hat{q}\}$. The advantages resulting from the reduction in elastic deformation $\{\delta q\}$ will lead to the wheelsets taking up more radial alignment. The direct benefits of the advantages are twofold: firstly, the contact forces between wheels and rails are reduced, which will reduce the wear between wheels and rails and decrease the track deformation, such that the cost of track and wheelset maintenance is reduced; and secondly, the potential of derailment can also be reduced, which improves safety.

On a uniform curve, relative displacements $\{\Delta q\}$ are constants and only the relative yaws $\{\Delta\psi\}$ in $\{\Delta q\}$ cause the elastic forces F_E for most of the configurations of railway vehicles, and thus only bending stiffnesses in vehicles contribute to the elastic forces, i.e. $F_E = E\{\Delta\psi\}$. The relative yaw angles $\{\Delta\psi\}$ on a same uniform curve are identical to any fore-and-aft symmetric railway bogie vehicles if the wheelset base $2a$ and the pivot distance $2l_0$ are equal, and thus the only way to reduce F_E is to optimise the elastic matrix E so that the elastic forces $E\{\Delta\psi\}$ can be minimised.

Since the relationships among the elements of $\{\Delta\psi\}$ are only decided by vehicle geometry on uniform curves, it is possible to set up relationships among the stiffnesses caused by the steering linkages in body-steered bogie vehicles, which can make the stiffnesses in the steering linkages not contribute any bending stiffness, such that $E\{\Delta\psi\} = 0$ if there are no other bending stiffnesses in the vehicle. The vehicle will be capable of perfect steering on steady state for any uniform curve with zero cant deficiency, and therefore, the key factor for a bogie vehicle to possess the capability of perfect steering is to find those relationships that let $E\{\Delta\psi\} = 0$.

Since the elastic matrix E is only determined by vehicle configuration and is independent of curve curvatures, the conditions for railway bogie vehicles being capable of perfect steering should be independent of curve geometry, in other words, perfect steering only depends on the configurations of railway bogie vehicles.

On the other hand, the realisation of perfect steering depends on whether the wheelsets of perfect steering vehicles can roll on their pure rolling lines on uniform curves, which turns out to be whether the distance between the pure rolling line and track central line is within the limitation of flange contact. If the distance is within this limitation, perfect steering can be achieved, otherwise, it cannot. Since track gauge usually has little alteration, Eq.(2-13) indicates that the distance between the pure rolling line and track central line is decided by wheel profile and curve curvature. In practice, it is unlikely to change the curvatures for existing railway lines, and thus the most effective method keeping the distance between the pure rolling line and track central line within the limitation of flange contact is to increase the equivalent conicities of wheelsets.

The lateral forces caused by cant deficiency will push the wheelsets away from their pure rolling lines, and displacements $\{\hat{q}\}$ will thus be produced. Since $E\{\Delta q\} = 0$ still exists in perfect steering vehicles, the associated displacement $\{\hat{q}\}$ will be much smaller than that in conventional bogie vehicles when cant deficiency exists. The capability of tolerating cant deficiency is therefore much improved in perfect steering vehicles.

When perfect steering vehicles negotiate a transition, the relative displacement $\{\Delta q\}$ is not constant and thus the elastic force $E\{\Delta q\} \neq 0$ exists. The analysis in section 3.5 has shown that $\{\Delta q\}$ of perfect steering vehicles is associated with the geometric parameters of the steering linkages and is much smaller than $\{\Delta q\}$ of conventional bogie vehicles on the transition curve, and the elastic forces produced by $\{\Delta q\}$ in perfect steering vehicles are thus much less than those in conventional bogie vehicles such that the displacement $\{\hat{q}\}$ of perfect steering vehicles on transition curves is greatly reduced. The ability of the vehicles to align to transition curves is therefore much improved, but the full understanding of the behaviour of perfect steering vehicles on transitions relies on dynamic models.

There are two instabilities in perfect steering vehicles: low conicity instability (comprising of low speed and dynamic instabilities) and conventional instability. In actual fact, conventional instability is one mode of dynamic instability, and the differences between dynamic instability in low conicity and conventional instability are the former only occurs on one bogie while the latter occurs on both bogies, and that the critical speed increases in the former and decreases in the latter as the conicity rises. Dynamic instability in low conicity disappears when the steering linkages are very stiff. Low speed instability of body-steered bogie vehicles has

been considered as divergent instability for long time. The theoretical analysis and the simulation results in Chapter 4 indicate, however, that low speed instability can be either divergent or oscillatory. Although the divergent instability has been noticed since the early 1980's[12,15,19], dynamic instability in low conicity has not been studied until now.

Since perfect steering vehicles allow their rigid bodies to take radial positions on curves, they are more flexible than conventional bogie vehicles, which directly affects vehicle stability. In the elastic sub-matrix E_T of the bogie sub-system, the effective stiffnesses of the steering linkages in Model I and Model II are on the same positions as the yaw stiffnesses of the suspensions in conventional bogie vehicles, and the steering linkages thus provide the yaw stiffnesses for the rigid bodies. Indeed, the yaw constraints for the wheelsets are only provided by the steering linkages in perfect steering vehicles, and therefore it is expected to apply stiff steering linkages in constraining wheelset movements and stabilising the systems. The stiffness of the steering linkages is however restricted by low conicity instability, especially by low speed instability.

Low conicity instability is an inherent property of perfect steering vehicles. Although the application of high conicity can improve low conicity instability and result in applying hard effective stiffnesses, perfect steering vehicles are going to be unstable at low speed even in high conicity if the steering linkages are very stiff. This is not only been proved from the results of simulation, but also by theoretical analyses. There are also two physical facts that explain these conclusions. Firstly, the effective stiffnesses between the inboard and outboard wheelsets of perfect steering vehicles are different such that perfect steering vehicles are effectively equivalent to asymmetric railway bogie vehicles. Wickens[25] has studied the instability modes of asymmetric two-axle vehicle and found that the asymmetric elasticity between wheelsets results in reducing the damping and inertia associated with instability in the steering mode, and thus static and dynamic instabilities occur if conicity is very low, and also that the appearance of instability depends on the direction of the moving vehicle. Secondly, steering linkages in body-steered bogie vehicles tend to force the wheelsets into having a yaw motion, but the only moment that can resist the wheelsets against the yaw motion caused by the steering mechanism is produced by longitudinal creepage. When the steering linkages are hard enough to force the wheelsets into having a yaw angle, the longitudinal creepage forces cannot restore the wheelsets back to their equilibrium positions, and static instability occurs. The longitudinal creepage forces become smaller as

conicity reduces and the tendency for the wheelsets to take up a yaw motion is enhanced by increasing the effective stiffnesses, and therefore, static instability is more obvious with low conicity and stiff steering linkage. The first reason explaining why static instability in body-steered bogie vehicles has not been considered before, whereas the second has been noted by several researchers [12,15,19] in the early 80's.

Stiff steering linkages can go towards preventing conventional instability of perfect steering vehicles while soft steering linkages can reduce the potential of low speed instability. An obvious conflict exists here between stiff and soft steering linkages in perfect steering vehicles, and optimising effective stiffnesses will thus become a major challenge in developing perfect steering vehicles.

The unequal distribution of effective stiffnesses between the wheelsets, bogie frames and carbody in Model I and Model II partly decouples the conflict between ride performance and stability. The effective stiffnesses dominate the constraints of yaw motions of the wheelsets and bogie frames, but only contribute a small proportion to the constraint of carbody yaw motion. An increment in effective stiffnesses can much strengthen the connection between the bogie frames and wheelsets, but will have little influence on the connection between the carbody and bogie frames. The steering linkage works as a double suspension system: stiff primary and soft secondary suspensions, and stiff steering linkages can therefore not only improve conventional stability, but also ride performance of Model I and Model II. This feature of steering linkages is also valid for other classes of body-steered bogie vehicle so long as their steering linkages possess similar configurations to those of Model I or Model II. The influence of the steering linkages on ride performance however relies on their configurations, and hard steering linkages can also deteriorate ride performance, as shown in Appendix A.

The geometric errors in steering linkages not only change effective stiffnesses, but also affect the compatibility matrix. The influence of the geometric errors on stability and ride performance can be roughly considered the same as those effects associated with effective stiffnesses, however, the effect of geometric errors on vehicle curving is different. As demonstrated in Section 3.1.2, the sufficient condition for a railway vehicle capable of perfect steering involves a condition that the geometric parameters of the steering linkages must satisfy, but the errors in these parameters mean that the sufficient condition cannot be satisfied, and thus the effective stiffnesses will contribute some bending stiffnesses when the geometric

errors exist. Since the effective stiffnesses are designed as hard as possible in obtaining better conventional stability and ride performance, the effect of the errors in the steering linkages on vehicle curving can be very obvious, even more serious than that effect associated with cant deficiency. The geometric parameters of the steering linkages should therefore be controlled very carefully and precisely in perfect steering vehicles.

In order to avoid low speed instability and to keep the distance between the pure rolling line and track central line within the limitation of flange contact, it is expected that high conicity will be applied to perfect steering vehicles, but low conicity gives better conventional stability and ride quality. In perfect steering vehicles then, conicity should be optimised to satisfy the requirements of both arguments, which is fundamentally different with conventional bogie vehicle design in which low conicity is always required. The results of simulation demonstrate that conicity in perfect steering vehicles should be higher than that of conventional bogie vehicles.

Given that the limitation of flange contact as being 5mm, the major performance index of Model I and Model II are listed in Table 6.1 and Table 6.2. If vehicle speed is 150km/h and conicity is 0.3, the maximum weighted rms's over the five points (the definitions of these points have been shown in Fig.5.2) are 12.57mg for Model I and 13.97mg for Model II respectively, and the minimum curve radius on which perfect steering vehicles can negotiate without flange contact is 216m.

For modern railways, passenger vehicles have three major applications: light railways and underground railways, new high speed railways and existing railways. The curves of light railway and underground railway have to be designed very sharp since they are clearly restricted by geographic objects such as buildings and streets. Flange contact specifically needs to be considered if perfect steering vehicles are applied in these lines. It is necessary to monitor conicity of perfect steering vehicles stringently if they are to be applied to new high speed lines since both low and high conicities can cause instability (either low conicity instability or conventional instability). Since perfect steering vehicles well decouple the conflict between conventional stability and curving, they can be widely applied to existing railways. The application of perfect steering vehicles on existing railways can not only increase vehicle speed, but also improve the safety against derailment and reduce maintenance costs of both wheelset and track.

In Model II, two of the three effective stiffnesses are independent. The effective stiffness between the wheelsets strengthens the constraints of wheelsets, and thus other two effective stiffnesses can be reduced. The reduction in these two effective stiffnesses results in two benefits: firstly, the tendency of the vehicle to become unstable at low speed is reduced and secondly, the stiffness between the wheelsets and body is cut down so that ride quality can be improved. The performance of Model II in stability and ride quality is therefore better than Model I.

Since there is neither primary non secondary yaw stiffnesses in the suspensions of perfect steering vehicles, any means that strengthen the yaw constraints of rigid bodies can stabilise the whole system. The conventional stability of perfect steering vehicles can thus be much improved upon by applying secondary yaw damping. Although the application of secondary lateral stiffness and damping to perfect steering vehicles is necessary for ride quality, they have little influence on stability around their practical application ranges.

Table 6.1 Major Performance Index of Model I

λ	0.05	0.1	0.15	0.2	0.25	0.3
$v_c(\text{km/h})$	287	312	269	229	200	182
max (rms)*	3.86	6.92	9.26	11.10	11.72	12.57

Table 6.2 Major Performance Index of Model II

λ	0.05	0.1	0.15	0.2	0.25	0.3
$v_c(\text{km/h})$	341	352	302	258	226	204
max (rms)*	2.76	5.25	7.55	9.71	11.81	13.97

* Weighted rms's at those five points as shown in Fig.5.2 when $v_0 = 150\text{km/h}$

**THE IMPROVEMENT OF
PERFECT STEERING BOGIE VEHICLE DYNAMICS
BY A RECONFIGURABLE MECHANISM**

The best advantage of perfect steering vehicles over conventional bogie vehicles is that they well decouple the conflict between curving and conventional stability, whilst their worst disadvantage is low conicity instability. On the other hand, low conicity instability does not occur in conventional bogie vehicles, but the conflict between curving and stability remains a major problem. The design of a railway bogie vehicle that possesses the advantages of both perfect steering vehicles and conventional bogie vehicles would be extremely useful, and a question thus arises: is there some mechanism or device that can achieve this purpose? This chapter will present the mechanism in question and will investigate the dynamic improvement when the mechanism is applied to Model I and Model II.

7.1 Reconfigurable Mechanism

7.1.1 Concept of the Reconfigurable Mechanism

In many physical systems, there are some conflicts associated with their performance in various working environments, and the conflicts cannot be solved easily if systems only work in one configuration even it is well optimised. The conflicts can, however, be decoupled and the overall performance can be much improved upon if the system configurations of can be changed according to their working environments. The reconfigurable mechanism is thus defined as a mechanism or device that can change the system configuration, and it can be electronic, mechanical, hydraulic, pneumatic or a combination of these.

If the suspension systems of a railway vehicle have several configurations and each of the configurations can be passive and/or active and be suitable to one or more of its working environments, the task of the reconfigurable mechanism is to change the system configuration as the working environments vary, i.e. the reconfigurable mechanism is initiated when the working environment varies, but after the system

has been switched from one configuration to another by the reconfigurable mechanism, the system works under a new configuration and the reconfigurable mechanism no longer affects the system. The reconfigurable mechanism, in simple terms, acts as a switch. The fundamental difference between the reconfigurable mechanism and other controlled suspension systems is that it switches the suspensions from one configuration to another depending on the working environments, rather than monitoring or controlling any individual component of the suspensions. Two features of the reconfigurable mechanism are noted from this difference:

- i) it only works for a short time and,
- ii) it does not supply or modulate the flow of energy in the system.

These two features result in two benefits:

- i) the reconfigurable mechanism only affects the transient characteristics of system responses and,
- ii) the power needed by the reconfigurable mechanism is merely to drive the switching mechanism and can be very small.

Applications of the reconfigurable mechanism in vehicle suspensions also possibly add some other advantages such as reliability, robustness, simplicity and ease of maintenance.

7.1.2 Reconfigurable Mechanism in Perfect Steering Vehicles

Usually, the lateral movement of a wheelset is larger on curves than on straight lines and increases as the curvature increases whilst the equivalent conicities will increase when the lateral movement of wheelset increases, and thus the equivalent conicities will rise as curves become sharper, and at least, the wheel profile can be designed to achieve the purpose. If the steering linkages are not too stiff, low speed instability occurs only when the equivalent conicity of perfect steering vehicles is low, and low speed instability therefore disappears if perfect steering vehicles only run on curves, especially on sharp curves. This implies that the fundamental conflict between stability (low conicity and conventional) and curving of a railway bogie vehicle can be well decoupled if a conventional bogie vehicle can be turned into a perfect steering configuration on sharp curves.

In each perfect steering vehicle, the steering linkages provide the constraints for yaw motions of vehicle's rigid bodies, especially with regard to wheelset yaw motion, while in conventional bogie vehicles, the yaw stiffnesses that contribute to bending stiffnesses constrain the yaw motions of the rigid bodies. If the reconfigurable mechanism can turn the effective stiffnesses in the steering linkages of perfect steering vehicles into the yaw stiffnesses in the suspensions, the perfect steering vehicles will become conventional bogie vehicles and vice versa.

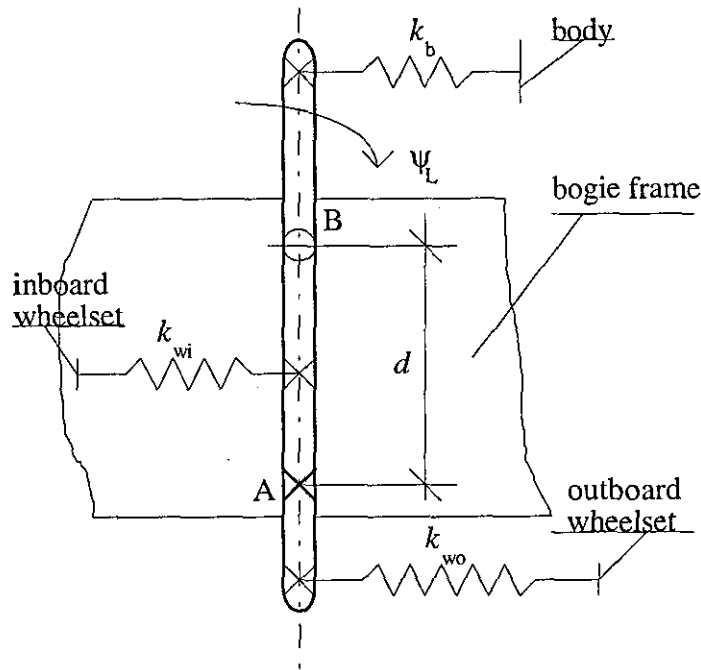


Figure 7.1 The concept of the reconfigurable mechanism in Model II

The diagram in Fig.7.1 shows the concept that turns the effective stiffnesses in the steering linkages of Model II into the yaw stiffnesses in the suspensions. In Fig.7.1, point A represents the joint between the bogie frame and the lever of the steering linkage. If point B is another joint between the bogie frame and the lever, the lever cannot turn related to the bogie frame, and the bogie frame and lever become one rigid body. Springs k_{wo} and k_{wi} become the primary longitudinal stiffness that forms the primary yaw stiffness while spring k_b becomes the secondary longitudinal stiffness that forms the secondary yaw stiffness, and thus the stiffnesses in the steering linkages are changed into the yaw stiffnesses in the suspensions so that the perfect steering vehicle (Model II) becomes a conventional bogie vehicle. When joint B is disconnected, the vehicle becomes a perfect steering vehicle again. If joint B can be disconnected on sharp curves and connected in other situations, the vehicle will be a perfect steering bogie vehicle on sharp curves and a conventional bogie vehicle on other circumstances, and the reconfigurable mechanism is therefore

realised. Obviously, there are many ways in which joint B can switch between being connected and unconnected. An analogous mechanism can also be applied to Model I.

It can be seen here that the reconfigurable mechanism itself does not affect the dynamics of the vehicle after the reconfiguration process has been completed. Indeed, the reconfigurable mechanism may only work on entering (to disconnect the joint B) and exiting (to connect the joint B) curves, or in other words, the reconfigurable mechanism may only work on transitions.

When the vehicles enter a curve, the reconfigurable mechanism should switch the vehicle from conventional configuration to perfect steering configuration, and joint B should be disconnected. The turning angles (ψ_L) of the levers of the steering linkages in Model I and Model II related to the bogie frame are zero when joint B is connected. Joint B should therefore produce enough force to hold the levers before it is disconnected when the vehicle enters a curve. If the distance d between joints A and B is 0.5m, the forces F_{pc} that should be applied on joint B are shown in Fig.7.2 when the vehicles move on the cubic parabola transition as defined by Fig.2.3.

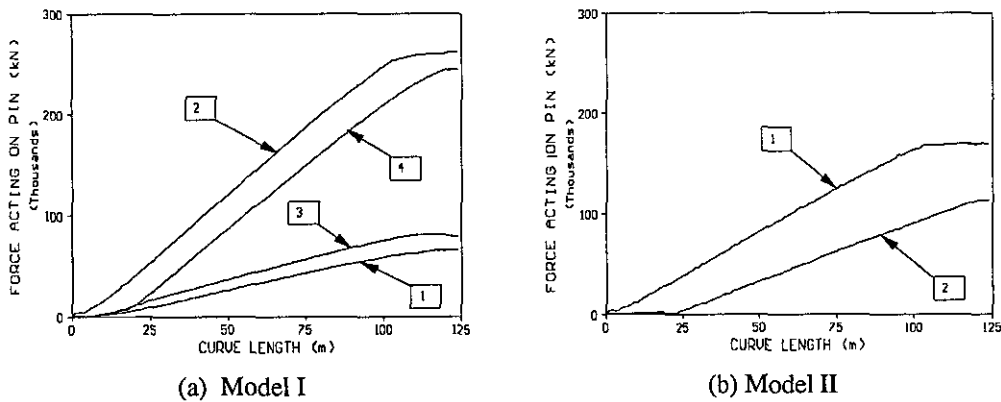


Figure 7.2 The forces F_{pc} in order to hold joint B when Model I and Model II enter the cubic parabola transition, stiff linkages

When the vehicles are on a curve (or a sharp curve), the vehicle configurations should be perfect steering form, and thus joint B is disconnected and the levers in the steering linkages can turn freely related to the bogie frame, i.e. $\psi_L \neq 0$. When the vehicles exit the curve, the reconfigurable mechanism should turn the vehicles from perfect steering configurations into conventional configurations, and thus joint B should be connected. Since $\psi_L \neq 0$, the task of the reconfigurable mechanism is i) to restore the steering levers back to their neutral positions ($\psi_L = 0$), and then ii) to

connect joint B, i.e. when the vehicles exit from curves. The working process of the reconfigurable mechanism can be divided into two steps: firstly restoring the levers and secondly, holding them. The turning angles (ψ_L) of the levers are shown in Fig.7.3 when the vehicles exit the same cubic parabola transition. If $d = 0.5\text{m}$, the forces F_{ps} that the reconfigurable mechanism should provide in restoring the levers back to their neutral positions along the transition are displayed in Fig.7.4.

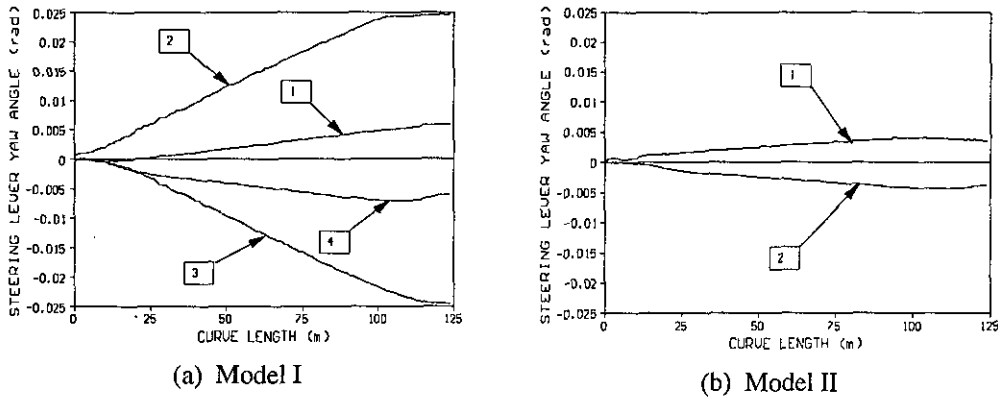


Figure 7.3 The turning angles (ψ_L) of the levers on the transition when Model I and Model II exit the cubic parabola transition, stiff linkages

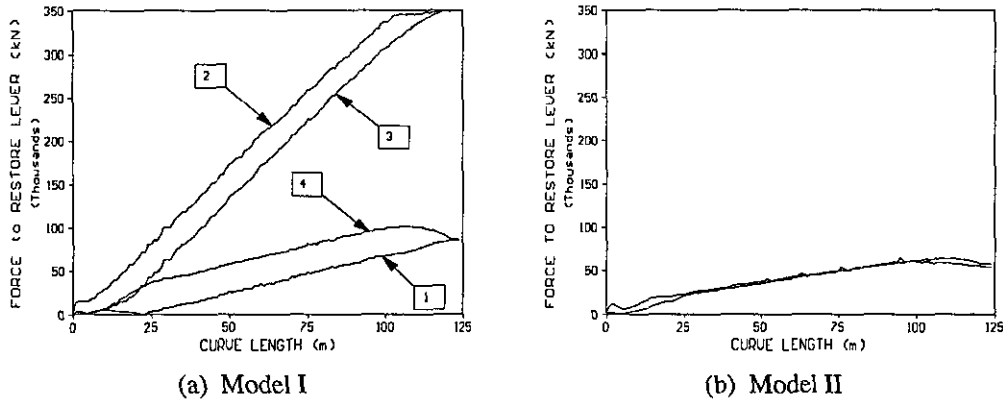


Figure 7.4 The forces F_{pc} in order to connect joint B when Model I and Model II exit the cubic parabola transition, stiff linkages

When perfect steering vehicles are on a uniform curve ($R = 200\text{m}$) with cant deficiency, the turning angles (ψ_L) of the steering levers are illustrated in Fig.7.5 for steady state. If joint B is disconnected, the levers of the steering linkages will rotate around joint A, and the displacements of joint B is listed in Table 7.1 when Model I and Model II are on curves. The shift of point B in Model II is much smaller than that in Model I, which implies that the reconfigurable mechanism is more easily achieved in Model II than in Model I.

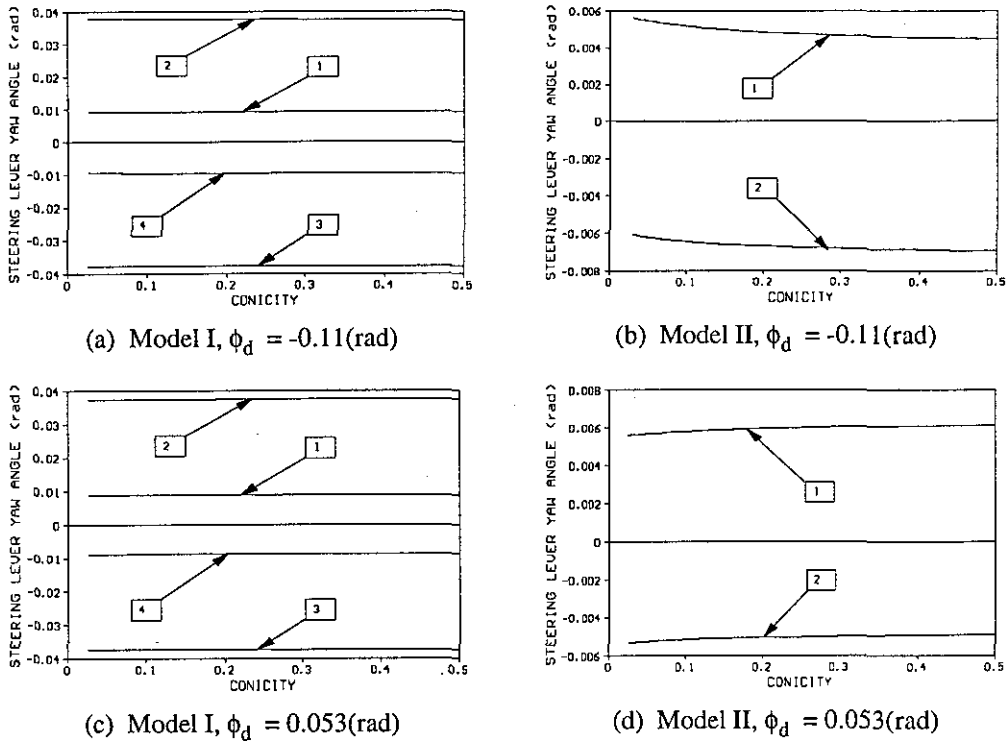


Figure 7.5 The angles of the levers versus conicity on a uniform curve, stiff linkages

Table 7.1 Possible linear shifts of point B

	cant deficiency	Model I $\max \psi <$	Model II $\max \psi <$
R = 200 meters	$\phi_d = -0.11$	0.04	0.007
	$\phi_d = 0.053$	0.04	0.007
R = 500 meters	$\phi_d = -0.11$	0.04	0.007
	$\phi_d = 0.053$	0.04	0.007
Cubic Parabola		0.025	0.005
$\Sigma \max \psi <$		0.065	0.012
500 mm $\times \Sigma \max \psi $		± 32.5 mm	± 6 mm

7.1.3 Two Devices

There are many possibilities with regard to the design of joint B. The configurations of two devices are outlined in Fig.7.6 and Fig.7.7. In Fig.7.6, a cored pin is mounted on the bogie frame and controlled by a force F. The clearance between the lever and the pin when the pin is on 0-0 position allows the lever to turn freely

around the joint A within the clearance between the lever and the pin. The clearance between the lever and pin is governed by the coned angle α and the pin stroke, and if the clearance is bigger than the maximum displacement of joint B in any circumstance, the vehicle has the perfect steering configuration. When the pin moves forward, the clearance decreases and finally disappears and the pin contacts the lever. If the force F driving the pin is increased further and pushes the pin into 1-1 position, the lever will be in its neutral position. The first step in restoring the lever back to its neutral position has now been completed. If there is enough force to hold the pin in 1-1 position, the second step is realised and the perfect steering vehicle is changed into a conventional bogie vehicle. When the pin is driven back to 0-0 position, the vehicle is turned back into the perfect steering configuration. The reconfigurable mechanism is thus achieved. The clearance between the pin and the lever should be wide enough for the lever to turn. The required stroke of the pin may be large than that achievable in practical applications if the displacement of the lever at joint B is too large. The device in Fig.7.7, however, can be used in the cases where the displacement of the lever at joint B is large.

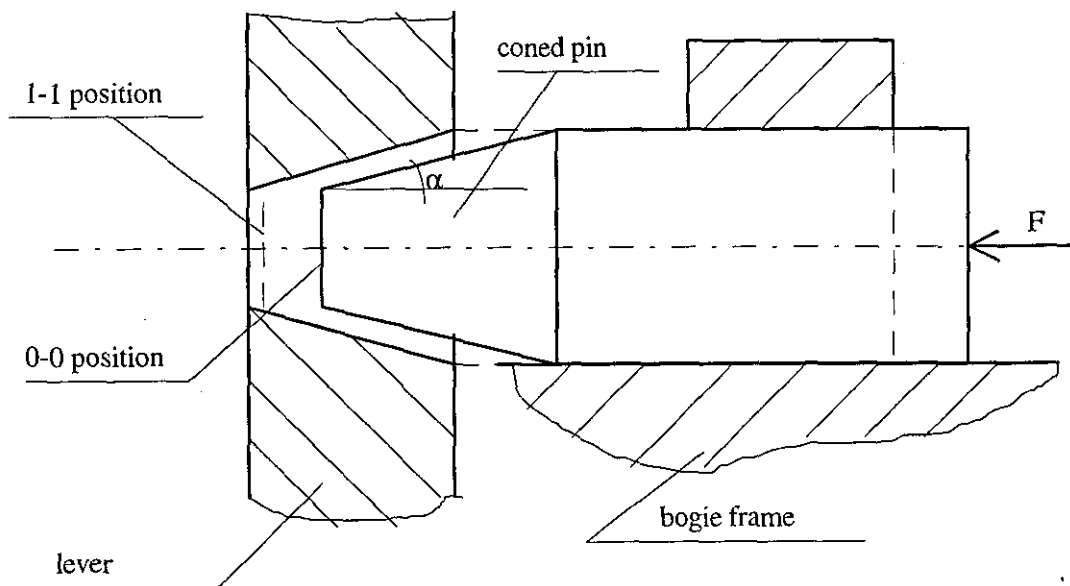


Figure 7.6 The coned pin system

In essence, there are two systems in Fig.7.7, one of which acts to restore the levers back to their neutral positions and the other is to hold them in place, the former being a gear system and the latter a pin device. When the power of gear C is switched off and pin D with the square head is removed, joint B in Fig.7.1 is disconnected and the lever can freely turn around joint A, and the vehicle configuration is that of perfect steering. When the vehicle demands conventional configuration, the power of gear C is first switched on to drive the lever back to its

neutral position through gears B and A. After the lever returns to its neutral position, pin D is pushed into shaft E and preventing it from turning so that the lever can not turn. The reconfigurable mechanism is therefore achieved once more. Since the primary purpose of this chapter is to develop merely the concept of the reconfigurable mechanism, only the cored pin-system in Fig.7.6 will be discussed further due to its simplicity.

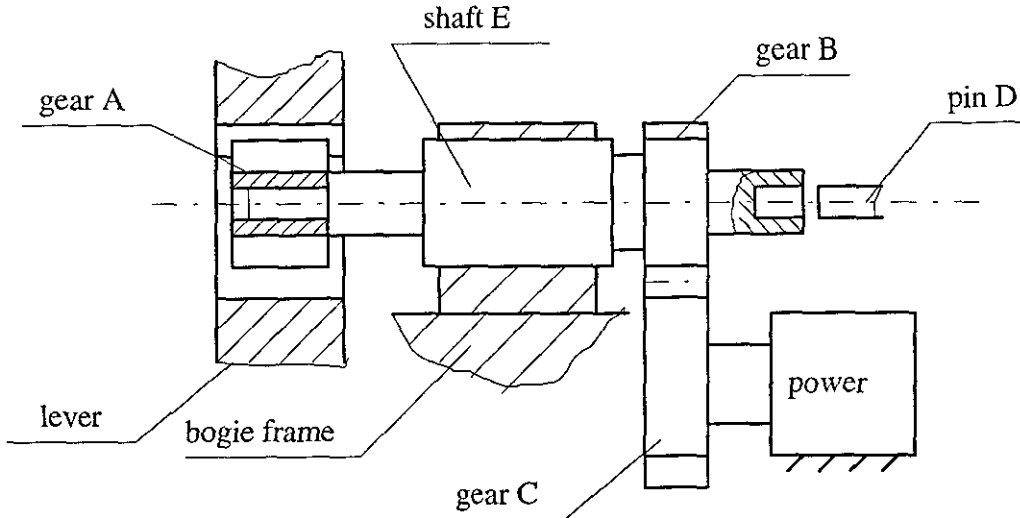


Figure 7.7 The gear system

The force diagram of the pin is schematically shown in Fig.7.8 when the pin is pushed into the lever in the system in Fig 7.6, where T is the force acting on the lever, F_f is the friction force and N_i the normal force. Since there are two contact surfaces, two normal forces and two friction forces will act on the pin. It can be derived that the force needed to push the pin into the lever is:

$$F_{in} \approx \mu T + \frac{(1 + \mu)(\mu \cos \alpha + \sin \alpha)}{\cos \alpha - \mu \sin \alpha} T \quad (7-1a)$$

where, μ is the coefficient of friction.

When the pin is pulled out of the lever, the friction forces will change direction, and thus the force needed to pull the pin out of the lever is:

$$F_{out} \approx \mu T + \frac{\mu \cos \alpha - \sin \alpha}{\cos \alpha + \mu \sin \alpha} T \quad (7-1b)$$

The above equations show that F_{in} and F_{out} are functions of the cored angle α and the coefficient of friction μ . Values of F_{in} and F_{out} for several pairs of α and μ are

listed in Table 7.2 and Table 7.3 respectively. The tabulated results indicate that a small value α and low friction can reduce F_{in} . The static friction coefficient lubricated by grease is about 0.11 [107], and if $\alpha = 5^\circ$, we have $F_{in} \approx 30\%T$ and $F_{out} \approx 14\%T$.

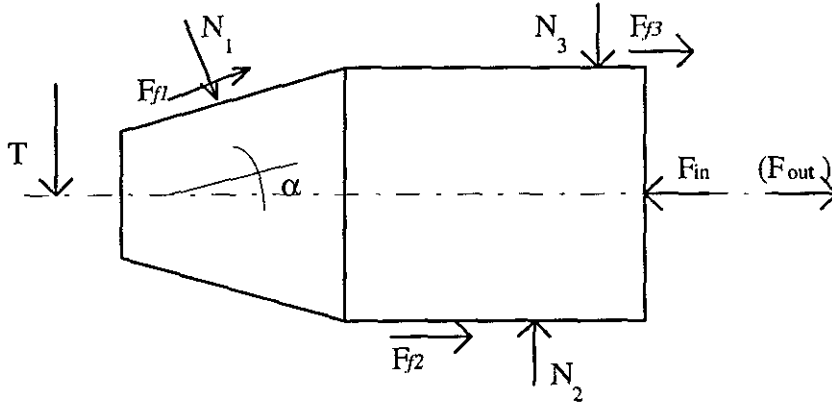


Figure 7.8 The force diagram of the pin

Table 7.2 $F_{in} (= T\%)$

F_{in}	μ	0.05	0.1	0.15	0.2	0.25	0.3
α							
	5°	19.50	30.80	42.67	55.11	68.13	81.73
	10°	28.98	40.94	53.54	66.81	80.75	95.38
	15°	38.84	51.59	65.08	79.33	87.54	110.29

Table 7.3 $F_{out} (= T\%)$

F_{out}	μ	0.05	0.1	0.15	0.2	0.25	0.3
α							
	5°	2.14	12.11	22.05	31.94	41.80	51.62
	10°	-0.75	4.25	14.18	24.03	33.81	43.52
	15°	-13.78	-3.40	6.30	16.18	25.94	35.59

Since F_{out} is the force required to pull the pin out of the lever, the pin cannot leave the lever if F_{out} is greater than or equal to zero. This means that the pin is self locked in the lever if F_{out} is positive. If there is not any contact between the pin and the lever, we have $F_{in} = 0$. When the pin contacts to the lever, we have $F_{in} \neq 0$, but suppose that F_{in} is not large enough to push the pin completely into the final position, with this condition, the lever does not return to its neutral position. If the pin is self locked, it cannot be pushed back by T only, and thus the lever cannot turn in one direction. When the lever tends to turn in another direction, T will decrease

and thus the pin is pushed a little further by F_{in} . The process will continue until the pin is pushed fully into the final position. This implies that F_{in} should not necessarily be very large in practical applications. In order to shorten the reconfigurable process, however, joint B should be connected as quickly as possible, and thus F_{in} should be large enough.

If the diameter of the actuator that drives the pin is 10cm, the area of one end of the piston is 78.5cm². The air pressure of the railway vehicle brake system is approximately 3bar, and thus the maximum output of the actuator is 2300N, moreover, the output of a real actuator will be even smaller than this[108]. Suppose that the pin of the system in Fig.7.6 should be pushed in or pulled out on the transition 25m away from the straight line, the forces that the actuator should provide are about 30kN, as seen in Fig.7.2 and Fig.7.4. It seems that the pneumatic actuator output is not sufficient enough to drive the pin in or out, if so, other systems can be applied to increase actuator output. If there is a hydraulic system on the bogie[109], the pneumatic system can be replaced by it, and the actuator output can be increased significantly as the pressure in hydraulic systems is much higher than that of pneumatic systems. If a hydraulic system is not available in a bogie, an intensifier can be used to raise the pressure of the pneumatic system.

The relative yaw angles between the carbody and bogies on curves are bigger than those when on straight lines, and these relative yaw angles can thus be used to examine whether the vehicle is on a curve or not. The technology of measuring the relative motion between the carbody and bogies developed by GEC ALSTHOM [110] can be used for this purpose.

The discussion above shows that it is possible to achieve the reconfigurable mechanism in Model I and Model II without adding any extra source of energy, which will greatly reduce the cost and complexity of manufacture and maintenance, and increase reliability and robustness.

When reconfigurable mechanism takes place in Model I and Model II, the vehicles basically work in two configurations: perfect steering and conventional. The vehicles take up the perfect steering configuration when they negotiate sharp curves, whilst on other track environments they become conventional bogie vehicles. When the vehicles are in one of their configurations, their dynamic behaviour will only depend on this configuration alone. However, when the reconfigurable mechanism takes place, the vehicle's dynamic behaviour depends on both configurations, and

the system is said to be in its transient state. The transient state will finally subside to the steady state when the vehicle takes on one of the configurations.

The behaviour in the transient state is useful in understanding what happens when the reconfigurable mechanism is working, and is especially important to reveal whether vehicle performance in this state is acceptable or not. After the transient period has passed, the system's behaviour will be finally governed by one of the configurations alone, and thus the most important aspect of the vehicle's dynamic characteristics is the behaviour in steady state. In the chapter, therefore, only steady state dynamic characteristics are considered. Another reason why the performance in transient states is not studied here is that it depends heavily on the vehicle detail and the physics of the reconfigurable mechanism. The results will not have general significance at this stage as both the vehicles and the mechanism may have many different forms in practical applications.

7.2 The Relationship Between Effective Stiffnesses and Yaw Stiffnesses

When joint B is connected, Model I and Model II take on the conventional configurations, and the yaw stiffnesses in the conventional configurations are defined by:

$$\begin{aligned} \text{Primary yaw stiffness:} \quad k_{p\psi_i} &= b^2 k_{w_i} & k_{p\psi_o} &= b^2 k_{w_o} \\ \text{Secondary yaw stiffness:} \quad k_{s\psi} &= b^2 k_b \end{aligned}$$

where, the meanings of k_γ 's and b can be found in Fig.7.1, Fig.3.2 and Fig.3.3. If the stiffness k_{w_i} is equal to the stiffness k_{w_o} (i.e. $k_{w_i} = k_{w_o} = k_w$), we have $k_{p\psi_i} = k_{p\psi_o} = k_{p\psi} = b^2 k_w$ and the conventional configurations of Model I and Model II are fore-and-aft symmetric such that the elastic matrix \mathbf{E} of the conventional configurations is a symmetric matrix. The elastic matrices \mathbf{E} 's of Model I and Model II themselves are, however, asymmetric even if the condition ($k_{w_i} = k_{w_o} = k_w$) is satisfied as seen in Eq.(3-1)--Eq.(3-5). This is the major difference in the structure of the elastic matrices \mathbf{E} 's with regard to conventional and perfect steering configurations. Moreover, there is another difference between the perfect steering form of Model II and its conventional configuration, which is that the perfect steering configuration of Model II has the inter wheelset stiffness k_{e3} while this stiffness disappears in its conventional form.

From Eq.(3-2) and Eq.(3-4), the relationships between the yaw stiffnesses of the conventional configurations and the effective stiffnesses of the perfect steering configurations can be found as:

For Model I

$$k_{e1} = \frac{k_{p\psi} k_{s\psi} / b^2}{l_1^2 k_{s\psi} + l_2^2 k_{p\psi}}; \quad k_{e2} = \frac{k_{p\psi} k_{s\psi} / b^2}{(l_3 + l_4)^2 k_{s\psi} + l_4^2 k_{p\psi}} \quad (7-2a)$$

For Model II

$$\begin{aligned} k_{e1} &= \frac{k_{p\psi} k_{s\psi} / b^2}{(l_1 + l_3)^2 k_{s\psi} + (l_3^2 + l_2^2) k_{p\psi}} \\ k_{e2} &= \frac{k_{p\psi} k_{s\psi} / b^2}{(l_1 + l_3)^2 k_{s\psi} + (l_3^2 + l_2^2) k_{p\psi}} \\ k_{e3} &= \frac{k_{p\psi}^2 / b^2}{(l_1 + l_3)^2 k_{s\psi} + (l_3^2 + l_2^2) k_{p\psi}} \end{aligned} \quad (7-3a)$$

Eq.(7-2) and Eq.(7-3) indicate that it is impossible to make the elastic matrix **E** symmetric for both perfect steering vehicle models if their conventional configurations are fore-and-aft symmetric. Applying the yaw stiffness ratio $\alpha = k_{p\psi} / k_{s\psi}$ to the formulas, Eq.(7-2) becomes:

$$k_{e1} = k_{e2} = \frac{k_{p\psi} / b^2}{l_1^2 + l_2^2 \alpha} \quad (7-2b)$$

since $l_1 = l_3 + l_4$, and Eq.(7-3) becomes:

$$\begin{aligned} k_{e1} = k_{e2} &= \frac{k_{p\psi} / b^2}{(l_1 + l_3)^2 + (l_3^2 + l_2^2) \alpha} \\ k_{e3} &= \frac{\alpha k_{p\psi} / b^2}{(l_1 + l_3)^2 + (l_3^2 + l_2^2) \alpha} \end{aligned} \quad (7-3b)$$

If $k_{e1} = k_{e2}$, two independent stiffnesses k_{e1} and k_{e2} in the perfect steering configuration become one in Model I, but for the conventional configuration of Model I, there are still two independent parameters ($k_{p\psi}$ and $k_{s\psi}$ or $k_{p\psi}$ and α), and therefore, for the same value of effective stiffnesses, one perfect steering configuration of Model I may have many combinations in its conventional

configuration. This implies that the conventional configuration of Model I can have more choices with regard to system elasticity. For Model II, there are still two independent stiffnesses (k_{e1} & k_{e3}) even though $k_{e1} = k_{e2}$.

Usually, $k_{p\psi} > k_{s\psi}$, so we have $\alpha > 1$, and if the geometric parameters of the steering levers are constant, the effective stiffnesses are the functions of the primary yaw stiffness $k_{p\psi}$ and the yaw stiffness ratio α . If the units of the stiffnesses are ignored, the effective stiffnesses are proportional to the primary stiffness, i.e. $k_e = \beta k_{p\psi}$, where the values of β are listed in Table 7.4 as a function of the ratio α .

Table 7.4 The stiffness ratio coefficient $\beta = k_e / k_{p\psi}$

β	α	1	10	20	40	60	80	100	150
k_e for Model I		1.10	0.93	0.80	0.62	0.50	0.43	0.37	0.28
k_{e1} for Model II		1.08	0.80	0.62	0.43	0.33	0.26	0.22	0.16
k_{e3} for Model II		1.08	7.95	12.23	17.02	19.48	21.00	22.04	23.58

7.3 Optimisation of Stiffnesses when the Reconfigurable Mechanism is Applied

The results in the last sub-section show that the effective stiffnesses in Model I and Model II are directly related to the yaw stiffnesses of their conventional configurations. Since the effects of effective stiffnesses on the vehicle dynamics of the perfect steering configurations are not completely coincident with the effects of the yaw stiffnesses on the vehicle dynamics, a comprehensive investigation has been carried out to optimise each stiffness suitable for both perfect steering configuration and conventional configuration.

In Eq.(7-2b) and Eq.(7-3b), the effective stiffnesses in the perfect steering configurations and the secondary yaw stiffness in the conventional configuration are determined by the ratio $\alpha (= k_{p\psi}/k_{s\psi})$ and the primary yaw stiffness $k_{p\psi}$. The results in Fig.7.9 give the critical speed of the conventional bogie vehicle versus the ratio $\alpha (= k_{p\psi}/k_{s\psi})$ and the primary yaw stiffness $k_{p\psi}$. The vehicle stability is improved when α is low, and the optimal value of the primary yaw stiffness is 20~30MN-m, however, the critical speeds are acceptable when the value of the primary yaw stiffness varies from 10MN-m to 100MN-m. Acceptable ride quality is achieved

with hard primary yaw stiffness, as seen in Fig.7.10, however, an optimised α ($= k_{p\psi} / k_{s\psi}$) can improve ride quality. From Fig.7.10, the optimal value of the yaw stiffness ratio α ($= k_{p\psi} / k_{s\psi}$) is around 50.

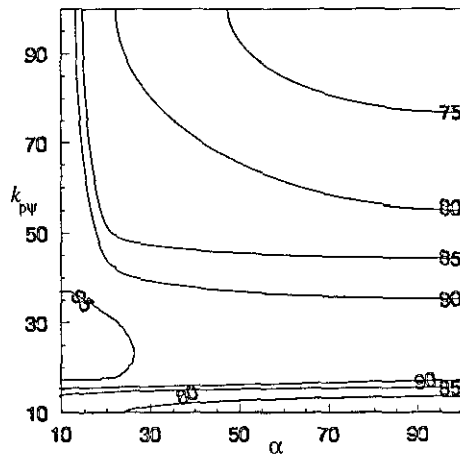


Figure 7.9 The critical speed versus α and $k_{p\psi}$ (MN-m) when $k_{py} = 40\text{MN/m}$ and $\lambda = 0.2$, the conventional bogie vehicle

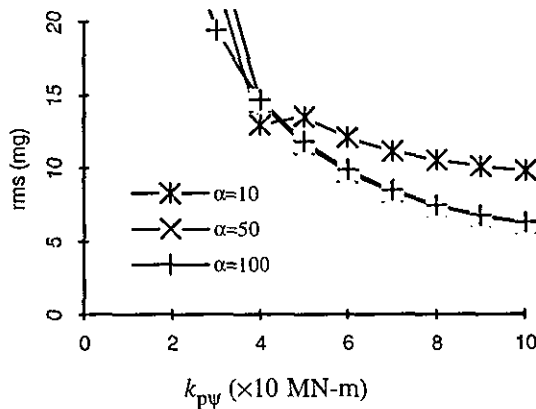


Figure 7.10 The maximum weighted rms's (mg) of accelerations versus of $k_{p\psi}$ when $k_{py} = 40\text{MN/m}$, $\lambda = 0.1$ and $v_0 = 200\text{km/h}$, the conventional bogie vehicle

The critical speeds versus k_{py} (primary lateral stiffness) and α are shown in Fig.7.11 and the maximum weighted rms's of the accelerations over 0.1-100.0Hz at the five points defined in Fig.5.2 are displayed in Fig.7.12 when $k_{p\psi} = 50\text{MN-m}$. The critical speeds in Fig.7.11 are acceptable when $k_{py} = 5\sim 50\text{MN/m}$ although the optimal value of the primary lateral stiffness k_{py} for stability is around 20MN/m . The ride quality does however become unacceptable when $k_{py} = 15\sim 35\text{MN/m}$, and it severely deteriorates when the primary lateral stiffness k_{py} is between 20MN/m and 30MN/m . The PSD's at points A, C and E (defined in Fig.5.2) are illustrated in Fig.7.13 respectively when $k_{py} = 10\text{MN/m}$, $k_{py} = 25\text{MN/m}$ and $k_{py} = 40\text{MN/m}$. It can be observed that the responses at the first natural frequency are very high, especially

the lateral acceleration (point C) when $k_{py} = 25\text{MN/m}$. This implies that the resonance effect is much higher when $k_{py} = 25\text{MN/m}$. Referring to the results in Chapter 5, the optimal value for the primary lateral stiffness k_{py} is approximately 10MN/m .

When the combining effect of the secondary lateral stiffness k_{sy} and the ratio α on ride quality are considered, one finds that high α can improve ride quality when the secondary lateral stiffness k_{sy} is very soft, whilst low α can benefit ride quality when k_{sy} becomes harder, as seen in Fig.7.14.

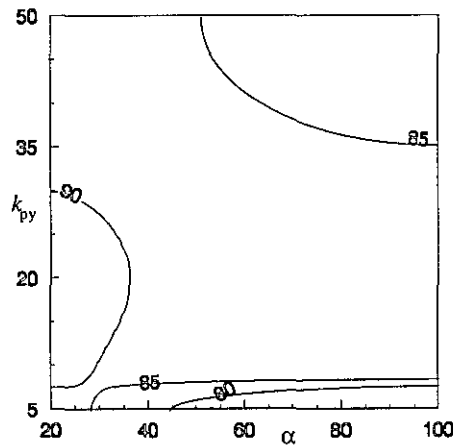
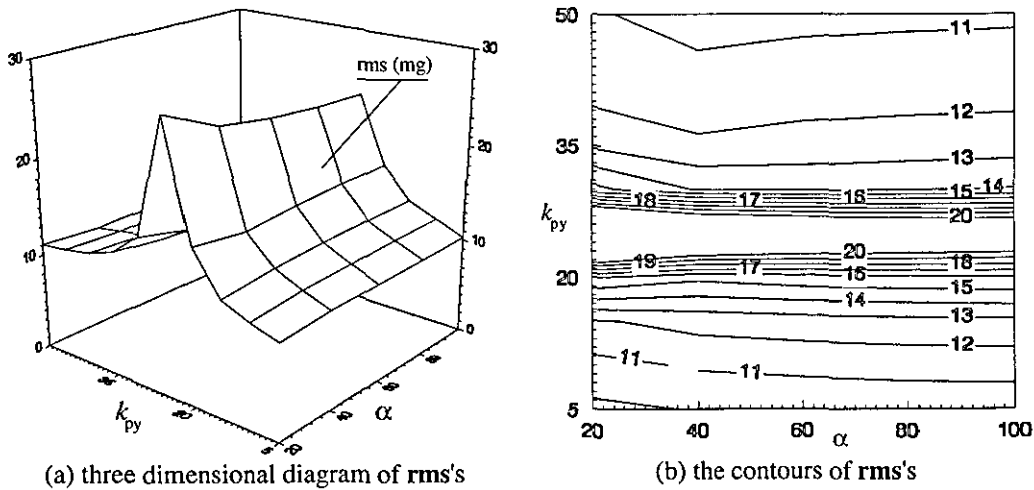


Figure 7.11 The critical speed versus α and k_{py} (MN/m) when $k_{p\psi} = 50\text{MN-m}$ and $\lambda = 0.2$, the conventional bogie vehicle



(a) three dimensional diagram of rms's
 (b) the contours of rms's
 Figure 7.12 The maximum weighted rms's (mg) versus α and k_{py} (MN/m) when $k_{p\psi} = 50\text{MN-m}$, $\lambda = 0.1$ and $v_0 = 200\text{km/h}$, the conventional bogie vehicle

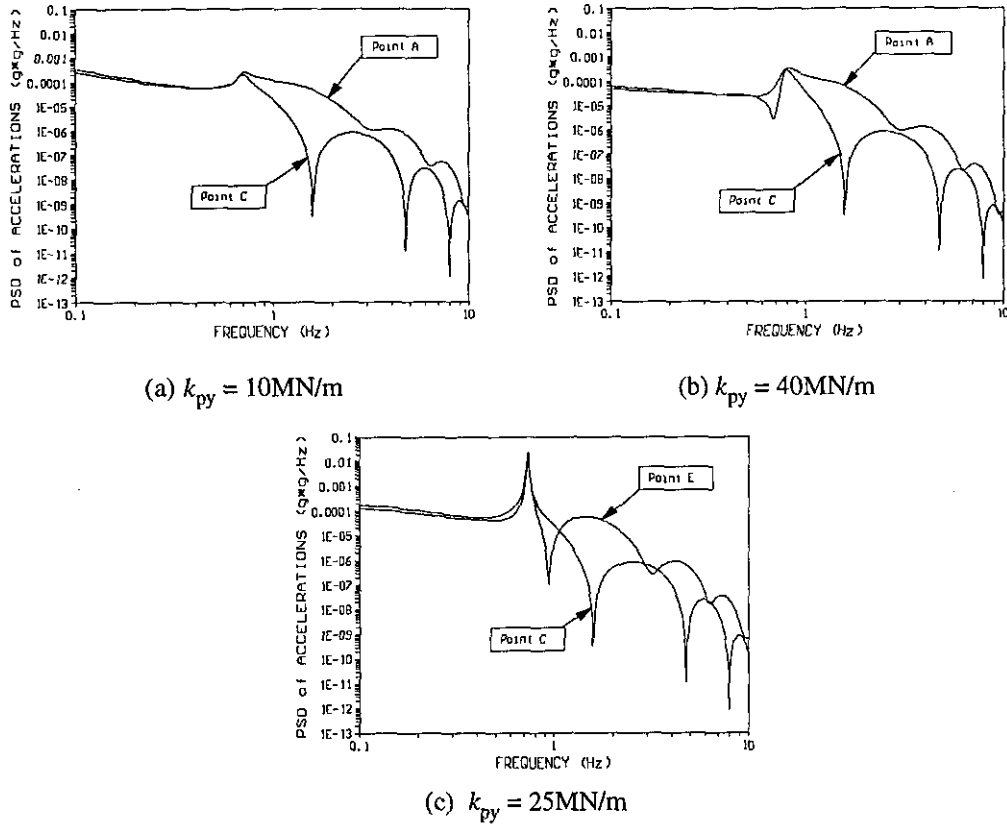


Figure 7.13 The PSD's of the accelerations, when $k_{p\psi} = 50\text{MN-m}$, $\lambda = 0.1$ and $v_0 = 200\text{km/h}$, points A, C and E are defined in Fig.5.2, the conventional bogie vehicle

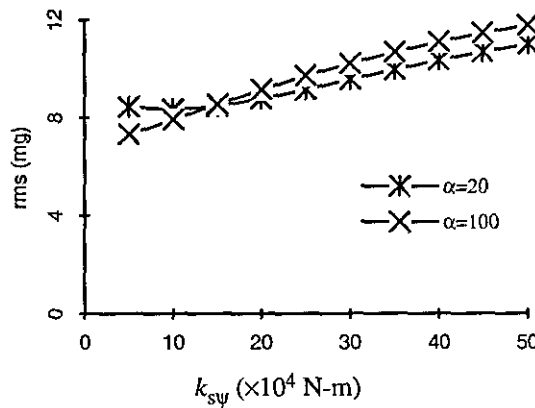


Figure 7.14 The maximum weighted rms's (mg) versus k_{sy} when $k_{py} = 10\text{MN/m}$, $k_{p\psi} = 50\text{MN-m}$, $\lambda = 0.1$ and $v_0 = 200\text{km/h}$, the conventional bogie vehicle

A brief summary on the effects of the stiffnesses on vehicle dynamics can now be given on the basis of the above results. When the perfect steering vehicles are converted into the conventional configurations, the primary yaw stiffness $k_{p\psi}$ should be equal to or greater than 50MN-m , the primary lateral stiffness k_{py} should be around 10MN/m and the yaw stiffness ratio α ought to be greater than 10. Vehicle

stability can be improved by further optimising the stiffnesses, but is acceptable for the ranges being studied, i.e.

$$10\text{MN-m} \leq k_{p\psi} \leq 100\text{MN-m}, \quad 5\text{MN/m} \leq k_{py} \leq 50\text{MN/m} \text{ and } \alpha > 10.$$

The values of the stiffnesses are therefore governed by the ride quality of the conventional configurations.

If $k_{p\psi} = 50\text{MN-m}$ and $20 \leq \alpha \leq 150$, the values of the effective stiffness k_e ($= k_{e1} = k_{e2}$) are:

$$\text{for Model I, } k_e = 1.3785 \times 10^7 \text{ } (\alpha = 150) \text{ and } k_e = 3.976 \times 10^7 \text{ } (\alpha = 20)$$

$$\text{for Model II, } k_e = 0.786 \times 10^7 \text{ } (\alpha = 150) \text{ and } k_e = 3.0825 \times 10^7 \text{ } (\alpha = 20)$$

Referring to Chapter 4 and Chapter 5, high effective stiffnesses can increase the critical speeds of Model I and Model II in conventional instability and improve their ride quality with the condition that low speed instability does not occur. An increment in $k_{p\psi}$ or a reduction in α will raise the effective stiffnesses (k_{e1} and k_{e2}), and therefore, if ride quality of the perfect steering vehicles is acceptable for a single value of the effective stiffness, the ride quality of the conventional configurations can be improved by applying hard $k_{p\psi}$ and high α (soft $k_{s\psi}$). This implies that the conventional configurations of the perfect steering vehicles potentially give some advantages in ride quality.

When $k_{p\psi}$ is 50MN-m and b (the distance between the longitudinal central line of vehicle and the steering linkage) is 0.9m, k_w is 61.73MN/m, which is a very hard spring, and if $k_{p\psi}$ is 60MN-m, k_w will be 74.07MN/m. It might not be a good practice if $k_{p\psi}$ is required to be increased further. k_w can be cut down by increasing the distance b .

7.4 Improvement in Dynamic Behaviour

If $k_{e1} = k_{e2} = k_e$, many combinations of $k_{p\psi}$ and α can form one value of k_e . This advantage can be used to improve the dynamic behaviour of the conventional configuration of Model I and Model II. The values of the effective stiffness k_e ($= k_{e1} = k_{e2}$) are 3.37553×10^7 for Model I and 0.94563×10^7 for Model II respectively. Some of combinations of $k_{p\psi}$ and α for the values are listed in Table 7.5 (Model I) and Table 7.6 (Model II). The results in the last section show that $k_{p\psi}$ should be around 50MN-m or over in order to achieve acceptable ride quality for the

conventional configurations, and thus the yaw stiffness ratio α should be around 30 or over for Model I and must be greater than 100 for Model II.

Table 7.5 Model I ($k_{e1} = k_{e2} = 3.37553 \times 10^7$)

α	20	30	40	50	60	70	80
$k_{pv} \times 10$ (MN-m)	4.245	4.860	5.475	6.090	6.705	7.321	7.935

Table 7.6 Model II ($k_{e1} = k_{e2} = 0.94563 \times 10^7$)

α	90	100	110	120	130	140	150	200
$k_{pv} \times 10$ (MN-m)	3.947	4.291	4.636	4.981	5.325	5.670	6.015	7.738
$k_{e3} \times 10^9$	0.851	0.946	1.040	1.135	1.229	1.324	1.419	1.891

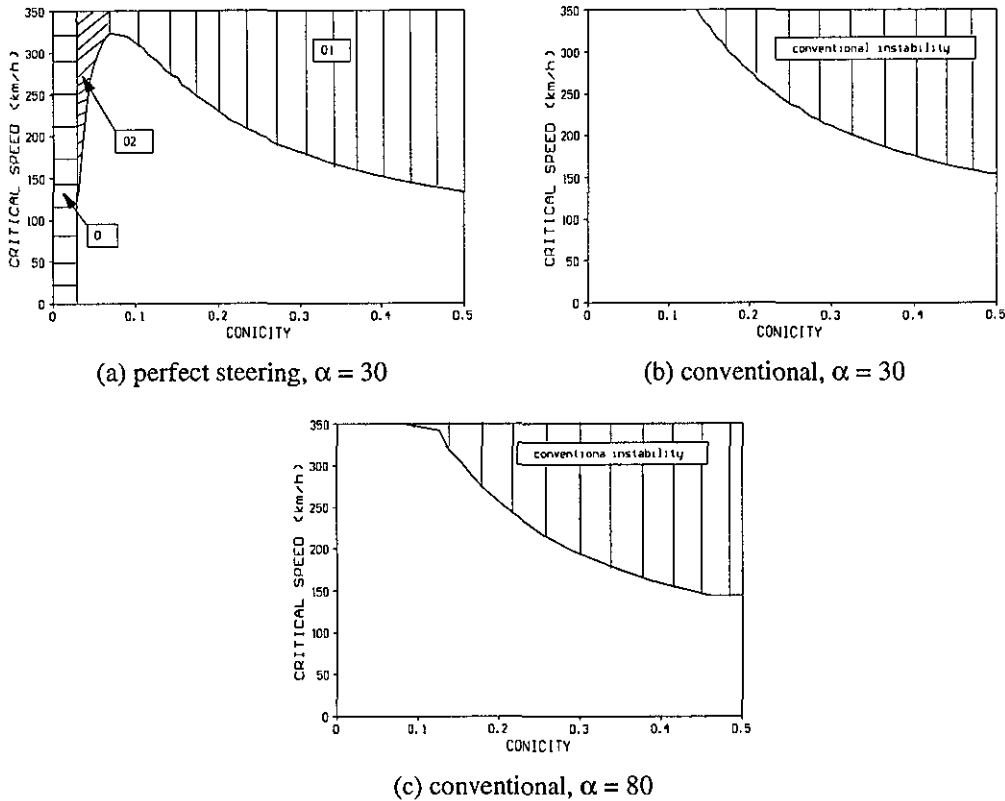
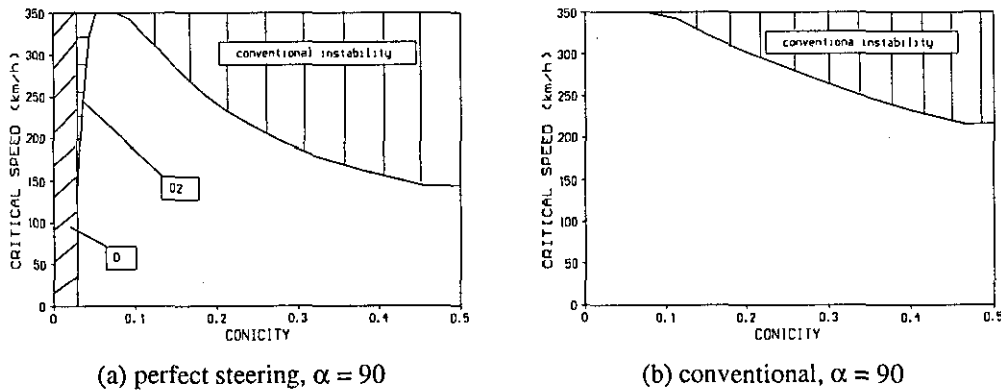


Figure 7.15 The critical speeds (versus conicity) of the perfect steering and conventional configuration of Model I

When the perfect steering vehicles are converted into conventional bogie vehicles, the most important improvement in their dynamics is the removal of low speed instability, as seen in Fig.7.15 (Model I) and Fig.7.16 (Model II). Usually, the equivalent conicities are smaller when the vehicles are on straight lines than those when they are on curves (at least this can be achieved by the wheel profile design).

The potential of low speed instability is much lower when the perfect steering vehicles are on curves than when on straight lines, and therefore, the possibility of low speed instability for each perfect steering vehicle is much reduced or even eliminated when they are equipped with the reconfigurable mechanism. Since the critical speeds of the conventional configurations of Model I and Model II in high conicity are higher than the perfect steering forms of Model I and Model II, the vehicle speed can be increased by applying the reconfigurable mechanism. The yaw stiffness ratio α does not affect the stability of Model I if the relation in Eq.(7-2b) is used, as seen in Fig.7.15, while the ratio α slightly affects the critical speeds of Model II, if the relation in Eq.(7-3b) is applied, as seen in Fig.7.16. The results in the last section indicate that the influence of the yaw stiffness ratio α on the stability of the conventional bogie vehicle is not very significant, which is also supported by the results shown in Fig.7.15 and Fig.7.16.

When the perfect steering vehicles are turned into the conventional bogie vehicles, the channels to transfer the track irregularities to the body are reduced from three to one, and thus the ride quality of the conventional configurations of Model I and Model II is potentially better than that of Model I and Model II themselves. The most evident improvement of ride quality is that the depression of the responses around the first natural frequency when the perfect steering vehicles change their configuration, as shown in Fig.7.17 (Model I) and Fig.7.18 (Model II). The reductions of rms's at points A, C and E (defined in Fig.5.2) are illustrated in Fig.7.19 when the perfect steering vehicles are in the conventional configurations. Since the reduction at point C is almost the same as that at points A & E, the decrease in rms's mainly comes from the lateral motion of the carbody, as is especially noticeable with Model II, which can be directly observed in Fig.7.17 and Fig.7.18.



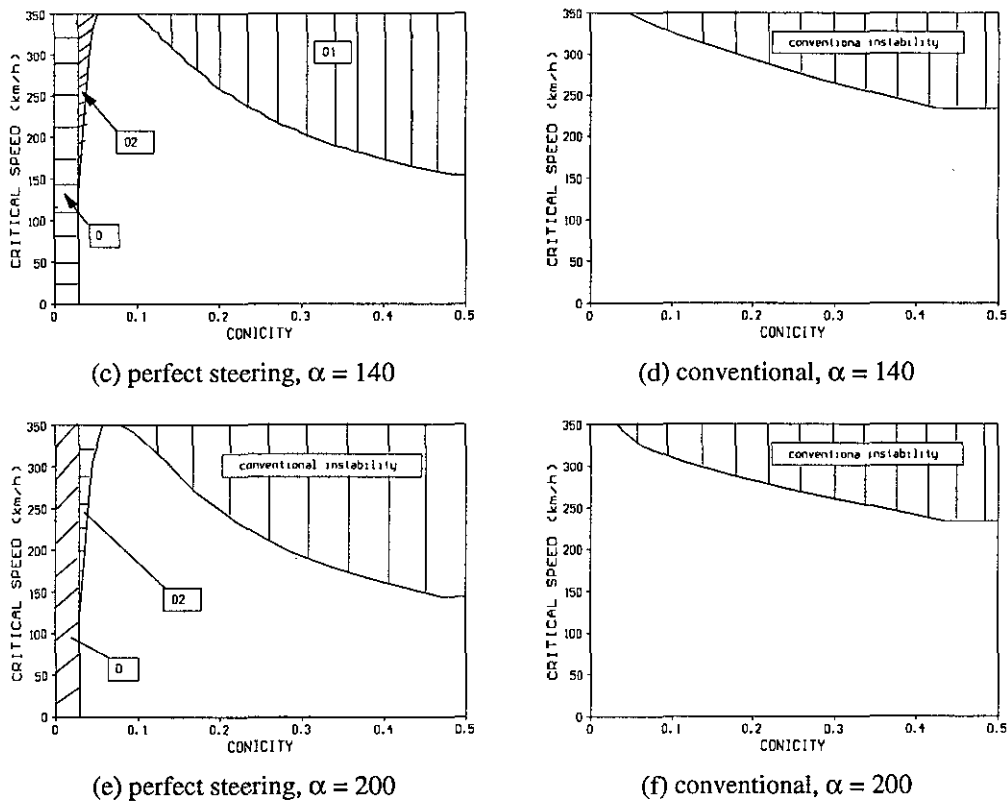


Figure 7.16 The critical speeds (versus conicity) of the perfect steering and conventional configuration of Model II

A further investigation is launched to study the effects of the yaw stiffness ratio α on ride quality. The maximum weighted **rms's** of the accelerations at the five points (defined in Fig.5.2) in question are displayed in Fig.7.20 (Model I) and Fig.7.21 (Model II). The maximum weighted **rms's** of all configuration are very sensitive to conicity, and the maximum weighted **rms's** related to conventional configuration are reduced by increasing α . This effect is most significant in Model I, and consequently, another advantage of the conventional configuration of Model I over the perfect steering form of Model I is that ride quality can be improved by raising $k_{p\psi}$ and α without changing the effective stiffnesses.

When $v_0 = 200\text{km/h}$ and $\lambda > 0.15$, the maximum weighted **rms's** of either Model II or its conventional configuration are too high to be tolerated even if $\alpha = 200$, as seen in Fig.7.21. The causes for this are that the primary and secondary lateral stiffnesses are higher in Model II than in Model I. If the secondary lateral stiffness of Model II is equal to that of Model I, i.e. $k_{sy} = 10\text{KN/m}$, the maximum weighted **rms's** of either Model II or its conventional configuration can be much reduced, as shown in Fig.7.22. It is found, however, that this reduction in k_{sy} does not affect the critical speed for both configurations. The decrease in the primary lateral stiffness

can also cut down the maximum weighted *rms*'s, but will reduce the critical speed. The results in these figures also indicate that a large yaw stiffness ratio α can improve ride quality, this implies that a hard k_w always benefits ride quality in all configurations.

When the vehicle speed is reduced to 150km/h, the ride quality is at an acceptable level (the maximum weighted *rms* $\leq 12\text{mg}$) for most of the cases considered. Usually, high equivalent conicities often occur when the vehicles negotiate very sharp curves[103]. Vehicle speeds in these circumstances are usually lower than those when in other circumstances, which implies that if the perfect steering configurations of Model I and Model II only work on sharp curves and their conventional configurations work on other circumstances, the ride quality of each perfect steering vehicle with the reconfigurable mechanism can be controlled to a reasonable level even if their normal speed is high.

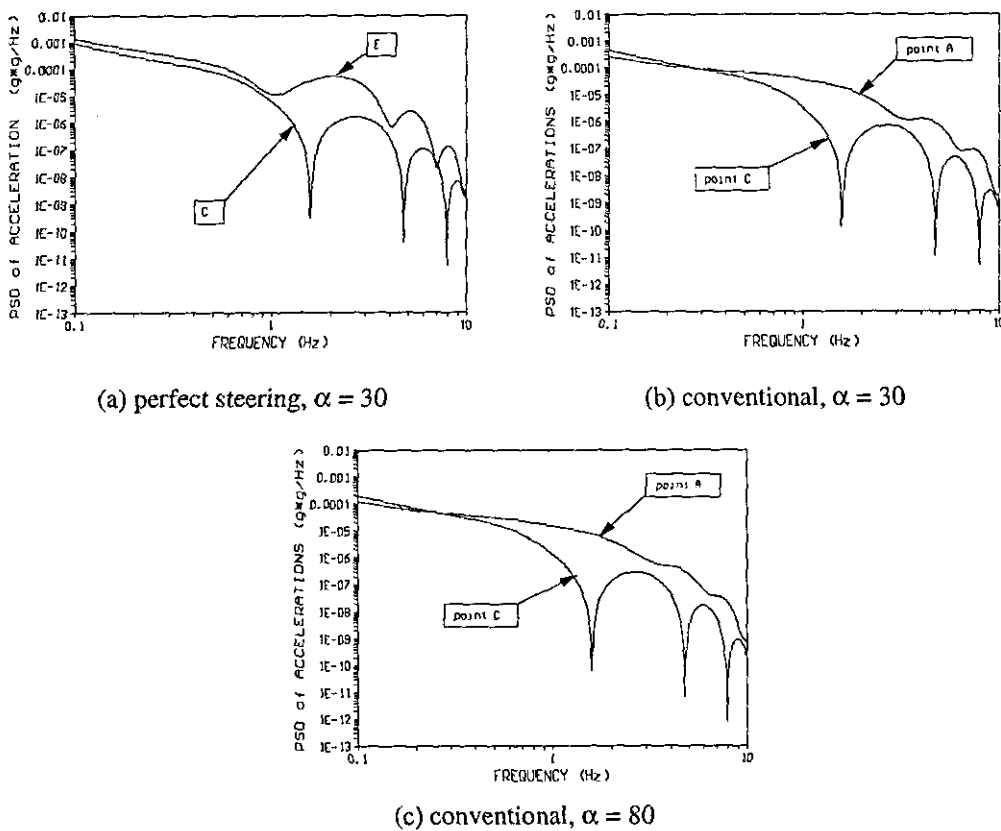


Figure 7.17 The acceleration PSD's of Model I and its conventional configuration $v_0 = 200\text{km/h}$ and $\lambda = 0.1$, points A, C and E are defined in Fig.5.2

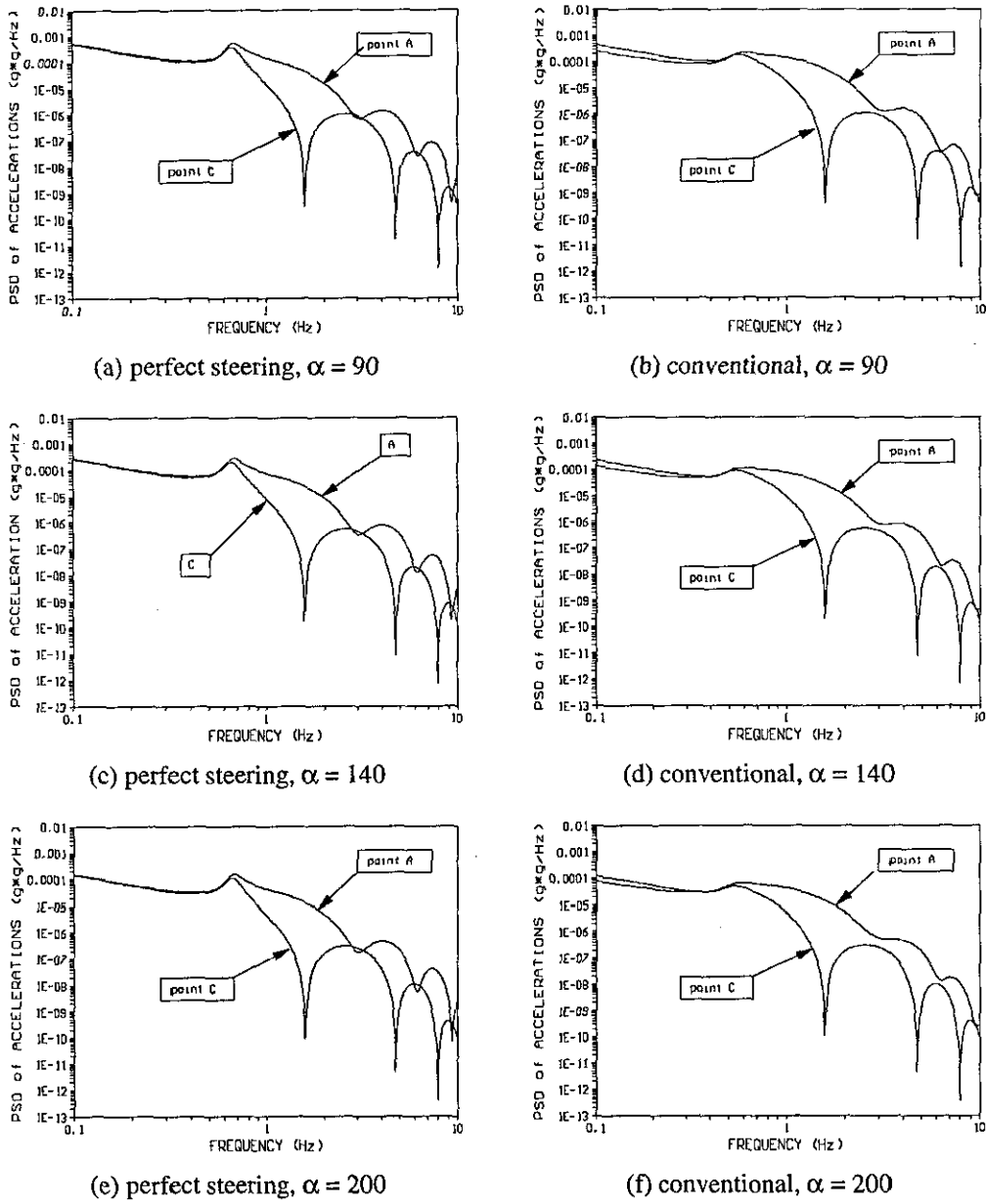


Figure 7.18 The acceleration PSD's of Model II and its conventional configuration when $v_0 = 200\text{km/h}$ and $\lambda = 0.1$, points A, C and E are defined in Fig.5.2

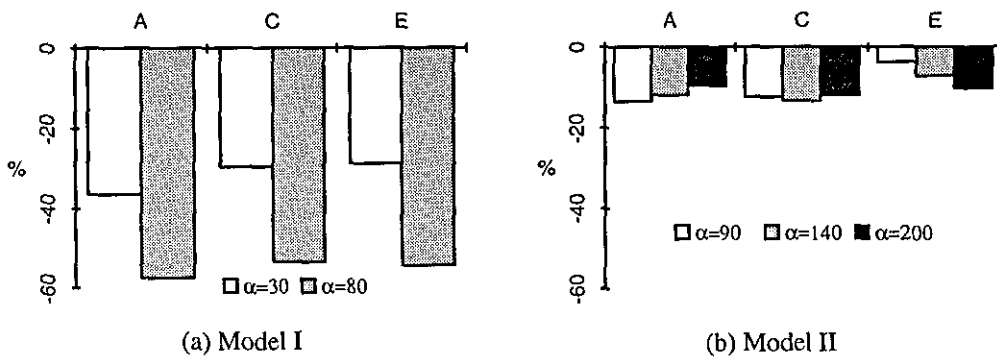


Figure 7.19 The reductions of rms's (mg) at points A, C and E for the conventional configurations of Model I and Model II, $v_0 = 200\text{km/h}$ and $\lambda = 0.1$

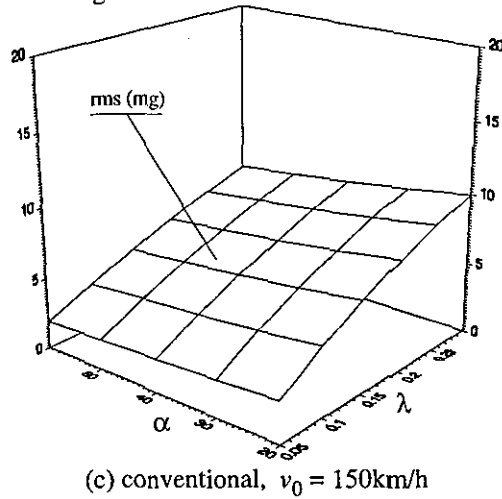
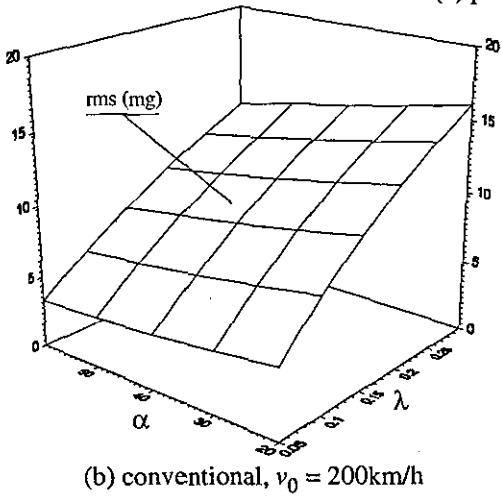
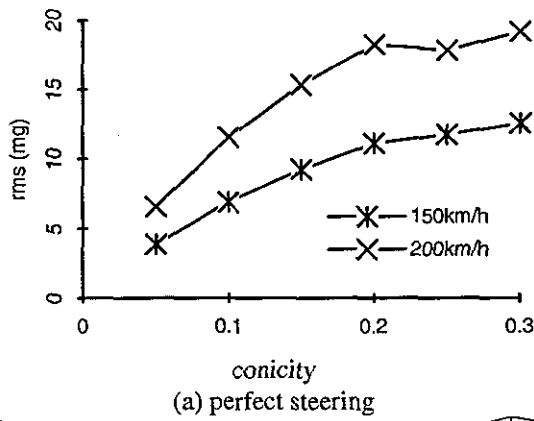
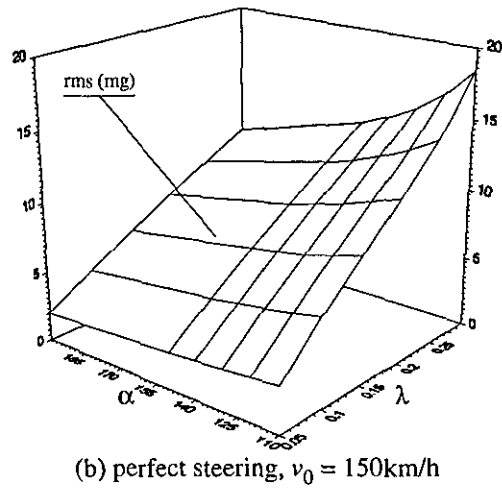
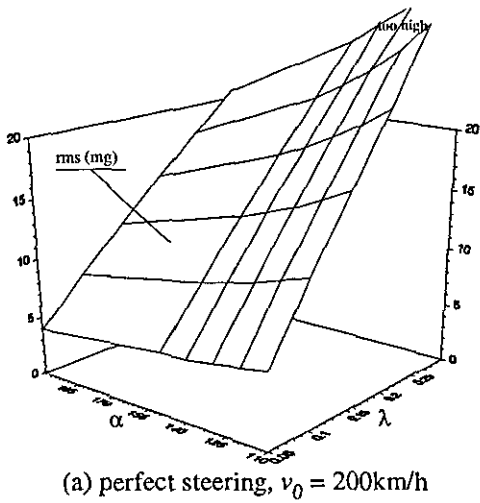
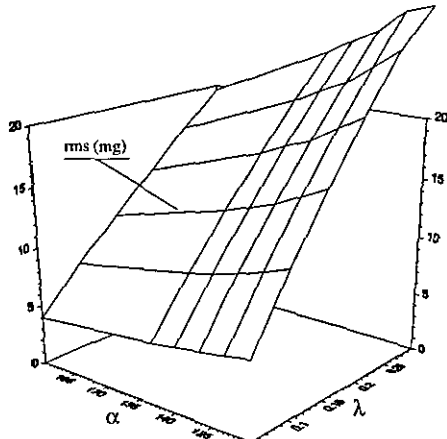
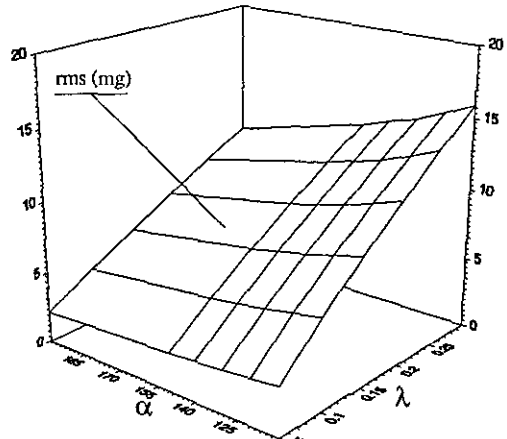


Figure 7.20 The maximum weighted rms's (mg) of the accelerations at the five points (defined in Fig.5.2) of Model I and its conventional configuration



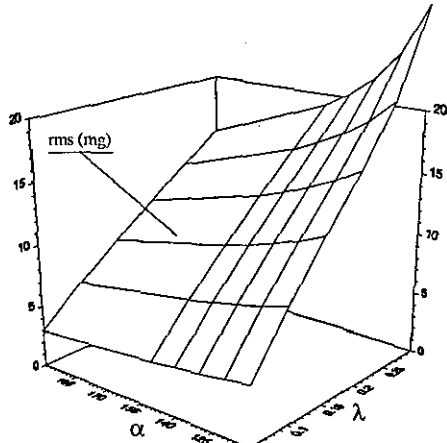


(c) conventional, $v_0 = 200\text{km/h}$

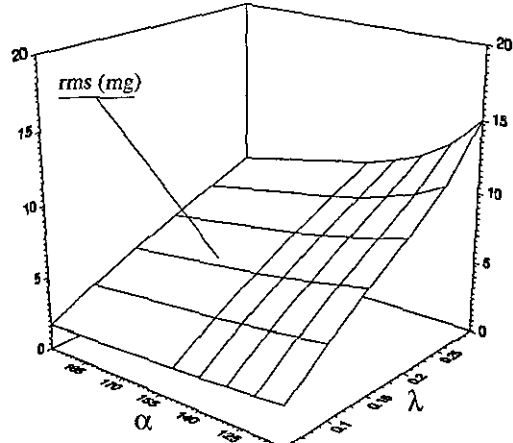


(d) conventional, $v_0 = 150\text{km/h}$

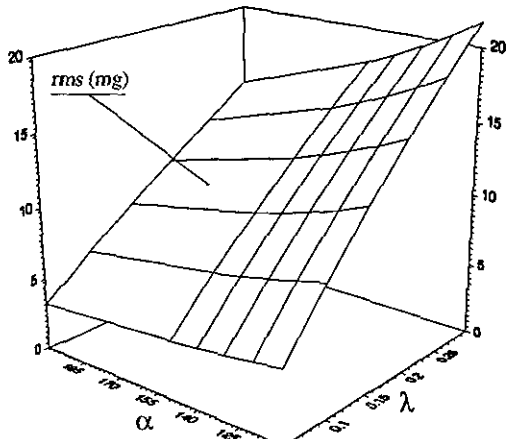
Figure 7.21 The maximum weighted rms's (mg) of the accelerations at the five points (defined in Fig.5.2) of Model II and its the conventional configuration



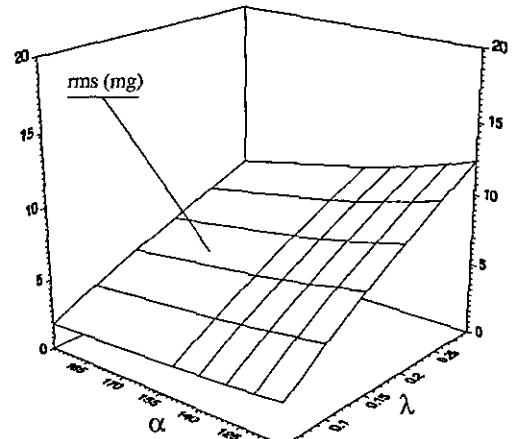
(a) perfect steering, $v_0 = 200\text{km/h}$



(b) perfect steering, $v_0 = 150\text{km/h}$



(c) conventional, $v_0 = 200\text{km/h}$



(d) conventional, $v_0 = 150\text{km/h}$

Figure 7.22 The maximum weighted rms's (mg) of the accelerations at the five points (defined in Fig.5.2) of Model II and its conventional configuration when $k_{sy} = 10\text{KN/m}$

7.5 Summary

The conflict between stability and curving in the lateral plane is fundamental with regard to conventional bogie vehicles. In actual fact, this conflict results in the knowledge of how to select yaw stiffnesses, especially with regard to the selection of the primary yaw stiffness. A hard primary yaw stiffness raises the critical speed, and increases the bending stiffness that causes a difficulty when vehicles negotiate curves. A perfect steering vehicle can steer itself well on sharp curves if there is sufficient flange clearance, however, a fundamental conflict exists in its stability itself, i.e. stiff steering linkages can improve the conventional stability of perfect steering vehicles, but cause low conicity instability. With the reconfigurable mechanism, a railway bogie vehicle can work in conventional configuration on straight lines and take on the perfect steering configuration on curves. This vehicle avoids low conicity instability on straight lines and negotiates curves well, and therefore, a perfect steering bogie vehicle with the reconfigurable mechanism decouple these fundamental conflicts well.

The reconfigurable mechanism only works when the vehicle changes its configuration. When the reconfigurable mechanism works, there is a transient state whereby the dynamic responses of the system change temporarily. The period of the transient state is governed by the reconfigurable mechanism as the time taken to change the configuration depends on the mechanism itself. After the transient period, the vehicle is in only one of the configurations and the reconfigurable mechanism is an independent system, and the mechanism itself does not, therefore, influence the dynamic behaviour of the vehicles in steady state. In other words, the dynamics of the vehicles in steady state is only decided by the vehicle configurations, which highlights the advantage in the simplicity over controlled suspensions. Comparing with controlled suspensions such as active and semi-active systems, the reconfigurable mechanism can be a more simple, less energy consuming and more robust system. Another benefit is that the system can avoid complicated feedback control philosophy. In actual fact, the reconfigurable mechanism for the perfect steering vehicles mainly depends on the turning angles of the levers in the steering linkages, and if the angles are small, the device can be very simple indeed as illustrated in Fig.7.6.

When the perfect steering vehicles are equipped with the reconfigurable mechanism, the dynamic behaviour is divided into two phases: the stability and ride quality of conventional configurations on straight lines and the stability and ride quality of

perfect steering configurations on curves. The critical speeds and maximum *rms* at those five points (defined in Fig.5.2) of Model I and Model II and of their conventional configurations are listed in Table 7.7 (Model I) and Table 7.8 (Model II) respectively when the parameters of Set 2 (stiff steering linkages) in Table 3.4 and in Table 3.5 are used. The critical speeds of the conventional configurations of Model I and Model II at high conicities are higher than those of Model I and Model II themselves, and ride quality of the conventional configuration of Model I are better than that of Model I itself whilst the ride quality of Model II and its conventional configuration are very close.

Since the equivalent conicity on curves is higher than that on straight lines, the effective stiffnesses of the perfect steering vehicles can be increased when the reconfigurable mechanism is applied. The results in Chapters 4 & 5 demonstrate that stiff steering linkages not only raise the critical speed, but also improve ride quality for the perfect steering vehicles. This effect can be more significant if the perfect steering configurations are only in effect when the vehicles are on sharp curves. The perfect steering vehicles with the reconfigurable mechanism are very useful implementations for railways with high speed in straight tracks and low speed on sharp curves.

Another advantage of the conventional configurations over the perfect steering vehicles is that any single value of the effective stiffnesses ($k_{e1} = k_{e2}$) can be formed from many combinations of the primary yaw stiffness $k_{p\psi}$ and the yaw stiffness ratio α . This gives the conventional configurations more choices in optimising their yaw stiffnesses and improving their dynamic behaviour, and this is very significant in Model I.

The reconfigurable mechanism can also be applied to other classes of body-steered bogie vehicles in improving their dynamic behaviour if their steering linkages have similar configurations as Model I or Model II. Furthermore, the reconfigurable mechanism also has a general application in other physical systems.

Table 7.7 Major performance index of Model I and its conventional configuration

Conicity λ	0.05	0.1	0.15	0.2	0.25	0.3
Model I v_0 (km/h)	287	312	269	229	200	182
Conventional	>360	>360	330	276	236	212
Model I, $v_0=150$ (km/h) rms_{max} (mg)	3.86	6.92	9.26	11.10	11.72	12.57
Conventional, $v_0=200$ (km/h)	4.36	7.26	9.72	11.81	13.60	15.15

the yaw stiffness ratio $\alpha = 30$

Table 7.8 Major performance index of Model II and its conventional configuration

Conicity λ	0.05	0.1	0.15	0.2	0.25	0.3
Model II v_0 (km/h)	341	352	302	258	226	204
Conventional	334	323	312	298	287	276
Model II, $v_0=150$ (km/h) rms_{max} (mg)	2.76	5.25	7.55	9.71	11.81	13.97
Conventional, $v_0=200$ (km/h)	4.22	7.59	10.59	13.39	16.02	18.49

the yaw stiffness ratio $\alpha = 140$

CONCLUSIONS AND FUTURE DEVELOPMENTS

Three configurations of railway bogie vehicles with the capability of perfect steering have been proposed, and their negotiating ability, stability and ride performance have been investigated. To overcome the disadvantages of perfect steering vehicles, a reconfigurable mechanism has been conceived, and the improvement in the dynamics of perfect steering vehicles with the reconfigurable mechanism has been studied. The dynamic performance of perfect steering vehicles has been summarised in Chapter 6, and the advantages of the reconfigurable mechanism with regard to improving the dynamics have been given in Section 7.5. This chapter will summarise the achievements of the research project, point out possible applications of the research results, and suggest possible future developments

8.1 Contributions and Findings

Chapter 1 indicated that the dynamic behaviour of perfect steering vehicles has not been studied well although the feasibility of bogie vehicles being capable of perfect steering has been proved. The results and analyses in this research project have great significance which will lead to the application of perfect steering vehicles. This section summarises the contributions and new findings of the research. Since perfect steering vehicles are one class of body-steered bogie vehicles, some of the results can in general be applied to other classes of body-steered bogie vehicle.

Contributions:

1. Three configurations of perfect steering vehicles have been proposed. The conditions for them to possess perfect steering have been postulated.
2. The effects of the perfect steering vehicles' elasticity on their curve negotiating ability (uniform curves with or without cant deficiency and transition) have been systematically investigated.
3. The effects of geometric errors in the steering linkages on the dynamic behaviour of perfect steering vehicles have been studied.

4. Two bogie sub-systems, one possessing three, and another four degrees of freedom, have been used to theoretically analyse the low conicity instability of perfect steering vehicles. It has been found that the bogie sub-system with four degrees of freedom more closely resembles the physical features of the bogie, and the results derived from this sub-system therefore match the simulation results more closely than those obtained from the bogie sub-system with three degrees of freedom.

5. The effect of each parameter in the suspensions and the steering linkages on the stability of perfect steering vehicles has been studied comprehensively. The results have very general significance with regard to the applications of body-steered bogie vehicles.

6. The effect of steering linkage on the transmissibility of body-steered bogie vehicles has been demonstrated theoretically. The influence of each parameter in the suspensions and the steering linkages on the ride performance of perfect steering vehicles has been investigated.

7. The reconfigurable mechanism for vehicle suspensions has been conceived, and the feasibility of applying the mechanism in perfect steering vehicles has been illustrated. The improvement in dynamics of the perfect steering vehicles with the reconfigurable mechanism has been studied.

Findings:

Negotiating Ability of Perfect Steering Vehicles

1. There is no bending stiffness in the suspensions of perfect steering vehicles. The sufficient condition for a bogie vehicle being capable of perfect steering is that the stiffness in the linkages does not make any contribution to the bending stiffness. This condition is independent of curvature and only depends on the configurations of bogie vehicles.

2. When perfect steering is realised, the wheelsets of the vehicles act as unconstrained wheelsets and roll on their pure rolling lines. This suggests that the yaw constraint of wheelset should be as flexible as possible in order to achieve better alignment on curves. This concept contradicts the traditional concept that a

steering mechanism should be applied to the wheelsets to assist in curve negotiation. This finding has general significance for other body-steered bogie vehicles, i.e. their steering linkages should be designed to minimise the bending stiffness of wheelset.

3. If the distance between the pure rolling lines of wheelsets and the track central line is larger than the restriction of flange contact, flange contact will occur before the wheelsets reach their pure rolling lines. Perfect steering cannot be achieved if flange contact occurs, and therefore, another condition for perfect steering is that flange clearance must be large enough to let the wheelsets roll on their pure rolling lines. Since the pure rolling line of wheelset is determined by the equivalent conicity of the wheelset and the curvature of curves, it is very difficult to realise perfect steering if curves are very sharp.

4. The capability of perfect steering vehicles with regard to negotiating curves is very sensitive to geometric errors in the steering linkages. The vehicles no longer possess the property of perfect steering if there are any geometric errors in their steering linkages. The geometrical accuracy of the steering linkages is therefore especially important in the applications of perfect steering vehicles.

5. Comparing with conventional bogie vehicles, perfect steering vehicles have much better alignment ability with regard to cant deficiency and curvature variation on transitions.

Stability of Perfect Steering Vehicles

1. There are three modes of instability with regard to the perfect steering vehicles: low speed instability, dynamic instability in low conicity and conventional instability. The instability modes of the perfect steering vehicles mainly depend on wheelset conicity. If the conicity is low, low speed instability (divergent or oscillatory) occurs and the vehicle critical speeds are very low. The critical speeds of perfect steering vehicles will increase as the conicity rises in dynamic instability in low conicity while the critical speed will decrease as the conicity becomes higher in conventional instability. When the steering linkages become very stiff, only low speed instability and conventional instability occur and dynamic instability in low conicity disappears. Although conventional instability is one kind of dynamic instability, the difference between dynamic instability in low conicity and conventional instability is that the former only occurs in one of the bogies whilst the latter occurs in both.

2. Since the condition for low speed instability is linked with the sufficient condition for the bogie vehicle being capable of perfect steering, low speed instability is unavoidable in perfect steering vehicles whenever their conicity is low or when the steering linkages are very stiff. This has been proved through both theoretical analysis and simulation. This is the first report regarding low speed instability in high conicity.

3. With regard to the stiffness of the steering linkages, there is a conflict between low speed instability and conventional instability. Soft steering linkages can prevent low speed instability whereas stiff steering linkages can improve conventional stability. It has also been found that the frequencies of the unstable motions in perfect steering vehicles are always associated with the kinematic frequencies of wheelset.

Ride Performance of Perfect Steering Vehicles

1. There are three channels capable of transferring track disturbances to the carbody of body-steered bogie vehicles: the coupling of primary/secondary suspensions (which only exist in conventional bogie vehicles), the steering linkages, and the coupling of the steering linkages/secondary suspension. These three channels are not, however, independent, such that the suspension coupling is complicated by the steering linkages in body-steered bogie vehicles. The transmissibility of body-steered bogie vehicles is potentially increased due to the steering linkages. Zero bending stiffnesses in the suspensions of perfect steering vehicles, however, simplifies the system coupling and reduces transmissibility. This effect will benefit ride performance of perfect steering vehicles.

2. The effects of the stiffness in the steering linkages of perfect steering vehicles on vehicle ride performance depend on the configurations of the steering linkages. If the steering linkages have similar configurations to those of Model I or Model II, the effective stiffnesses in the steering linkages unequally distribute in the connection between the wheelsets and bogie frames, and in the connection between the bogie frames and carbody. The increment in the effective stiffnesses of the steering linkages can strengthen the connection between the wheelsets and bogie frames, but makes little contribution to the strength of the connection between the bogie frames and carbody. The steering linkages effectively work as a double suspension system with a hard primary suspension and a soft secondary suspension,

and thus stiff steering linkages can improve the ride performance of perfect steering vehicles. The effects of steering linkages on ride performance, however, depend on their configurations, and stiff steering linkages can also deteriorate ride performance.

Overall Dynamic Performance of Perfect Steering Vehicles

The sufficient condition of perfect steering is independent of steering linkage stiffness whilst stiff steering linkages can raise the critical speed in conventional instability. Perfect steering vehicles, therefore, partly decouple the fundamental conflicts between curving and stability. Furthermore, if the configurations of the steering linkages are similar to those of Model I or Model II, stiff steering linkages also improve the ride performance of perfect steering vehicles. Stiff steering linkages can thus also partly decouple the basic conflict between stability and ride performance.

The Reconfigurable Mechanism

1. The reconfigurable mechanism is much simpler than controlled suspension systems because it does not control any of the components in the suspensions, and more generally, it does not control any of system state variables. Indeed, the reconfigurable mechanism can be considered as an independent system. It only affects the transient dynamics of the vehicles, and when the vehicles are in one of the configurations alone, their dynamics is only governed by this single configuration (which can be passive, active, semi-active or a combination of them). The simplicity of the reconfigurable mechanism can offer other advantages over controlled suspension systems such as cost, reliability, robustness and maintenance.

2. When the perfect steering vehicles are equipped with the reconfigurable mechanism, they can work in two configurations. They are perfect steering vehicles when on curves (or on sharp curves) but become conventional bogie vehicles when in other circumstances. The perfect steering vehicles with reconfigurable mechanism thus possess the advantages of both perfect steering vehicles and conventional bogie vehicles.

3. The vehicles with the reconfigurable mechanism can be controlled such that their perfect steering configurations only work under high equivalent conicity. This can not only eliminate low conicity instability, but also increase the stiffness of the steering linkages, which can improve conventional stability and ride performance. The stiffness in the steering linkages is turned into yaw stiffnesses in suspensions

when in the conventional configurations. It has been shown that stiff steering linkage in the perfect steering configuration can be changed into hard primary yaw stiffness and soft secondary yaw stiffness in the suspensions in conventional configuration. This can improve the ride quality of the conventional configurations without much deterioration in stability. The basic conflicts between curving, stability and ride performance are thus well solved in perfect steering vehicles with the reconfigurable mechanism.

8.2 Commercial Application Remarks

Perfect Steering Vehicles

Perfect steering vehicles presented in this thesis can be applied whenever the conflict between stability and curving becomes the major problem. They are especially useful for existing railway lines with sharp curves in raising train speed without causing problems during curve negotiation.

The stiffness in the steering linkages is limited by low conicity instability, which will produce negative effects on stability and ride performance. Other approaches need to be applied if perfect steering vehicles are used in a new high speed railway.

The realisation of perfect steering is dictated by the need for sufficient flange clearance to let the wheelsets move on their pure rolling lines. It is difficult to avoid flange contact for perfect steering vehicles when curvature is too large; for example in light railways or in underground railways.

Perfect Steering Vehicles with The Reconfigurable Mechanism

The applications of perfect steering vehicles are increased when they are equipped with the reconfigurable mechanism. It is possible to apply perfect steering vehicles with reconfigurable mechanism in new high speed railways. The reconfigurable mechanism cannot, however, alleviate flange contact when curves are very sharp.

Reconfigurable Mechanism

The concept of the reconfigurable mechanism has general significance and can be used in many physical systems. The reconfigurable mechanism of perfect steering vehicles can also be applied to other body-steered bogie vehicles.

8.3 Future Development Remarks

In order to develop perfect steering bogie vehicles into products, and apply the reconfigurable mechanism in body-steered bogie vehicles, further research is required and is given below.

1) More configurations of perfect steering bogie vehicles should be set up and their dynamic behaviour investigated. The purpose of research in this area has objectives: firstly to further explore the physical features of perfect steering bogie vehicles, secondly, to reveal the mechanisms behind these features, and finally, to optimise the configurations of perfect steering bogie vehicles with regard to their dynamics.

2) To understand the dynamics of perfect steering bogie vehicles in details, and to expose more physical features, it is necessary to simulate the dynamic responses of perfect steering vehicles in the time domain. In this computer model, the following aspects are of concern:

- influences of non-linear factors, especially flange contact,
- dynamic responses on special sections such as on switches, transitions and reverse curves,
- transient responses occurring when the reconfigurable mechanism is used.

3) The development of the reconfigurable mechanism can be divided in two fields. Firstly, the feasibility of the reconfigurable mechanism working correctly in each configuration of perfect steering bogie vehicles should be investigated, and secondly, the physical features of the reconfigurable mechanism with special regard to transient state should be studied. Some of the research in this area can be undertaken through computer simulation, but a physical system will lead to better results.

REFERENCES

- [1] **V.K Garg & R.V. Dukkipati**, 'Dynamics of Railway Vehicle Systems', Academic Press, 1984, ISBN 0 12 275950 8.
- [2] **F.W. Carter**, 'On the Action of a Locomotive Driving Wheel', Proceedings of the Royal Society of London, Vol.112, Ser.A, 1926, pp.151-157.
- [3] **J.J Kalker**, 'On the Rolling Contact of Two Elastic Bodies in the Presence of Dry Friction', Doctoral Thesis, Delft University of Technology, 1967.
- [4] **J.J Kalker**, 'The Contact between Wheel and Rail', Processings of First Course on *Advanced Vehicle System Dynamics*, International Centre for Transportation Studies, 1982.
- [5] **A.H. Wickens**, 'The Dynamic Stability of Railway Vehicle Wheelsets and Bogies Having Profiled Wheels', *Int., J. Solid Structures*, Vol.1, 1965, pp319-341.
- [6] **A. H. Wickens**, 'Steering and Dynamic Stability of Railway Vehicles', *Vehicle System Dynamics*, Vol.5, 1975/76, pp.15-46.
- [7] **A.H. Wickens**, 'Steering and Stability of Unsymmetric Articulated Railway Vehicles', ASME, J. of Dynamics Systems, Measurement, and Control, Vol.101, 1979, pp.256-262.
- [8] **A.H. Wickens**, 'Steering and Stability of the Bogie: Vehicle Dynamics and Suspension Design', *Proc Instn Mech Engrs*, Vol.205, 1991, pp.109-122.
- [9] **H. Scheffel**, 'A New Design Approach for Railway Vehicle Suspension', *Rail International*, Vol.638, Oct.1974.
- [10] **B.T. Scales**, 'Behaviour of Bogies on Curve', *Railway Eng.*, Dec. 1972.

- [11] **H.A. List**, 'Means for Improving the Steering Behaviour of Railway Vehicles', *Annual Meeting of the Transportation Research Board*, Washington, D.C., Jan. 1976.
- [12] **C.E. Bell & J.K. Hedrick**, 'Forced Steering of Rail Vehicles: Stability and Curving Mechanics', *Vehicle System Dynamics*, Vol.10, 1981, pp.357-386.
- [13] **J.A. Clement Fortin & R.J. Anderson**, 'Steady-State and Dynamic Predictions of the Curving Performance of Forced-Steering Rail Vehicles', *8th IAVSD-IUTAM Symposium*, 1983, pp.179-192.
- [14] **J.A.C. Fortin, etc.**, 'Validation of A Computer Simulation of Forced-Steering Rail Vehicles', *9th IAVSD Symposium*, 1985, pp.100-111.
- [15] **R.J. Anderson & C. Fortin**, 'Low Conicity Instabilities in Forced-Steering Railway Vehicles', *10th IAVSD Symposium*, 1987, pp.17-28.
- [16] **R.E. Smith**, 'Forced-Steering Truck and Vehicle Dynamic Modes-Resonance Effects Due to Car Geometry', *10th IAVSD Symposium*, 1987, pp.423-434.
- [17] **R. Weeks**, 'The Design and Testing of a Bogie with a Mechanical Steering Linkage', *10th IAVSD Symposium*, 1987, pp.497-508.
- [18] **Zhiyun Shen, etc.**, 'Dynamical Behaviour of A Forced-Steering Three-Piece Freight Car Truck', *10th IAVSD Symposium*, 1987, pp.542-551.
- [19] **R.E. Smith & R.J. Anderson**, 'Characteristics of Guided-Steering Railway Trucks', *Vehicle System Dynamics*, Vol.17, 1988, pp.1-36.
- [20] **R.E. Smith**, 'Dynamic Characteristics of Steered Railway Vehicles and Implications to Design', *Vehicle System Dynamics*, Vol.18, 1988, pp.45-69.
- [21] **D. Liechty**, 'Das Bogenlaeufige Eisenbahn-Fahrzeug', 1934, pp.21 (Schulthess, Zurich).

- [22] **D. Liechty**, 'Das Gleitende Flugelrad', *Glaser's Annln*, Vol.112, 1933, pp.62-67.
- [23] **U. Schwanck**, 'Wheelset Steering for Bogies of Railway Vehicles', *Rail Engineering International*, Oct.1974, pp.352-359.
- [24] **A.H. Wickens**, 'Stability Criteria for Articulated Railway Vehicles Possessing Perfect Steering', *Vehicle System Dynamics*, Vol.7, 1978, pp.165-182.
- [25] **A.H. Wickens**, 'Static and Dynamic Stability of Unsymmetric Two-Axle Railway Vehicles Possessing Perfect Steering', *Vehicle System Dynamics*, Vol.11, 1982, pp.89-106.
- [26] **A.H. Wickens**, 'Stability Optimization of Multi-Axle Railway Vehicles Possessing Perfect Steering', *ASME, J.of Dynamic Systems, Measurement, and Control*, Vol.110, 1988, pp.1-7.
- [27] **A.H. Wickens**, 'Railway Vehicles with Generic Bogie Capable of Perfect Steering', accepted by *Vehicle system Dynamics*.
- [28] **A.H. Wickens**, 'Static and Dynamic Instabilities of Bogie Railway Vehicles with Linkage Steered Wheelsets', accepted by *Vehicle System Dynamics*.
- [29] **R.M. Goodall & W. Kortum**, 'Active Controls in Ground Transportation - A review of the State-of-Art and Future Potential', *Vehicle System Dynamics*, Vol.12, 1983, pp.225-257.
- [30] **J.K. Hedrick & D.N. Wormley**, 'Active Suspensions for Ground Transport Vehicles - A State of the Art Review', In: *Mechaninc of transportation Suspension Systems*, Eds. B Paul et al., ASME AMD-Vol.15, 1975, pp.21-40.
- [31] **M. Panzer**, 'The Theory and Synthesis of Active Suspension Systems', Doctoral Thesis, Polytechnic Institute of Brooklyn, 1960.

- [32] **S.Rakheja, H. Su & T.S. Sankar**, 'Analysis of a Passive Sequential Hydraulic Damper for Vehicle Suspension', *Vehicle System Dynamics*, Vol.19, 1990, pp.289-312.
- [33] **Ye Lin & H.P. Willumeit**, 'The Dynamics of the Vibrator-Controlled Adaptive Damper and Its Potentials in Vibration Isolation', *Vehicle System Dynamics*, Vol.20, 1991, pp.353-369.
- [34] **A.G. Thompson & B.R. Davis**, 'Optimal Active Suspension design Using a Frequency-Shaping PID Filter', *Vehicle System Dynamics*, Vol.21, 1992, pp.19-37.
- [35] **A.G. Thompson**, 'Optimal and Suboptimal Active Suspensions for Road Vehicles', *Vehicle System Dynamics*, Vol.13, 1984, pp.61-72.
- [36] **D.A. Wilson et al**, 'The Application of Linear Optimal Control Theory to the Design of Active Automotive Suspensions', *Vehicle System Dynamics*, Vol.15, 1986, pp.105-118.
- [37] **M.M. Elmadany**, 'Stochastic Optimal Control of Highway Tractors with Active Suspensions', *Vehicle System Dynamics*, Vol.17, 1988, pp.193-210.
- [38] **S. Roukieh & A Titli**, 'On the Model-based Design of Semi-active and Active Suspension for Private Cars', *C389/289 IMechE*, 925105, 1992, pp.305-318.
- [39] **E.K. Bender**, 'Optimum Linear Preview Control with Application to Vehicle Suspension', *ASME Journal of Basic Engineering*, 1968, pp.213-221.
- [40] **M. Tomizuka**, 'Optimum Linear Preview Control with Application to Vehicle Suspension - Revisited', *ASME J.of Dynamic Systems, Measurement, and Control*, Vol.98, 1976, pp.309-315.
- [41] **R.G.M. Huisman et al**, 'Preview Estimation and Control for (Semi-) Active Suspensions', *Vehicle System Dynamics*, Vol.22, 1993, pp.335-346.

- [42] **A. Moran and M. Nagai**, 'Optimal Preview Control of Rear Suspension Using Nonlinear Neural Networks', *Vehicle System Dynamics*, Vol.22, 1993, pp.321-334.
- [43] **R.S. Sharp & D.A. Crolla**, 'Road Vehicle Suspension System Design -a Review', *Vehicle System Dynamics*, Vol.16,1987, pp.167-192.
- [44] **R.L. Jeffcoat & D.N. Wormley**, 'Improvement of Rail vehicle Lateral Dynamics, Performance Through Active Control', *Vehicle System Dynamics*, Vol.4, 1975, pp.169-172.
- [45] **P.K. Sinna, etc.**, 'Rail Passenger Vehicle Lateral Dynamic Performance Improvement Through Active Control', *ASME J. of Dynamic Systems, Measurement, and Control*, Vol.100, 1978, pp.270-283.
- [46] **J.K. Hedrick**, 'Railway Vehicle Active Suspensions', *Vehicle System Dynamics*, Vol.10, 1981, pp.267-283.
- [47] **G.W. Ceiniker & J.K. Hedrick**, 'Rail Vehicle Active Suspensions for Lateral Ride and Stability Improvement', *ASME J. of Dynamic Systems, Measurement, and Control*, Vol.104, 1982, pp.100-106.
- [48] **F.T. Buzan & J.K. Hedrick**, 'Lateral Active Pneumatic Suspensions for Rail Vehicle Ride Control', *Processing of the 1983 American control Conference*, 1983, pp.263-269.
- [49] **D. Cho & J.K. Hedrick**, 'Pneumatic Actuators for Vehicle Active Suspension Applications', *ASME J. of Dynamic Systems, Measurement, and Control*, Vol.107, 1985, pp.67-72.
- [50] **R.M. Goodall etc.**, 'Railway Vehicle Active Suspensions in Theory and Practice', *7th IAVSD-IUTAM Symposium*, 1981, pp.301-316.
- [51] **M.G. Pollard**, 'Passenger Comfort - The Role of active Suspensions', *Proc. Instn Mech Engrs*, Vol.198D, No.11, 1984, pp.161-175.

- [52] **R.A. Williams**, 'Active Suspensions Classical or Optimal', *9th IAVSD Symposium*, 1985, pp.607-620.
- [53] **A. Nishio et al**, 'High Speed Tilting Vehicles Controlled by Airspring', *Sumitomo Metals Research*, Vol24, No.1, Jan.1972, pp.71-78.
- [54] **U. Kayserling**, 'Power Bogies of the DB 200km/h ET405 Incorporating Body-tilt through the Secondary Air Suspension', *Rail Eng. Int.*, Vol.4, No.9, 1974, pp.414-418.
- [55] **A. Toran**, 'Tilting Train: A Practical Application of the Principle of Natural Pendulation to the Talgo System', Paper given at *Railway Dynamics Symposium*, Asociaion de Investigacion dek Transporte, May 1977.
- [56] **J. Gonzales**, 'Passengers will Sample Tilting Train this Spring', *Railway Gazette Int.*, Vol.133, No.2, 1977, pp.56-59
- [57] **D. Boocock & M. Newman**, 'The Advanced Passenger Train', Presented at *Railway Division of IMechE*, London, 1976.
- [58] **J.J. Mashall & D. Helpenny**, 'Tilt Technology', Presented at *Railway Division of IMechE*, London, 1977.
- [59] **R.M. Goodall**, 'Active Railway Suspensions - Potential and Applications', *Proc. IMech Seminar No.S181 on Vehicle/Track Interface Dynamics*, London, 1994.
- [60] **A.H. Wickens and R.M. Goodall**, 'The Mechtronic Bogie', *9th International Conference on Systems Engineering*, 1992, pp.413-419.
- [61] **A. J. Powell and A.H. Wickens**, 'Active Guidance of Railway Vehicle Using Traction Motor Torque Control', persented at *14th IAVSD*, Michigan, Aug. 1995.

- [62] **Y. Suda**, 'High Speed Stability and Curving Performance of Longitudinally Unsymmetric Trucks with Semi-Active Control', *Vehicle System Dynamics*, Vol.23, 1994, pp.29-52.
- [63] **D.H. Allen**, 'Active Bumpstop Hold-off Device', RailTech 1994, The Railway Technology Event, Seminar 5, *Bogie, Suspension and Transmissions I Demand Versus Technology*, 1994.
- [64] **F.W. Carter**, 'On the Stability of Running of Locomotive', *Proc. R. Soc.*, 1928, Ser.A, Vol.121, pp.585-611.
- [65] **A.D. De Pater**, 'Optimal Design of Running Gears', *Vehicle System Dynamics*, Vol.18, 1989, pp.243-300.
- [66] **G. Yang**, 'Dynamic Analysis of Railway Wheelsets and Complete Vehicle Systems', Doctoral Thesis of Delft University of Technology, 1993, ISBN 90 370 0080 0
- [67] **T. Matsudaira**, 'Hunting Problem of High-Speed Railway Vehicles with Special Reference to Bogie Design for the New Tokaido Line', *Proc Instn Mech Engrs*, Vol.180, part 3F, 1965-1966, pp.58-66.
- [68] **B.L. King**, 'The measurement of the Mode of Hunting of a Coach Fitted with Standard Double-bolster Bogie', *British Railways report E439*, 1963.
- [69] **R.A. Pooley**, 'Assessment of the Critical Speeds of Various Types of Four-Wheeled Vehicles', *British Railways Report E557*, 1965.
- [70] **A.O. Gilchrist et al**, 'The Rideing of Two Particular Designs of Four Wheeled Vehicle', *Proc. Instn. Mech. Engrs.*, Vol.180, 1965, pp.99-113.
- [71] **V.K. Garg et al**, 'Technical Documentation for the Locomotive Truck Hunting Model', *Research Report R-219*, Association of American Railroads, Chicago,1976.

- [72] **Y.H. Tse, V.K. Garg & A. Lo**, 'Validation of the Freight Car Hunting (Non-Linear/Linear) Model', *Research Report R-324*, Association of American Railroads, Chicago, May 1979.
- [73] **N.J. Darien**, 'Field Test for Truck Hunting Model Validation', *Research Report R-378*, Association of American Railroads, Chicago, Jan. 1980.
- [74] **S.M.A. Hussain et al**, 'Technical Documentation for the Freight Car Linear Hunting Model', *Research Report R-460*, Association of American Railroads, Chicago, Dec. 1980.
- [75] **D.E. Newland**, 'Steering Characteristics of Bogies', *Railway Gazette*, Vol.124, 1968, pp.745-750.
- [76] **D. Boocock**, 'Steady-State Motion of Railway Vehicles on Curved Track', *J., Mech. Engng. Sci.*, Vol.11(6), 1969, pp.556-566.
- [77] **M.L. Nagurka et al**, 'Computational Methods for Rail Vehicle Steady-State Curving Analysis', *Computation Methods in Ground Transportation Vehicles*, AMD-Vol.50, ASME/WAM, Nov,1982.
- [78] **J.A. Elkins & R.J. Gostling**, 'A General Quasi-Static Curving Theory for Railway Vehicles', *5th IAVSD Symposium*, 1978, pp.388-406.
- [79] **J.K. Hedrick et al**, 'Freight Car Dynamic Curving Model', *Technical Documentation*, Vol.1, Research Report R-557, prepared for the Association of American Railroads, Chicago, by the Mech. Eng. Dept., M.I.T., July, 1983.
- [80] **J.N. Siddall et al**, 'On the effect of Track Irregularities on the Dynamic Response of Railway Vehicle', *ASME paper*, 73-WA/RT-1, Nov.1973.
- [81] **R.E. Rinehart**, 'Locomotive Response to Random Track Surface Irregularities', *ASME paper*, 78-WA/RT-12, Dec.1978.
- [82] **R.A. Clark et al**, 'Prediction of the Dynamic Response of Vehicles to Lateral Track Irregularities', *7th IAVSD Symposium*, 1981, pp.535-548.

- [83] **A. Hamid and T.L. Yang,** 'Analytical Descriptions of Track Geometry Variations', ENSCO Transportation Technology Engineering Division, Springfield, Virginia, Oct. 1981.
- [84] **A.H. Wickens & A.O. Gilchris,** 'Railway Vehicle Dynamics - The Emergence of a Practical Theory', Council of Engineering Institutions *MacRobert Award Lecture*, 1977.
- [85] 'Equations of Motion of A Railway Vehicle', *ORE Question C 116*, 1974.
- [86] **A.H. Wickens,** 'Steering and Dynamic Stability of Railway Vehicles', *Vehicle System Dynamics*, Vol.5, 1975/1976, pp.15-46.
- [87] **A.H. Wickens,** 'Steering and Stability of Unsymmetric Articulated Railway Vehicles', ASME, *J. of Dynamic Systems, Measurement and Control*, Vol.101, 1979, pp.256-262.
- [88] **J.K. Hedrick et al,** 'Performance Limits of rail Passenger Vehicles: Evaluation and Optimization', *Report DOT-RSPA-DPB-50-79-32*, U.S. Department of Transportation, Washington, D.C., Dec. 1979.
- [89] **J.K. Hedrick et al,** 'Performance Limits of rail Passenger Vehicles: Conventional, Radial and Innovative Trucks', *Report DOT-RSPA-DPB-50-81-28*, U.S. Department of Transportation, Washington, D.C., Dec. 1979.
- [90] VAMPIRE. Descriptive Brochure, British Rail Research, 1989.
- [91] **Oskar Wallrapp & Clause Fuhrer,** 'MEDYNA - An Interactive Analysis and Design Program for Geometrically Linear and Flexible Multibody Systems', *Multibody System Handbook*, Springer-Verlag Berlin, 1990, pp.203-223.
- [92] **R.V. Dukkipati & J.R. Amyot,** 'Computer-Aided Simulation in Railway Dynamics', Marcel Dekker Inc, 1988, ISBN 0 8247 7787 5.
- [93] **R.C. Hibbeler,** 'Engineering Mechanics - Dynamics', Third edition, Macmillan Publishing Co., Inc, 1974, ISBN 0 02 354250 0.

- [94] **G.H Cope**, 'British Railway Track-Design, Construction and Maintenance', Sixth Edition, 1993, Echo Press, Loughbo. Leics. England, ISBN 0 903489 03 1.
- [95] **D.E. Newland**, 'An Introduction to Random Vibrations and Spectral Analysis', Longman, London, 1975, ISBN 0 582 463335 1.
- [96] **W.A. Gardner**, 'Introduction to Random Processes - with Applications to Signals and Systems', Second Edition, Mcgraw-Hill Publishing Company, 1989, ISBN 0 07 022855 8.
- [97] **J.B. Roberts & P.D. Spanos**, 'Random Vibration and Statistical Linearization', John Wiley & Sons, 1990, ISBN 0 471 91699 4.
- [98] **P.F. Cunniff**, 'Environmental Noise Pollution', John Wiley & Sons, 1977, ISBN 0 471 18943 X.
- [99] **Leo L. Beranek**, 'Noise and Vibration Control', McGraw-Hill Inc. Washington DC, Revised Edition, 1988, ISBN 0 9622072 0 9.
- [100] **J.B. Scarborough**, 'Numerical Mathematical Analysis', fifth edition, The Johns Hopkins Press, 1962.
- [101] **R.E. Hohn**, 'Elementary Matrix Algebra', third edition, The Macmillan Company, New York, 1973.
- [102] **NAG FORTRAN Library Manual Mark 16**, The Numerical Algorithms Group Limited, 1993, ISBN 1 85206 091 3
- [103] **W. Li**, 'Some Results of BR's Computer Model for Predicting Wheel Wear', *Technical Report*, VDYN-174, British Railway Technical Centre, Feb. 1990.
- [104] **B. Porter**, 'Stability Criteria for Linear Dynamical Systems', Oliver & Boyd Ltd, 1967.

- [105] **S. Barnett and C. Storey**, 'Matrix Methods in Stability Theory', Thomas Nelson and Sons Ltd, 1970, ISBN 17 761617 2
- [106] Draft International Standard ISO/DIS 2631/1-1, 1994.
- [107] **B. Bhushan & B. Gupta**, 'Tribology Handbook', McGraw-Mill Inc, New York, ISBN 0 07 005249 2, 1991.
- [108] **R Brunell**, 'Hydraulic & Pneumatic Cylinders', Trade & Technical Press Ltd, Morden, Surrey, England, ISBN 85461 049 9.
- [109] 'Hydraulics Saves Weight and Space', *Railway Gazette International*, Aug.1993, pp.571.
- [110] Patent News 466.449 - GEC Alsthom Ltd, *Railway Gazette International*, Dec.1992, pp.863.

Appendix A

The Dynamic Behaviour of A Body-Steered Bogie Vehicle with the Capability of Perfect Steering in the Lateral Plane

W. LI*

SUMMARY

The configuration of a body-steered bogie vehicle without primary nor secondary yaw stiffnesses has been proposed. Its outboard wheelsets are directly connected to the carbody and there is a linkage between its inboard and outboard wheelsets. The conditions for the vehicle to possess the capability of perfect steering has been set up, which only depend on the geometric parameters of the steering linkage. There is no any bending stiffness in the vehicle if the steering linkage satisfies these conditions. The stability, curving and ride performance of this vehicle in the lateral plane have been investigated. Two instabilities, namely steering instability (low speed and dynamic) and conventional instability, have been identified, and steering instability has been theoretically analysed. The results show that this vehicle can partly decouple the conflict between the stability and curving.

1. INTRODUCTION

Generally, the suspensions of a railway vehicle should provide strong enough constraints to the wheelsets in order to prevent them from being unstable. On the other hand, the wheelsets ought to be as free as possible so that they can take more radial alignment on curves. The former results in hard suspensions while the latter requires soft suspensions. This fundamental trade-off between stability in the lateral plane and steering ability on curves in railway bogie vehicles has been well studied[2-3]. It is well known that this basic conflict between stability and curving cannot be solved very well in conventional bogie vehicles.

To moderate the conflict between stability and curving, several configurations of body-steered bogie vehicles have been proposed [3-11] and some have been applied in practice. A body-steered bogie vehicle has a linkage between its carbody and wheelsets, and the presence of force on the axles is a function of the relative displacements between the carbody and wheelsets such that the relative displacements between the carbody and wheelsets can assist the wheelsets to take more radial alignment on curves.

* Department of Mechanical Engineering, Loughborough University of Technology

DYNAMICS OF A STEERING BOGIE VEHICLE

Wickens[1] has proved that it is possible to design a bogie vehicle with the capability of perfect steering which has non-zero critical speed if it has at least three wheelsets. He defined the concept of perfect steering as zero creep between wheelsets and rails when the vehicle moves steadily on a uniform curve with zero cant deficiency, and then the wheelsets act as unconstrained wheelsets when perfect steering is achieved.

If the primary and secondary yaw stiffnesses are removed from a conventional bogie vehicle with four wheelsets, the vehicle's bending stiffnesses disappear and the wheelsets can negotiate a uniform curve with zero cant deficiency by taking their radial positions. In this case, there is no creep between wheelset and track, and perfect steering is therefore realised. Wickens[1] has proved, however, that the critical speed of this vehicle is zero and another two independent stiffnesses for each bogie at least are required to stabilise the vehicle, and these two stiffnesses should not contribute any bending stiffness to the vehicles if perfect steering is required.

This paper demonstrates a body-steered bogie vehicle that does not possess the primary nor secondary yaw stiffnesses, and another two independent stiffnesses are added to each bogie by the steering linkage between its carbody and wheelsets and between its outboard and inboard wheelsets. The condition for the vehicle to possess perfect steering will be derived, and its steering capability, stability and ride performance in the lateral plane are also going to be investigated.

NOTATION

a_0	half gauge (0.72m)	a_i	geometric parameters of vehicle in the horizontal plane
a	half wheelset base (1.25m)	\mathbf{a}	compatibility matrix
\mathbf{A}	disturbance gain matrix	c_{ij}	viscous damping coefficient
\mathbf{C}	viscous damping matrix	\mathbf{E}	elastic matrix
f_{ij}	creepage coefficient	h_i	geometric parameters of vehicle in the vertical plane
F_E	elastic force caused by curvature	\mathbf{G}	creepage stiffness matrix
k_{ij}	stiffness	l_0	length between vehicle body weight centre and bogie pivot (8.75m)
\mathbf{M}	inertia matrix	\mathbf{N}	creepage damping matrix
\mathbf{q}	general coordinate vector	\mathbf{Q}	force vector
r_0	wheel radius (0.45m)	R	curve radius
v_0	vehicle forward speed	x	longitudinal coordinate or displacement

DYNAMICS OF A STEERING BOGIE VEHICLE

<p>y track irregularity vector</p> <p>z vertical coordinate or displacement</p> <p>ϕ_d curve cant deficiency</p> <p>λ_e wheelset equivalent conicity</p> <p>ψ yaw angle</p>	<p>y lateral coordinate or displacement</p> <p>ϕ roll angle</p> <p>λ wheelset conicity</p> <p>λ_n necessary conicity to avoid flange contact</p>
--	---

Subscript

<p>b body</p> <p>s secondary</p> <p>w wheelset</p> <p>ψ yaw freedom</p>	<p>p primary</p> <p>T bogie</p> <p>y lateral freedom</p> <p>ϕ roll freedom</p>
--	---

2. THE CONFIGURATION AND ITS CURVING MECHANISM

2.1 Motion Equations

If a railway bogie vehicle is considered as a system of rigid bodies possessing n degrees of freedom connected by m massless elastic elements and m massless viscous dampers, the dynamic equation of the vehicle can be defined as:

$$M\ddot{\mathbf{q}} + (\mathbf{G} + \mathbf{C})\dot{\mathbf{q}} + (\mathbf{N} + \mathbf{E})\mathbf{q} = \mathbf{Q} \quad (1)$$

Where, \mathbf{G} and \mathbf{N} come from the creepage and can be easily found based on the dynamic equation of an unconstrained wheelset[12]; \mathbf{E} and \mathbf{C} are called the elastic matrix and the viscous damping matrix respectively; \mathbf{Q} is the force vector and \mathbf{q} is the general coordinate vector (displacement vector).

For a fore-and-aft symmetric bogie vehicle with four wheelset, the vehicle can be simplified as a system with seventeen degrees of freedom in the lateral plane: two for each wheelset (lateral shift y_w and yaw angle ψ_w), three for each bogie frame (lateral shift y_T , yaw angle ψ_T and roll angle ϕ_T) and three for its carbody (lateral shift y_b , yaw angle ψ_b and roll angle ϕ_b), and thus the general coordinate vector \mathbf{q} is:

$$\mathbf{q} = \{ y_{w1} \ \psi_{w1} \ y_{w2} \ \psi_{w2} \ y_{w3} \ \psi_{w3} \ y_{w4} \ \psi_{w4} \ | \ y_{TL} \ \psi_{TL} \ \phi_{TL} \ y_{TR} \ \psi_{TR} \ \phi_{TR} \ | \ y_b \ \psi_b \ \phi_b \} \quad (2)$$

Applying the compatibility matrix method suggested by Wickens[1], the elastic matrix \mathbf{E} and the viscous damping matrix \mathbf{C} of the system are given by:

DYNAMICS OF A STEERING BOGIE VEHICLE

$$\mathbf{E} = \mathbf{a}^T [\mathbf{k}] \mathbf{a} \quad \mathbf{C} = \mathbf{a}^T [\mathbf{c}] \mathbf{a} \quad (3)$$

where, \mathbf{a} is called the $m \times n$ compatibility matrix and is governed by vehicle configuration, and $[\mathbf{k}]$ (or $[\mathbf{c}]$) is an $m \times m$ diagonal matrix of stiffness (damping) corresponding to the strains (strain rate) represented by the i 'th row of \mathbf{a} .

For steady state, Eq.(1) is simplified as:

$$(\mathbf{N} + \mathbf{E}) \mathbf{q} = \mathbf{F}_{\text{creep}} + \mathbf{F}_{\text{E}} + \mathbf{F}_{\text{cant}} \quad (4)$$

where, $\mathbf{F}_{\text{creep}}$ is the creepage force vector caused by curvature, \mathbf{F}_{E} is the system elastic force vector caused by curvature and \mathbf{F}_{cant} is the force caused by cant deficiency. It can be proved that $\mathbf{F}_{\text{creep}}$ is defined by:

$$\mathbf{F}_{\text{creep}} = \begin{Bmatrix} 0 & -2a_0^2 f_{11}/R & 0 & -2a_0^2 f_{11}/R & 0 & -2a_0^2 f_{11}/R & 0 & -2a_0^2 f_{11}/R \\ 0 & 0 & 0 & 0 & 0 & 0 & 0 & 0 \end{Bmatrix} \quad (5)$$

and \mathbf{F}_{E} is given by:

$$\mathbf{F}_{\text{E}} = - \sum_{i=1}^m k_i \{a_{in}\}^T \{a_{in}\} \{q_i\} \quad (6)$$

and \mathbf{F}_{cant} is:

$$\mathbf{F}_{\text{cant}} = \begin{Bmatrix} W_w \phi_d & 0 & W_w \phi_d & 0 & W_w \phi_d & 0 & W_T \phi_d & 0 & W_T \phi_d & 0 & 0 \\ & & & & & & W_T \phi_d & 0 & 0 & W_T \phi_d & 0 & 0 \end{Bmatrix} \quad (7)$$

Since $\frac{dq}{dt} = \frac{dq}{dx} \frac{dx}{dt} = v_0 \frac{dq}{dx} = v_0 q'$, for kinematic state ($v_0 \rightarrow 0$), Eq.(1) becomes:

$$\mathbf{G} \mathbf{q}' + (\mathbf{N} + \mathbf{E}) \mathbf{q} = \mathbf{F}_{\text{cant}} + \mathbf{F}_{\text{creep}} + \mathbf{F}_{\text{E}} \quad (8)$$

If the track irregularities are taken into account in a straight line, Eq.(1) becomes:

$$\mathbf{M} \ddot{\mathbf{q}} + (\mathbf{G} + \mathbf{C}) \dot{\mathbf{q}} + (\mathbf{N} + \mathbf{E}) \mathbf{q} = \mathbf{A} \mathbf{y} \quad (9)$$

The definition of the disturbance coefficient matrix \mathbf{A} and the disturbance vector \mathbf{y} can be found in reference [17] if the cross-level and alignment track irregularities are only

DYNAMICS OF A STEERING BOGIE VEHICLE

considered as the system disturbances. The parameters for Class 6 Track in American Railroad Standard [18] are used to define the track irregularities in the simulation.

2.2 Configuration

A body-steered bogie vehicle model without the primary and secondary yaw stiffnesses, as shown in Fig.1, is set up in the research. Two independent stiffnesses are added in the system by a spring with stiffness k_7 between the outboard wheelsets and carbody and by a spring with stiffness k_{11} between the inboard and outboard wheelsets. For this configuration, any of the relative displacements (lateral, yaw and roll) between its carbody and outboard wheelsets will cause the deformation of the spring k_7 . This deformation can force the outboard wheelset to have a yaw angle, and thus any of these relative displacements is one of the steering inputs.

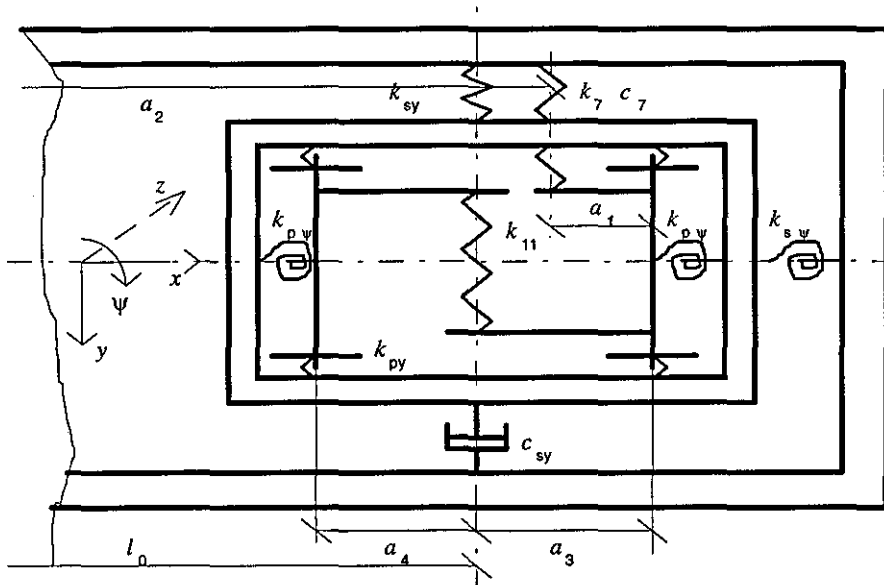


Figure 1. The Configuration of A Body-Steered Bogie Vehicle

If the diagonal elements of $[k]$ are arranged as:

$$\{k_{ii}\} = \{k_{py} \quad k_{p\phi} \quad k_{py} \quad k_{p\phi} \quad k_{py} \quad k_{p\phi} \quad k_{py} \quad k_{p\phi} \mid k_{11} \quad k_{11} \quad k_7 \quad k_7 \mid k_{sy} \quad k_{s\phi} \quad k_{sy} \quad k_{s\phi}\} \quad (10)$$

DYNAMICS OF A STEERING BOGIE VEHICLE

the compatibility matrix \mathbf{a} is listed in Table A and the elastic force F_E in Table B.

Since the sufficient condition for a railway vehicle being capable of perfect steering is $F_E = 0$, the geometric parameter a_1 of the linkage between the carbody and outboard wheelsets must satisfy:

$$a_1 = al_0 / (a + l_0) \quad (11)$$

and the geometric parameters a_2 and a_3 of the linkage between the outboard and inboard wheelsets should have the relationship:

$$a_3 = a_4 \quad (12)$$

and thus $a_1 = 1.09375\text{m}$ and $a_3 = a_4 = 1.25\text{m}$ can be obtained if $a = 1.25\text{m}$ and $l_0 = 8.75\text{m}$, and $a_1 = 1.0938\text{m}$ are used in the simulation. Eq.(11) and Eq.(12) indicate that the condition for a railway bogie vehicle being capable of perfect steering is independent of the parameters associated with curves and is only governed by the geometric parameters of the vehicle.

2.3 Steering Ability

In steady state, the wheelset attack angles are zero and perfect steering is achieved when the steering linkage satisfies the condition Eq.(11) & Eq.(12) and when cant deficiency is zero, and then the wheelsets act as unconstrained wheelsets and move on their pure rolling lines. The distance between the pure rolling line of unconstrained wheelset and track central line can be derived from the motion equations of an unconstrained wheelset on steady state and is given by:

$$y = -\frac{a_0 r_0}{R \lambda_e} \quad (13)$$

This distance becomes shorter when there is an inboard cant deficiency, and becomes longer when there is an outboard cant deficiency.

If this distance is equal to or greater than the flange clearance, flange contact occurs, which causes two major problems: firstly, it forces the wheelsets to leave their pure rolling lines and results in creep so that perfect steering cannot be achieved, and

DYNAMICS OF A STEERING BOGIE VEHICLE

secondly, it increases the wear between rails and wheels and increases the tendency of derailment. A reduction in the potential of flange contact is therefore highly desirable.

From Eq.(13), the equivalent conicity λ_e must be equal to or greater than 0.324 to avoid flange contact if the flange clearance is 5mm and the curve radius $R = 200m$. The wheelset lateral displacements of the body-steered bogie vehicle in steady state are illustrated in Fig.2 when the curve radius $R = 200m$. The minimum equivalent conicity in avoiding flange contact is defined as the necessary conicity λ_n . In Fig.2a, the cant deficiency is equal to zero, and the necessary conicity λ_n is equal to the value theoretically predicted by Eq.(13) if taking the calculation accuracy into account. An inboard cant deficiency causes wheelsets to have a positive lateral shift so that the absolute lateral displacements of wheelsets reduce while an outboard cant deficiency forces wheelsets to have a negative lateral displacement so that the absolute lateral displacements increase. The necessary conicity λ_n therefore reduces when there is an inboard cant deficiency while it increases when there is an outboard deficiency, as illustrated in Fig.2c&d. Comparing with the necessary conicity λ_n when $\phi_d = 0$, and the alteration in the necessary conicity λ_n is slight when $\phi_d \neq 0$, which indicates that the vehicle has a very good ability in accommodating cant deficiency.

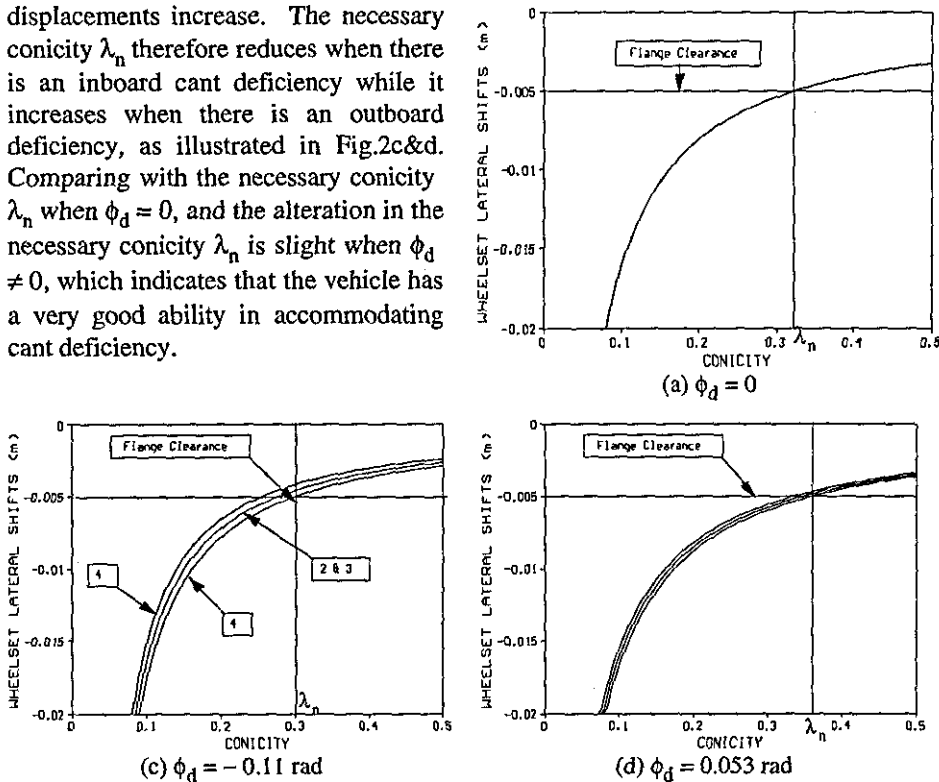


Figure 2. The wheelset lateral displacements versus conicity, steady state, No.1--4, wheelset sequence, $R = 200m$.

DYNAMICS OF A STEERING BOGIE VEHICLE

When there is an error in the geometric parameters of the steering linkage, the steering linkage does not satisfy the conditions Eq.(11) and Eq.(12), and will produce bending stiffness and thus cause attack angles and creep. For example, when $a_1 = 1\text{m}$, the lateral shifts and resultant creepages of the wheelsets are displayed in Fig.3. The results show that its necessary conicity λ_n is not greatly affected by the geometric error in the steering linkage although this error causes creep between the wheelsets and tracks.

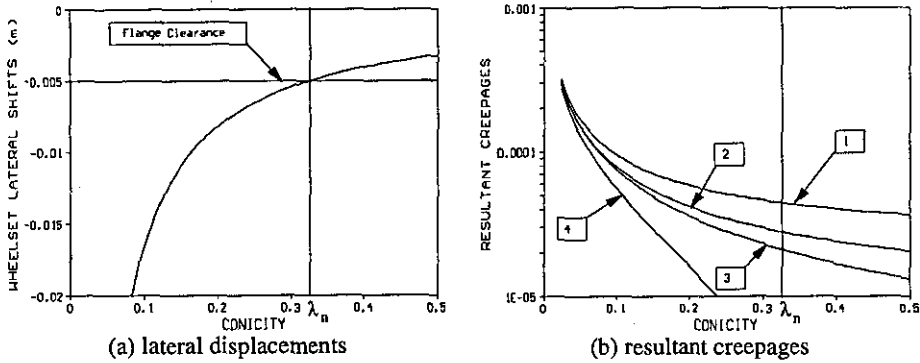


Figure 3. The lateral displacements and resultant creepages versus conicity when $a_1 = 1\text{m}$, steady state, $R = 200\text{m}$ and $\phi_d = 0$.

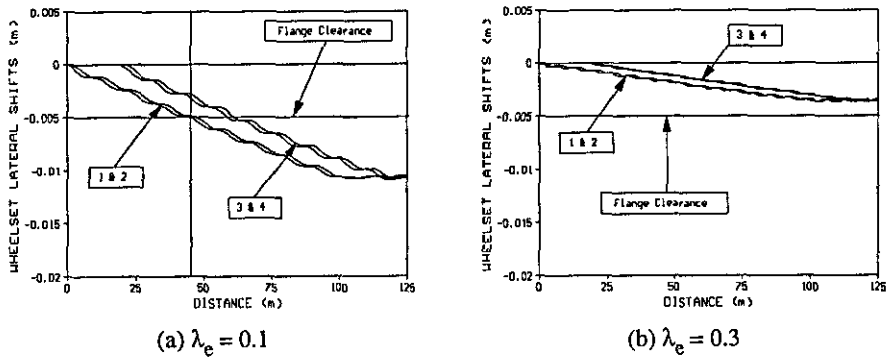


Figure 4. The wheelset lateral displacements on the transition

On transitions, the curvature at each point is not a constant, the curvature difference along transitions will cause the elastic force F_E even if the steering linkage satisfies the

DYNAMICS OF A STEERING BOGIE VEHICLE

conditions Eq.(11) & Eq.(12). A cubic parabola is used as the transition connected to a uniform curve with $R = 305\text{m}$. The wheelset lateral displacements of the vehicle capable of perfect steering are shown in Fig.4 when $\lambda_e = 0.1$ and $\lambda_e = 0.3$ and the cant deficiency is neglected. For $R = 305\text{m}$, the distance between the pure rolling line of unconstrained wheelset and the track central line is 10.6mm when $\lambda_e = 0.1$ and is 3.54mm when $\lambda_e = 0.3$. The wheelset lateral displacements in Fig.4 are smaller than those values along the transition and finally converge to those values on the uniform curve. One can see from the results that the bogie vehicle capable of perfect steering have a great advantage in reducing the potential of flange contact. The reason for this is that the steering linkage is designed to reduce the forces produced by elastic deformation due to curvature and this function of the steering linkage is still effective even on transitions. For example, the elastic moment $M_{\psi w1}$ acting on the outboard wheelset of the leading bogie due to variation of curvature on transition can be found as:

$$M_{\psi w1} = a_2 k_7 (a_0 \psi_{bTL} - a_2 \psi_{bw1}) + a_3^2 k_{11} (2\psi_{bTL} - \psi_{bw1} - \psi_{bw2})$$

where, ψ_{bTL} is the relative yaw between the carbody and the leading bogie due to curvature; ψ_{bw1} is the relative yaw between the carbody and the outboard wheelset due to curvature; and ψ_{bw2} is the relative yaw between the carbody and the inboard wheelset due to curvature. Usually, the second term $a_3^2 k_{11} (2\psi_{bTL} - \psi_{bw1} - \psi_{bw2})$ of the equation above is much smaller than the first term and can be ignored. For a conventional bogie vehicle, the elastic moment $M_{\psi w1}$ acting on the outboard wheelset of the leading bogie due to variation of curvature on transition is:

$$M_{\psi w1} = k_{pb} (\psi_{bTL} - \psi_{bw1})$$

where, k_{pb} is the bending stiffness between wheelsets. Since there are:

$$a_0 > a_2 \quad \text{and} \quad \psi_{bTL} < \psi_{bw1}$$

we have

$$|\psi_{bTL} - \psi_{bw1}| > |a_0 \psi_{bTL} - a_2 \psi_{bw1}|$$

The elastic moment $M_{\psi w1}$ of this body-steered bogie vehicle due to variation of curvature on transition is smaller than that of a conventional bogie vehicle, and thus the

DYNAMICS OF A STEERING BOGIE VEHICLE

displacements of this body-steered bogie vehicle due to variation of curvature on transition are reduced.

3. INSTABILITY

3.1 Instability Modes

The critical speeds of the vehicle capable of perfect steering are demonstrated in Fig.5 as a function of wheelset conicity. There are three modes of instability in Fig.5: the critical speed is very low and the instability is defined as low speed instability when the wheelset conicity is very low; and then the critical speed goes up as the conicity rises and the instability here is called dynamic instability in low conicity; and finally the critical speed reduces as the conicity becomes higher and the instability here is called conventional instability. Both low speed instability and dynamic instability in low conicity are defined as steering instability, and conventional instability can be observed in conventional bogie vehicles.

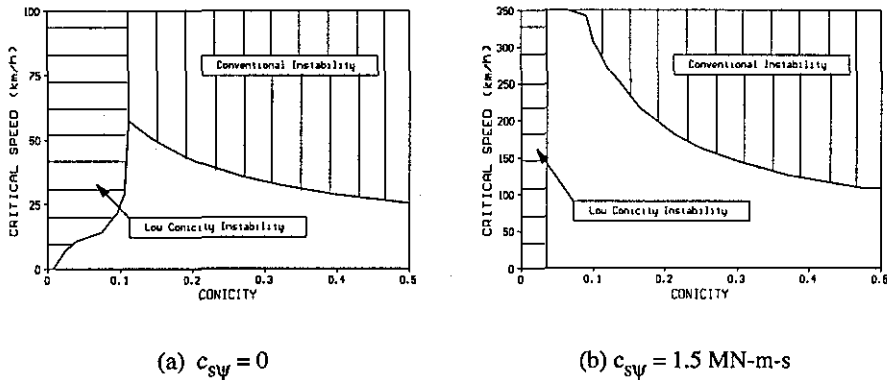


Figure 5. The critical speed versus λ of the vehicle capable of perfect steering

The eigenvalues of instability modes are illustrated in Fig.6. Since the frequencies of these instability modes are close to the kinematic frequency of unconstrained wheelset

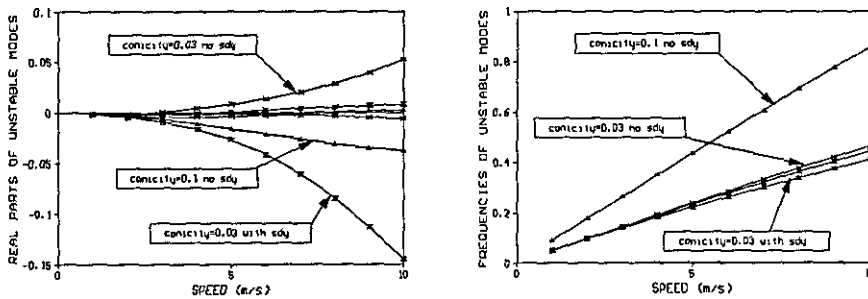
$$(2\pi f = v_0 \sqrt{\lambda_e / a_0 r_0}),$$

the unstable mode mainly associates with the wheelset motions.

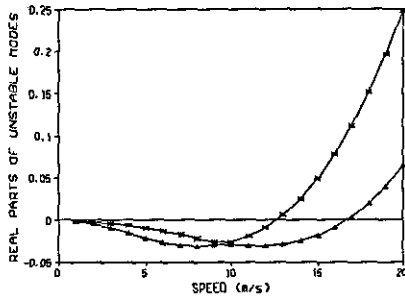
In steering instability, as shown in Fig.6a, only one real part of these eigenvalues becomes larger and finally becomes positive while another becomes smaller as the vehicle speed rises. This indicates that only one of the motions with this frequency is

DYNAMICS OF A STEERING BOGIE VEHICLE

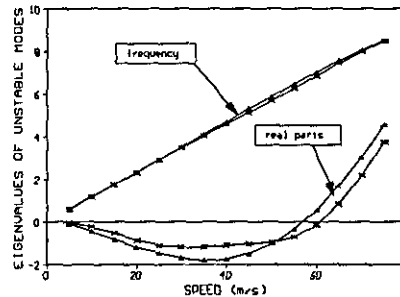
unstable in steering instability, which implies that steering instability only appears in one of the bogies. In conventional instability, as illustrated in Fig.6b&c, both real parts of the eigenvalues become positive as vehicle speed rises, which means that conventional instability occurs in both bogies. The fundamental difference between steering instability and conventional instability is thus that steering instability only occurs in one of the vehicle bogies while conventional instability occurs in both. Although both bogies are unstable in conventional instability, one of the bogies becomes unstable at a lower speed than the other, and this tendency becomes more obvious when there is no secondary yaw damping, as shown in Fig.6b. The unequal stability performance between the bogies of this vehicle comes from the asymmetric elasticity between the outboard and inboard wheelsets, which was studied by Wickens[19].



(a) steering instability, $s_{dy} = c_{s\psi}$



(b) conventional instability,
 $\lambda = 0.2, c_{s\psi} = 0$



(c) conventional instability,
 $\lambda = 0.2, c_{s\psi} = 1.5 \text{ MN-m-s}$

Figure 6, The eigenvalues of unstable modes (versus speed) of the vehicle capable of perfect steering

DYNAMICS OF A STEERING BOGIE VEHICLE

3.2 Theoretical Prediction of Steering Instability

A relatively simple physical explanation can be given for the steering unstable behaviour of body-steered bogie vehicles. The steering linkage will produce a steering angle in wheelsets, and there is not enough longitudinal creepage between wheel and rail in low conicity to restore the wheelsets back to the balance position, and the vehicle is therefore unstable. Bell and Hedrick[2] first theoretically proved the existence of steering instability when they investigated the kinematic stability of the bogie sub-system of a body-steered bogie vehicle. Smith, Anderson and Fortin[8][13] later gave the physical explanation of steering instability when they studied the bogie sub-system of another configuration of body-steered bogie vehicles. Recently, Wickens[14] used more a general bogie sub-system to identify this problem.

In their models, the wheelsets, bogie frame and carbody are connected by the steering linkages, and the bogie motions, especially yaw motion, interfere with the steering mechanism. Since vehicle speed is very low in low speed instability, the carbody can be considered as an inertia reference, and therefore a bogie sub-system is a suitable model allowing the analysis of steering instability in these body-steered bogie vehicles. In the configuration of Fig.1, the outboard wheelsets are directly connected with the carbody, and the bogie frame motions do not interfere with the steering mechanism. Moreover, another major difference between the configuration in Fig.1 and the body-steered bogie vehicles studied by other researchers is that all relative displacements between the carbody and the outboard wheelsets are the steering inputs in the former while only the relative yaw angles are the steering input in the latter ones. A bogie sub-system is therefore not an ideal model with which to study steering instability of this body-steered bogie vehicle.

For the configuration in Fig.1, the steering mechanism is produced by the relative motions between the carbody and outboard wheelsets. The steering mechanism mainly affects the motions of the outboard wheelsets if the carbody is considered as an inertia body when the vehicle speed is very low. Only the outboard wheelset is thus used as the model to investigate steering instability for the configuration in Fig.1, and other mass components of the vehicle are considered as inertia references. Under these assumptions, the dynamic equations of the outboard wheelset become:

$$\begin{aligned}
 m\ddot{y} + \frac{2f_{22}}{v_0}\dot{y} + (k_{py} + k_7 + k_{11})y - (2f_{22} + a_1k_7 + a_3k_{11})\psi &= 0 \\
 I\ddot{\psi} + \frac{2a^2f_{11}}{v_0}\dot{\psi} + (a_1^2k_7 + a_3^2k_{11})\psi + \left(\frac{2af_{11}\lambda}{r_0} - a_1k_7 - a_3k_{11}\right)y &= 0
 \end{aligned}
 \tag{14}$$

DYNAMICS OF A STEERING BOGIE VEHICLE

So, the characteristic equation of the system is:

$$p_4 s^4 + p_3 s^3 + p_2 s^2 + p_1 s + p_0 = 0 \quad (15)$$

where,

$$\begin{aligned} s &= d/dt & p_4 &= mI & p_3 &= 2(ma^2 f_{11} + If_{22}) \\ p_2 &= (mK_3 v_0^2 + IK_1 v_0^2 + 4a^2 f_{11} f_{22}) / v_0^2 \\ p_1 &= 2(a^2 f_{11} K_1 + 2f_{22} K_3) / v_0 \\ p_0 &= K_1 K_3 + \frac{2af_{11}\lambda}{r_0} (2f_{22} + K_2) - K_2 (2f_{22} + K_2) \\ K_1 &= k_{py} + k_7 + k_{11} & K_2 &= a_1 k_7 + a_3 k_{11} \\ K_3 &= a_1^2 k_7 + a_3^2 k_{11} \end{aligned} \quad (16)$$

Applying Routh's stability criterion, the necessary condition for the system to be stable is:

$$p_0 > 0 \quad p_1 > 0 \quad p_2 > 0 \quad p_3 > 0 \quad \text{if} \quad p_4 > 0 \quad (17)$$

So, from $p_0 > 0$, the following relationship can be set up:

$$\lambda > [K_2 (2f_{22} + K_2) - K_1 K_3] r_0 / [2af_{11} (2f_{22} + K_2)] \quad (18)$$

For conventional bogie vehicles, $K_1 = k_{py}$, $K_2 = 0$ and $K_3 = k_{p\psi}$ are true and therefore, the necessary condition Eq.(18) is satisfied if the conicity $\lambda > 0$ exists.

For this body-steered bogie vehicle, Eq.(18) becomes:

$$\lambda > \frac{[k_7 k_{11} (a_1 - a_3)^2 + 2f_{22} (a_1 k_7 + a_3 k_{11}) - k_{py} (a_1^2 k_7 + a_3^2 k_{11})] r_0}{2af_{11} (2f_{22} + a_1 k_7 + a_3 k_{11})} \quad (19)$$

The right hand side of Eq.(19) can be positive in some cases, which means that the vehicle can be unstable even for $\lambda > 0$ if some conditions are satisfied, and also the instability is divergent since Eq.(19) is derived from $p_0 > 0$. The same analysis can be applied to the outboard wheelset of the trailing bogie. It has been found that the right hand side of Eq.(19) for the outboard wheelset in the trailing bogie is negative, which

DYNAMICS OF A STEERING BOGIE VEHICLE

indicates that steering instability only appears in one of the bogies and depends on the vehicle's moving direction.

The first term of the numerator in the right side of Eq.(19) is governed by the stiffness of the steering linkage and the condition of perfect steering, and steering instability is thus promoted by a stiff steering linkage, whilst the sum of the last two terms depends on the lateral creepage f_{22} and the primary lateral stiffness k_{py} , which seems that the increment in the primary lateral stiffness and the reduction in lateral creepage can reduce the potential of steering instability. The effects of these parameters on steering instability will be further discussed at later points.

3.3 Influences of the suspensions and steering linkage parameters on the instabilities

Steering instability

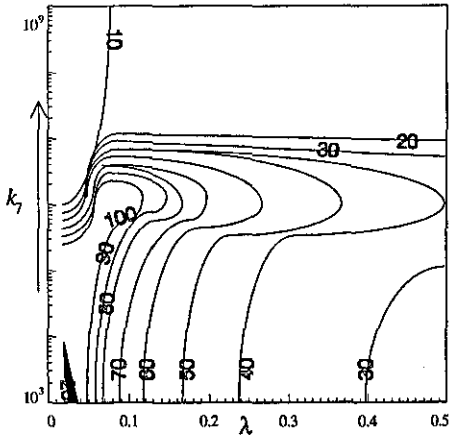
The results in Fig.7 show that the effective factors that influence steering instability are the stiffness k_7 , the damping c_7 , the stiffness k_{11} , the primary lateral stiffness k_{py} and the secondary yaw damping c_{sy} . The steering force produced in the steering linkage rises as k_7 and c_7 increase, and thus the steering instability becomes more serious as the steering linkage becomes stiff, as illustrated in Fig.7a&b. Furthermore, steering instability even appears in high conicity when the values of k_7 and c_7 become very high.

When k_{11} increases, the connection between the outboard wheelset and inboard wheelset is strengthened, and thus the steering mechanism needs to produce more force to steer the outboard wheelset. In other words, the steering effect from the steering linkage is reduced by the stiff connection between the outboard wheelset and inboard wheelset, and steering instability is therefore improved by employing hard k_{11} , as shown in Fig.7c.

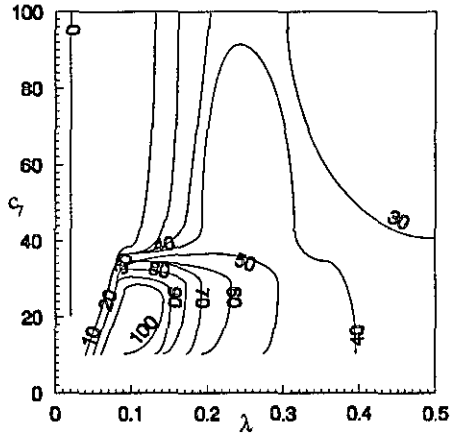
The influence of the primary stiffness k_{py} on steering instability is more complex than that of the steering linkage, as displayed in Fig.7d. Steering instability is improved as k_{py} increases if k_{py} is not very hard, whilst steering instability is promoted by the increment in k_{py} if k_{py} is hard. These facts can be explained as the following: the steering mechanism in the configuration of Fig.1 not only affects the outboard wheelset yaw motion, but also its lateral motion, such that a hard primary lateral stiffness strengthens the connection between the bogie frame and outboard wheelset, and that the steering linkage needs to produce more force to steer the outboard wheelset, and thus the tendency of steering instability is reduced as the primary lateral stiffness becomes harder; but, when k_{py} is hard enough, the bogie frame and wheelsets tend to become

DYNAMICS OF A STEERING BOGIE VEHICLE

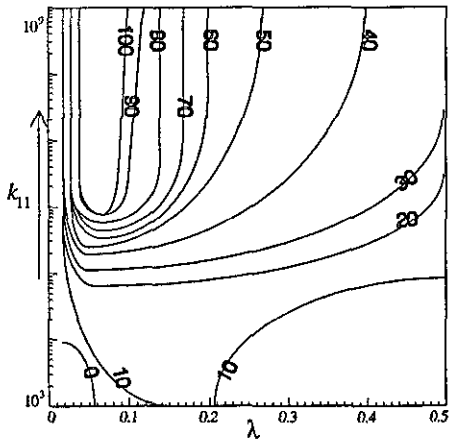
one mass, and steering instability can be promoted by further increasing the primary lateral stiffness k_{py} .



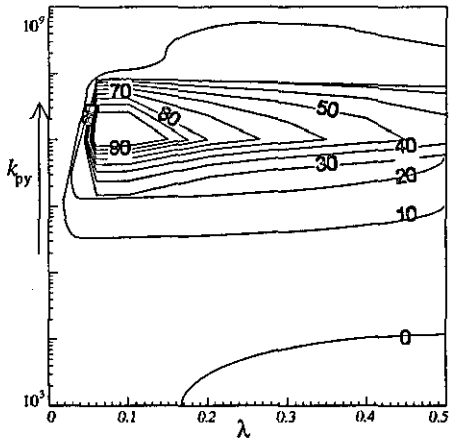
(a) critical speed contours versus k_7 (N/m) and conicity



(b) critical speed contours versus c_7 (kN-s/m) and conicity

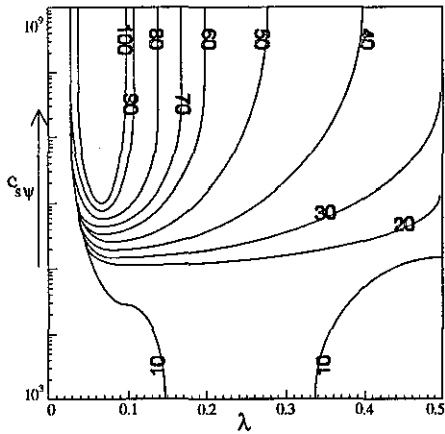


(c) critical speed contours versus k_{11} (N/m) and conicity

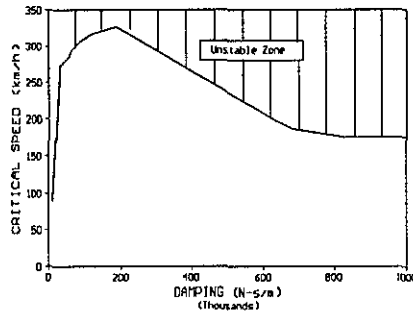


(d) critical speed contours versus k_{py} (N/m) and conicity

DYNAMICS OF A STEERING BOGIE VEHICLE



(e) critical speed contours versus c_{sy} (N-m-s) and conicity



(f) critical speed versus c_{sy} when $\lambda = 0.1$

Figure 7 The critical speed contours of the bogie vehicle capable of perfect steering

Low speed instability mode in steering instability is not greatly affected by secondary yaw damping because viscous damping is not active in low frequencies, but the critical speed in both dynamic mode of steering instability and conventional instability can be much increased by applying secondary yaw damping, as is illustrated in Fig.7c. Since there is neither primary nor secondary yaw stiffness, the yaw constraints of the inertia bodies are not strong enough to restrict them. The yaw damping can strengthen the yaw constraints and thus improve stability. Simulation has shown that the vehicle speed can also be increased if the primary yaw damping is applied instead of secondary yaw damping.

Conventional instability

The constraints of the inertia components can be strengthened by stiff springs and high dampings, and thus hard stiffnesses or high dampings can improve the conventional stability. When springs are already stiff enough or dampings are already high enough,

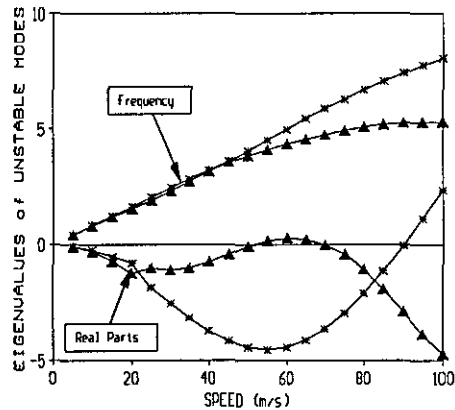


Figure 8, The eigenvalues of unstable modes $\lambda=0.1$ and $c_{sy} = 85 \text{ kN-s/m}$

DYNAMICS OF A STEERING BOGIE VEHICLE

however, this effect may be limited such that any further increments may not improve the stability any further, as shown in Fig.7c&e, because the system tends to become a single mass body as the springs and dampings increase in magnitude.

Since a bogie vehicle is a multi-body system, the motions of inertia bodies are coupled, and an increase in one parameter may decrease the effects of other parameters, and thus may promote other unstable modes. For example, the appearance of the unstable modes in Fig.8, in which the secondary lateral damping c_{sy} is high, is different from those in Fig.6c.

Steering instability prevents the application of hard primary lateral stiffness k_{py} and stiff steering linkage k_7 , which weakens the constraints of the wheelset motions, and the critical speed of the body-steered bogie vehicle thus reduces and is very sensitive to conicity in conventional stability, as shown in Fig.6b. There is a conflict between conventional instability and steering instability: to reduce the potential of steering instability, k_{py} and k_7 should be soft while hard k_{py} and k_7 are expected to improve conventional stability of the vehicle. One also finds that the instability of the body-steered bogie vehicle always appears on the motions linked with the kinematic frequency of wheelset no matter if in steering instability or in conventional instability.

Other parameters such as primary roll stiffness and damping, secondary lateral stiffness and secondary roll stiffness and damping do not have much effect on stability of the vehicle.

4. RIDE PERFORMANCES

The system dynamic equation Eq.(1) can be written as Eq.(20) in the frequency domain if only track irregularities are considered as the system disturbances;

$$\mathbf{P}(\omega)\mathbf{q}(\omega) = \mathbf{Q}(\omega) \quad (20)$$

where,

$$\mathbf{q}(\omega) = \{\mathbf{q}_w(\omega) : \mathbf{q}_T(\omega) : \mathbf{q}_b(\omega)\}^T, \quad \mathbf{Q}(\omega) = \{\mathbf{F}(\omega)\mathbf{Y}(\omega) : \mathbf{0} : \mathbf{0}\}^T$$

and

$$\mathbf{P}(\omega) = \begin{bmatrix} \mathbf{P}_1(\omega) & \mathbf{P}_2(\omega) & \mathbf{P}_3(\omega) \\ \mathbf{P}_4(\omega) & \mathbf{P}_5(\omega) & \mathbf{P}_6(\omega) \\ \mathbf{P}_7(\omega) & \mathbf{P}_8(\omega) & \mathbf{P}_9(\omega) \end{bmatrix}$$

DYNAMICS OF A STEERING BOGIE VEHICLE

So, Eq.(20) can be divided into three group equations as:

$$\begin{aligned}
 \mathbf{q}_w(\omega) + \mathbf{P}_1^{-1}(\omega)\mathbf{P}_2(\omega)\mathbf{q}_T(\omega) + \mathbf{P}_1^{-1}(\omega)\mathbf{P}_3(\omega)\mathbf{q}_b(\omega) &= \mathbf{P}_1^{-1}(\omega)\mathbf{F}(\omega)\mathbf{Y}(\omega) \\
 \mathbf{P}_5^{-1}(\omega)\mathbf{P}_4(\omega)\mathbf{q}_w(\omega) + \mathbf{q}_T(\omega) + \mathbf{P}_5^{-1}(\omega)\mathbf{P}_6(\omega)\mathbf{q}_b(\omega) &= 0 \\
 \mathbf{P}_9^{-1}(\omega)\mathbf{P}_7(\omega)\mathbf{q}_w(\omega) + \mathbf{P}_9^{-1}(\omega)\mathbf{P}_8(\omega)\mathbf{q}_T(\omega) + \mathbf{q}_b(\omega) &= 0
 \end{aligned} \tag{21-a}$$

Be letting $\mathbf{H}_k(\omega) = \mathbf{P}_i^{-1}(\omega)\mathbf{P}_j(\omega)$, Eq.(21-a) becomes:

$$\begin{aligned}
 \mathbf{q}_w(\omega) + \mathbf{H}_{T_w}(\omega)\mathbf{q}_T(\omega) + \mathbf{H}_{b_w}(\omega)\mathbf{q}_b(\omega) &= \mathbf{H}_{Y_w}(\omega)\mathbf{Y}(\omega) \\
 \mathbf{H}_{w_T}(\omega)\mathbf{q}_w(\omega) + \mathbf{q}_T(\omega) + \mathbf{H}_{b_T}(\omega)\mathbf{q}_b(\omega) &= 0 \\
 \mathbf{H}_{w_b}(\omega)\mathbf{q}_w(\omega) + \mathbf{H}_{T_b}(\omega)\mathbf{q}_T(\omega) + \mathbf{q}_b(\omega) &= 0
 \end{aligned} \tag{21-b}$$

The power spectral densities (PSD) of the carbody responses are:

$$\mathbf{S}_b(\omega) = \mathbf{H}(\omega)\mathbf{S}_y(\omega)(\mathbf{H}^*(\omega))^T \tag{22}$$

where,

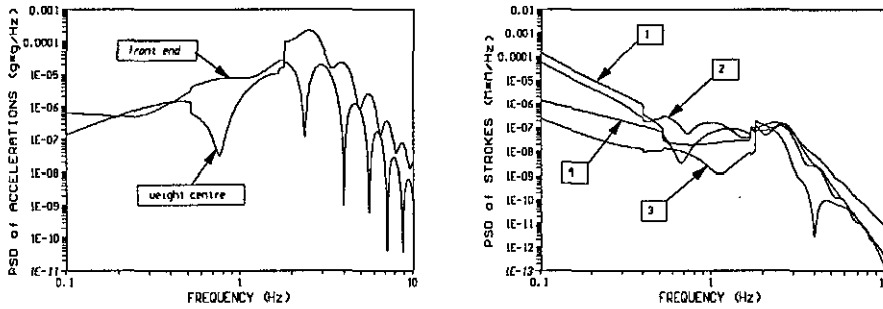
$$\mathbf{H}(\omega) = \Delta_2(\omega)\Delta_3^{-1}(\omega)\mathbf{H}_{Y_w}(\omega) \tag{23}$$

and

$$\begin{aligned}
 \Delta_1(\omega) &= [\mathbf{I} - \mathbf{H}_{b_T}(\omega)\mathbf{H}_{T_b}(\omega)]^{-1}[\mathbf{H}_{b_T}(\omega)\mathbf{H}_{w_b}(\omega) - \mathbf{H}_{w_T}(\omega)] \\
 \Delta_2(\omega) &= -\mathbf{H}_{T_b}(\omega)\Delta_1(\omega) - \mathbf{H}_{w_b}(\omega) \\
 \Delta_3(\omega) &= \mathbf{I} + \mathbf{H}_{T_w}(\omega)\Delta_1(\omega) + \mathbf{H}_{b_w}(\omega)\Delta_2(\omega)
 \end{aligned} \tag{24}$$

The PSD's of the accelerations at five points on the carbody, and the primary and secondary strokes are calculated. These five points are at both carbody ends, two pivots and carbody centre on the carbody floor level in the longitudinal central line. The acceleration PSD's at the front end and weight centre of the carbody, and the PSD's of the strokes are illustrated in Fig.9. For the acceleration PSD's in Fig.9a, the highest responses are between 1.0-2.0Hz, while the highest values of the stroke PSD's, as shown in Fig.9b, are at low frequencies. The rms's of accelerations and the rms's of the strokes have been integrated at three frequency bands (0.1-0.315Hz, 0.315-4.0Hz and 4.0-10.0Hz). The percentages of the rms's at each band over all frequencies (0.1-10.0Hz) are demonstrated in Fig.10. The results show that the acceleration rms's and the primary stroke rms's at the band of 0.315-4.0Hz are much higher than those at other two frequency bands whilst the secondary stroke rms's at the band of 0.1-0.315Hz is much higher than those at other two frequency bands.

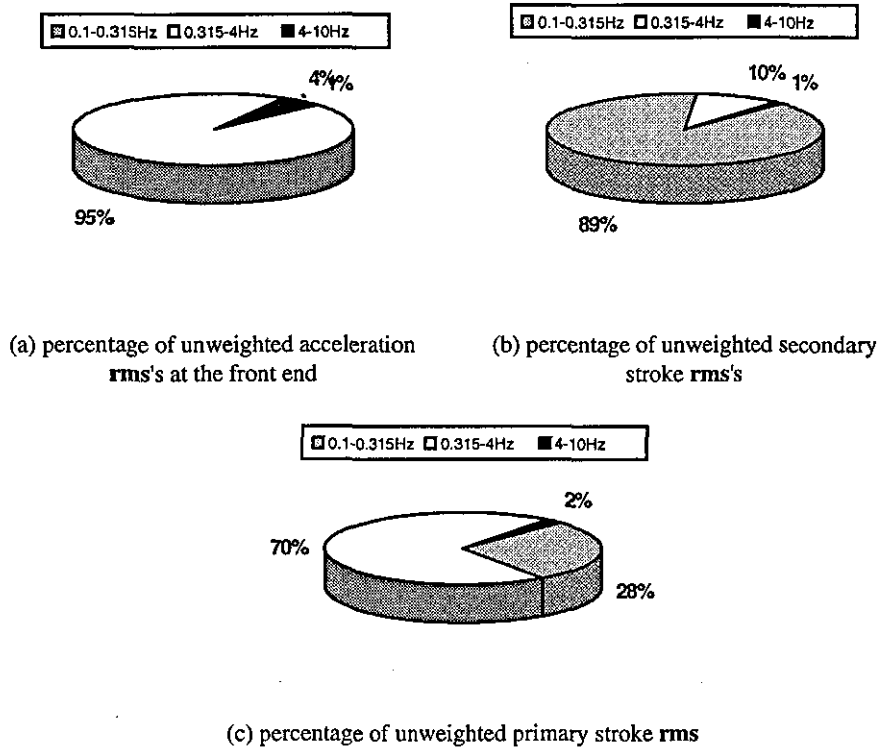
DYNAMICS OF A STEERING BOGIE VEHICLE



(a) PSD's of accelerations

(b) PSD's of strokes, 1 & 2-secondary strokes, 3 & 4-primary strokes

Figure 9 The acceleration and stroke PSD's, $\lambda = 0.1$ and $v_0 = 100\text{km/h}$



(a) percentage of unweighted acceleration rms's at the front end

(b) percentage of unweighted secondary stroke rms's

(c) percentage of unweighted primary stroke rms

Figure 10. The percentages of rms in three bands, $\lambda = 0.1$ and $v_0 = 100\text{km/h}$

DYNAMICS OF A STEERING BOGIE VEHICLE

The filters suggested by ISO/DIS[20] are used to weight the acceleration rms's, and according to this standard, the weighting factors between 0.315Hz and 4.0Hz are larger than 0.5. Combining this with the results in Fig.10a, it can be understood that the major effort in improving the ride quality of the body-steered bogie vehicle is to reduce the responses in the frequency band of 0.315-4.0Hz.

A railway bogie vehicle with two suspension systems can be roughly considered as a system with two parallel filters: the primary suspension system acts as a high pass filter and the secondary suspension acts as a low pass filter. The central frequencies of the filters can be approximately considered as the first two natural frequencies of the vehicle. Usually, the combination of a low central frequency for the low pass filter and a high central frequency for the high pass filter promotes the isolating effect of the filters, which means that the primary suspension should be stiff and the secondary suspensions should be soft. In this body-steered bogie vehicle, the primary lateral stiffness is the main stiffness in the primary suspension, and thus the primary lateral stiffness of this vehicle should be hard in improving its ride quality, as shown in Fig.11, but hard primary lateral stiffness may promote steering instability, which brings out one of the conflicts between the stability and ride quality. In the other hand, when the primary lateral stiffness is very hard, the wheelsets and bogie frame tend to become a single mass body such that the ride quality may also be deteriorated.

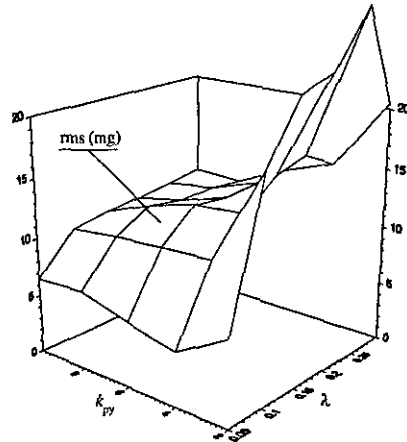


Figure 11, The maximum weighted rms's (mg) of acceleration over 0.315-4.0Hz, $v_0 = 100\text{km/h}$

The ride performance of railway vehicles is governed by two factors: the vehicle disturbances and the system transmissibility. In this section, the system disturbances do not change, and thus the results and analysis can be used to evaluate the transmissibility of the vehicle. In actual fact, the system transmissibility is dictated by the transfer function $\mathbf{H}(\omega)$ that is decided by Eq.(24), and thus it is worth of discussing the transfer function here. The component $\Delta_2(\omega)$ of the transfer function $\mathbf{H}(\omega)$ in Eq.(24) can be expressed as:

DYNAMICS OF A STEERING BOGIE VEHICLE

$$\Delta_2(\omega) = \mathbf{H}_{\gamma_b}(\omega)[\mathbf{I} - \mathbf{H}_{b_T}(\omega)\mathbf{H}_{\gamma_b}(\omega)]^{-1}\mathbf{H}_{w_T}(\omega) - \mathbf{H}_{\gamma_b}(\omega) - \mathbf{H}_{\gamma_b}(\omega)[\mathbf{I} - \mathbf{H}_{b_T}(\omega)\mathbf{H}_{\gamma_b}(\omega)]^{-1}\mathbf{H}_{b_T}(\omega)\mathbf{H}_{w_b}(\omega) - \quad (25)$$

The first term of $\Delta_2(\omega)$ is governed by the primary and secondary suspensions, the second term only depends on the steering linkage, and the last term depends on the secondary suspension and steering linkage. Since there is no direct connection between the carbody and wheelsets in a conventional bogie vehicle, $\mathbf{H}_{w/b}(\omega) = \mathbf{H}_{b/w}(\omega) = 0$ can be easily found, and so only the last term exists in $\Delta_2(\omega)$ for a conventional vehicle. For this body steered bogie vehicle, the outboard wheelsets are connected to the carbody such that $\mathbf{H}_{w/b}(\omega) \neq 0$ and $\mathbf{H}_{b/w}(\omega) \neq 0$ are true. The track irregularities can therefore be transferred into the carbody through other two channels--directly through the steering linkage and through the coupling between the linkage and secondary suspension, and the transmissibility of the body-steered vehicle is therefore potentially increased. The stiff linkage (k_7) between the wheelsets and carbody enhances the effect and thus deteriorates ride quality, as shown in Fig.12a, whilst the increment in k_{11} will strengthen the constraint between the wheelsets and carbody, which effectively increases the wheelset inertia, and improves ride quality, but this effect is not very effective such that ride quality can be improved but only slightly as k_{11} gets harder, as seen in Fig.12b. Since the channels to transfer track irregularities into the carbody are not independent, the system coupling is complicated by the steering linkage and it is more difficult to identify the influence of a single parameter on the transmissibility of this vehicle.

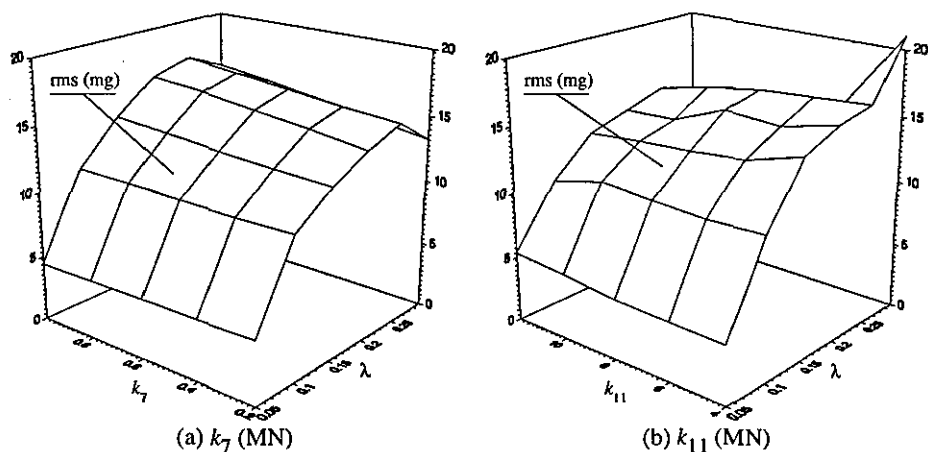


Figure 12, The maximum weighted rms's of acceleration over 0.315-4Hz, $v_0 = 100\text{km/h}$

DYNAMICS OF A STEERING BOGIE VEHICLE

5. CONCLUSION

The configuration of a simple body-steered bogie vehicle capable of perfect steering has been set up to explore the dynamic behaviour of this class of railway bogie vehicle. The conditions for this vehicle capable of perfect steering are independent of curve parameters and only governed by the geometric parameters of the steering linkage. When the steering linkage satisfies these conditions, all bending stiffnesses in this vehicle are eliminated, which not only greatly reduces the wheelset lateral displacements and attack angles even if cant deficiency exists, but also greatly reduces the effect of curvature variation on vehicle alignment in transition. These effects much improve the capability of accommodating cant deficiency and the ability in negotiating transitions, which significantly increase the safety with regard to derailment as well as the cost of maintenance for both wheelset and track. This vehicle therefore greatly decouples the conflict between the stability in lateral plane and curving of railway bogie vehicles. The simplicity of the steering linkage in this vehicle will also boost its advantages in practical applications.

When perfect steering is achieved, the wheelsets take their radial positions and act as unconstrained wheelsets. This means that wheelset constraints should be as flexible as possible to let the vehicle accommodate curve geometry. The fundamental purpose of steering linkages in body-steered bogie vehicles is to produce forces that can balance the forces produced by the bending stiffnesses in the suspensions when the vehicles are on curves. If the bending stiffnesses are equal to zero, the steering linkage should not contribute any bending stiffness. This concept has a very general significance for railway body-steered bogie vehicles.

On the other hand, the wheelsets will move on the pure rolling line when perfect steering is realised. The wheelset lateral displacements are restricted by flange clearance. Since the pure rolling line is mainly dictated by wheelset conicity and curvature, perfect steering is hardly achieved on very sharp curves.

The steering linkage in the body-steered bogie vehicle causes steering instability, which can be either static mode or dynamic mode, and this is the major drawback for the body-steered bogie vehicle and should be aware in practical application.

The connection between the wheelsets and carbody adds up the channels to transfer track irregularities into the carbody, and the transmissibility is potentially increased, which gives a negative effect on the ride performance of the vehicle. The ride performance of this vehicle can, however, be improved by applying other technology such as active or semi-active systems[21].

DYNAMICS OF A STEERING BOGIE VEHICLE

REFERENCES

1. Wickens, A.H. "Railway Vehicle With Generic Bogie Capable Of Perfect Steering", accepted by Vehicle System Dynamics.
2. Wickens, A.H. "Steering and Dynamic Stability of Railway Vehicles", Vehicle System Dynamics, Vol.5, pp.15-46, 1975/6.
3. Bell, C.E. and Hedrick, J.K. "Forced Steering of Rail Vehicles: Stability and Curving Mechanics", Vehicle System Dynamics, Vol.10, No.6, pp.357-385, 1981.
4. Wickens, A.H. "Stability Criteria for Articulated Railway Vehicles Possessing Perfect Steering", Vehicle System Dynamics, Vol.7, pp.165-182, 1978.
5. Schwanck, U. "Wheelset Steering for Bogies of Railway Vehicles", Rail Engineering International, Vol.4, pp.352-359, 1974.
6. Scheffel, H. "Self-steering Wheelsets Will Reduce Wear and Permit Higher Speeds", Railway Gazette International, December 1976, pp.453.
7. Fortin, J.A.C. "Steady-state and Dynamic Predictions of the Curving Performance of Forced-steering Rail Vehicle", 8th IAVSD-IUTAM Symposium on the Dynamics of Vehicles on Roads and Tracks, Cambridge, 1983, pp.223-228.
8. Shen, Z.Y., Yan, J.M., and Liu, J.X. "Dynamical Behaviour of a Forced-Steering Three-Piece Freight Car Truck", 10th IAVSD Symposium on The Dynamics of Vehicles on Roads and Tracks, pp.407-418, 1987.
9. Weeks, R. "The Design and Testing of a Bogie with a Mechanical Steering Linkage", 10th IAVSD Symposium on the Dynamics of Vehicles on Roads and Tracks, pp.497-508, 1987.
10. Smith, R.E. and Anderson, R.J. "Characteristics of Forced-Steering Railway Trucks", Vehicle System Dynamics, Vol.17, No.1-2, pp.1-36, 1988.
11. Smith, R.E. "Dynamics Characteristics of Steered Railway Vehicles and Implications to Design", Vehicle System Dynamics, Vol.18, pp.45-69, 1988.
12. Yang, G. "Dynamic Analysis of Railway Wheelsets and Complete Vehicle System", Ph.D Thesis of Delft University of Technology, 1993.
13. Anderson, R.J. and Fortin, C. "Low Conicity Instability in Forced-steering Railway Vehicles", 10th IAVSD Symposium on the Dynamics of Vehicles on Roads and Tracks, pp.17-28, 1987.
14. Wickens, A.H. "Static and Dynamic Instabilities of Bogie Railway Vehicles with Linkage Steered Wheelsets", accepted by Vehicle System Dynamics.
15. Matsudaria, T. "Hunting Problem of High-speed Railway Vehicles with Special Reference to Bogie Design for The New Tokaido Line", Proc Instn Mech Engrs, Vol.180, Part F, pp.58-66, 1965-1966.
16. Wickens, A. H. "Steering and Stability of The Bogie: Vehicle Dynamics and Suspension Design", Proc Instn Mech Engrs, Vol.205, Part F, pp.109-122, 1991.
17. "Equations of Motion of A Railway Vehicle", ORE Question C 116, 1974.
18. V.K. Garg & R.V. Dukkipati, "Dynamics of Railway Vehicle Systems", Academic Press, ISBN 0 12 275950 8, 1984.

DYNAMICS OF A STEERING BOGIE VEHICLE

19. A.H. Wickens, "Static and Dynamic Stability of Unsymmetric Two-Axle Railway Vehicles Possessing Perfect Steering", *Vehicle System Dynamics*, Vol.11, pp.89-106, 1982.
20. Draft International Standard ISO/DIS 2631/1-1, 1994.
21. W. Li, 'Active and Semi-Active Systems for Optimisation of Bogie Vehicle Primary and Secondary Suspensions in Lateral Plane', IAVSD, 13th symposium, Chengdu, pp.297-307, 1993.

Table A Compatibility matrix

1	0	0	0	0	0	0	0	-1	$-a_0$	h_1	0	0	0	0	0	0
0	1	0	0	0	0	0	0	0	-1	0	0	0	0	0	0	0
0	0	0	0	0	0	0	0	0	0	-1	0	0	0	0	0	0
0	0	1	0	0	0	0	0	-1	a_0	h_1	0	0	0	0	0	0
0	0	0	1	0	0	0	0	0	-1	0	0	0	0	0	0	0
0	0	0	0	0	0	0	0	0	0	-1	0	0	0	0	0	0
0	0	0	0	1	0	0	0	0	0	0	-1	$-a_0$	h_1	0	0	0
0	0	0	0	0	1	0	0	0	0	0	0	-1	0	0	0	0
0	0	0	0	0	0	0	0	0	0	0	0	0	-1	0	0	0
0	0	0	0	0	0	1	0	0	0	0	-1	a_0	h_1	0	0	0
0	0	0	0	0	0	0	1	0	0	0	0	-1	0	0	0	0
0	0	0	0	0	0	0	0	0	0	0	0	0	-1	0	0	0
1	$-a_3$	-1	$-a_4$	0	0	0	0	0	0	0	0	0	0	0	0	0
0	0	0	0	1	$-a_4$	-1	$-a_3$	0	0	0	0	0	0	0	0	0
1	$-a_1$	0	0	0	0	0	0	0	0	0	0	0	0	-1	$-a_2$	h_4
0	0	0	0	0	0	-1	$-a_1$	0	0	0	0	0	0	-1	$-a_2$	h_4
0	0	0	0	0	0	0	0	1	0	h_2	0	0	0	-1	$-l_0$	h_3
0	0	0	0	0	0	0	0	0	1	0	0	0	0	0	-1	0
0	0	0	0	0	0	0	0	0	0	1	0	0	0	0	0	-1
0	0	0	0	0	0	0	0	0	0	0	1	0	h_2	-1	l_0	h_3
0	0	0	0	0	0	0	0	0	0	0	0	1	0	0	-1	0
0	0	0	0	0	0	0	0	0	0	0	0	0	1	0	0	-1

DYNAMICS OF A STEERING BOGIE VEHICLE

Table B Elastic force vector \mathbf{F}_E caused by curve geometry

$$\begin{bmatrix}
 \frac{a_0 l_0 - a_1(l_0 + a_0)}{R} k_7 + \frac{a_0(a_3 - a_4)}{R} k_{11} \\
 \frac{a_0 l_0 - a_1(l_0 + a_0)}{R} a_0 k_7 - \frac{a_0(a_3 - a_4)}{R} a_3 k_{11} \\
 -\frac{a_1(a_3 - a_4)}{R} k_{11} \\
 -\frac{a_1(a_3 - a_4)}{R} a_4 k_{11} \\
 -\frac{a_0(a_3 - a_4)}{R} k_{11} \\
 \frac{a_0(a_3 - a_4)}{R} a_4 k_{11} \\
 -\frac{a_0 l_0 - a_1(l_0 + a_0)}{R} k_7 + \frac{a_0(a_3 - a_4)}{R} k_{11} \\
 -\frac{a_1 l_0 - a_2(l_0 + a_1)}{R} a_0 k_7 + \frac{a_1(a_3 - a_4)}{R} a_3 k_{11} \\
 0 \\
 0 \\
 0 \\
 0 \\
 0 \\
 0 \\
 \frac{a_1 l_0 - a_2(l_0 + a_1)}{R} 2k_7 \\
 0 \\
 -\frac{a_0 l_0 - a_1(l_0 + a_0)}{R} h_4 k_7
 \end{bmatrix}$$

Active and Semi-Active Systems for Optimisation of Bogie Vehicle
Primary and Secondary Suspensions in the Lateral Plane

W. LI*

SUMMARY

The application of an actuator in the secondary suspension of a body-steered bogie vehicle without any yaw stiffness in both the primary and the secondary suspension has been studied. The improvements in ride quality are investigated when the actuator works in the active and the semi-active states. Without reducing stability, for American track standard class 6 track, the body acceleration rms is reduced by 33% when the actuator is in the active state; for a bump track input, a reduction of 11% is possible when the actuator is in a semi-active state, compared with passive suspensions.

1. INTRODUCTION

In conventional bogie vehicles, primary suspensions are used to satisfy the requirements of stability and steering, while secondary suspensions are used to improve the ride performance. The perfect steering law, demonstrated by Wickens [1], shows that all yaw stiffness in both suspensions must be zero in order to achieve curve negotiation without creep. In other words, yaw stiffness in both suspensions should be as small as possible to provide good steering. It is very unlikely that this can be achieved by conventional bogie vehicles.

It seems that body steered bogie vehicles provide a good approach to this problem. Many configurations of steering bogies have been cited by Wickens [1]. Generally, body steered bogie vehicles have a linkage between the vehicle body and the wheelsets. This linkage will lead the wheelsets to take a radial position when the wheelsets follow a curve. This linkage may also provide the possibility to build bogie vehicle with neither primary nor secondary yaw stiffness.

In fact, this linkage can be considered to be the third suspension in the vehicle. Therefore, the coupling among suspensions in the vehicle will be complicated by this linkage.

* Department of Mechanical Engineering, Loughborough University of Technology,
Loughborough, Leicestershire, LE11 3TU, UK.

2 MODEL AND DYNAMICS

2.1 Passive System

A steering bogie vehicle model in the lateral plane, shown in Fig.1, has been set up for this research. This vehicle has two bogies each with two wheelsets. There are two degrees of freedom for each wheelset -- lateral displacement and yaw angle, three degrees of freedom for each bogie -- lateral displacement, yaw angle and roll angle, and three degrees of freedom for vehicle body -- lateral displacement, yaw angle and roll angle. There is a total of seventeen degrees of freedom system.

The vehicle body directly connects with the first wheelset and with the fourth wheelset separately by spring k_7 (parallel with damper d_7 or without damper d_7). The wheelsets in the same bogie are connected by spring k_{11} . With this configuration, each mode of vehicle body -- lateral displacement, yaw angle and roll angle -- has an effect on steering in a curve. On the other hand, the wheelset movement will be directly transferred to the body through the linkage and the ride quality will be degraded. There is no yaw stiffness in the primary and secondary suspensions. Kalker's linear creepage law is used to define the creepage between wheelsets and rails.

The assumptions to set up the dynamics equations of the model are:

- a perfect cone profile for the tread of wheel,
- wheelset neither leaving the rail nor two point contact,
- no elastic deformation of the track,
- creepages are small enough to maintain its linearity,
- no elastic deformation of any parts of vehicle except the springs,
- all springs and dampers are linear, and
- the vehicles is symmetrical in lateral plane.

For the purpose of illustration, American track standard [7] is used to define track irregularities. The power spectrum densities (PSD) of track irregularities are defined as:

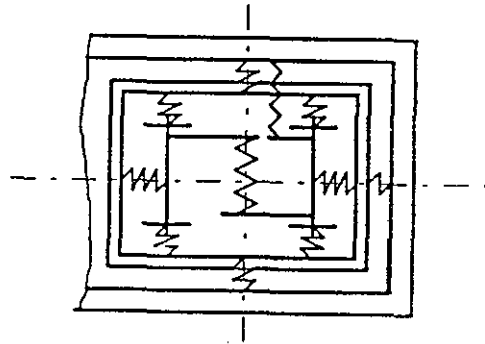


Fig.1 Configuration of Vehicle

if only track irregularities are considered as the system disturbances.

The elastic matrix E and damping matrix C can be formed by using the assembled matrix technique[1].

$$\begin{aligned} E &= \mathbf{a}^T[\mathbf{k}]\mathbf{a} \\ C &= \mathbf{a}^T[\mathbf{c}]\mathbf{a} \end{aligned} \quad (11)$$

where, $[\mathbf{k}]$ is stiffness coefficient matrix, and
 $[\mathbf{c}]$ is damping coefficient matrix.

2.4 Active System and Semi-Active System Configuration

Actuator is fixed between the car body and bogie in the lateral direction shown in Fig.2. The output of the actuator will produce a lateral force and a roll moment in the bogie frame and a lateral force, yaw moment and roll moment in the vehicle body.

The output of actuator is defined by

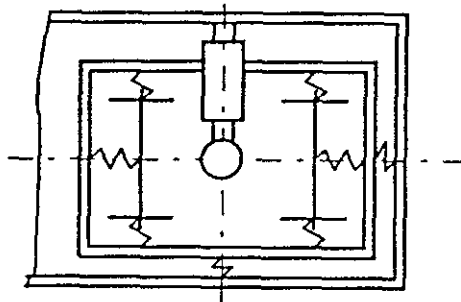


Fig.2 Actuator arrangement

for leading bogie:

$$\begin{aligned} U_L &= A_1 \ddot{y}_b + A_2 \ddot{\psi}_b + A_3 \ddot{\phi}_b + A_4 \dot{y}_b + A_5 \dot{\psi}_b + \\ &+ A_6 \dot{\phi}_b + A_7 y_b + A_8 \psi_b + A_9 \phi_b \end{aligned} \quad (12)$$

for trailing bogie:

$$\begin{aligned} U_T &= B_1 \ddot{y}_b - B_2 \ddot{\psi}_b + B_3 \ddot{\phi}_b + B_4 \dot{y}_b - B_5 \dot{\psi}_b + \\ &+ B_6 \dot{\phi}_b + B_7 y_b - B_8 \psi_b + B_9 \phi_b \end{aligned} \quad (13)$$

The range of possibilities implicit in these control laws have not been fully evaluated. A_i and B_i are artificially chosen as discussed below and are restricted by the system stability. Usually, $A_i = B_i$.

The body acceleration rms (root-mean-square) is used to evaluate the model ride quality. The accelerations of three points on the body floor level along the central line are measured. They are on the body front end (point A), on the body rear end (point B) and on the body geometric centre (point C). The accelerations at those points are calculated by

responsible for the high body yaw acceleration. The most effective approach to improve the ride quality is to reduce the body yaw acceleration.

3.2 Active System

To investigate the possibility to improve the ride quality of body steered vehicles by applied the control unit, the actuator is first considered as in the active state. The improvements in ride quality against some feedback coefficients in Eq.12 and Eq.13 are shown in Fig.5 -- Fig.8 when the actuator is in the active state with a band pass filter 1Hz--10Hz. The body acceleration feedbacks have the most significant influences on the ride quality, especially the body yaw acceleration feedback. But, the further increases in the body acceleration feedback will reduce the system critical speed.

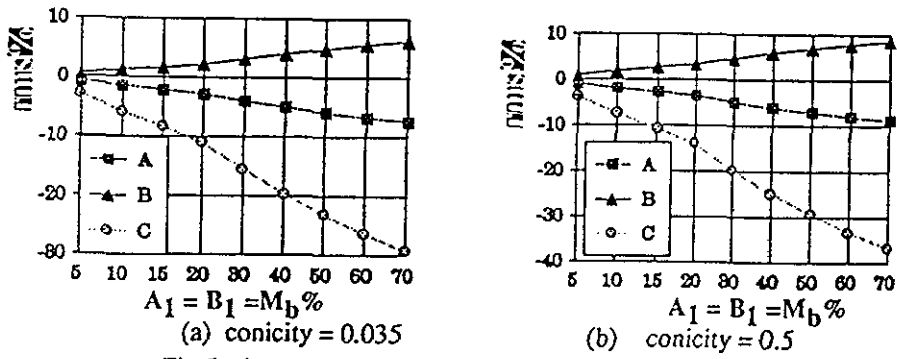


Fig.5 change in rms, $v = 100\text{km/h}$; $\lambda_{\min} = 0.03$ and $v_{\lambda = 0.5} = 107\text{km/h}$ when $A_1 = B_1 = 70\% M_b$

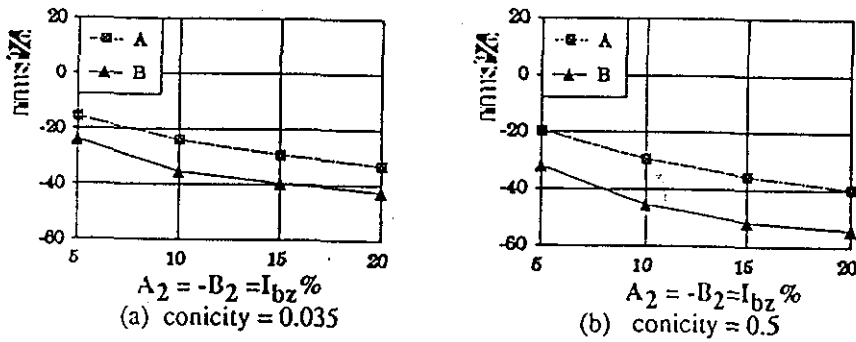


Fig.6 change in rms, $v = 100\text{km/h}$; $\lambda_{\min} = 0.04$ and $v_{\lambda = 0.5} = 103\text{km/h}$ when $A_2 = -B_2 = 20\% I_{bz}$

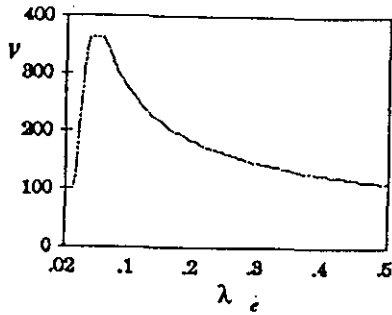


Fig.9 Critical speed (km/h)
 $\lambda_{\min} = 0.035$ and $v_{0.5} = 110.8\text{km/h}$.

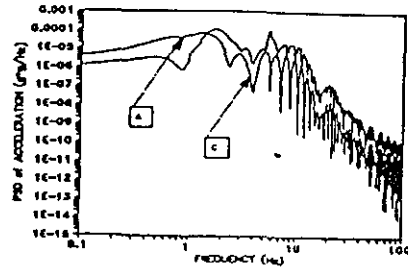


Fig.10 PSD of accelerations
 $v = 100\text{km/h}$

Better results would be achieved if different band pass filter were used for different modes in this research. But, suspension coupling and variation of conicity will affect unstable modes in a bogie vehicle. Consequently, it is very difficult to apply this idea to a bogie vehicle. However, it might be helpful to use a different band pass filter for the feedback of body velocities. This area is going to be investigated in near future.

3.3 Semi-active System

The output of the actuator will not only depend on Eq.12 and Eq.13 but also Eq.1 when the control unit is in a semi-active state. The system works like a combination of two systems. When the actuators need energy supply, they are switched off and the model becomes a passive system. When the actuator do not need power supply, they are switched on and the system is in the active state. So, the system becomes a parametrically adjustable system. It is difficult to analyse the ride quality in the frequency domain.

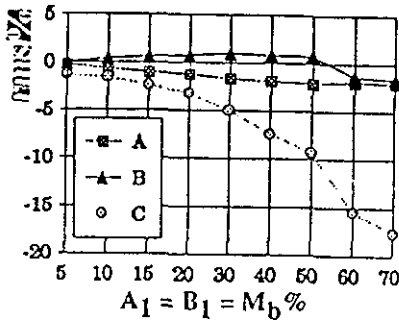


Fig.11 change in rms, $v = 100\text{km/h}$
 and conicity = 0.5.

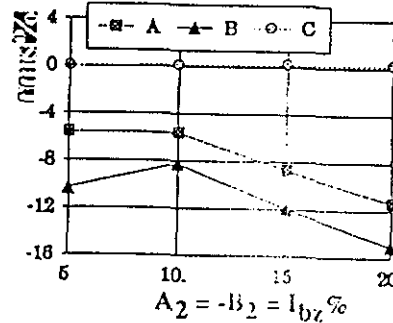


Fig.12 change in rms, $v = 100\text{km/h}$
 and conicity = 0.5.

REFERENCE

1. Wickens A., 'Railway Vehicles with Generic Bogie Capable of Perfect Steering', to be published.
2. Hedrick J.K. and Wormley D.N., 'Active Suspensions for Ground Transport Vehicle - A State of the Art Review', *Mechanics of Transportation suspension Systems*, eds.B. Paul et al., ASME AMD-Vol.15, 1975, pp.21-40.
3. Goodall R. M. and Kortum W., 'Active Control in Ground Transportation - A Review of the State-of-the-Art and Future Potential', *Vehicle System Dynamics*, Vol.12, 1983, pp.225-257.
4. Goodall R. M. and Kortum W., 'Active Suspensions for Railway Vehicle -- an Avoidable Luxury or an Inevitable Consequence?', *Proceedings of IFA conference*, 1990, pp.219-225.
5. Redfield R. C., 'Performance of Low-bandwidth, Semi-active Damping Concepts for Suspension Control', *Vehicle System Dynamics*, Vol.20, 1991, pp.245-267.
6. Lin Y. and Willumeit H.P., 'The Dynamics of the Vibrator-controlled Adaptive Damper and Its Potential in Vibration Isolation', *Vehicle System Dynamics*, Vol.20, 1991, pp. 353-369.
7. Garg V.K. and Dukkipati Rao V., 'Dynamics of Railway Vehicle Systems', Table 3.6, pp89, Academic Press Canada, 1984.
8. Wickens A., 'The Dynamics Stability of Railway Vehicle Wheelsets and Bogies Having Profiled Wheels', *Ins. J. Solids Structure*, Vol.1, 1965, pp. 319-341.
9. 'Equations of Motion of a railway Vehicle', ORE, Question C 116, Report No.4, 1974.
10. Yang G., 'Dynamic Analysis of Railway Wheelsets and Complete Vehicle Systems', Ph.D Theises of Delft University of Technology, 1993.
11. Li W., 'The Dynamics of A Body Steering Bogie Vehicle in the Lateral Plane', to be published.

THE MODELLING OF RAILWAY PASSENGER VEHICLES IN THE LATERAL PLANE

Li

Department of Mechanical Engineering, Loughborough University of Technology, Loughborough, LE11 3TU, K.

A computer program is set up to investigate the railway vehicle stability, ride quality and curve negotiation in the lateral plane. The parameters in the vehicle suspensions can be studied individually. This program allow the user to apply active and semi-active systems on the vehicle suspensions. The process and some techniques used to model the railway vehicle are demonstrated in this paper.

INTRODUCTION

Railway vehicles usually consist of wheelsets, bogie frames and car body which are connected by suspensions. The suspension between wheelsets and bogie frames is called the primary suspension and the suspension between bogie frames and car body is called the secondary suspension. The elements in these two suspensions can be passive, active, semi-active or combinations of them. The physical system of railway vehicles is nonlinear. The nonlinearity comes from two sources, one of which is the nonlinear suspension elements such as Coulomb friction, air springs, dead end of dampers and bumps, and another is the contact forces of wheel/rail. The contact forces between wheel and rail are called creepage forces and are well known as nonlinear [1]. Track irregularities are well understood as random processes, which are the main sources of disturbances in railway vehicle systems. Therefore, the railway vehicle is a nonlinear system with random inputs. The modelling of this system can be very complex. However, the system can be simplified according to research interest. The system can be considered as a linear multi-body system, when the following assumptions are made in this simulation:

- all suspension elements are linear except semi-active actuators,
- Kalker's linear theory [1] is used to find creepage forces,
- uniform conicity is for wheel profile and there is no flange contact,
- all springs and dampers are massless.

The dynamic equations of railway vehicles can be decoupled into two groups if the vehicles are longitudinally symmetric. One of them is in the lateral plane and another is in the longitudinal plane. The inherent "snake movement" of wheelset [2] raises the unstable problem in the lateral plane. In order to keep wheelsets on straight track, strong constraint on the wheelsets is required. But, to let the wheelsets follow a curve, the constraint should be released as much as possible. Usually, the former requires hard suspensions and the latter requires soft suspensions. The trade-off between vehicle tangent stability and curve negotiation is fundamental in railway vehicles. Moreover, vehicle ride quality is a requirement for the vehicle suspension. Generally, the ride quality is benefited from soft suspensions. But, the static deformations of suspension springs and the rattle spaces need to be considered. Therefore, the vehicle stability, ride quality and curve negotiation in the lateral plane are investigated in the research.

Two approaches are considered here to solve those problems above. One of them is to innovate new configurations to decouple or at least to reduce the tradeoff of stability/curving. Another is to apply active and/or semi-active systems to improve the ride quality. A computer simulation model has been set up to investigate the effects of vehicle configurations on the inherent tradeoff of stability/curve negotiation of railway vehicle. The configurations of vehicles and the parameters in suspension can be easily changed so that the program is suitable for many class vehicles. The program also allows the user to add the active or semi-active actuators in the secondary suspension. The results are expected to lead to innovate some new ideas for new generation railway vehicles. It should be pointed out that the research is to explore the applications of new techniques and the results are theoretical at this stage. Although a few of multibody dynamics program packages are available now, non of them can satisfy the research purpose here. Of course, their cost is another reason.

DYNAMIC BEHAVIOUR OF RAILWAY VEHICLES

For a linear multi-body system, the equations of motion can be expressed as:

The damping yielded by the creepage between rail and wheel is proportional to $1/V_0$ (V_0 is the vehicle forward speed m/s). The investigation of railway vehicle stability is to find the maximum vehicle speed (it is called the vehicle critical speed) without violating Eq.7.

Ride Quality

The response power spectral density $S_x(\omega)$ of a linear system is

$$S_x(\omega) = H(\omega)S_y(\omega)(H^*(\omega))^T \quad (8)$$

Where, $H(\omega)$ is the system transfer function and $H^*(\omega)$ is its conjugate. $S_y(\omega)$ is the power spectrum density of the system disturbance. If the track irregularities are only the system disturbances, Eq.8 cannot be applied here directly. Having applied Laplace transform to Eq.1, it can be arranged as:

$$\begin{aligned} P_1(\omega)X_w(\omega) + P_2(\omega)X_T(\omega) + P_2(\omega)X_b(\omega) &= F(\omega)Y(\omega) \\ P_4(\omega)X_w(\omega) + P_5(\omega)X_T(\omega) + P_6(\omega)X_b(\omega) &= 0 \\ P_7(\omega)X_w(\omega) + P_8(\omega)X_T(\omega) + P_9(\omega)X_b(\omega) &= 0 \end{aligned} \quad (9)$$

Subscript w, T and b are represented as wheelset, bogie and car body respectively. So the system response power spectral density PSD related to track irregularities are

$$\begin{aligned} S_w(\omega) &= H_1(\omega)S_y(\omega)(H_1^*(\omega))^T \\ S_T(\omega) &= H_2(\omega)S_y(\omega)(H_2^*(\omega))^T \\ S_b(\omega) &= H_3(\omega)S_y(\omega)(H_3^*(\omega))^T \end{aligned} \quad (10)$$

Where, $H_1(\omega)$, $H_2(\omega)$ and $H_3(\omega)$ can be derived from Eq.9.

Two kinds of track irregularities affect the ride quality of railway vehicles in the lateral plane. They are cross-level irregularity and alignment irregularity. They are close to Gaussian process and not correlated [4]. There are different standards to define them. Class 6 of track in American track standard [4] is used here. Supposed that all wheelsets in the vehicle pass through the same point on track in different time, the cross-PSD between wheelset is

$$S_{wij}(\omega) = S_{wii}(\omega)e^{-i\omega t_k} \quad (11)$$

where t_k is a time delay which is a function of the vehicle geometry and the vehicle speed V_0 . The relationship between single sided spectrum and double sided spectrum is [5]:

$$W(f) = 4\pi S(\omega), \quad \omega = 2\pi f \quad (12)$$

Three indices are used to evaluate the vehicle ride quality. They are PSD of the primary strokes, the secondary strokes and the accelerations. The accelerations are calculated at five points on the floor level of the car body. The weighted RMS of the accelerations at those points are calculated. The filter recommended by ISO-2631 [6] is used as the weighting function.

Curve Negotiation

ere, A is a constant and $x = \int_0^t V_0 dt$.

SIMULATION

A computer program, shown in Figure 1, is made to simulate the vehicle's dynamic behaviour as discussed in the last section. The program has four parts, vehicle model and track specification, stability analysis, ride quality analysis and steady state curving analysis.

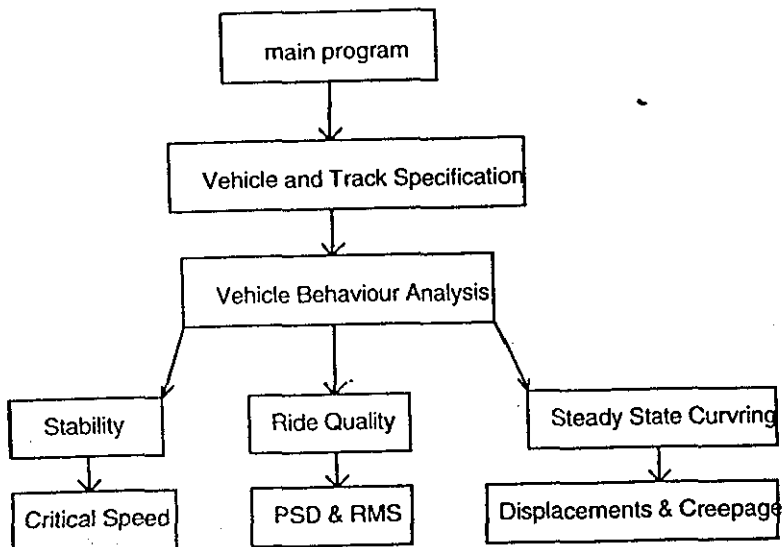
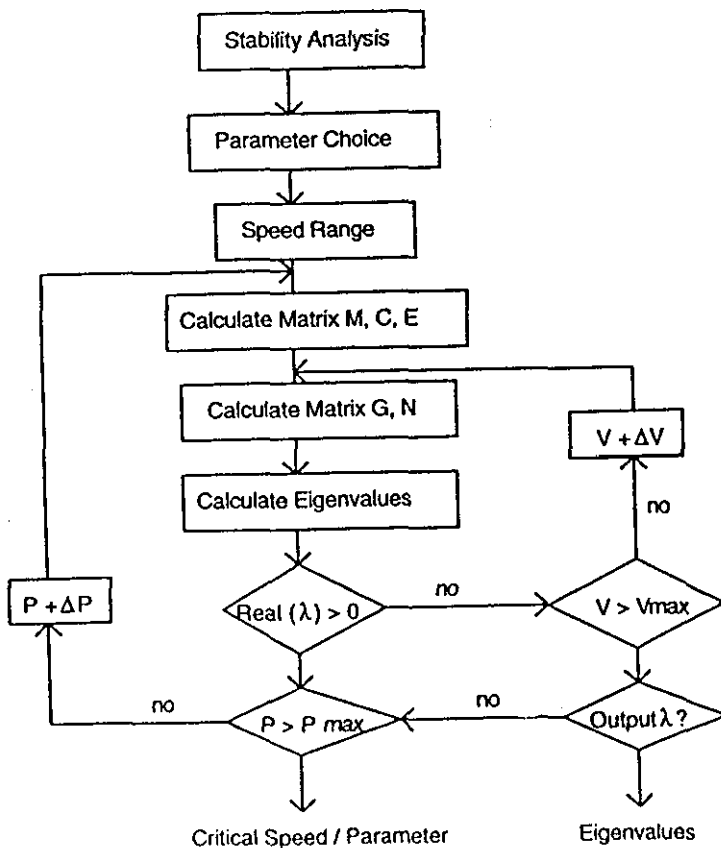


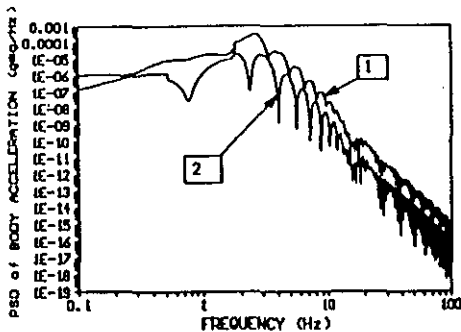
Figure 1. Program block diagram

In the vehicle model and track specification part, the following system parameters should be defined:

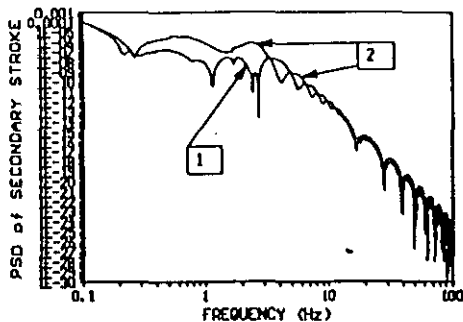
- degrees of freedom in the system,
- geometric parameters of vehicle,



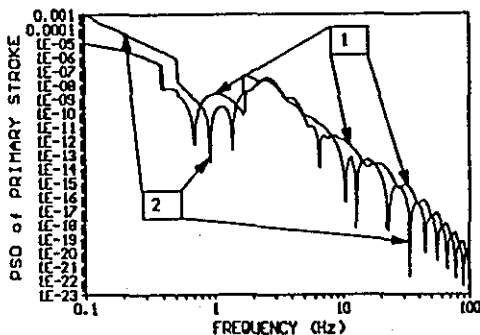
(a) block diagram



(b) PSD and weighted RMS of accelerations
weighted RMS: 1--11.68mg, 2--9.79mg



(c) PSD of the secondary strokes
RMS: 1-- 1.56mm, 2 -- 2.06mm



(b) PSD of the primary strokes
RMS: 1-- 0.86mm, 2 -- 5.33mm

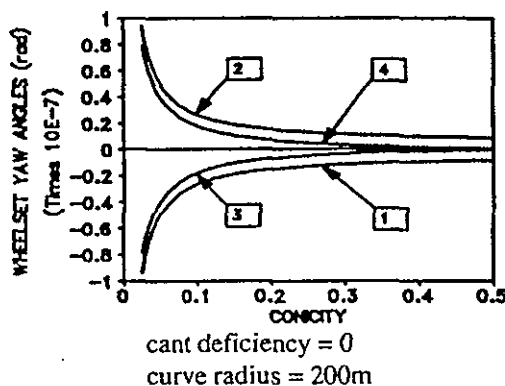


Figure 4, Wheelset yaw Angles

Figure 3, Ride quality analysis block diagram and results, $V_0 = 100\text{km/h}$, conicity = 0.1

In the stability analysis subroutine shown in Figure 2, each stiffness and each damping in the suspensions as well as wheelset conicity is considered as an independent parameter. Therefore, their effects on the vehicle stability can be investigated individually. This subroutine can calculate the eigenvalues of the whole vehicle and the vehicle critical speed against each parameter in the vehicle's suspensions. The vehicle's natural frequencies against the vehicle forward speed V_0 are used to identify the unstable modes. The results in Figure 2 (b) and (c) are the examples.

The ride quality analysis subroutine is divided into two sections. When the actuators work in a semi-active state, the simulation is carried out in time domain and the system responses are the time series. Without carrying out frequency analysis, the RMS of the system accelerations are directly calculated from their time series. In this case, ISO-2631 filter is not used and RMS is unweighted. When the elements in the system are only passive or the actuators work in active state, the analysis is carried out in the frequency domain. The program can output PSD of the accelerations, primary strokes and secondary strokes, their unweighted RMS and the weighted RMS of accelerations based on ISO-2631 filter. The programming block diagram and the results are shown in Figure 3.

The programming of steady state curving analysis is rather simpler than the stability analysis and ride quality analysis. When the vehicle model and track specifications are decided, the equations in Eq.15 are linear and can be solved easily. The outputs of this subroutine are the displacements (absolute and relative) in all degrees of freedom of the vehicle mass elements and the creepages between wheelsets and rail. In the subroutine, each stiffness in the system can be changed individually. Some of results are shown in Figure 4.

Validation

The computer modelling of a physical system is usually divided into two steps. First, a mathematical model is set up from the physical system by simplifying some conditions. Then a computer program is made to simulate the mathematical model. Therefore, there are two questions relating to the validation of computing simulation. Is the mathematical model correct and does the computer program correctly simulate the mathematical model? The answer to the first question is decided by the research purpose and the understanding of the physical system. The second question is the computing program itself.

The validation of this modelling is supported by the following facts:

Computer Program Instruction

Name: **RVDSP**

Stand for

Railway
Vehicle
Dynamics
Simulation
Program

Supporting facility: NAG Library

Language: FORTRAN 77

System: UNIX

Part I, Data Files

A, *Preparation Data Files*

Before carrying out any simulation by **RVDSP**, the following data files should be produced. **RVDSP** has set the options to build up those data files. The meaning of each data on those files is defined in **RVDSP**.

ASMT.DAT	non-zero elements of compatibility matrix a
COS.DAT	contact parameters
CVS.DAT	curve definition
CVDP.DAT	yaw angles caused by the curvature of a uniform curve and related to the carbody
CVLD.DAT	forces F_{cant} and F_{creep} on steady state

DMS.DAT	dampings
GES.DAT	geometric parameters
MAS.DAT	mass & inertia
PXIN.DAT	transition definition
RDPS.DAT	track irregularity definition
STS.DAT	stiffnesses

B, *Intermediate Data Files*

DMAT.DAT	non-zero elements of damping matrix D
DPMX.DAT	dampings correspondent to compatibility matrix a
MMAT.DAT	non-zero elements of inertia matrix M
SCMX.DAT	stiffnesses correspondent to compatibility matrix a
SMAT.DAT	non-zero elements of stiffness matrix K
SDFM.DAT	F_E on steady state
EDFM.DAT	$F_E + F_C$ on transition
PSIN.DAT	yaw angles and radius of local coordinates related to reference on transition

C, *Results*

Stability:

*EAGEN.DAT	eigenvalues
STALIT.DAT	critical speeds and frequency of unstable mode

Ride Performance:

RIDE.DAT	PSD and rms of accelerations
RIDES.DAT	PSD of strokes

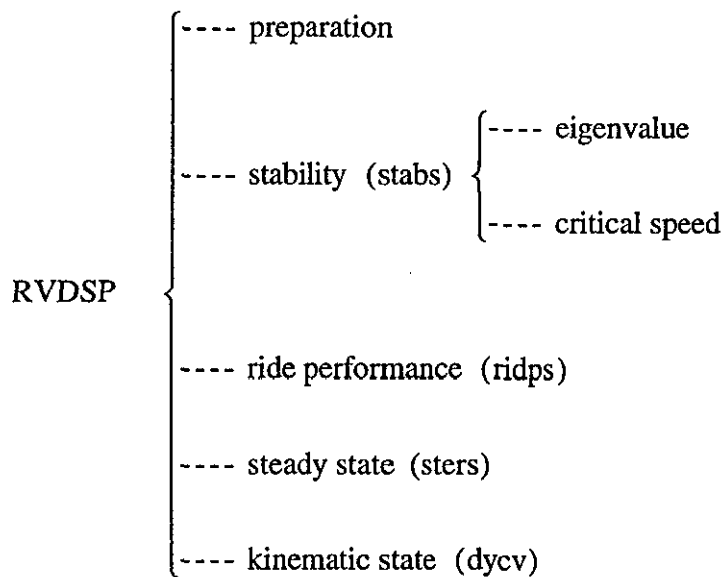
Steady State:

SDST.DAT	displacements on steady state
SDLY1.DAT	turning angles of steering level of Model I on steady state
SDLY2.DAT	turning angles of steering level of Model II on steady state

Kinematic State:

SHL.DAT	lateral displacements on transition
SHR.DAT	roll angles on transition
SHY.DAT	yaw angles on transition
DYLY1.DAT	turning angles of steering level of Model I on transition
DYLY2.DAT	turning angles of steering level of Model II on transition

Part II, Structure of Program



Part III, Running Commands and Process

A, *Start*

For initiate the program, Type `rvdsp` and then press ENTER

The following sentences is appearing on screen:

```
" Welcome To Use RVDSP "  
" Have you made the data files ready  
Type YE for yes or NO for no "
```

If you type 'YE' or 'ye', you are going to carry out simulation.

If you type 'NO' or 'no', you are going to prepare the data files.

The instruction to prepare the data files are well described in the program. Just follow the instructions on screen.

Suppose you answer is 'yes', you will read the following words on screen:

```
" Input the degrees of freedom of this system"
```

Type: **17**

```
" Input the number of the springs "
```

Type: **18** ----- for conventional bogie vehicle
26 ----- for Model I and Model in Appendix D
30 ----- for Model II

```
" Type of bogie:  
1 ----- conventional bogie vehicle  
2 ----- Model in Appendix D  
3 ----- Model I  
4 ----- Model II "
```

Type: **one** of these numbers

" Options:

- End of the program ----- 0
- Stability ----- 1
- Ride Performance ----- 2
- Steady State ----- 3
- Kinematic State ----- 4
- Dynamic State ----- 5 (going to be developed)
- Time Response ----- 6 (going to be developed)
- Prepare Compatibility Matrix ----- 7 "

Type: **one** of these numbers

B, *Simulation*

The simulation start after you choose one of the options. The results will be store to the data files listed above. The program will return to the options after the simulation completes and another option but not the same one can be selected.

